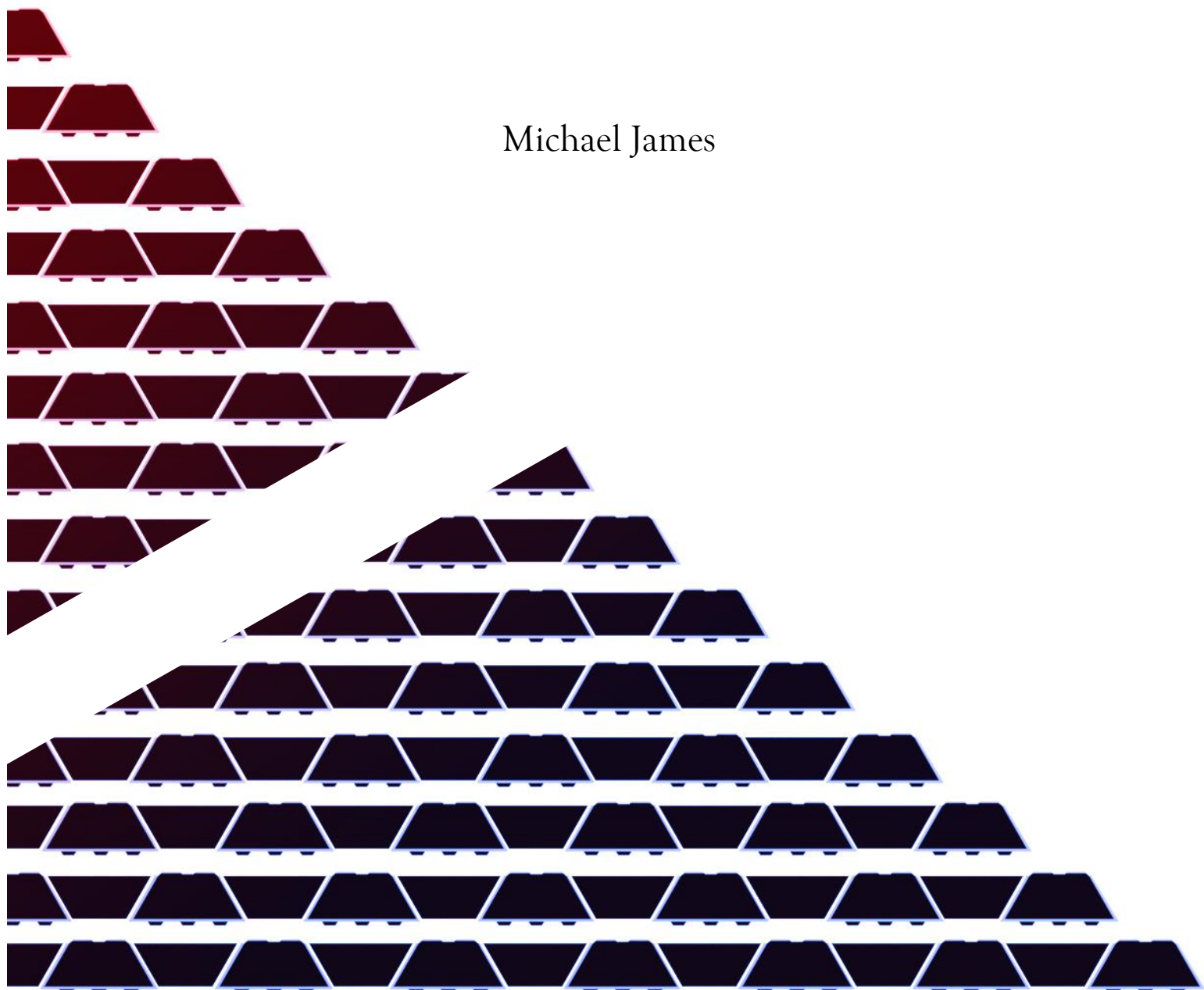


The Segment barrier

A case study on the applicability of new conceptual designs for a storm surge barrier at Long Island Sound, USA

Michael James



The Segment barrier

A case study on the applicability of new conceptual designs for a storm surge barrier at Long Island Sound, USA

Master of Science Thesis

by

Michael Plasido Jacinto James

in partial fulfillment of the requirements to obtain the degree of

Master of Science

in Civil Engineering at the Delft University of Technology, Department of Hydraulic Engineering,
to be defended on Thursday January 21, 2021 at 15:00 PM.

Student number: 4105605

Thesis committee:	Prof. dr. ir. S.N. (Bas) Jonkman	Chairman	TU Delft
	Prof. ir. R. (Rob) Nijssen	Supervisor	TU Delft
	Dr. ing. M.Z. (Mark) Voorendt	Supervisor	TU Delft
	Ir. N.A. (Niek) van der Leer	Supervisor	Witteveen+Bos
	Ir. J. (Joost) Lansink	Supervisor	Witteveen+Bos

Preface

This master thesis has been conducted to fulfil the academic requirement to obtain the degree of master of science in civil engineering at the Delft University of Technology. I would like to extend my gratitude to the university and company supervisors for sharing their expertise and providing me with the opportunity to gain experience at Witteveen+Bos.

My time at the university has empowered me with knowledge and strengthened my conviction to be a positive force in society. With a new degree in hand, the sense of responsibility to share knowledge and help those who are less fortunate has grown ever stronger. The pandemic has been a personal reminder of the many challenges the world faces of which the climate crisis could be the most defining of our time. It is my hope to contribute in finding solutions for these global challenges through the discipline of civil engineering.

To all my friends and family members who have supported me on my academic journey, my sincerest appreciation. It is simply impossible to describe the depth of my gratitude.

Finally, I want to thank the most sacred person in my life, my mother, who has supported and witnessed my journey from beginning to end. With the completion of this thesis, I am able to turn the final page on a decade long chapter defined by adversity and perseverance.

Mother, with this achievement, we can finally end our truly extraordinary journey.

Michael James
Delft, January 2021

Summary

The Segment barrier is a conceptual design for a storm surge barrier consisting of individual concrete segments which can be combined to form a barrier. The structure is designed with the ability to expand in size to deal with the uncertainties of global mean sea level rise by stacking the individual segments into various configurations. At its core, the Segment barrier is a temporary structure that can be assembled before the advent of a storm surge and dismantled afterwards with the intent of mitigating the long-term environmental and ecological impact associated with permanently fixed hydraulic structures. However, the Segment barrier is equally able to function as a typical structure with a long design life if necessary. Long Island Sound served as a case study for the development of this concept. The severity and frequency of annual hurricanes is expected to increase within this century and recent examples of hurricanes have already shown the devastating impact to New York City and the wider coastal region. The area of Long Island Sound is expected to have a crucial role in providing protection for millions of people through the development of flood protection measures. The development of this concept involved analyses on the structure's overall stability, local wave climate, structural design of prestressed concrete elements and the applicability of the barrier for this region. An important aspect of this concept is optimization for which a number of suggestions are provided to inspire further research and design efforts. This thesis establishes the foundation for a new type of storm surge barrier and aims to convey the potential of this concept for wider applicability around the world.



Table of Contents

PREFACE	I
SUMMARY	II
LIST OF FIGURES	VII
LIST OF TABLES	X
LIST OF ACRONYMS	XI
CHAPTER 1 INTRODUCTION	1
CHAPTER 1 ABSTRACT	1
1.1 MOTIVATION AND RELEVANCY	2
1.2 INITIAL EXPLORATION OF THE MAIN THREATS	3
1.3 DESIGN OBJECTIVE	4
1.4 METHODOLOGY	5
1.5 REPORT STRUCTURE	6
CHAPTER 2 SYSTEM ANALYSIS	7
CHAPTER 2 ABSTRACT	7
2.1 THE IMPACT OF HURRICANE SANDY	8
2.1.1 Storm development and trajectory	8
2.1.2 Damage to New York coastal region	12
2.2 LONG ISLAND SOUND	14
2.2.1 Flood prone areas	14
2.2.2 Long Island Sound ecosystem.....	15
2.2.3 West Sound priority map.....	16
2.3 STAKEHOLDER ANALYSIS	17
2.4 NYNJHAT CONCEPTUAL BARRIER DESIGN	18
2.4.1 Barrier features.....	18
2.4.2 Barrier location.....	19
2.4.3 Geometric design.....	19
2.4.4 Gate type selection.....	20
2.4.5 Discussion	20
CHAPTER 3 REQUIREMENTS AND BOUNDARY CONDITIONS	21
CHAPTER 3 ABSTRACT	21
3.1 FUNCTIONAL REQUIREMENTS	22
3.2 ENVIRONMENTAL BOUNDARY CONDITIONS	22
3.2.1 Astronomical tides.....	22
3.2.2 Sea level rise	23
3.2.3 Tidal flows	24
3.2.4 Water level head difference	24
3.2.5 Wind data.....	24
3.2.6 Vessel dimensions.....	24
3.2.7 Water depth and wave height.....	25
3.2.8 Geological data.....	25
CHAPTER 4 LOCATION SELECTION	26
CHAPTER 4 ABSTRACT	26
4.1 INTRODUCTION	27
4.2 LOCATION SELECTION CRITERIA	27
4.3 BARRIER LOCATION OPTIONS	28
4.4 LOCATION DISCUSSION	33
CHAPTER 5 DEVELOPMENT AND ANALYSIS OF CONCEPTS	34
CHAPTER 5 ABSTRACT	34

5.1 CONCEPTUAL DESIGN 1: THE SEGMENT BARRIER	35
5.1.1 <i>Introduction</i>	35
5.1.2 <i>Expandability of the barrier</i>	36
5.1.3 <i>Geometry</i>	36
5.2 CONCEPTUAL DESIGN 2: RISING TOWER BARRIER	37
5.2.1 <i>Introduction</i>	37
5.2.2 <i>Tower parts</i>	37
5.3 CONCEPTUAL DESIGN 3: THE RISING WALL BARRIER	39
5.4 CONCEPTUAL DESIGN 4: THE HORIZONTAL SLIDING BARRIER	42
5.5 CONCEPTUAL DESIGN 5: FLAP GATE	44
5.6 CONCEPTUAL DESIGN 6: FLOATING SECTOR GATE	45
5.7 CONCEPTUAL DESIGN 7: LIFT GATE	46
5.8 VERIFICATION OF CONCEPTS	47
5.9 EVALUATION OF THE CONCEPTS	48
5.9.1 <i>Multiple-criteria decision analysis</i>	48
5.9.2 <i>Evaluation criteria</i>	48
5.9.3 <i>Weight Factors</i>	49
5.9.4 <i>MCA results</i>	50
5.9.5 <i>MCA Conclusions</i>	52
5.9.6 <i>Final Choice</i>	52
CHAPTER 6 BARRIER CONFIGURATIONS.....	53
CHAPTER 6 ABSTRACT	53
6.1 INTRODUCTION	54
6.2 CONSTRUCTION PROCESS	56
6.2.1 <i>Barrier layout</i>	56
6.2.2 <i>Shoreline connections</i>	59
6.2.3 <i>Transport of heavy equipment</i>	60
6.2.4 <i>Foundation</i>	63
6.2.5 <i>Cross-section assembling</i>	64
6.2.6 <i>Watertightness</i>	65
CHAPTER 7 STRUCTURAL DESIGN.....	69
CHAPTER 7 ABSTRACT	69
7.1 SEGMENT CROSS-SECTIONAL DESIGN	70
7.1.1 <i>Introduction</i>	70
7.1.2 <i>Crest elevation of the barrier</i>	70
7.1.3 <i>Loads on the barrier</i>	71
7.1.4 <i>Concrete & steel design</i>	72
7.2 DETAILING	75
7.2.1 <i>Lifting connection</i>	75
7.2.2 <i>Chloroprene synthetic gasket</i>	76
7.3 COST ANALYSIS	77
7.3.1 <i>Estimations</i>	77
7.3.2 <i>Discussion</i>	79
7.4 SEGMENT DETERIORATION	80
7.4.1 <i>Causes of damage</i>	80
7.4.2 <i>Repairing methods</i>	81
7.5 TECHNICAL DESIGN CHOICES	83
CHAPTER 8 EVALUATION.....	84
CHAPTER 8 ABSTRACT	84
8.1 EVALUATION MATRIX	85
8.2 ECOLOGICAL CONSTRUCTION STRATEGIES	88
CHAPTER 9 CONCLUSIONS AND RECOMMENDATIONS.....	90
CHAPTER 9 ABSTRACT	90

9.1 CONCLUSIONS	91
9.1.1 <i>The Segment barrier</i>	91
9.1.2 <i>Applicability</i>	91
9.2 RECOMMENDATIONS	92
REFERENCES	95
APPENDIX A: MATHEMATICAL DERIVATION OF THE BASIC GEOMETRY	100
APPENDIX B: CREST ELEVATION OF THE BARRIER	103
B1 INTRODUCTION	103
B1.2 <i>Steep slopes</i>	105
B1.3 <i>Gentle slopes</i>	106
B1.4 <i>Discussion</i>	107
B2 SEA LEVEL RISE SCENARIOS	108
B3 DISCUSSION	110
APPENDIX C: LOADS ON THE BARRIER	111
C1 INTRODUCTION	111
C2 MECHANICAL MODEL	111
C3 CONTEMPORARY LOAD SCENARIO	112
C3.1 <i>Hydrostatic loads</i>	112
C3.2 <i>Dynamic wave Loads</i>	113
C3.3 <i>Self-weight</i>	116
C3.4 <i>Load combinations</i>	116
C4 EXTREME LOAD SCENARIO	117
APPENDIX D: CONCRETE & STEEL DESIGN	118
D1 INTERNAL ANGLE	118
D2 CONCRETE & STEEL DESIGN	120
D2.1 <i>Material properties</i>	120
D2.2 <i>Prestress losses</i>	124
D2.3 <i>Friction loss</i>	124
D2.4 <i>Creep</i>	125
D2.5 <i>Shrinkage</i>	125
D2.6 <i>Relaxation</i>	125
D2.7 <i>Elastic deformation</i>	126
D2.8 <i>Summary of all losses</i>	126
D2.9 <i>Bending moment capacity</i>	127
D2.10 <i>Shear reinforcement</i>	130
D2.11 <i>Final Results</i>	132
D2.12 <i>Reinforcement only</i>	133
APPENDIX E: STABILITY	134
E1 BUOYANCY	134
E2 ROTATIONAL STABILITY	136
E3 VERTICAL STABILITY	137
E4 HORIZONTAL STABILITY	138
E5 PIPING RESISTANCE	138
APPENDIX F: GATE TYPES	139
APPENDIX G: EARTHEN EMBANKMENT AND CONCRETE SEGMENT COMPARISONS	141
APPENDIX H: TIDAL RANGES	142

List of Figures

FIGURE 1.1 NEW YORK CITY (MAPTILER, N.D.).....	2
FIGURE 1.2 LONG ISLAND SOUND (MAPTILER, N.D.).....	3
FIGURE 1.3 BASIC CIVIL ENGINEERING DESIGN CYCLE.	5
FIGURE 2.1 HURRICANE SANDY’S TRAJECTORY (THE NEW YORK TIMES, 2012).	8
FIGURE 2.2 HURRICANE SANDY’S TRAJECTORY DAYS BEFORE LANDFALL (NATIONAL HURRICANE CENTER [NHC], 2013, p. 156).	9
FIGURE 2.3 WATER LEVELS AT KINGS POINT NY (CENTER FOR OPERATIONAL OCEANOGRAPHIC PRODUCTS AND SERVICES, N.D.).	10
FIGURE 2.4 WATER LEVELS AT THE BATTERY NY (CENTER FOR OPERATIONAL OCEANOGRAPHIC PRODUCTS AND SERVICES, N.D.).	10
FIGURE 2.5 MAXIMUM WIND GUST (KNOT) TAKEN FROM 24 M OR LESS (NATIONAL HURRICANE CENTER [NHC], 2013, p. 141).	11
FIGURE 2.6 MAXIMUM SUSTAINED WIND (KNOT) TAKEN FROM 24 M OR LESS (NATIONAL HURRICANE CENTER [NHC], 2013, p. 139)	11
FIGURE 2.7 HURRICANE SANDY RETURN PERIOD ESTIMATION (LOPEMAN, DEODATIS, & FRANCO, 2015, p. 379).....	12
FIGURE 2.8 THE DEVASTATION OF HURRICANE SANDY. TOP LEFT: SEA WATER FLOODING GROUND ZERO CONSTRUCTION SITE (MINCHILLO, 2012). TOP RIGHT: BURNED-OUT HOMES IN THE BREEZY POINT SECTION OF THE QUEENS BOROUGH (GROLL, 2012). BOTTOM LEFT: PEOPLE WADE AND PADDLE DOWN A FLOODED STREET AS HURRICANE SANDY APPROACHES (DECROW, 2012). BOTTOM RIGHT: NEW YORK SKYLINE AND HARBOR (LENNIHAN, 2012).....	13
FIGURE 2.9 FLOOD PRONE AREAS BASED ON ADCIRC MODELING (USACE ET AL., 2019, p. 71).	14
FIGURE 2.10 CATEGORY 4 HURRICANE INUNDATIONS (UNITED STATES DEPARTMENT OF COMMERCE [USDC]; NATIONAL OCEANIC AND ATMOSPHERIC ADMINISTRATION [NOAA]; NATIONAL OCEAN SERVICE [NOS], 2020).....	14
FIGURE 2.11 WEST SOUND REGION (MAPTILER, N.D.).....	15
FIGURE 2.12 WEST SOUND PRIORITY MAP.	16
FIGURE 2.13 PROPOSED FLOOD PROTECTION MEASURES BY THE USACE (USACE ET AL., 2019, p. 83).....	18
FIGURE 2.14 CONSIDERED LOCATIONS FOR THE THROGS NECK BARRIER (USACE ET AL., 2019B, p. 106).....	19
FIGURE 2.15 THROGS NECK BARRIER CONCEPT BY USACE (USACE ET AL., 2019B, p. 61).....	19
FIGURE 3.1 EXPECTED GLOBAL MEAN SEA LEVEL RISE FOR THE 21 ST CENTURY (USADC ET AL., 2017, p. 12).....	23
FIGURE 3.2 EXPECTED GMSLR SCENARIOS BASED ON GREENHOUSE EMISSIONS AND ICE LOSS (LINDSEY, 2020).	23
FIGURE 3.3 SURFICIAL SEDIMENT OF LONG ISLAND SOUND (POPPE, KNEBEL, MŁODZINSKA, HASTINGS, & SEEKINS, 2000).	25
FIGURE 4.1 AREA WHERE A BARRIER IS ASSUMED TO ALREADY BE PRESENT (MAPTILER, N.D.).....	27
FIGURE 4.2 PROPOSED BARRIER LOCATION FOR WEST SOUND (MAPTILER, N.D.).....	28
FIGURE 4.3 DAVENPORT PARK CONNECTION POINT (MAPTILER, N.D.).....	29
FIGURE 4.4 SANDS POINT CONNECTION POINT (MAPTILER, N.D.).....	29
FIGURE 4.5 ROCKY POINT CONNECTION POINT (GOOGLE EARTH).....	30
FIGURE 4.6 PEACOCK POINT CONNECTION POINT (GOOGLE EARTH).	30
FIGURE 4.7 BATHYMETRY BETWEEN DAVENPORT PARK – SANDS POINT (NOAA, N.D.).....	31
FIGURE 4.8 BATHYMETRY PEACOCK POINT – ROCKY POINT (NOAA, N.D.).....	31
FIGURE 4.9 SCHEMATIC OF THE PROTECTED COASTLINE LENGTH BY THE NEW BARRIER (MAPTILER, N.D.).....	33
FIGURE 5.1 THE SEGMENT BARRIER CONCEPT, CROSS-SECTION.....	35
FIGURE 5.2 THE SEGMENT BARRIER, SIDE VIEW.....	35
FIGURE 5.3 RISING TOWER BARRIER PART IN OPENED AND CLOSED POSITION.	37
FIGURE 5.4 ENTRANCHED FOUNDED RISING TOWER BARRIER IN CLOSED POSITION.	38
FIGURE 5.5 RISING TOWER BARRIER IN DEEP WATER WITH A CONCRETE SILL IN OPENED POSITION.	38
FIGURE 5.6 RISING WALL BARRIER PART IN FULLY RAISED POSITION.....	39
FIGURE 5.7 RISING WALL BARRIER PART IN CLOSED POSITION.....	39
FIGURE 5.8 SUBMERGED RISING WALL BARRIER PART.	40
FIGURE 5.9 RISING WALL BARRIER CUT-OUTS WITH PISTON PLACEMENTS.....	41
FIGURE 5.10 RISING WALL BARRIER WIRE FRAME VIEW.	41

FIGURE 5.11 HORIZONTAL SLIDING BARRIER.....	42
FIGURE 5.12 SUPPORT BARS (RED) THAT SLIDE IN THE FOUNDATION TO PROVIDE EXTRA SUPPORT.....	42
FIGURE 5.13 HORIZONTAL SLIDING BARRIER IN CLOSED POSITION (TOP VIEW).....	43
FIGURE 5.14 HORIZONTAL SLIDING BARRIER IN OPEN POSITION (TOP VIEW).....	43
FIGURE 5.15 PNEUMATIC FLAP GATE, ITALY (STANCATI & SYLVERS, 2019).....	44
FIGURE 5.16 MAESLANTKERING, THE NETHERLANDS (RIJKSWATERSTAAT, N.D.).....	45
FIGURE 5.17 EASTERN SCHELDT STORM SURGE BARRIER, THE NETHERLANDS (WATERSNOODMUSEUM, N.D.).....	46
FIGURE 6.1 A SEGMENT BARRIER SECTION DESIGNED TO WITHSTAND FORCES SIMILAR TO HURRICANE SANDY.....	54
FIGURE 6.2 BARRIER LAYOUT BETWEEN ROCKY POINT - PEACOCK POINT (TOP VIEW).....	54
FIGURE 6.3 BARRIER LAYOUT 1 (TOP VIEW).....	56
FIGURE 6.4 BARRIER LAYOUT 2 (TOP VIEW).....	56
FIGURE 6.5 BARRIER LAYOUT BETWEEN DAVENPORT PARK – SANDS POINT (TOP VIEW).....	57
FIGURE 6.6 BARRIER LAYOUT BETWEEN THROGS POINT – WILLETS POINT.....	57
FIGURE 6.7 SHORELINE CONNECTION OPTION 1.....	59
FIGURE 6.8 SHORELINE CONNECTION OPTION 2.....	59
FIGURE 6.9 SHORELINE CONNECTION OPTION 3.....	59
FIGURE 6.10 LONG AND HEAVY TRANSPORT EQUIPMENT INCLUDING A 70 M LONG WIND TURBINE BLADE (FAYMONVILLE, N.D.).....	60
FIGURE 6.11 SCHEMATIC REPRESENTATION OF THE SMALLEST SEGMENT CROSS-SECTION.....	61
FIGURE 6.12 MIDDLE SIZE SEGMENT OF THE BARRIER CROSS-SECTION CONSISTING OF 100 SEGMENTS.....	61
FIGURE 6.13 BARRIER CONSISTING OF 36 LARGE SEGMENTS.....	61
FIGURE 6.14 ASIAN HERCULES II VESSEL WITH A LIFT CAPACITY UP TO 3200 TONS (ROYAL BOSKALIS WESTMINSTER N.V., N.D.).....	62
FIGURE 6.15 ROLLER DECK FOR TRANSPORTING SEGMENT (AIRPORT TECHNOLOGY, 2016).....	62
FIGURE 6.16 PILE FOUNDATION (CROSS-SECTIONAL VIEW).....	63
FIGURE 6.17 PROFILED CONCRETE FLOOR (CROSS-SECTIONAL VIEW).....	63
FIGURE 6.18 DIRECT FOUNDATION ON THE SUBSOIL (CROSS-SECTIONAL VIEW).....	63
FIGURE 6.19 CROSS-SECTIONAL VIEW OF THE STACKING SEQUENCE FOR THE LARGE SIZE SEGMENTS.....	64
FIGURE 6.20 LONGITUDONAL VIEW OF THREE BARRIER PARTS (FRONT VIEW).....	64
FIGURE 6.21 CONSTRUCTION LOOP EXAMPLE FOR THREE LIFTING VESSELS.....	64
FIGURE 6.22 BASE LAYER OF SEGMENTS WITH NEOPRENE (RED) THAT PROVIDES WATERTIGHTNESS IN HORIZONTAL DIRECTION.....	65
FIGURE 6.23 TOP VIEW SCHEMATIC OF THE BARRIER IN STACK BOND PATTERN WITH A VERTICAL WATERTIGHT SOLUTION.....	65
FIGURE 6.24 STACK PATTERN SCALE REPRESENTATION (TOP VIEW).....	66
FIGURE 6.25 STACK PATTERN ON SCALE REPRESENTATION (PERSPECTIVE VIEW).....	66
FIGURE 6.26 TOP VIEW OF THE CORE ROW OF THE BRICK PATTERN CONFIGURATION WHICH IS WATERTIGHT.....	67
FIGURE 6.27 TOP VIEW OF THE BRICK PATTERN CONFIGURATION.....	67
FIGURE 6.28 BRICK PATTERN TOP VIEW ON SCALE REPRESENTATION.....	67
FIGURE 6.29 BRICK PATTERN PERSPECTIVE VIEW ON SCALE REPRESENTATION.....	68
FIGURE 6.30 GINA GASKET BEFORE CONTACT (GLERUM, VRIJLING, & BAKKER, 2018, P. 126).....	68
FIGURE 7.1 MECHANICAL MODEL OF THE BARRIER.....	71
FIGURE 7.2 LOAD COMBINATION ON THE STRUCTURE.....	71
FIGURE 7.3 CROSS-SECTION OF A SEGMENT’S TOP, BOTTOM OR DIAGONAL SIDE.....	72
FIGURE 7.4 ECCENTRICITIES OF THE FICTITIOUS TENDON (YELLOW) RELATIVE TO THE CENTROIDAL AXIS (RED).....	73
FIGURE 7.5 SHADED TENDON PLACEMENT AREA (PRESTRESSED CONCRETE, 2019, P. 4-39).....	73
FIGURE 7.6 FORCES IN THE CROSS-SECTION.....	74
FIGURE 7.7 FINAL RESULT OF THE CROSS-SECTION.....	74
FIGURE 7.8 PADEYE AND STEEL BAR USED FOR LIFTING OF A BARRIER SEGMENT.....	75
FIGURE 7.9 PADEYES AND STEEL BARS USED FOR LIFTING OF A BARRIER SEGMENT (WIREFRAME VIEW).....	75
FIGURE 7.10 A- AND V SEGMENT INSIDE CONNECTIONS (WIREFRAME VIEW).....	76
FIGURE 7.11 VERTICAL CHLOROPRENE WATERTIGHT SEAL FOR SEGMENTS AT THE CENTER OF THE BARRIER.....	76
FIGURE 7.12 REDIRECTING THE LOAD PATH AROUND A MAJOR DAMAGED AREA.....	81

FIGURE 8.1 CONCRETE PRODUCTION LOCATION (MAPTILER, N.D.).....	88
FIGURE 9.1 STEEL RODS FITTED THROUGH THE FRONT AND BACK COVER TO PROVIDE ADDITIONAL STRENGTH AND STABILITY.	93
FIGURE 9.2 ALTERNATE SEGMENT CONFIGURATIONS FOR FURTHER RESEARCH.	94
FIGURE A.1 TRAPEZIUM GEOMETRY DEFINITION.	100
FIGURE A.2 EXAMPLE OF UNIFORMLY SCALED TRAPEZIA WITH EVENLY THICK SIDES.	101
FIGURE A.3 LARGE SEGMENT CROSS-SECTION RELATING TO TABLE A.1.	102
FIGURE B.1 HURRICANE SANDY’S TRACK, INTENSITY AND NOAA NDBC BUOY LOCATIONS (UNITED STATES GEOLOGICAL SURVEY [USGS], 2014, P. 3).	103
FIGURE B.2 DEFINITION OF THE WAVE RUN-UP HEIGHT $R_{U2\%}$ ON A SMOOTH IMPERMEABLE SLOPE (EUROTOP, 2007, P. 69)	104
FIGURE B.3 SEASIDE SLOPE SEGMENTS UNDER STEEP AND GENTLE ANGLES.....	107
FIGURE B.4 DIAGRAM FOR ESTIMATING THE FETCH LENGTH (GOOGLE MAPS).	108
FIGURE C.1 BASIC MECHANICAL MODEL WITH HYDROSTATIC LOADS (RED) AND SELF-WEIGHT (BLUE).....	111
FIGURE C.2 AXIAL FORCES WITHIN THE STRUCTURE.	111
FIGURE C.3 MECHANICAL MODEL OF THE STRUCTURE.	112
FIGURE C.4 HYDROSTATIC LOADS ON THE STRUCTURE.	112
FIGURE C.5 GODA’S WAVE PRESSURE MODEL (TU DELFT, 2016, P. 111).	113
FIGURE C.6 DYNAMIC WAVE LOADS ON THE STRUCTURE.	115
FIGURE C.7 SELFWEIGHT OF THE STRUCTURE.....	116
FIGURE C.8 LOAD COMBINATION ON THE STRUCTURE.....	117
FIGURE D.1 MECHANICAL SCHEME FOR THE BASE SEGMENT GEOMETRY.....	118
FIGURE D.2 INTERNAL MOMENT OF ONE SEGMENT UNDER VARIOUS ANGLES.....	119
FIGURE D.3 CROSS-SECTION OF A SEGMENT’S SIDE (TOP, BOTTOM OR DIAGONAL).....	120
FIGURE D.4 ECCENTRICITIES OF THE FICTITIOUS TENDON (YELLOW) RELATIVE TO THE CENTROIDAL AXIS (RED).....	121
FIGURE D.5 SHADED AREA IN WHICH THE TENDONS CAN BE PLACED IN ACTUALITY (PRESTRESSED CONCRETE, 2019, PP. 4-39).....	121
FIGURE D.6 MECHANICAL SCHEME OF THE BENDING MOMENT CONTRIBUTION BY THE PRESTRESSED TENDON.	122
FIGURE D.7 CONCRETE CROSS-SECTION AND STRAIN DISTRIBUTION DIAGRAM.	128
FIGURE D.8 FORCES IN THE CROSS-SECTION.	129
FIGURE D.9 SHEAR REINFORCEMENT SCHEMATIC (PRESTRESSED CONCRETE, 2019, P. 8-9).....	131
FIGURE D.10 FINAL RESULT OF THE CONCRETE AND STEEL PRESTRESSED DESIGN.....	132
FIGURE D.11 FORCES IN THE CROSS-SECTION.....	133
FIGURE E.1 DEFENITION OF THE SUBMERGED DISTANCE.....	134
FIGURE E.2 POSSIBLE FLOATING ORIENTATION OF A TRAPEZIUM.....	135
FIGURE E.3 SEGMENT WITH FRONT AND BACK COVER WIDTH FOR A V-SEGMENT (SIDE VIEW).....	135
FIGURE E.4 SCHEMATIC REPRESENTATION OF THE FORCES ON THE STRUCTURE.....	136
FIGURE G.1 EARTHEN DYKE FAILURE MECHANISMS (TU DELFT, FLOOD DEFENCES LECTURE NOTES CIE5314, 2017, P. 20).	141

List of Tables

TABLE 1.1 CHAPTERS, DESIGN CYCLES AND DESIGN PROCESS STEPS RELATION.....	6
TABLE 2.1 WIND SPEED MEASUREMENTS AT KINGS POINT (NATIONAL HURRICANE CENTER [NHC], 2013, p. 56).....	11
TABLE 2.2 MINIMUM NAVIGATION CHANNEL DIMENSIONS (USACE ET AL., 2019, p. 141).	20
TABLE 3.1 TIDAL DATUMS USED FOR WEST SOUND (CO-OPS, 2018).....	22
TABLE 3.2 TIDAL FLOWS (USACE ET AL., 2019B, PP. 27-28).....	24
TABLE 3.3 WATER LEVEL HEAD DIFFERENCE (USACE ET AL., 2019B, P. 33).	24
TABLE 3.4 VESSEL DIMENSIONS (USACE ET AL., 2019B, P. 35).	24
TABLE 4.1 WESTCHESTER COUNTY POPULATION AND HOUSING (UNITED STATES CENSUS BUREAU, N.D.), (POINT2, N.D.).	32
TABLE 4.2 NASSAU COUNTY POPULATION AND HOUSING (UNITED STATES CENSUS BUREAU, N.D.), (POINT2, N.D.).	32
TABLE 5.1 MCA WEIGHT FACTORS.....	49
TABLE 5.2 PRIORITY LIST FOR THE EVALUATION CRITERIA.	50
TABLE 5.3 MCA SCORES.	50
TABLE 6.1 ASSEMBLING TIME FOR DIFFERENT LOCATIONS.	58
TABLE 7.1 NUMBER OF REQUIRED SEGMENTS FOR VARIOUS SLR SCENARIOS AND SLOPES.....	70
TABLE 7.2 INTERNAL FORCES OF THE STRUCTURE FOR CONTEMPORARY AND EXTREME GMSLR SCENARIOS.	71
TABLE 7.3 MATERIAL PROPERTIES OF ONE SEGMENT.....	72
TABLE 7.4 ESTIMATED CONSTRUCTION COST AND DURATION FOR THE STORM SURGE BARRIERS (NEW YORK-NEW JERSEY [NYNJ] INTERIM REPORT COST APPENDIX, 2019, P. 6)	77
TABLE 7.5 ROCKY POINT – PEACOCK POINT BARRIER COST ASSUMING THE EXISTING OR SEGMENT GATES.	77
TABLE 7.6 MATERIAL COST ESTIMATION PER SEGMENT.....	78
TABLE 7.7 SEGMENT MATERIAL COST ESTIMATION PER BARRIER PART EQUAL TO 50 M.	78
TABLE 7.8 SEGMENT MATERIAL COST ESTIMATION PER SECTION OF THE ENTIRE BARRIER.	78
TABLE 7.9 THROGS POINT – WILETS POINT BARRIER COST ASSUMING THE EXISTING OR SEGMENT GATES.....	79
TABLE 8.1 EVALUATION MATRIX.....	87
TABLE A.1 DIMENSIONS OF THE CROSS-SECTION FOR THE FINAL CONCEPT. INPUT VALUES COLORED RED.....	102
TABLE B.1 ULS AND SLS REQUIREMENTS FOR OVERTOPPING (TU DELFT, 2016, P. 104).....	104
TABLE B.2 TOTAL BARRIER HEIGHTS ACCOUNTING FOR DIFFERENT SEA LEVEL RISE SCENARIOS AND OUTER SLOPES.....	109
TABLE B.3 INTENSIFIED WAVE DEVELOPMENT FOR THE DETERMINATION OF THE BARRIER HEIGHTS ACCOUNTING FOR DIFFERENT SEA LEVEL RISE SCENARIOS AND OUTER SLOPES.	109
TABLE B.4 NUMBER OF REQUIRED SEGMENTS FOR DIFFERENT SLOPES.....	110
TABLE C.1 INTERNAL FORCES ON THE STRUCTURE FOR CONTEMPORARY AND EXTREME GMSLR SCENARIOS.....	117
TABLE D.1 MATERIAL PROPERTIES.	120
TABLE E.1 FORCES ON THE STRUCTURE.	136
TABLE H.1 TIDAL RANGES (CO-OPS, 2018).....	142

List of Acronyms

AEP	Annual Exceedance Probability
CO-OPS	Center for Operational Oceanographic Products and Services
CSRM	Coastal Risk Management
FPM	Flood Protection Measures
FR	Functional Requirement
GR	Gate Requirements
GMSLR	Global Mean Sea Level Rise
GDP	Gross domestic product
HAT	Highest Astronomical Tide
LAT	Lowest Astronomical Tide 1-21-1996
MHW	Mean High Water
MHHW	Mean Higher High Water
MHHW	Mean Higher-High Water
MLW	Mean Low Water
MLLW	Mean Lower-Low Water
MSL	Mean Sea Level
MN	Mean Tidal Range
MCA	Multiple-Criteria Decision Analysis
NDBC	National Data Buoy Center
NHC	National Hurricane Center
NOS	National Ocean Service
NOAA	National Oceanic and Atmospheric Administration
NYC	New York City
NYS	New York State
NAVD88	North American Vertical Datum of 1988
NTS	Not to Scale
HATS	NY & NJ Harbor & Tributaries Focus Area Feasibility Study
PPT	Parts Per Thousand
USACE	United States Army Corps of Engineers
USDC	United States Department of Commerce
USEPA	United States Environmental Protection Agency
USA, U.S.	United States of America

CHAPTER 1

Introduction

Contents

CHAPTER 1 INTRODUCTION	1
CHAPTER 1 ABSTRACT	1
1.1 MOTIVATION AND RELEVANCY	2
1.2 INITIAL EXPLORATION OF THE MAIN THREATS.....	3
1.3 DESIGN OBJECTIVE.....	4
1.4 METHODOLOGY.....	5
1.5 REPORT STRUCTURE	6

Chapter 1 Abstract

This chapter introduces the reader to the tidal strait of Long Island Sound, USA, and explains why this location is relevant for the protection of the metropolitan city of New York. After an initial exploration of the main threats, the main design objective is presented which is the conceptual design of a new type of storm surge barrier for which Long Island Sound serves as a case study area. Finally, the chapter closes with an explanation on the design methodology that was part of this thesis and how it relates to each chapter of the report.

1.1 Motivation and relevancy

The largest metropolitan city of The United States of America (USA): New York City (NYC), shown in Figure 1.1, with a population of almost 19 million and gross domestic product (GDP) over \$1.5 trillion (2018), is one of the most valuable regions on the globe. As the climate crisis intensifies, this city is increasingly at risk of rising sea levels and fiercer storm surges. Solutions to these threats are needed with urgency.

The U.S. Army Corps of Engineers (USACE) carries the main responsibility for protecting the nation's coastal areas against natural disasters through the development of civil infrastructure. In accordance with their mission statement, several researches have been conducted into the North Atlantic coastal area to provide scientific data for coastal planning purposes.

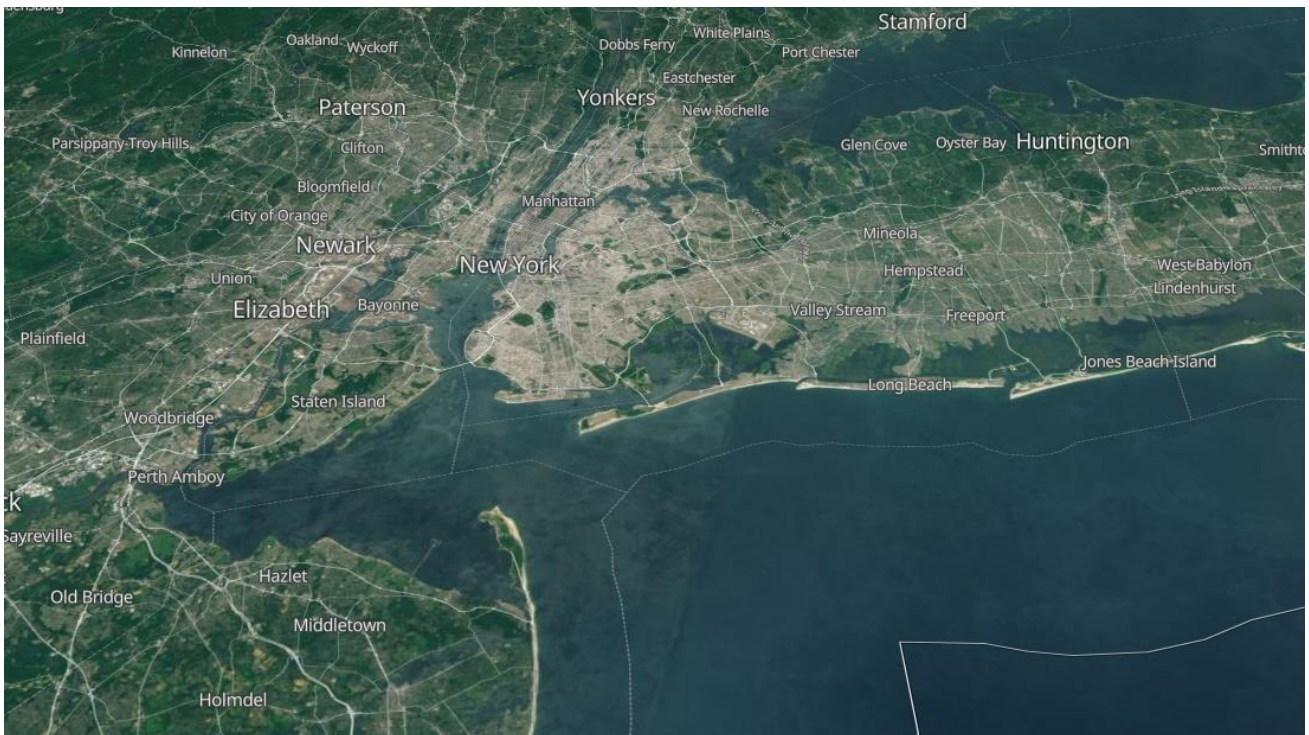


Figure 1.1 | New York City (MapTiler, n.d.).

The coastal areas of New York and New Jersey have always endured severe storms and hurricanes with one of the most damaging in recent years being Hurricane Sandy in 2012. The U.S. government is examining the possibilities to reduce the impact of these storms by developing a system of storm surge barriers and coastal flood protection measures. As of this writing, the interim research results have been published and serve as an important source of information for this thesis (NY & NJ Harbor & Tributaries Focus Area Feasibility Study (HATS), 2019) in which a conceptual design for a storm surge barrier is developed.

1.2 Initial exploration of the main threats

The issues threatening the entire coastal region of New York state can be subdivided into multiple categories. This section discusses a number of issues and challenges that need to be addressed in order to mitigate the consequences and cyclic threat of flooding in this region.

The fundamental issue and threat for the state of New York – in particular the city – is the development of storm surges due to the yearly hurricane seasons.

These storm surges waves have a direct and severe impact on people’s lives. Tangible are the inundations, damaged property, power outages and destroyed infrastructure (U.S. Energy Information Administration, 2012). Followed by the short or long term psychological and mental challenges faced by those who have experienced the effects of severe flooding (Schwartz et. al., 2015, pp. 363-369).

Then there is the problem of sea level rise which can exacerbate the developments of storm surges. Moreover, sea lever rise will permanently inundate the majority of New York City in the long run without any protective measures. This is a more indirect issue that cannot be solved by one party alone. Instead, it requires a global effort from all nations of the world to act by reducing greenhouse gas emissions proportionately, and with urgency. Further complicating the matter is the complex geography, including the multitude of rivers that stream into the area. Long Island Sound is essentially a tidal straight, meaning the water body connects to the ocean on both outer ends. Therefore, a storm surge could migrate towards the city from two directions as shown in Figure 1.2.

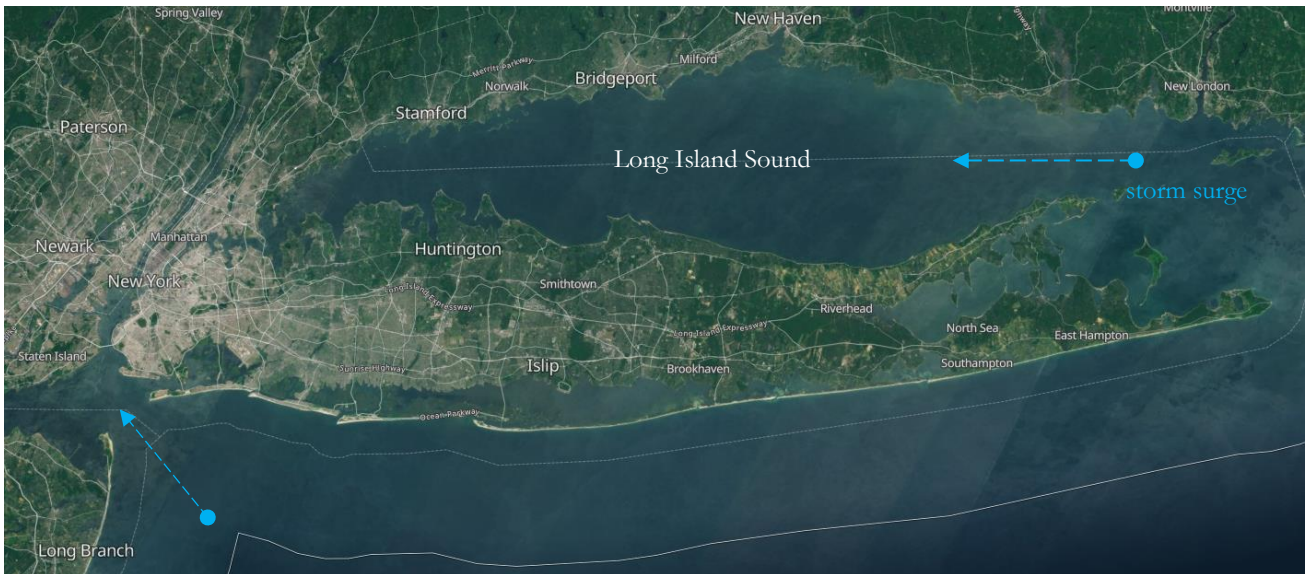


Figure 1.2 | Long Island Sound (MapTiler, n.d.).

Furthermore, the coastlines along Long Island Sound within the state of New York are extremely irregular and densely populated which further complicates the application of flood protection measures. The reader is referred to chapter 4 for a detailed location analysis.

Finally, existing studies such as the NY & NJ Harbor & Tributaries Focus Area Feasibility Study (HATS) (USACE, n.d.) focus on flood protection measures for this area that are based on conventional types of storm surge barriers (Appendix F). The development of innovative and new types of barriers as a solution are comparatively less prioritized.

1.3 Design objective

The main objective of this thesis is to develop a conceptual design for a new type of storm surge barrier and study its applicability at Long Island Sound with the purpose of protecting New York City and the coastlines of Long Island Sound within the state border from storm surges that migrate from the east side of Long Island Sound towards the city (Figure 1.2).

Closing off parts of a waterway with structures such as dams or storm surge barriers can have serious environmental consequences. It is possible that the entire tidal straight of Long Island Sound needs to be closed off and ends up becoming a reservoir to combat sea level rise. With storm surge barriers it is possible to influence an estuarine system to some extent, however its presence alone will have a disturbing effect on the environment. In general, dams and storm surge barriers are known to impact the environment as follows (Elgershuizen, 1981):

- Sediment can be (partially) held back, which carries minerals for many aquatic species needed to sustain the ecosystem. Its distribution over an estuarine is also dependent on the flow patterns and speed.
- Biodiversity can be significantly reduced.
- Certain parts can erode or accrete due to insufficient sediment input.
- Changes in flow velocity, circulation patterns and benthic animals will all have an effect on the suspension rate of sediment.
- Depending on the degree and duration of closure, storm surge barriers can reduce the tidal area, mean tidal amplitude and tidal phase. A tidal wave phase difference might also disturb the exchange of salinity between the ocean (35 ppt) and the Western end of Long Island Sound (23 ppt) (Long Island Sound Study, n.d.), which could be undesirable for certain plants or animals.

Therefore, the goal is to design a barrier that is reconstructable and can function as a temporary structure to avoid long term environmental and ecological impact. In order to achieve this, the concept is centered around two aspirations:

- *Simplification*
There are many different types of storm surge barriers built around the world (Appendix F) which are complex structures and usually tailor-made for a specific location. The new barrier should be designed in such a way that its components can be assembled before the advent of a storm surge and dismantled afterwards in a relatively simple manner.
- *Modularity*
The new barrier should be able to deal with the uncertainties of sea level rise by increasing in size.

In this thesis, the main focus lies on the conceptual and structural design of the barrier.

1.4 Methodology

The engineering design process – adjusted for civil engineering – which stems from the learnings of professor Norbert Roozenburg and professor Johannes Eekels, serves as a guiding methodology for this thesis. The design process is iterative, meaning assumptions and decisions are frequently subject to change or reconsidered based on new information. Figure 1.3 shows the theoretical basis of this method and the chapters of this thesis corresponding to different steps.

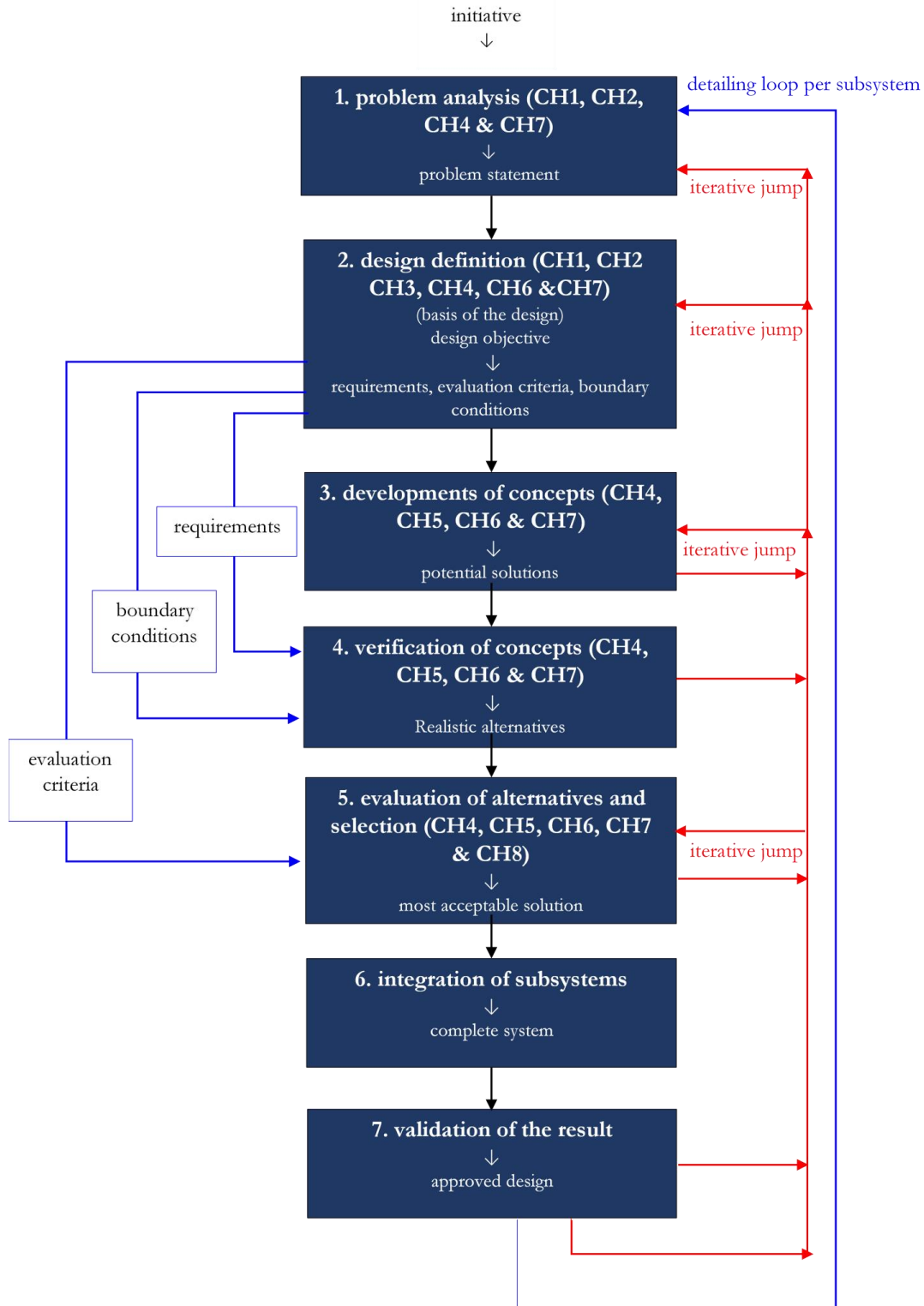


Figure 1.3 | Basic civil engineering design cycle.

The problem analysis (step 1) and design definition (step 2) involve literature study with different objectives. Initially, the focus is on gathering relevant information on the region (chapter 2) and environmental boundary conditions (chapter 3) that provides a basis from which a technical design can be made (chapter 6 and 7). Then there is literature on the impact of flooding, which helps the reader understand the severity of the situation (chapter 2). Although literature has an important role in the early stages of the process, it remains relevant throughout all chapters. The design cycles were applied revolved around location selection, development of concepts and structural design with many iterative jumps between step 1 and 5. The development of concepts involves many hand drawings and sketches which starts by keeping the structure’s fundamental purpose in mind – stopping storm surges – and then focusing on the geometric design. Once the basic geometry is established, a refinement process begins which involved fitting the structure into the environment and reducing the complexity of the design where possible. All conceptual designs are verified (step 4) and compared (step 5) using the multiple-criteria decision analysis (MCA) method which takes into account non-monetary decision criteria (Beheshti, 1999, p. 194). However, it should be mentioned that this process has its limitations and does not directly lead to an optimal solution. The MCA is a tool used in service of achieving the design objectives.

1.5 Report structure

The reader is guided through the development of a conceptual design for a storm surge barrier. Table 1.1 summarizes how each chapter relates to a particular design cycle and which basic steps of the civil engineering design process (Figure 1.3) are part of the chapter. It is noted that the general evaluation (chapter 8) and thesis conclusions and recommendations (chapter 9) are not part of any design cycle.

	design cycle			basic civil engineering design steps						
	location analysis	conceptual design	structural design	1	2	3	4	5	6	7
Chapter 1 introduction										
Chapter 2 System Analysis										
Chapter 3 Requirements and Boundary Conditions										
Chapter 4 Location Selection										
Chapter 5 Development and Analysis of Concepts										
Chapter 6 Barrier Configuration Design										
Chapter 7 Structural Design										
Chapter 8 Evaluation										
Chapter 9 Conclusions and Recommendations										

Table 1.1 | Chapters, design cycles and design process steps relation.

CHAPTER 2

System Analysis

Contents

CHAPTER 2 SYSTEM ANALYSIS	7
CHAPTER 2 ABSTRACT	7
2.1 THE IMPACT OF HURRICANE SANDY	8
2.1.1 <i>Storm development and trajectory</i>	8
2.1.2 <i>Damage to New York coastal region</i>	12
2.2 LONG ISLAND SOUND	14
2.2.1 <i>Flood prone areas</i>	14
2.2.2 <i>Long Island Sound ecosystem</i>	15
2.2.3 <i>West Sound priority map</i>	16
2.3 STAKEHOLDER ANALYSIS	17
2.4 NYNJHAT CONCEPTUAL BARRIER DESIGN	18
2.4.1 <i>Barrier features</i>	18
2.4.2 <i>Barrier location</i>	19
2.4.3 <i>Geometric design</i>	19
2.4.4 <i>Gate type selection</i>	20
2.4.5 <i>Discussion</i>	20

Chapter 2 Abstract

Long Island Sound serves as a case study for the new conceptual design; therefore, a system analysis of the area is provided in this chapter. The development and impact of seasonal storms are discussed as well as the local environment and stakeholder views. The final part of this chapter includes an analysis on the storm surge barrier type that was chosen by the USACE for reference purpose. Descriptions on many other types of barriers are provided in Appendix F.

2.1 The impact of Hurricane Sandy

2.1.1 Storm development and trajectory

Tropical cyclones begin their formation above the Atlantic Ocean near the equator where warm waters (26 degrees Celsius) are present and uninterrupted winds travelling skyward dominate. As these storms gain strength, their classification changes from a tropical disturbance – rain clouded area over warm water – to tropical depressions, tropical storms and eventually a hurricane with winds speeds reaching 119 km/h or higher. A hurricane consists of three areas: the calmer eye, eye wall – most violent winds and rainfalls –, and rain bands containing thunderstorms and tornados (May, 2017).

On October 29, 2012 Hurricane Sandy arrived at the New York-New Jersey coastal region leading to massive disruptions, property damage and fatalities. As of this writing, it has been the most damaging hurricane in the history of the New York City. This section details what made this storm such a significant event and why it serves as a case study for the conceptual design of a storm surge barrier. It was the combination of the storm's trajectory, severity and high tides which had a devastating effect on the area. Figure 2.1a shows the storm's trajectory from its formation in the Caribbean Sea towards the east coast of the United States where it ultimately hit land at Atlantic City, New Jersey (USACE et al., 2019, pp. 5-6).

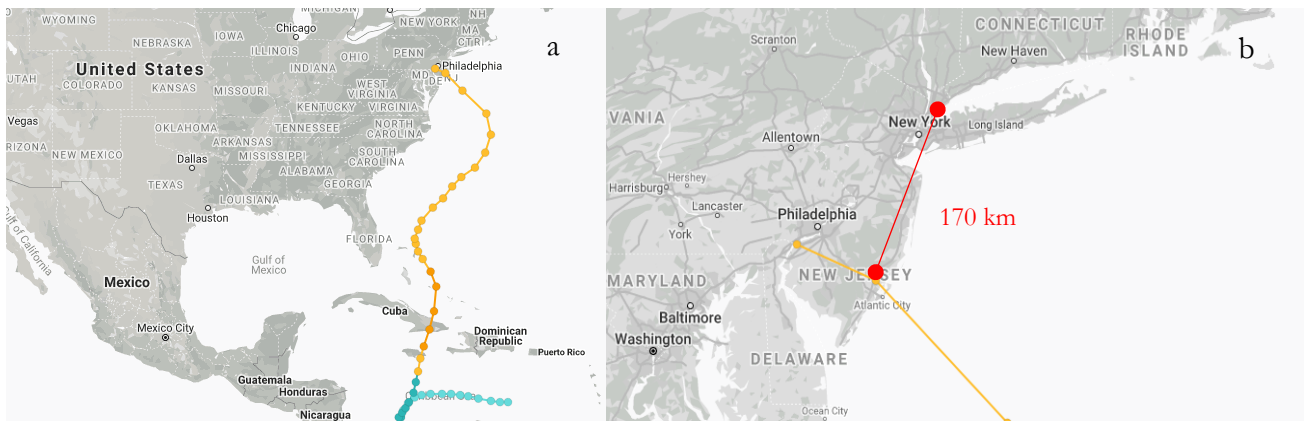


Figure 2.1 | Hurricane Sandy's trajectory (The New York Times, 2012).

The distance from the storm's epicenter at the location where it first hit land (Atlantic City) to New York City is approximately 170 km as shown in Figure 2.1b.

The initial recording of Hurricane Sandy's formation was on October 22, 2012 in the Caribbean and intensified over Cuba, the Bahamas and Jamaica until it reached the east coast of the United States on October 29, 2012. Predictions of its trajectory led to the following output shown in Figure 2.2 (National Hurricane Center [NHC], 2013). The white dotted line is Hurricane Sandy's actual trajectory and the colored dotted lines are different model predictions days before landfall.

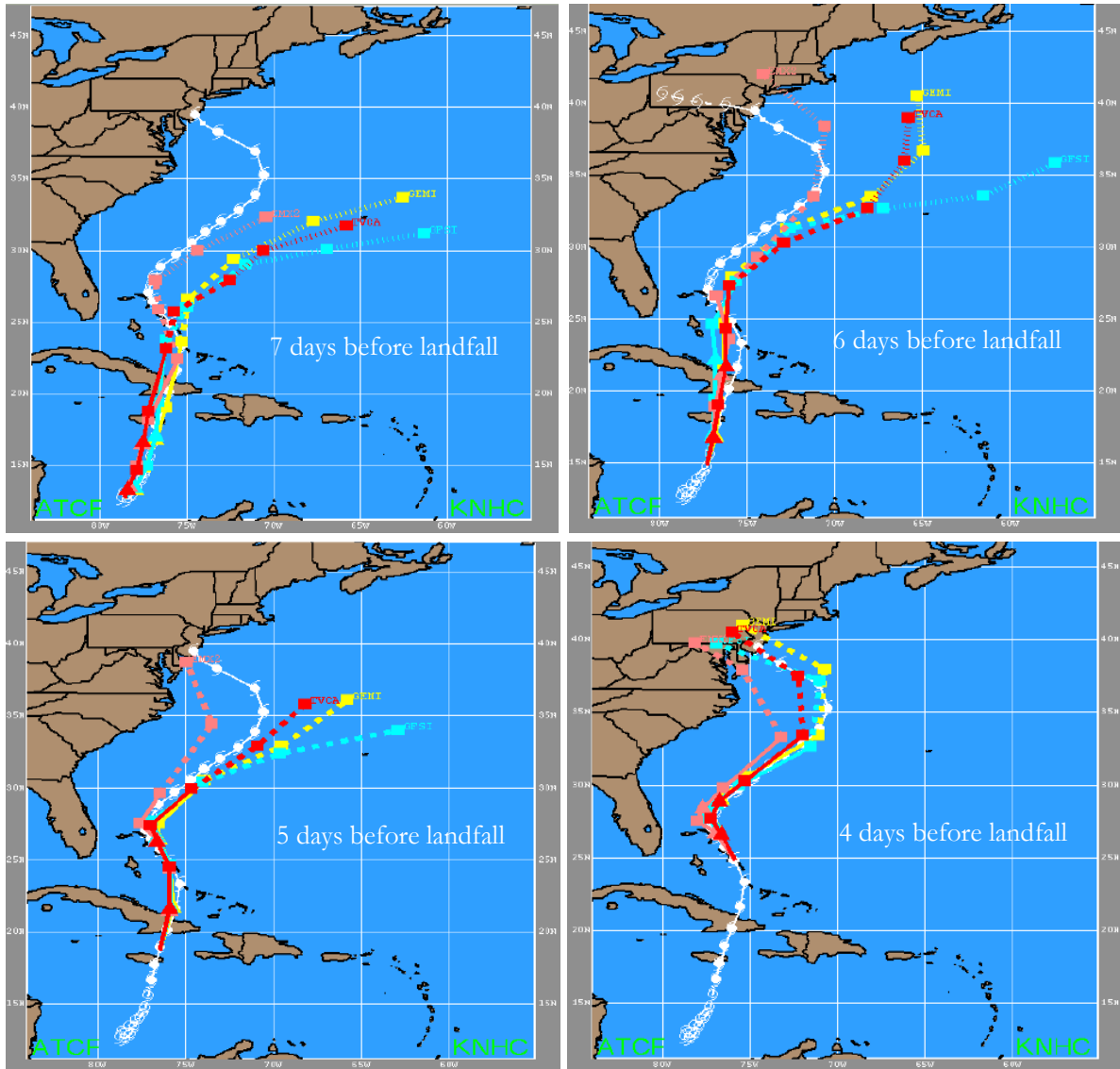


Figure 2.2 | Hurricane Sandy's trajectory days before landfall (National Hurricane Center [NHC], 2013, p. 156).

It was possible to predict the formation of Hurricane Sandy seven days in advance and with increased accuracy in the following days. Figure 2.2 shows there were seven days before Hurricane Sandy's arrival from the moment it was being generated at sea. It takes one or two days to determine with sufficient accuracy if the storm's trajectory coincides with a specific area of interest.

In the western part of Long Island Sound – where a storm surge passes through before reaching New York City – at Kings Point, the highest recorded storm surge¹ was 3.86 m above Mean Lower-Low Water (MLLW). Figure 2.3 shows that the verified observed water levels deviated substantially from the predicted values. The highest recorded water levels were 4.63 m above MLLW while the predicted water levels at the same time were 1.76 m. The inundation levels caused by Hurricane Sandy in The Bronx – adjacent to Long Island Sound – were measured between 0.61 and 1.2 m (NHC, 2013, p. 8).

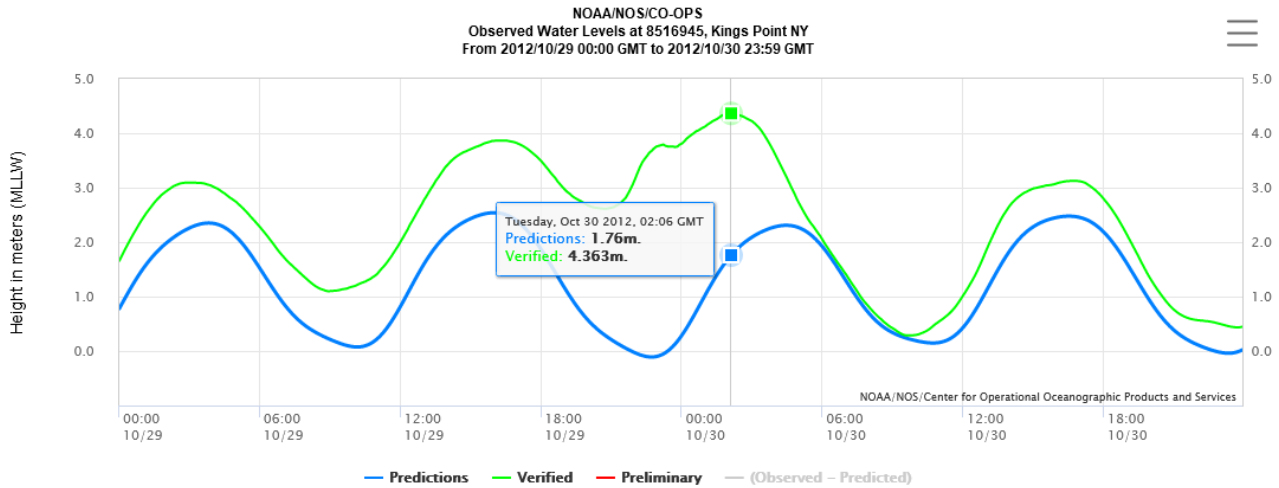


Figure 2.3 | Water levels at Kings Point NY (Center for Operational Oceanographic Products and Services, n.d.).

High water levels first arrived at The Battery as shown in Figure 2.4 with a maximum value of 4.28 m (MLLW) on 01:24 GMT. The highest recorded water level at Kings Point was recorded at 02:06 GMT showing the storm surge propagated along the East River into Long Island Sound.

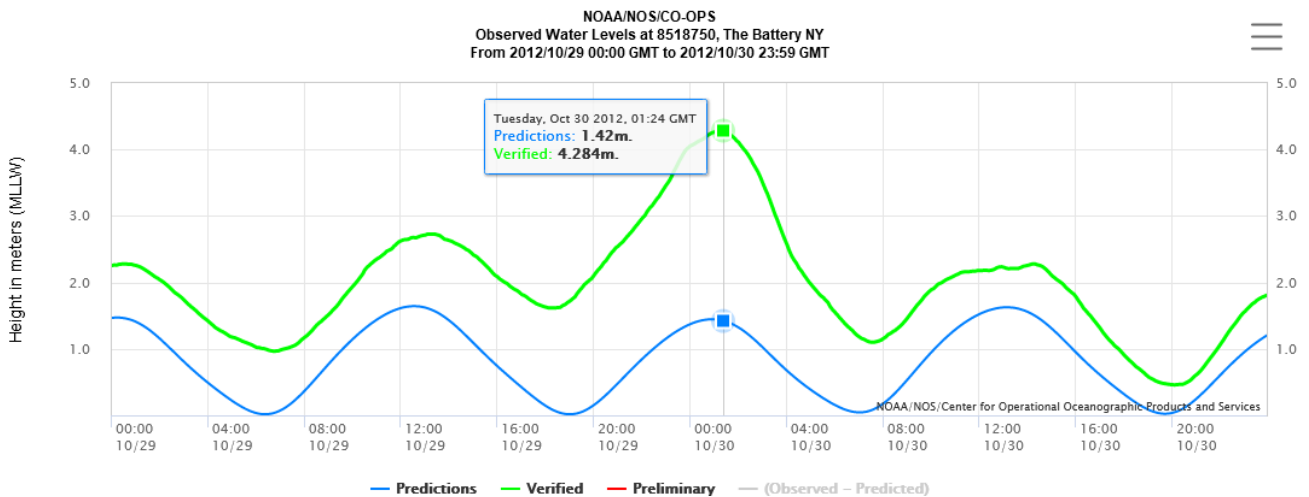


Figure 2.4 | Water levels at The Battery NY (Center for Operational Oceanographic Products and Services, n.d.).

¹ A **storm surge** is defined as the rise of water above the predicted astronomical tide and expressed in terms of height above normal tide levels and *not* referenced to a vertical datum (e.g., NAVD88). **Storm tide** is the combination of a storm surge and astronomical tide and expressed as height above vertical datum. **Inundation** is the water level above normally dry ground due to storm tides. Normally dry ground is usually defined from a Mean Higher High Water (MHHW) reference point (National Hurricane Center [NHC], 2013, p. 9).

Table 2.1 summarizes the observed wind speeds during the hurricane at King’s Point.

Kings Point NOS (KPTN6) 40.81N 73.77W Height: 10.0 m	minimum sea level pressure		maximum surface wind speed		
	Date/time (UTC)	Press. (mb)	Date/time (UTC)	Sustained (km/h)	Gust (km/h)
	29/2200	965.7	29/2106	46	76

Table 2.1 | Wind speed measurements at Kings Point (National Hurricane Center [NHC], 2013, p. 56).

To get a better overview of the wind speeds during the storm, Figure 2.5-6 show the recorded windspeeds for the east coast of the United States and parts of Canada. Measurements show a maximum sustained wind speed of 56 knot (104 km/h) and a maximum gust of approximately 75 knots (139 km/h) in the western part of Long Island Sound.

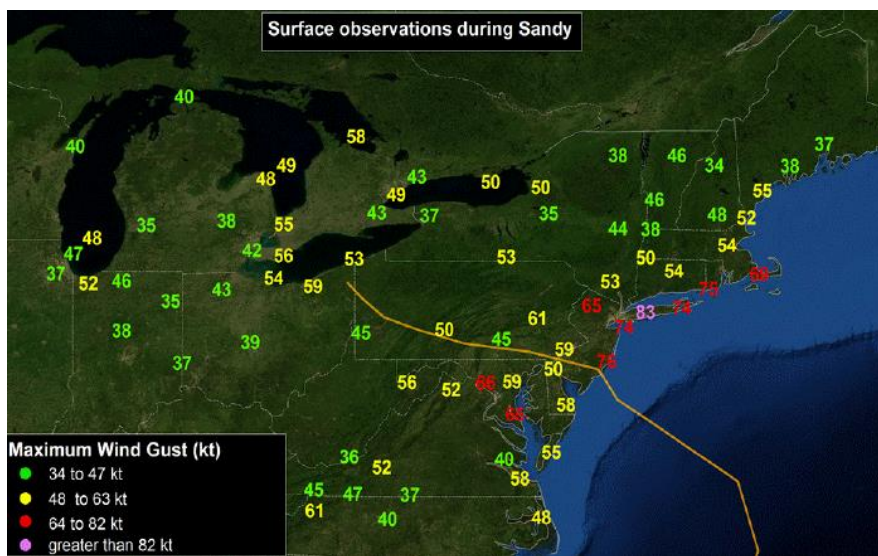


Figure 2.5 | Maximum wind gust (knot) taken from 24 m or less (National Hurricane Center [NHC], 2013, p. 141).

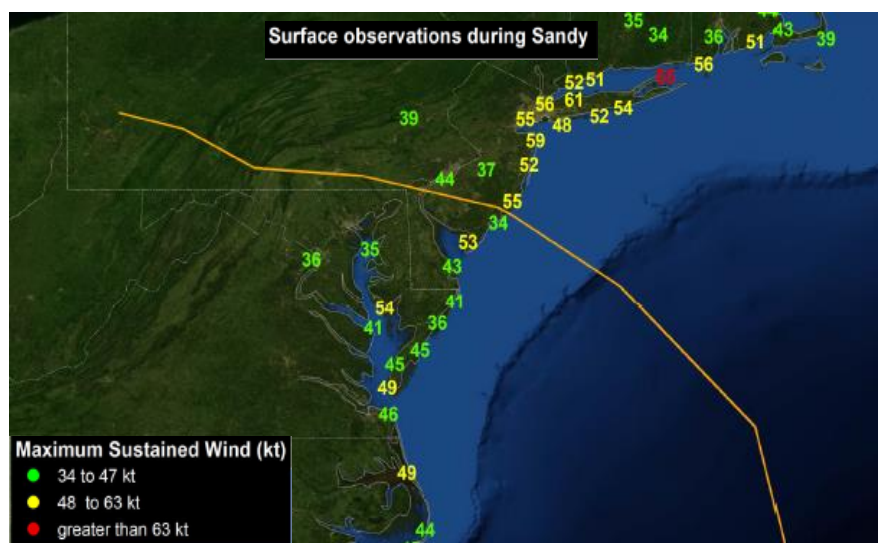


Figure 2.6 | Maximum sustained wind (knot) taken from 24 m or less (National Hurricane Center [NHC], 2013, p. 139)

What made Hurricane Sandy so powerful was its extratropical transition that combined it with a winter storm. This resulted in a hybrid storm with water levels 2.75 m above the expected tidal cycle mean high water (MHW) at The Battery, equal to 5.27 m above station datum² (STND) which corresponded to a return period of 1/500-years (Aerts et al., 2013, pp. 11-12). It should be noted that research on hybrid storms is currently limited, however, another study by (Lopeman, Deodatis, & Franco, 2015) suggests that these severe storms are becoming more frequent with a higher probability of occurrence as shown in Figure 2.7.

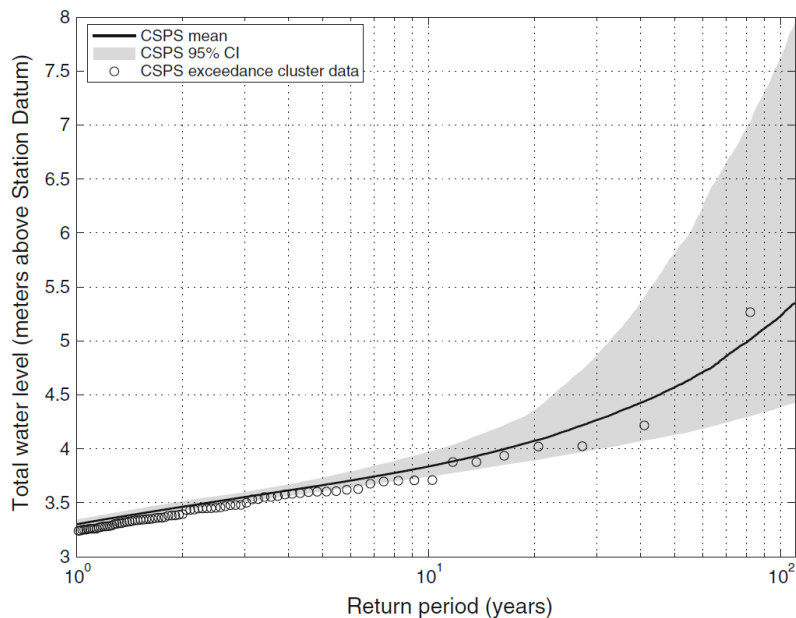


Figure 2.7 | Hurricane Sandy return period estimation (Lopeman, Deodatis, & Franco, 2015, p. 379).

Their simulation resulted in a 1/103-year return period for Hurricane Sandy’s peak water level (5.27 m) and a 1/100-year return period of 5.23 m at tidal gauge station 8518750, The battery, New York.

2.1.2 Damage to New York coastal region

Hurricane Sandy serves as a reference storm for this thesis. As of this writing, it has been the only real event of such magnitude and devastation in the region. According to the data shown in Figure 2.7 such storms could become more common and severe in the future. Moreover, if the new barrier is designed with a service life of 100 years (5.23 m STND, peak water level), it is very likely that a storm with the magnitude of Hurricane Sandy will occur at least once in its lifetime. Further research into the probability of occurrence of severe storms is outside the scope of this thesis.

There are millions of people at risk of flooding in New York City alone. The low-lying areas are densely populated and primarily inhabited by low-income households and elderly that are in need of governmental support for public housing. Most residents do not have direct access to vehicular transportation. Many New Yorkers also have a different native language other than English. This could prove to be a challenge in times of flood disasters when clear and fast communication can save lives (USACE et al., 2019, p. 9).

The damage of Hurricane Sandy has been substantial with 48 deaths in New York City. Streets and houses have been inundated and infrastructure (e.g., tunnels, highways, railway stations) were either heavily

² The NOAA tidal gauges have fixed elevation called **Station Datum (STND)**. To convert measurements referenced from STND to NAVD88 at The Battery, subtract by 1.85 m.

disrupted or rendered unusable such as the subway station South Ferry/Whitehall Street in lower Manhattan. The infrastructure and state agencies which are critical in times of disaster such as, police, fire fighters and hospitals were experiencing difficulties. Schools and businesses had to stay closed and power outages and gas shortages were a reality. The New York City Metropolitan Transit Authority concluded the subway system never had sustained this much damage in its entire history with the total cost for New York City estimated at \$19 billion which included all private, public and indirect costs of which an estimated \$4.5 billion alone was damage to Housing Administration and the Health and Hospitals corporation. Eight tunnels were inundated costing \$5 billion. The remaining transportation infrastructure had \$2.5 billion worth of damage (National Hurricane Center [NHC], 2013, p. 18). As of this writing, many areas are still recovering from the damages while every hurricane season brings its own new set of damages to the area. In response, \$50 billion has been allocated by the government to, “reduce future flood risk in ways that will support the long-term resilience of vulnerable coastal communities” (USACE et al., 2019, p. 9). The photographs presented in Figure 2.8 show only a fraction of the devastation caused by Hurricane Sandy.

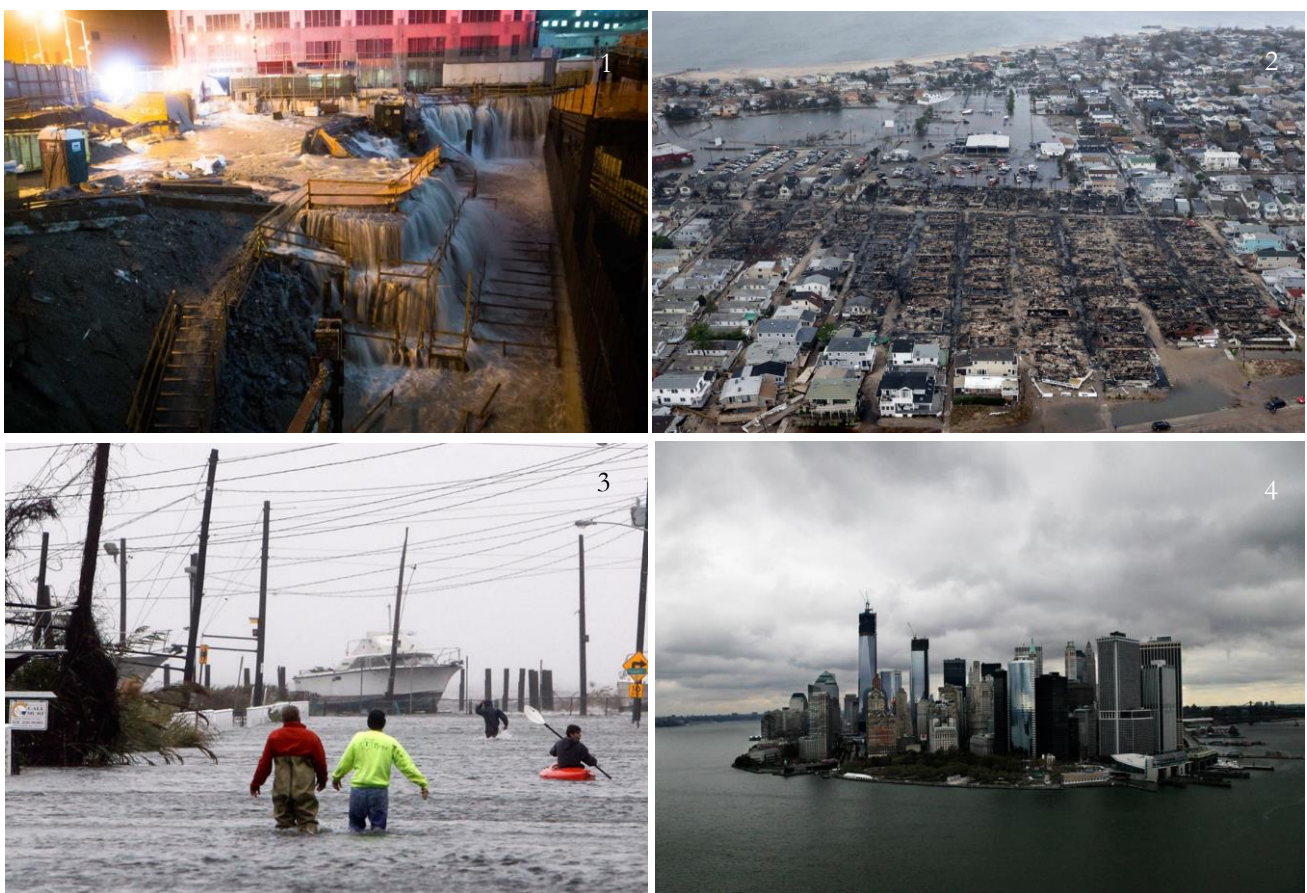


Figure 2.8 | The devastation of Hurricane Sandy. Top left: Sea water flooding Ground Zero construction site (Minchillo, 2012). Top right: Burned-out homes in the Breezy Point section of the Queens borough (Groll, 2012). Bottom left: People wade and paddle down a flooded street as Hurricane Sandy approaches (DeCrow, 2012). Bottom right: New York skyline and harbor (Lennihan, 2012).

This thesis focuses storm surges with a similar wave climate as that of Hurricane Sandy, however, due to the expected increase in severity and frequency of seasonal storms, the aim is to develop a barrier which is able to deal with higher storm surges by expanding the barrier’s size overtime if necessary.

2.2 Long Island Sound

2.2.1 Flood prone areas

Figure 2.9 shows the flood prone areas for the entire New York coastal region with high and low probability of occurrence based on hydrodynamic models (USACE et al., 2019, p. 50).

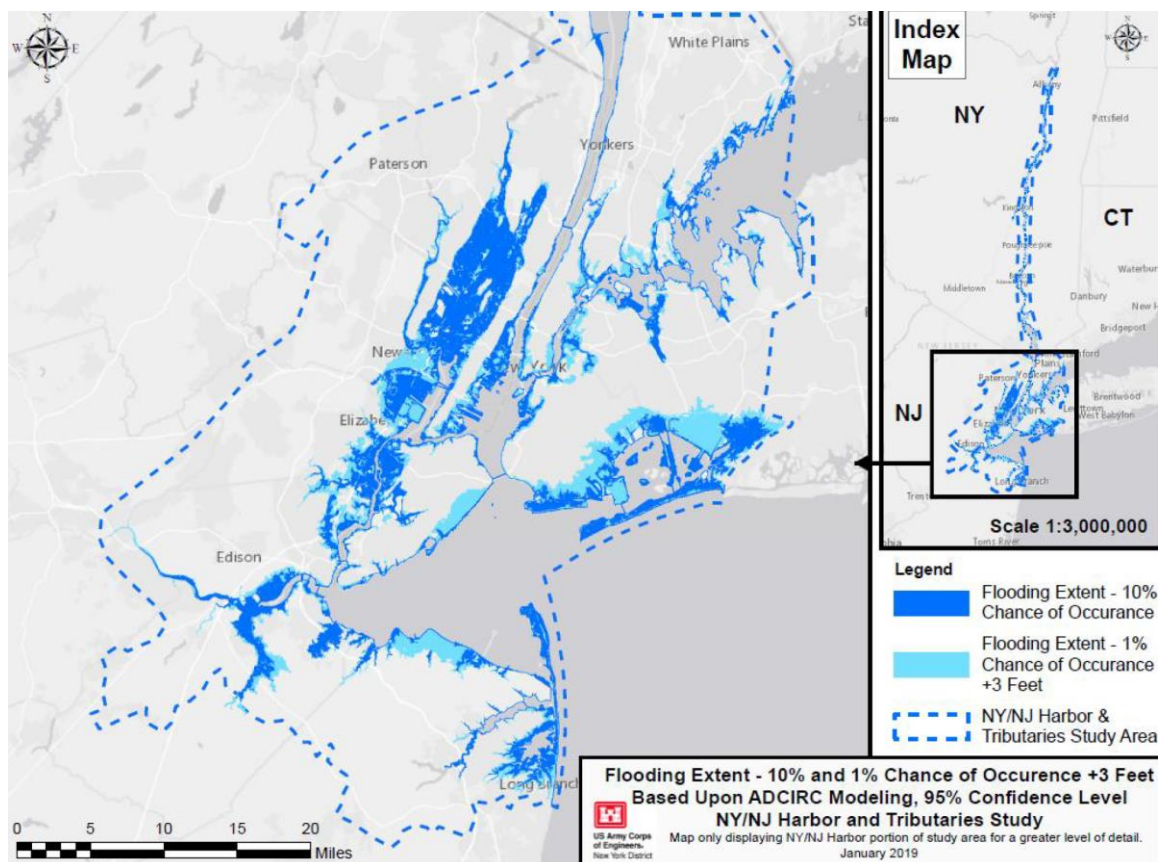


Figure 2.9 | Flood prone areas based on ADCIRC modeling (USACE et al., 2019, p. 71).

Figure 2.10 shows which areas are flooded in the advent of a category 4 hurricane. The majority of the region's coastlines would experience inundation level up to 9 feet (≈ 2.74 m).

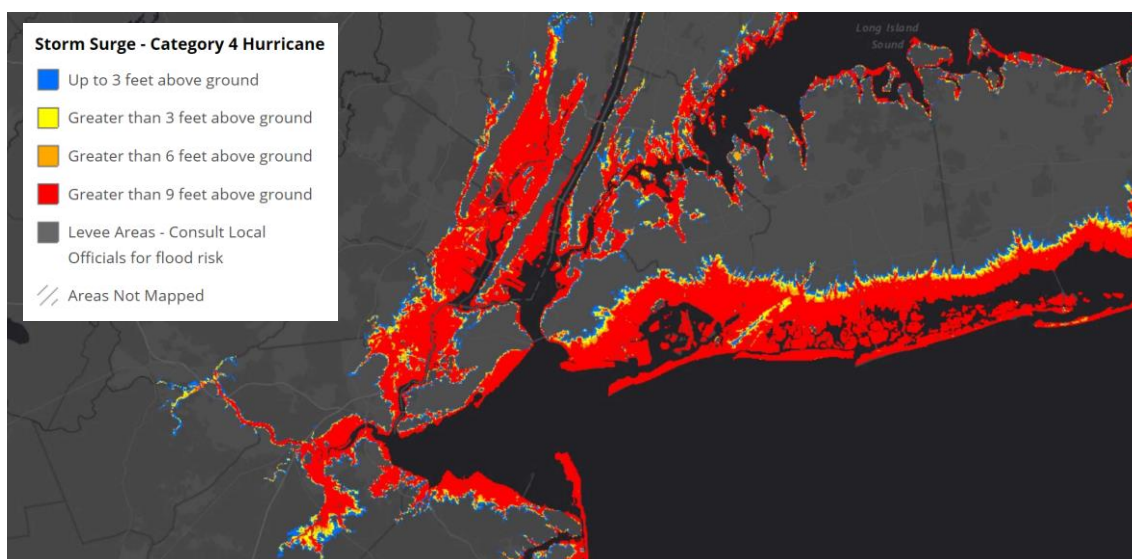


Figure 2.10 | Category 4 hurricane inundations (United States Department of Commerce [USDC]; National Oceanic and Atmospheric Administration [NOAA]; National Ocean Service [NOS], 2020).

2.2.2 Long Island Sound ecosystem

The flood prone maps in section 2.2.1 show the vulnerability of the entire region to inundation. Storm surge waves first arrive at Long Island Sound before reaching the city, therefore a suitable location for a barrier can be searched for in this area (chapter 4). In this section an analysis is given on the western region of Long Island Sound, hereinafter referred to as ‘West Sound’ shown in Figure 2.11. The area of interest remains within the boundaries of the state of New York for this thesis. West Sound can be qualified as a tidal straight, i.e., the waterbody connects to the Atlantic Ocean through the East river and the outer east end of Long Island Sound. Multiple tributaries flow into West Sound and the coast lines are filled with recreational areas, housing and natural ecosystems. Living or working in this flood prone area poses higher risks to millions of people.



Figure 2.11 | West Sound region (MapTiler, n.d.).

The counties surrounding West Sound are inhabited by approximately 3,032,000 citizens, sixty-eight percent are considered environmental justice communities. These are communities that are statistically most impacted by environmental harms and risks (United States Environmental Protection Agency, n.d.). There are six tributaries that flow into West Sound: The Bronx River, Flushing Creek, Westchester Creek, Hutchinson River, Mamaroneck River, and Byram River. Large estuarine wetlands are located at Little Neck Bay, parts of Sands Point, Hen Island and Milton Harbor, Mamaroneck River including its tributaries and Pelham Bay Park. Figure 2.12 highlights these locations. Pelham Bay Park is characterized by large marsh systems that support nesting shorebirds. The entire area is important for migratory fish and the many bays support marine life of which Little Neck Bay, Manhasset Bay and Hempstead Bay are popular recreational fishing areas. Popular recreational areas include Orchard Beach and Rye Playland Beach (USACE et al., 2019, p. 36).

2.2.3 West Sound priority map

Figure 2.12 provides a comprehensive overview of West Sound and important areas within the system.

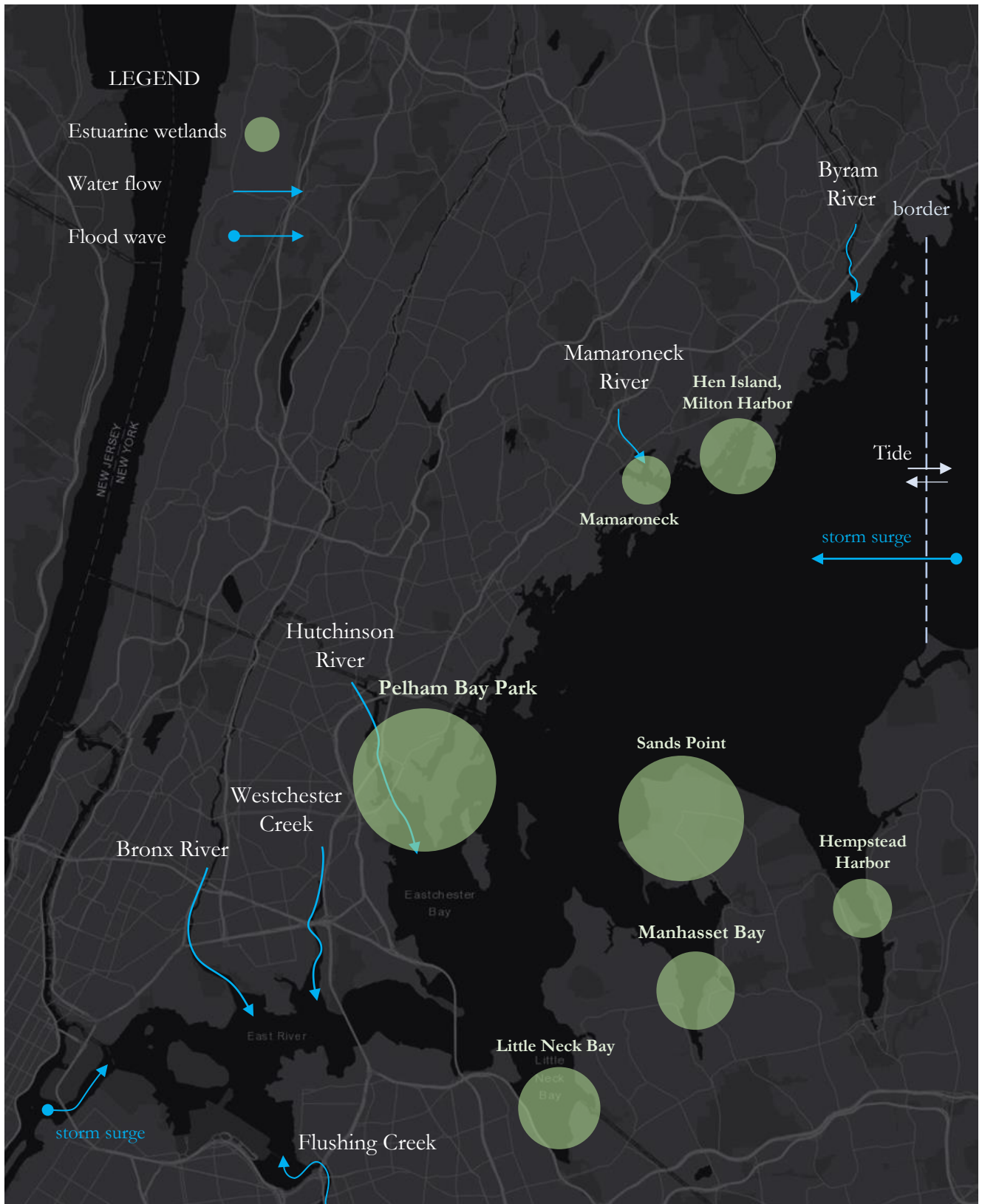


Figure 2.12 | West Sound priority map.

2.3 Stakeholder Analysis

The views on flood protection measures (FPM) from the authorities, communities or any other stakeholders are of importance. According to the USACE – responsible for FPM –, “Proposed CSRMs alternatives should either minimize exacerbating riverine/fluvial flooding, covered under the Flood Risk Management mission of USACE, or include measures to alleviate any induced flooding” (USACE et al., 2019, p. 8). The involved governmental agencies expressed their thoughts on what should be taken into consideration when addressing issue of flooding which are described as follow (USACE et al., 2019, pp. 11-12):

- There is a need for collaboration and coordination across different levels of government to achieve adequate coastal risk management measures.
- An evaluation of a single or series of storm surge barriers which include flood risk management benefits and costs. The impact on the environment, people, property and local economies must be considered.
- Public engagements, education and communication of the risks are important for future support.
- The impact on transportation infrastructure and evacuation routes, power generation and supply, and wastewater infrastructure.
- Addressing the uncertainty regarding appropriately defining the design conditions and thus, the selection and incorporation of a sea level change scenario.
- Addressing uncertainty regarding the occurrence and timing of fluvial flooding with coastal flooding. The concern is that storm surge barriers will worsen fluvial flooding
- Structural measures that negatively impact the environments, especially the Hudson river.
- Funding, time, legislation and bureaucracy slowing down coastal management implementations.

Other stakeholders, which include individual inhabitants, local municipalities, community boards, the US Fish and Wildlife Service and Housing and Urban Development have been involved with the intent of receiving feedback and address concerns. The inhabitants have a better understanding of the effects of these storms on their daily lives and the concerns among different communities. Engaging the public can provide useful input for coastal protection measures and increase public and political support for large scale environmental interventions by the government. The questions and concerns of the public are summarized as follow (USACE et al., 2019, pp. 16-20):

- Sea level rise, as this results in permanent flooded areas. Shoreline-based solution were preferred for it was expected to have less of an impact on the area.
- There is broad concern of the impact on the environment such as:
 - Tidal flows and water quality.
 - Polychlorinated Biphenyls or sewer overflow.
 - Flora and fauna. The inability for animals to move between areas blocked by a barrier.
 - Sedimentation rate.
- Disruption of traffic flow.
- There is concern that non-governmental parties decide to quit their financial contributions.
- The selection criteria for the design alternatives.
- Induced flooding, meaning flooding from two direction. Freshwater from behind the barrier and flood waves reflecting from the gates.

2.4 NYNJHAT Conceptual Barrier Design

2.4.1 Barrier features

The United States government is investigating flood protection measures for New York City and has published several preliminary studies which include conceptual designs of storm surge barriers for multiple locations within the region. A brief overview and discussion of their conceptual design for a barrier at Throgs Neck is given in this section. The analysis serves as a reference to understand what type of barriers were considered and why this location was chosen. The reader is referred to Appendix F for a list of different type of barriers.

Throgs Neck is a neighborhood in the southeastern part of the Bronx and the first locations through which hurricane Sandy's storm surge wave migrated before entering West Sound. This location was chosen by the USACE for its potential to "conceptually broadly address coastal storm surge and wave attack from either the New York Bight or Long Island Sound to the vast majority of the study area" (USACE et al., 2019, p. 77). There are two alternative concepts featuring a barrier at Throgs Neck. The first 'Alternative 2 - NY-NJ Harbor-Wide Surge Gates/Beach Restoration' and second 'Alternative 3A - Upper Bay-Newark Bay Surge Gate and Jamaica Bay Surge Gate Plan' for which the main features are a combination of levee, berm and surge gate/barrier system. A small embankment at Pelham Bay Park is part of this plan. This alternative will also include relocations, acquisitions and building retrofits behind the surge gates to address sea level rise and combat storms for which the gates will not be closed (USACE et al., 2019, pp. 77-84). Figure 2.13 shows the proposed location for Alternative 2 with a barrier at Throgs Neck.

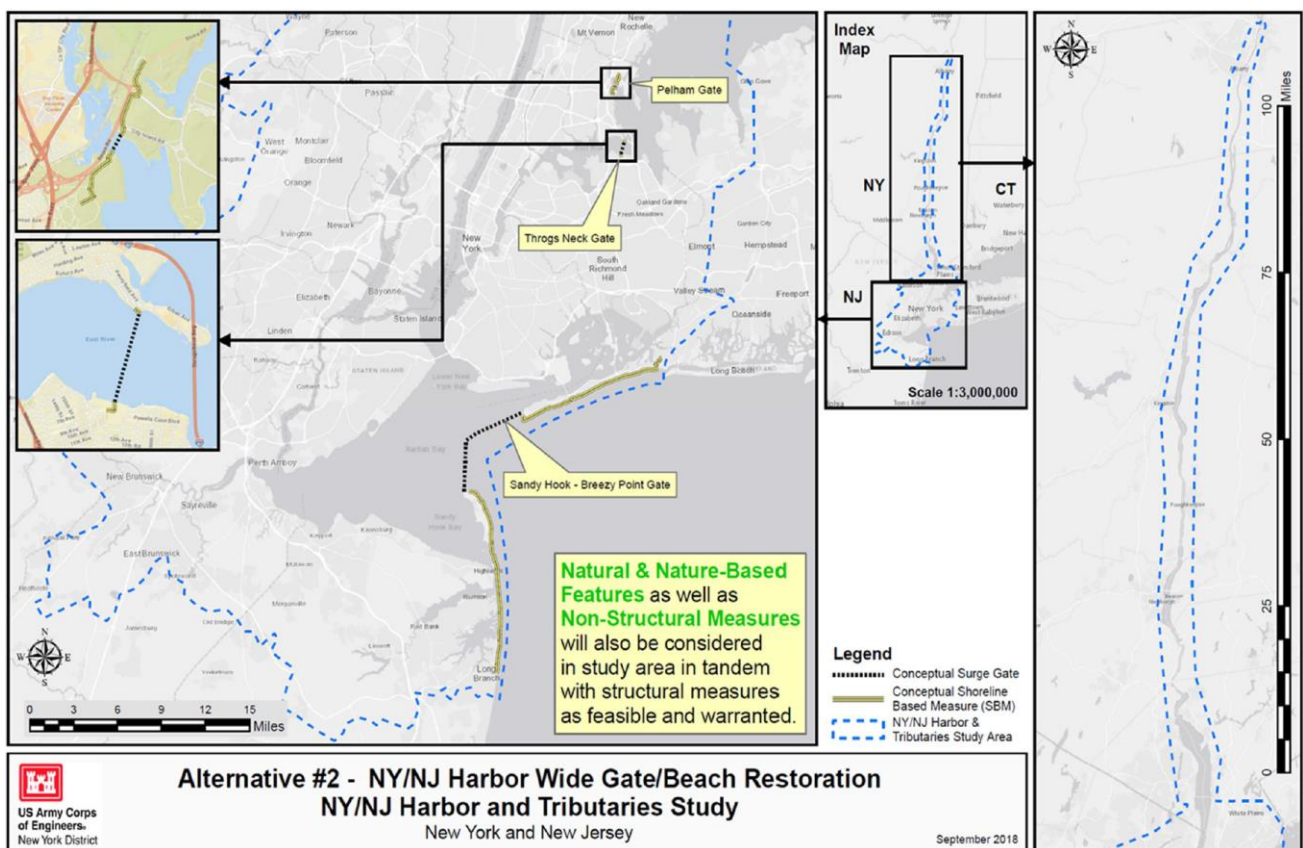


Figure 2.13 | Proposed flood protection measures by the USACE (USACE et al., 2019, p. 83).

2.4.2 Barrier location

The USACE considered five locations at Throgs Neck that could potentially be suitable for a storm surge barrier shown in Figure 2.14 as dotted white lines. The choice for these locations is based on: a fairly similar geotechnical condition, a bathymetry which is preferred to be as shallow as possible and the start and end of the barrier which are preferred to be sheltered to reduce wave exposure. Furthermore, the total length of the barrier should be kept to a minimum and as straight as possible. The average barrier length in Figure 2.14 is 1370 m and average depth between 12.2 and 15.2 m. The option ‘ThrogsNeck04’ has been suggested for a preliminary design for its favorable water depths and short tie-in structures to land (USACE et al., 2019, p. 11).



Figure 2.14 | Considered locations for the Throgs Neck barrier (USACE et al., 2019b, p. 106).

2.4.3 Geometric design

The first concept of the USACE has led to the design shown in Figure 2.15. It is noted that a substantial amount of conceptual design work is still needed. The original flow area at ThrogsNeck04 was 15900 m². With this conceptual design in place, this space would be reduced to 9890 m² (62% of the original flow space).

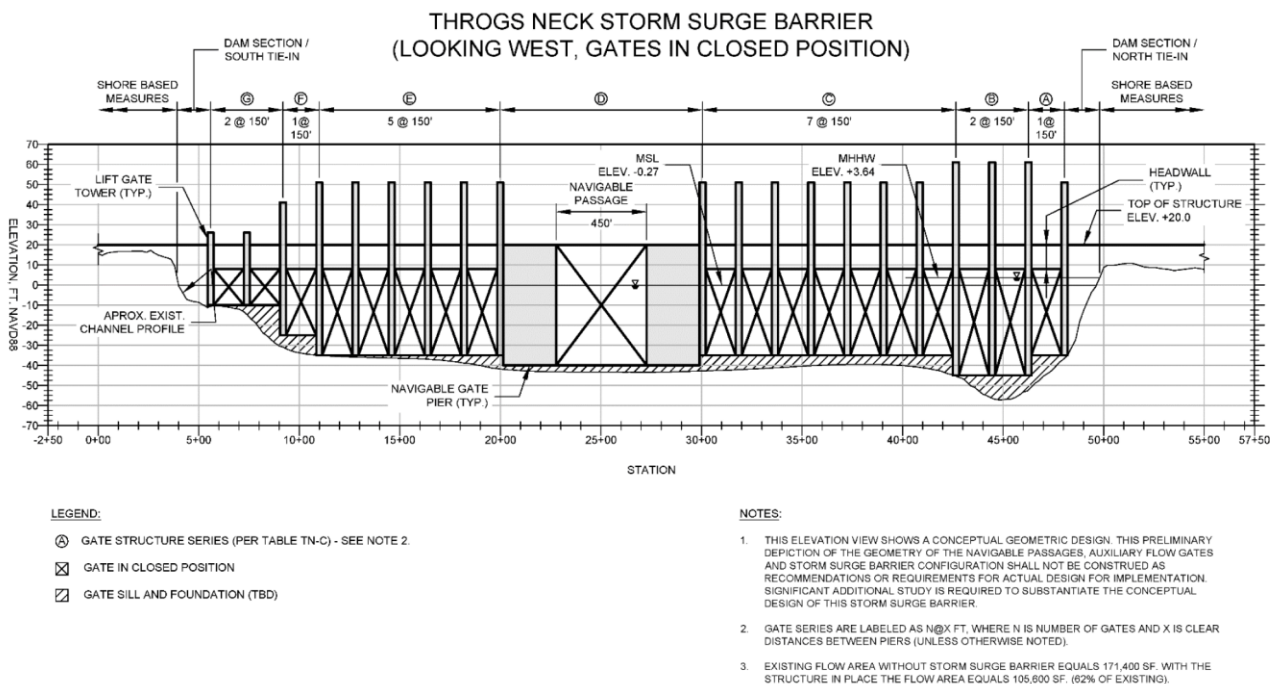


Figure 2.15 | Throgs Neck barrier concept by USACE (USACE et al., 2019b, p. 61).

Examining the image from right to left, shore-based measures and a dam section connect the barrier to the shore. The top of the structure – relative to NAVD 88 – is +6.1 m. With mean sea level (MSL) at -0.08 m and mean higher high water (MHHW) at +1.1 m the difference in water surface elevation is 1.02 m. A series of auxiliary gates are situated from section ‘A’ to ‘C’ in closed position which are similar to the lift gates of the Eastern Scheldt barriers (section 5.7 and Appendix F). The piers are assumed high and strong enough to lift the gates above MHHW. The sill and foundation are designed to equalize the bathymetry for the gates to align properly. At section ‘D’ a gate similar to the floating sector gate (section 5.6 and Appendix F) allows for navigable passage. Section ‘E’ to ‘G’ have lift gates and finally, the barrier connects the shore again with an embankment.

2.4.4 Gate type selection

The minimum requirements for Throgs Neck gate dimensions are summarized in Table 2.2. It should be noted that these are preliminary assumptions. A thorough simulation and verification process is expected to ultimately refine these values.

Location	Federal Channel	Existing Depth (m)	Minimum Practical Width of Opening (m)	Minimum Depth of Opening (m MLLW)	Minimum Depth of Opening (m NAVD88)	Air Clearance (m NAVD99)
Throgs Neck	Throgs Neck	12.2-16.8	137.2	11.3	-12.2	Unrestricted

Table 2.2 | Minimum navigation channel dimensions (USACE et al., 2019, p. 141).

In general, the floating sector gate is chosen for larger navigable spaces considering it is a proven concept which can span large channel cross-sections. Lift gates are used for smaller passages. Another considered option was the flap gate. However, it is not considered suitable for reverse head conditions and challenging to maintain. Then there was the vertical rising gate which was considered too challenging to maintain and had no proven concept for such large span.

The following gate types were considered unsuitable. The sector gate (vertical axis type), barge gate, rotating segment gate and the inflatable gate or dam are unsuitable for large and deep spans and have no proven concepts. The miter gate is unsuitable for large spans and head differences. Unrestricted air clearance makes vertical lift gates and tainter gates no options. A horizontal rolling gate required much space for docking the entire gate, thus considered impractical (USACE et al., 2019, p. 142). An inventory list has been made to determine the suitability for each hydraulic gate type per location. The reader is referred to Appendix F for a complete overview of the different barrier types including the USACE’s view on the suitability of each gate type.

2.4.5 Discussion

Although this is a preliminary design by the USACE, an important missing aspect is the reasoning and decision on which areas to protect – and which not – and why. This information is welcome as it can inform the design decisions of the new barrier in this thesis. A barrier at Throgs Neck will not protect the coastlines of West Sound in the event of a storm surge migrating towards New York City from Long Island Sound. The city may be protected, but there are over 100 km of coastlines along West Sound full of residential areas left unprotected (Figure 2.9). If there are, for example, financial reasons not to develop a longer barrier, an additional challenge would be to develop a new concept that is more cost effective. Another point of discussion are the advantages and disadvantages of the combination of floating sector gates and lift gates and how they exactly fit within the cross-section which is not elaborated in detail. The choice for these gates seems an to be an automatic one.

CHAPTER 3

Requirements and Boundary Conditions

CHAPTER 3 REQUIREMENTS AND BOUNDARY CONDITIONS.....	21
CHAPTER 3 ABSTRACT.....	21
3.1 FUNCTIONAL REQUIREMENTS.....	22
3.2 ENVIRONMENTAL BOUNDARY CONDITIONS.....	22
3.2.1 <i>Astronomical tides</i>	22
3.2.2 <i>Sea level rise</i>	23
3.2.3 <i>Tidal flows</i>	24
3.2.4 <i>Water level head difference</i>	24
3.2.5 <i>Wind data</i>	24
3.2.6 <i>Vessel dimensions</i>	24
3.2.7 <i>Water depth and wave height</i>	25
3.2.8 <i>Geological data</i>	25

Chapter 3 Abstract

This chapter presents the functional requirements for the conceptual design of the new barrier. In addition, publicly available resources are used to describe the environmental boundary conditions which are the natural conditions that will affect the barrier.

3.1 Functional Requirements

Functional requirements are specification to which the structure must adhere in order to fulfil its purpose, i.e., providing protection against storm surges. The functional requirements that apply to the conceptual design in this thesis are described as follow:

- F1 – the barrier is designed with a service life of 100 years.
- F2 – the barrier is able to adapt to different sea level rise scenarios, including the most extreme estimation.
- F3 – the minimum navigation width is 140 m and depth 12.2 m (Table 2.2).
- F4 – the navigable sections of the barrier are able to close at least once per year.
- F5 – the navigational sections of the barrier are designed to close within one day.

The location selection criteria are detailed in section 4.2 and structural requirements in Appendix D2.11. The evaluation criteria for the comparison of different concepts are detailed in section 5.9.2.

3.2 Environmental boundary conditions

This section provides an overview of the environmental boundary conditions in West Sound which are used as reference data for this thesis. Any deviation from these conditions will be mentioned.

3.2.1 Astronomical tides

The astronomical tides are measured at Kings Point and shown in Table 3.1 (Center for Operational Oceanographic Products and Services [CO-OPS], 2018). The reader is referred to Appendix H for a complete list of tidal range values.

Tidal datums for station 8516945, Kings Point, NY		
datum	value (m)	description
Max Tide	3.073	Highest Observed Tide
HAT	1.674	Highest Astronomical Tide
MHHW	1.109	Mean Higher-High Water
MHW	0.999	Mean High Water
NAVD88	0	North American Vertical Datum of 1988
MSL	-0.082	Mean Sea Level
MLW	-1.183	Mean Low Water
MLLW	-1.268	Mean Lower-Low Water
LAT	-1.761	Lowest Astronomical Tide 1-21-1996
Min Tide	-2.491	Lowest Observed 2-2-1976
MN	2.182	Mean Tidal Range

Table 3.1 | Tidal datums used for West Sound (CO-OPS, 2018).

3.2.2 Sea level rise

The extent of global mean sea level rise (GMSLR) by the end of the 21st century is uncertain. Some models predict sea levels to rise as much as 1.83 m by the year 2100 in the case of a rapid ice melting scenario (NYS 2100 Commission, 2013, pp. 20-21). Other models consider sea levels as high as 2.0 m to be possible by the year 2100 as shown in Figure 3.1 (United States of America Department of Commerce [USADC], USGS, United States Environmental Protection Agency [USEPA], Rutgers University, 2017, p. 12).

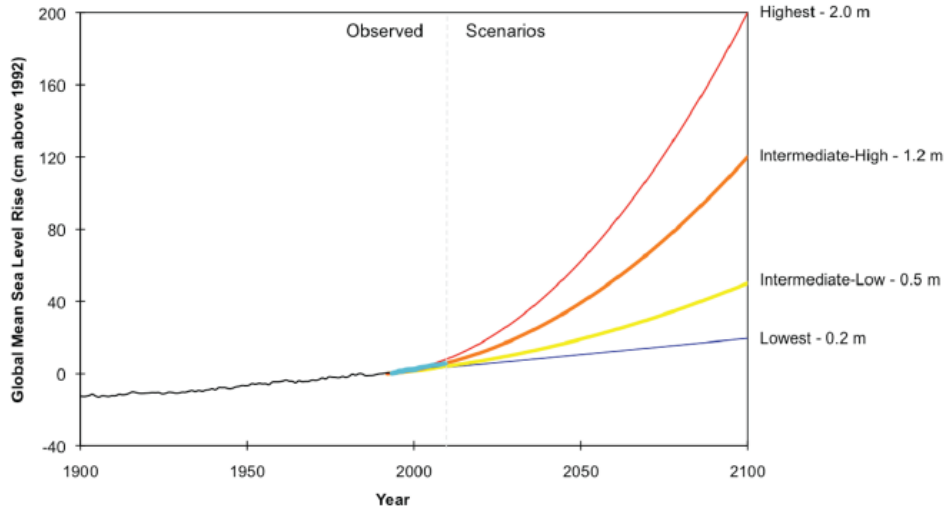


Figure 3.1 | Expected global mean sea level rise for the 21st century (USADC et al., 2017, p. 12).

Rising sea levels are increasing the high-tide flooding frequency, which is defined as a half meter water level increase above the daily high-tide. The NOAA estimated that this trend is accelerating. The high tide-flooding frequency could triple by 2030 and between five to 15 times are frequent by 2050 (Flavelle, 2020).

NOAA scientist presented future sea level rise estimates based on greenhouse gas emission projections shown in Figure 3.2. For low emissions, a 0.3 m increase is expected to occur and for the most extreme case 2.5 m which takes into account ice loss from Antarctica (Lindsey, 2020).

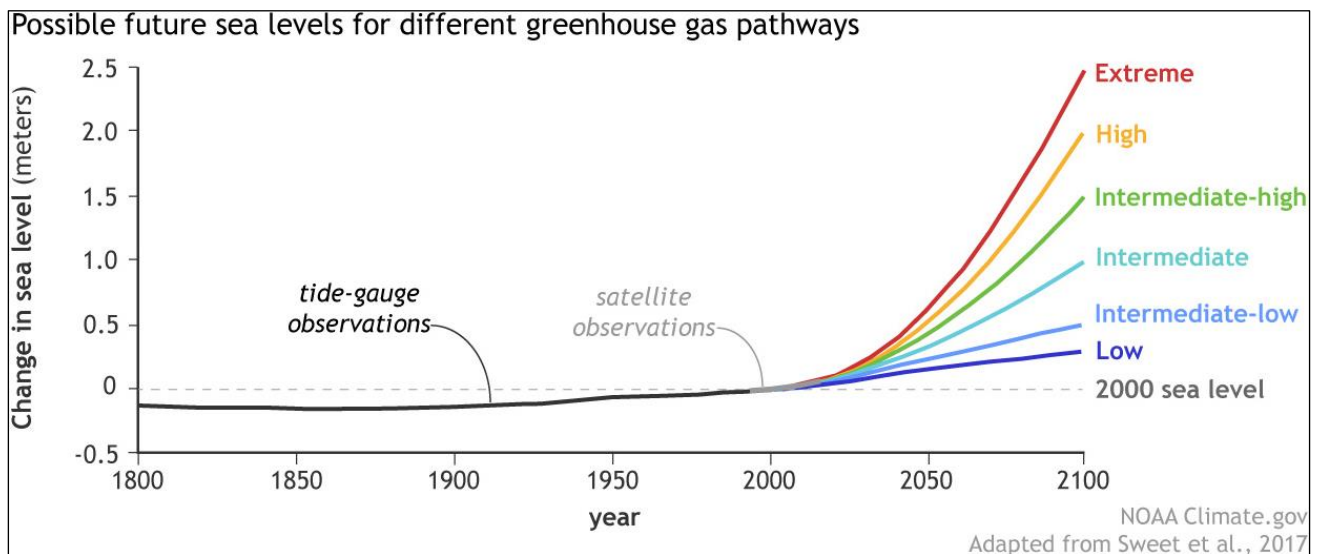


Figure 3.2 | Expected GMSLR scenarios based on greenhouse emissions and ice loss (Lindsey, 2020).

Uncertainty regarding sea level rise is taken into consideration by designing an expandable barrier which is detailed in chapter 6 and further detailed in Appendices.

3.2.3 Tidal flows

The mean and maximum tidal flows are shown in Table 3.2. The tidal currents show tidal surface currents at the Throgs Neck area and are the resulted average between ebb and flood flows for conditions without a storm surge barrier (USACE et al., 2019b, pp. 27-28).

Flows			
location	output	mean tidal flow [m ³ /s]	maximum tidal flow [m ³ /s]
Throgs Neck		5800	13000
	V4	mean tidal current magnitude [m/s]	maximum tidal current magnitude [m/s]
		0.548	1.34

Table 3.2 | Tidal flows (USACE et al., 2019b, pp. 27-28).

3.2.4 Water level head difference

High storm surges on the ocean side which lead to wave overtopping, large setups due to strong winds or high river discharges on the protected side can result in large head differences between both sides of the barrier. Table 3.3 shows the direct and reverse head differences (USACE et al., 2019, p. 33) for storms with a 100-year return period with the flood side (Long Island Sound) and protected side (East River).

Direct and Reverse Head difference for 1% AEP conditions for storm surge barriers			
Throgs Neck			
parameter	flood side water level	protected side water level	difference
	NAVD88 [m]	NAVD 88 [m]	[m]
direct head (1% AEP)	4.33	-0.79	5.12
reverse head (1% AEP)	-1.58	1.65	-3.23

Table 3.3 | Water level head difference (USACE et al., 2019b, p. 33).

The water level head difference values in Table 3.3 are considered a minimum requirement. This table takes into account 50 years of sea level rise (until 2070). For the load analysis (section 7.1.3), larger water level differences are used based on GMSLR and the maximum and minimum observed tides (Table 3.1).

3.2.5 Wind data

The maximum sustained wind speed measured at Kings Point is 46 km/h and Gust 76 km/h as described in section 2.2.1, Table 2.1. These values are used for design purpose in section 7.1.2 and further elaborated in Appendix B.

3.2.6 Vessel dimensions

The required vessel dimensions to cross the barrier are given in Table 3.4 (USACE et al., 2019b, p. 35).

Design Vessels for the Navigation Passages				
Location	Design Vessel Category	LOA [m]	beam [m]	draft [m]
Throgs Neck	Tanker	179.9	30.6	7.9

Table 3.4 | Vessel dimensions (USACE et al., 2019b, p. 35).

3.2.7 Water depth and wave height

The design water depth is based on observations of the bathymetry at the selected barrier location (chapter 4) equal to 20 m. The governing wave height $H_s = 9.9$ m and wave period $T_s = 13$ s are based on the highest observed wave heights during Hurricane Sandy measured 28 km southeast of Breezy Point, N.Y (United States Geological Survey [USGS], 2014, p. 4). It should be noted that the USACE used a 100-year significant wave height at Throgs Neck of 1.3 m and Sandy Hook-Rockaway – near Breezy Point – of 5.0 m based on “NACCS and the Simulation of Waves Nearshore (SWAN)” (USACE et al., 2019b, pp. 9,18). However, the Sandy Hook-Rockaway simulation result is still well below the actual measured wave height at Breezy Point. It is unclear whether wave heights of this magnitude (or higher) can develop in Long Island Sound, however, the possibility cannot be ruled. Therefore, it is assumed that a storm surge of the same magnitude can migrate from Long Island Sound towards the city.

3.2.8 Geological data

Information on the subsoil is very limited and can be summarized as follow for Throgs Neck (USACE et al., 2019b, p. 137):

- Recent Alluvium. Organic soft silts with varying amounts of fine sand, 7.62 m thick over the majority of the alignment.
- Glacial till. Mainly medium dense to very dense sands and gravels with lesser amounts of silts and clays.
- Lloyd Sand. Mainly medium dense to very dense sands and gravels with minor amounts of silts and clays.
- Raritan Clay.

Based in this information and the surficial sediment of Long Island Sound shown in Figure 3.3, the surface layers of the bathymetry of the area of interest in West Sound is assumed to be of a weak clayey silt material spanning the entire channel in West Sound.

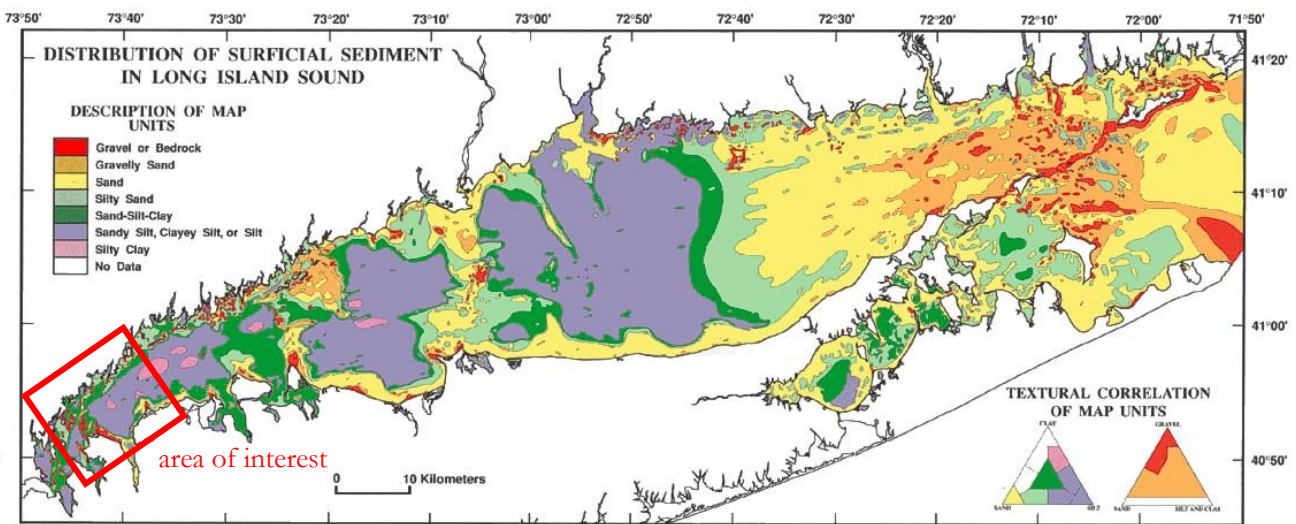


Figure 3.3 | Surficial sediment of Long island Sound (Poppe, Knebel, Mlodzinska, Hastings, & Seekins, 2000).

Further assumptions include the presence of a sand layer beneath the soft layer for which the bearing capacity is assumed to be sufficient.

CHAPTER **4**

Location Selection

CHAPTER 4 LOCATION SELECTION.....	26
CHAPTER 4 ABSTRACT.....	26
4.1 INTRODUCTION.....	27
4.2 LOCATION SELECTION CRITERIA	27
4.3 BARRIER LOCATION OPTIONS.....	28
4.4 LOCATION DISCUSSION	33

Chapter 4 Abstract

In this chapter a number of possible locations for a storm surge barrier are analyzed. Location selection criteria are devised to assist in the decision-making process on the preferred location as well as local population and housing unit data in the region.

4.1 Introduction

The geography of Long Island Sound is complex due to the irregular and densely populated shorelines. Long Island Sound can be characterized as a tidal straight connecting two sides of the ocean through one water body, therefore, one barrier will not protect New York City or the surrounding shorelines due to the fact that a storm surge can reach the city from two directions. Therefore, multiple barriers are needed. For this thesis it is assumed a barrier is already constructed near Sandy Hook – Breezy Point preventing a storm surge from further propagating towards the city as shown in Figure 4.1.

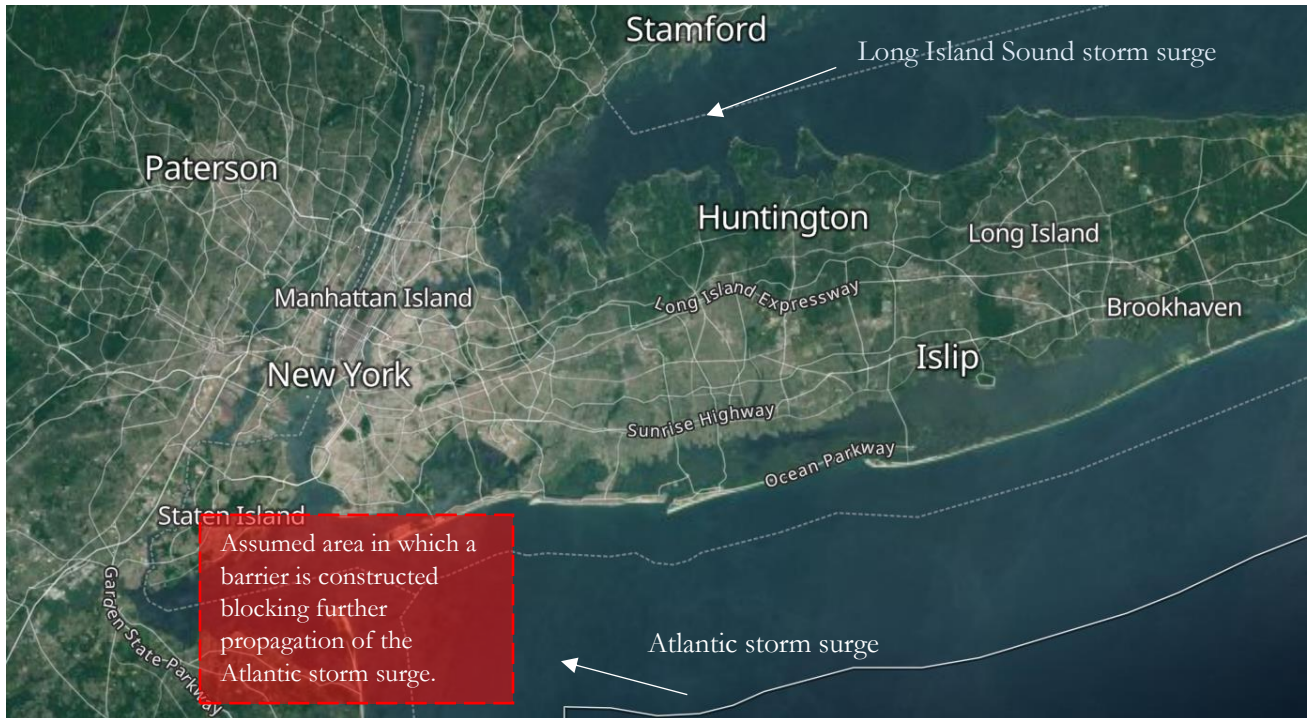


Figure 4.1 | Area where a barrier is assumed to already be present (MapTiler, n.d.).

4.2 Location selection criteria

The following criteria are devised to assist in determining the preferred location for the barrier:

- The *protection range*, i.e., length of protected shorelines which are inhabited or where there is economic activity, needs to be as large as possible.
- The location is limited to the geographical boundary of New York state.
- No permanent relocation of inhabitants should be the result of the selected location.
- The bathymetry should be fairly uniform, i.e., variations in water depth along the channel length should be minimal.
- The northern and southern shoreline connection locations should be chosen such that the barrier remains relatively parallel to the width of the channel.

Although one location will be designated as the preferred destination for the barrier, other locations will remain part of the applicability analysis throughout subsequent chapter. It should be noted that at this stage of the design, there is no maximum barrier length requirement. Clearly, a longer barrier is more expensive. If it is possible to provide the same level of protection for an area with a shorter barrier, a different location is should be investigated.

4.3 Barrier location options

Figure 4.2 shows a perspective view of West Sound with the northern shoreline on the right side of the image and southern shoreline on the left side. In order to find a suitable location, the number of inhabitant and housing units that are protected for each location is taken into account. The northern shoreline is highly irregular and almost entirely predominated by housing making it difficult for the barrier to connect to the shore without disrupting local neighborhoods. In general, the southern shoreline is less densely populated compared to the northern shoreline and has more connection possibilities. However, shoreline connections should be chosen such that the barrier remains relatively parallel to the width of the channel in order to maintain a shorter distance (Figure 4.2).

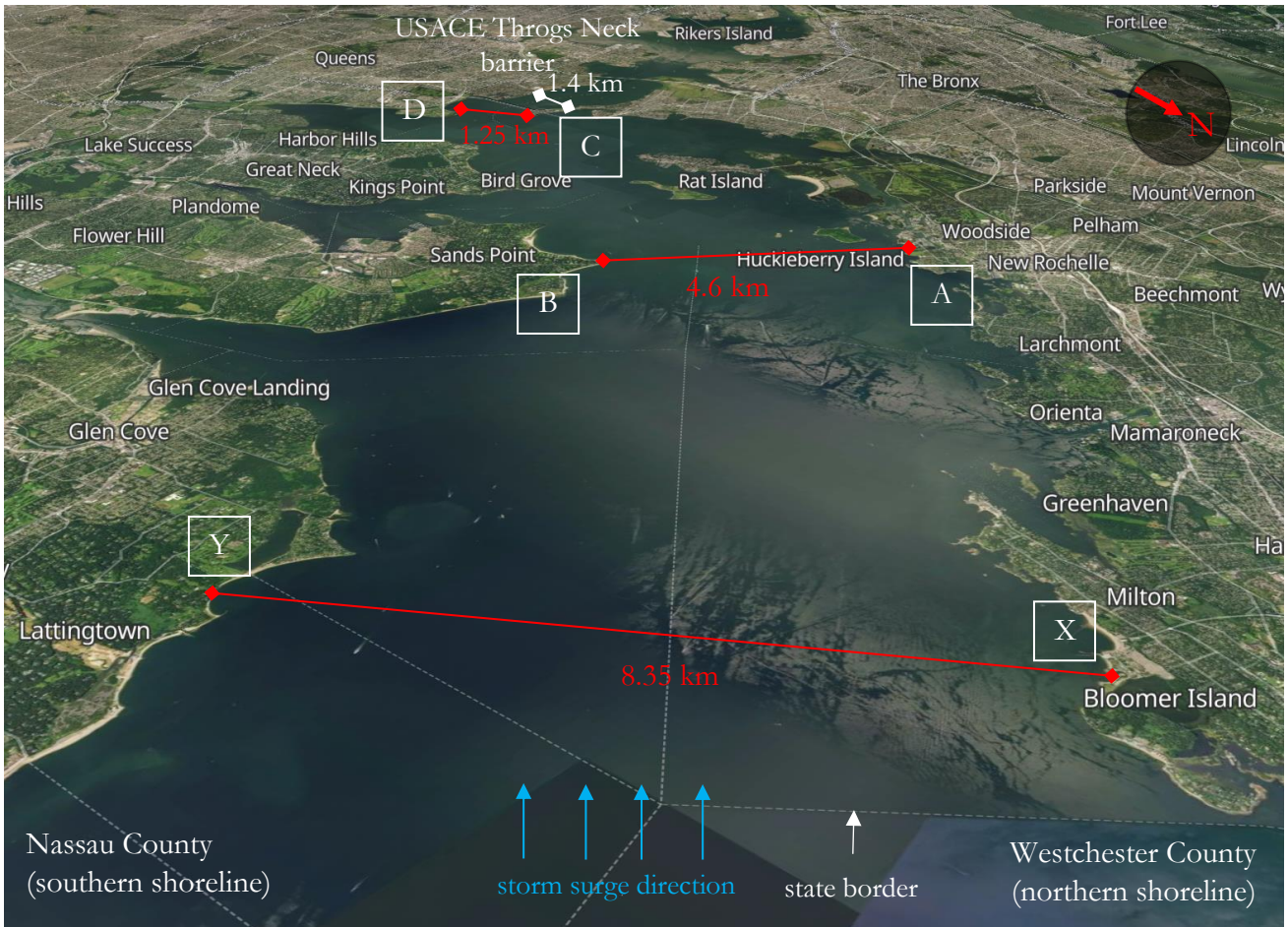


Figure 4.2 | Proposed barrier location for West Sound (MapTiler, n.d.).

The storm surge migrates from northeast to southwest as shown in Figure 4.2. Noteworthy is the overall decreasing channel width in the propagation direction which could lead to an increase in wave height as the waves propagate through the channel. Further research could prove this. The applicability of the barrier is analyzed for three locations: A barrier between Throgs Point (C) – Willets Point (D), Sands Point (B) – Davenport park (A) and Peacock Point (Y) – Rocky Point (X).

In this analysis, the barrier at Throgs Point – Willets Point only serves as a reference location from which the housing units and shore-line area populations are counted up to the state border. The Throgs Point – Willets Point location is further analyzed in chapter 6 with regards to the barrier layout.

Figures 4.3-4 show close-up images of the shorelines connecting Davenport Park and Sands Point. Davenport Park has sufficient space for the barrier to connect to the shore without having a significant impact on the neighborhood. The symbol 'A' indicates the connection point in Figure 4.3.

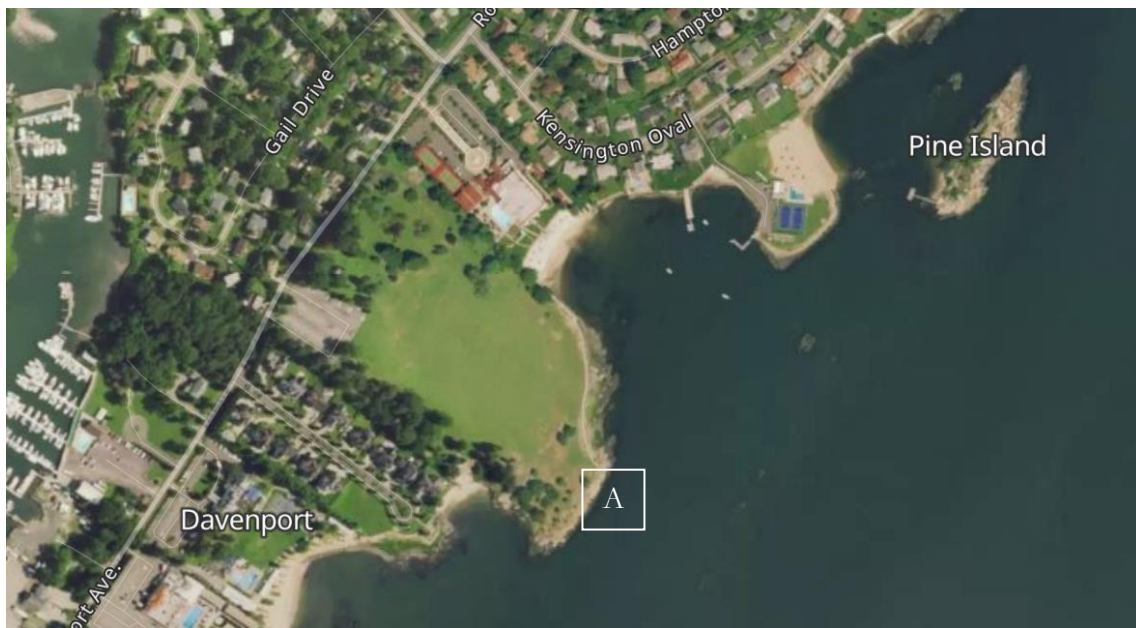


Figure 4.3 | Davenport park connection point (MapTiler, n.d.).

The connection point 'B' in Figure 4.4 at Sands Point is more complicated due to housing along the shoreline. It could be necessary to extend the shoreline away from the houses if construction activities are expected to have too much impact on residents.

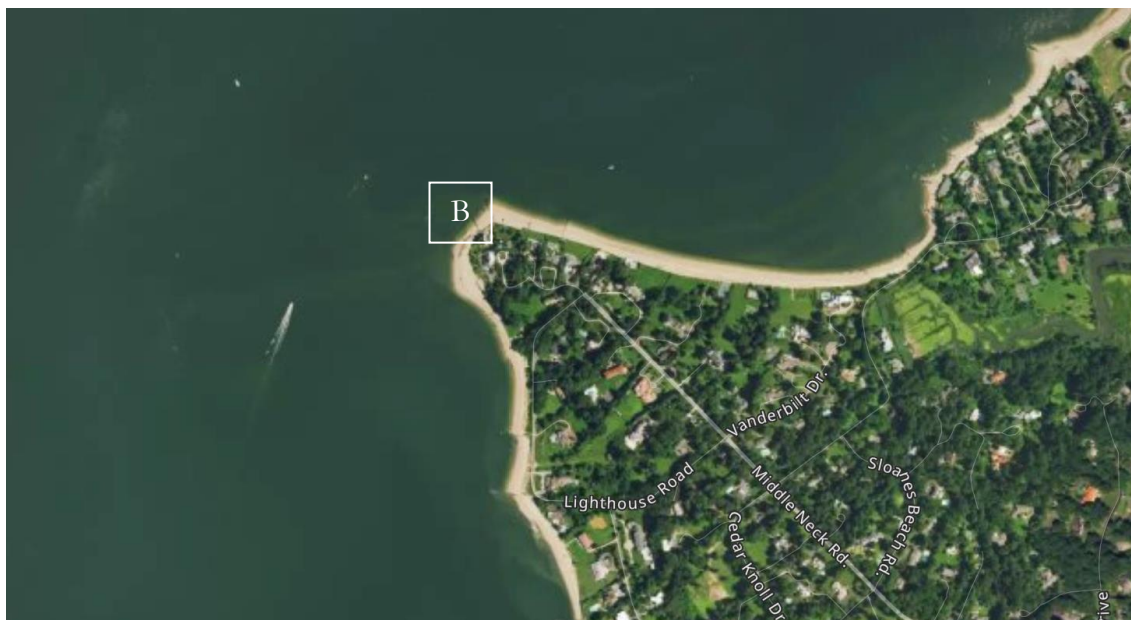


Figure 4.4 | Sands Point connection point (MapTiler, n.d.).

A disadvantage of this location is the proximity to Davids Island, Huckleberry Island and Pea Island which are located near Davenport. These are uninhabited wildlife refuges that would be impacted by construction activities and pollution.

The second possible location is between Peacock Point – Rocky Point spanning 8.35 km. The entire northern shoreline is densely urbanized with housing and recreational areas. There are few locations that would be ideal for minimizing construction nuisance and environmental impact for nearby residents. The most suitable location for the northern connection point would be in the small suburban city of Rye in Westchester County. A piece of land denoted ‘X’ in Figure 4.5 connecting a theme park ‘1’ and natural wildlife sanctuary ‘2’ is the desired location. The theme park ‘1’ should be (temporary) relocated. This would provide enough space for construction activity at a distance from the adjacent neighborhoods. Moreover, the already existing parking space ‘3’ can be used for the project.



Figure 4.5 | Rocky Point connection point (Google Earth).

The southern shoreline connection is shown in Figure 4.6. East Island ‘4’ is densely urbanized, thus considered unqualified. Moreover, if a storm breaches a weak spot, for example ‘5’, water will flow around the barrier. The desired location for connecting the barrier to the mainland along East Beach is at Peacock Point denoted ‘Y’ where there is sufficient space.

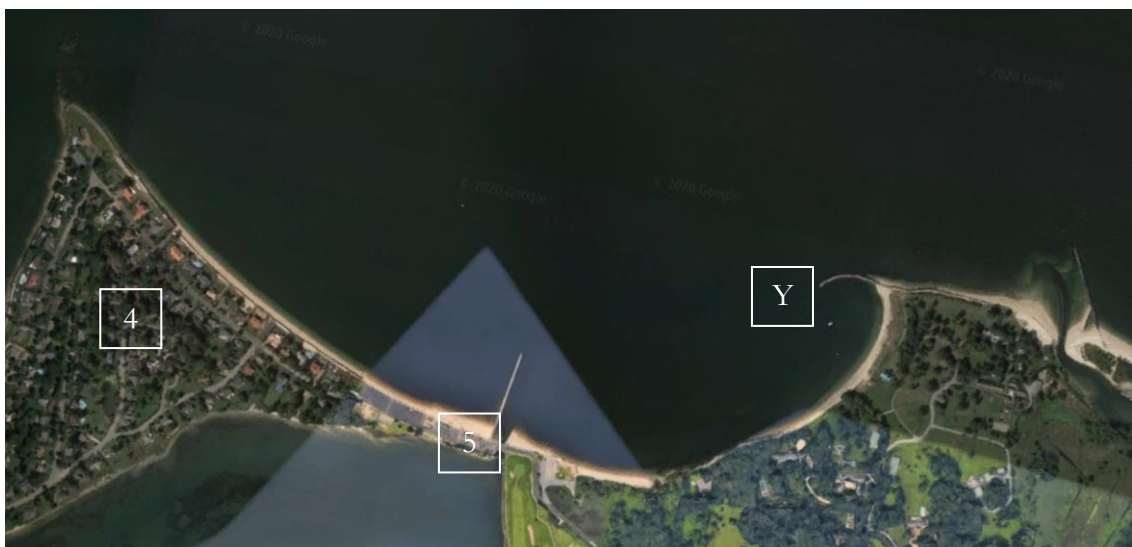


Figure 4.6 | Peacock Point connection point (Google Earth).

The bathymetry for Davenport Park – Sands Point varies significantly over the length of the barrier as shown in Figure 4.7. The deepest regions (dark green) vary between 26 and 33 m on average.

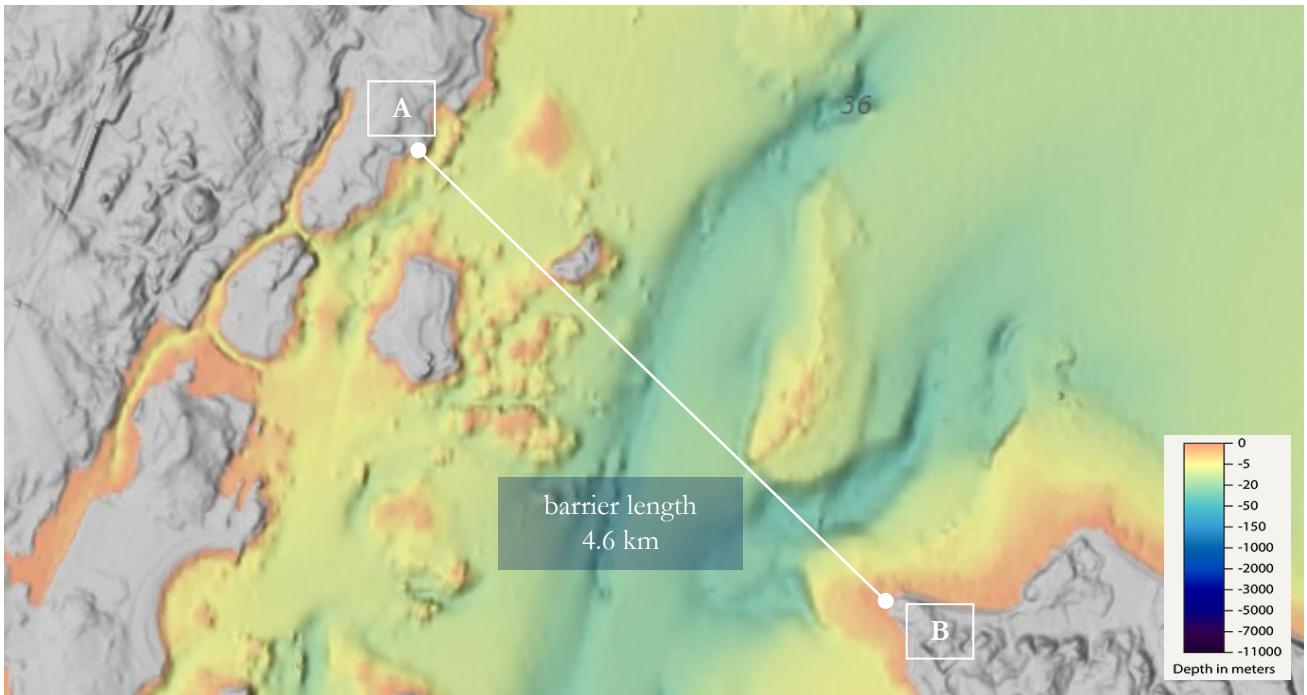


Figure 4.7 | Bathymetry between Davenport Park – Sands Point (NOAA, n.d.).

The bathymetry of Peacock Point – Rocky Point is relatively uniform along the channel width as shown in Figure 4.8. The largest water depths vary between 15 and 20 m (dark green) on average.

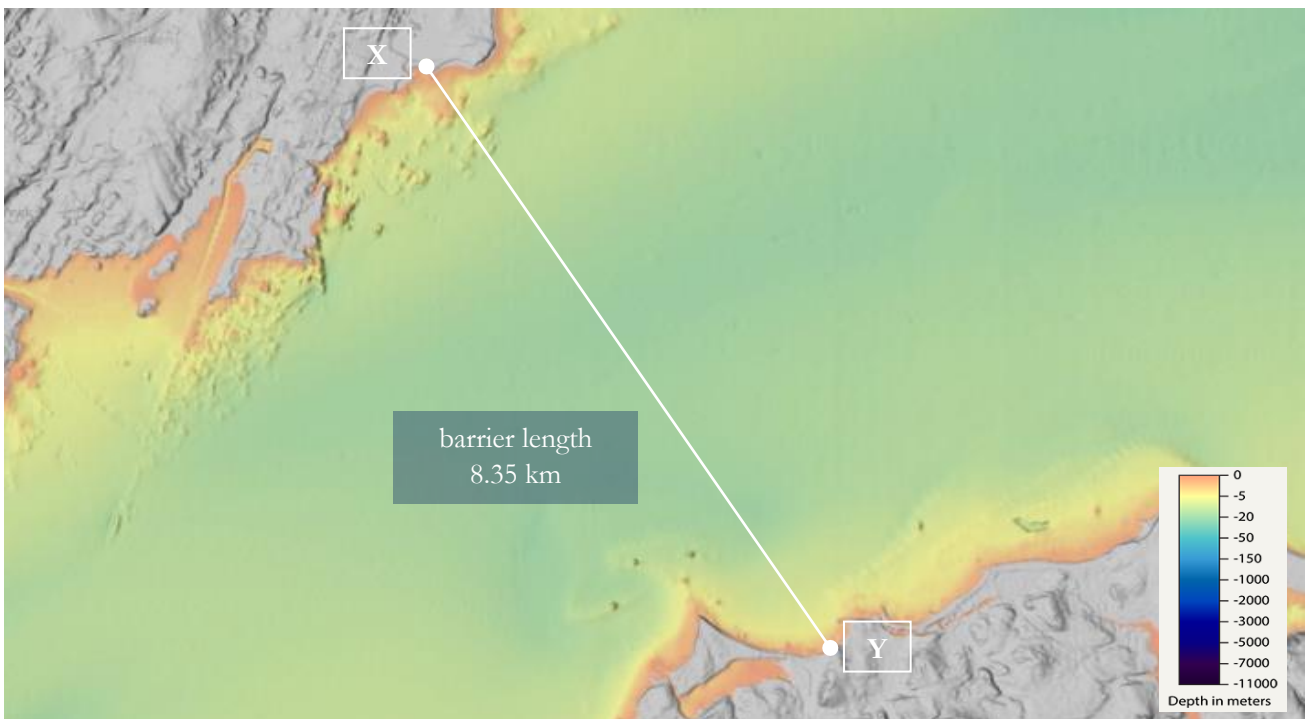


Figure 4.8 | Bathymetry Peacock Point – Rocky Point (NOAA, n.d.).

Although the barrier would be shorter between Davenport Park – Sands Point, the larger depth and irregularity of the bathymetry is considered a disadvantage compared to Peacock Point – Rocky point.

Tables 4.1-2 provide information on the populations and housing units for each city, town or village along the northern and southern shorelines between Throgs Neck and the state border (Figure 4.2). It is assumed that the entire population of each location will be affected by a storm surge.

Westchester County				
location	population estimate	housing units	protected by the barrier at	
			Davenport Park - Sands Point	Peacock Point-Rocky Point
Throgs Neck	44,000	16,842	yes	yes
Pelham Manor	5,500	1,770	yes	yes
City Island	4,400	2,157	yes	yes
Co-Op City	43,200	19,080	yes	yes
Country Club	17,400	6,375	no	yes
New Rochelle	78,500	29,645	no	yes
Larchmont	6,100	2,033	no	yes
Mamaroneck	19,100	7,424	no	yes
Rye	15,700	5,813	no	yes
Total	233,900	91,139		
Total number of protected population			97,100	233,900
Total number of protected housing units			39,849	91,139

Table 4.1 | Westchester County population and housing (United States Census Bureau, n.d.), (Point2, n.d.).

Nassau County				
location	population estimate	housing units	protected by the barrier at	
			Davenport Park - Sands Point	Peacock Point-Rocky Point
Little Neck	17,800	2,767	yes	yes
Great Neck Estates	2,800	1,111	yes	yes
Saddle Rock	980	3,141	yes	yes
Kings Point	5,300	1,499	yes	yes
Great Neck	10,215	3,386	yes	yes
Thomaston	2,600	1,004	yes	yes
Manhasset	8,100	2,980	yes	yes
Plandome	1,500	418	yes	yes
Plandome heights	850	331	yes	yes
Port Washington	15,600	6,261	yes	yes
Sands Point	2,900	1,023	yes	yes
Roslyn Harbor	1,100	368	no	yes
Glenwood Lading	3,900	1,379	no	yes
Sea Cliff	5,050	2,012	no	yes
Glen Cove	27,200	10,475	no	yes
Lattingtown	1,800	737	no	yes
Total	107,695	38,892		
Total number of protected population			68,645	107,695
Total number of protected housing units			23,921	38,892

Table 4.2 | Nassau County population and housing (United States Census Bureau, n.d.), (Point2, n.d.).

Tables 4.1-2 quantify the protection range and shows the difference in population and housing protection for the two barrier locations. In summary, constructing the barrier between Peacock Point – Rocky Point instead of Davenport Park – Sands Point, protects an additional 175,850 residents and 66,261 housing units.

Finally, it should be emphasized that an 8.35 km long storm surge barrier between Peacock Point – Rocky Point protects an approximate 120 km of additional shoreline compared to the Throgs Neck location. Furthermore, the decision to build a barrier instead of an embankment along the shorelines is expected to be more feasible based on the distance alone. Figure 4.9 shows the shoreline lengths protected for each possible barrier location and summarizes the population and housing units that would be protected.

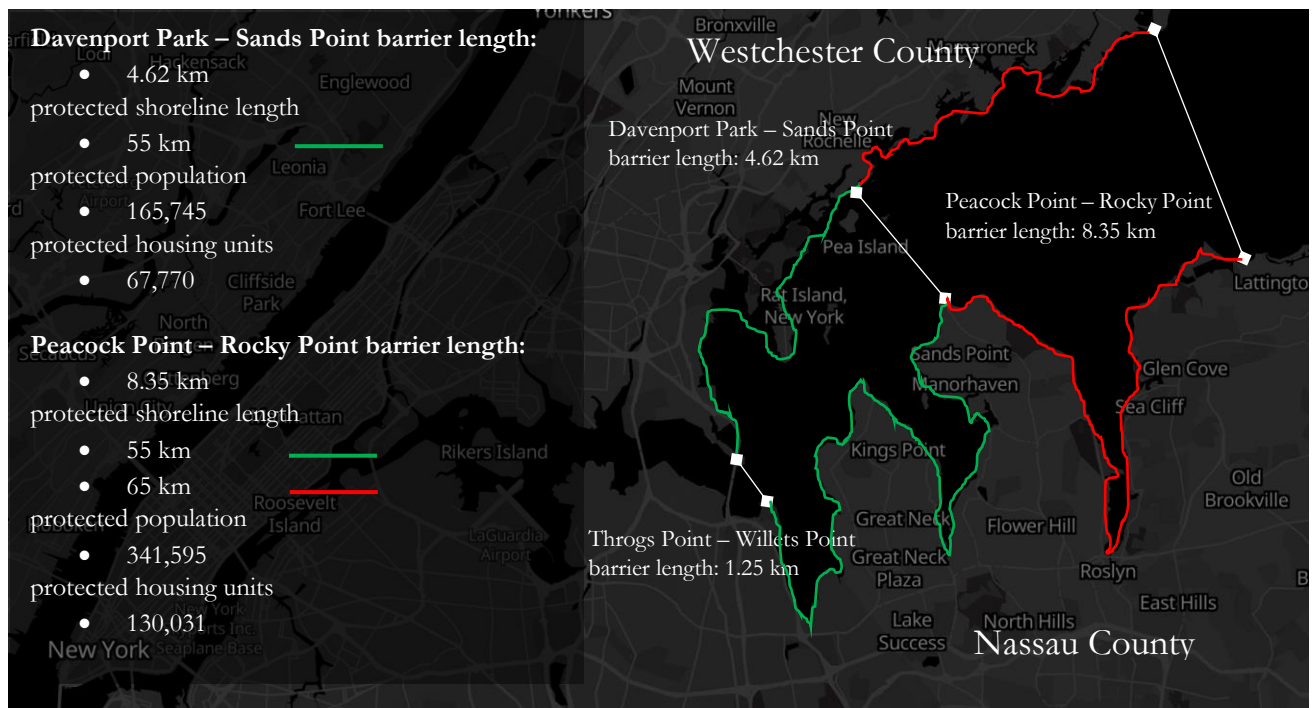


Figure 4.9 | Schematic of the protected coastline length by the new barrier (MapTiler, n.d.).

4.4 Location Discussion

Tables 4.1-2 and Figure 4.9 show the degree of protection a barrier would provide when constructed at Peacock Point – Rocky Point versus Davenport Park – Sands Point, i.e., an additional 175,850 residents and 66,261 housing units would be protected if the barrier would be constructed between Peacock Point – Rocky Point. The total number of protected populations for this location is 341,595 and housing units 130,031. However, the length of the barrier is 3.7 km longer than a barrier constructed between Davenport Park – Sands Point, which is the only real advantage of this location, the shorter distance. The irregular, relative deep bathymetry and the barrier’s close proximity the natural wildlife refuges are undesirable.

The fact that the bathymetry is fairly uniform between Peacock Point – Rocky Point is considered a positive observation. Local flow velocities are therefore expected to remain relatively constant in this area. Lastly, it is noted that the funnel shaped geography of Long Island Sound limits the options for an effective location selection, i.e., protecting as many populations and housing units for the shortest possible barrier length. Ultimately, the question is whether the additional protection provided by a Peacock Point – Rocky Point over Davenport Park – Sands Point is worth the investment. This question can be answered after an in-depth cost analysis and discussion between the public and the government. However, for this case study, the decision is made to designate Peacock Point – Rocky Point as the preferred location to provide the largest possible protection considered the protection range is largest, bathymetry fairly uniform and no residential areas need to be relocated.

CHAPTER 5

Development and Analysis of Concepts

CHAPTER 5 DEVELOPMENT AND ANALYSIS OF CONCEPTS	34
CHAPTER 5 ABSTRACT	34
5.1 CONCEPTUAL DESIGN 1: THE SEGMENT BARRIER	35
5.1.1 Introduction	35
5.1.2 Expandability of the barrier	36
5.1.3 Geometry	36
5.2 CONCEPTUAL DESIGN 2: RISING TOWER BARRIER	37
5.2.1 Introduction	37
5.2.2 Tower parts	37
5.3 CONCEPTUAL DESIGN 3: THE RISING WALL BARRIER	39
5.4 CONCEPTUAL DESIGN 4: THE HORIZONTAL SLIDING BARRIER	42
5.5 CONCEPTUAL DESIGN 5: FLAP GATE	44
5.6 CONCEPTUAL DESIGN 6: FLOATING SECTOR GATE	45
5.7 CONCEPTUAL DESIGN 7: LIFT GATE	46
5.8 VERIFICATION OF CONCEPTS	47
5.9 EVALUATION OF THE CONCEPTS	48
5.9.1 Multiple-criteria decision analysis	48
5.9.2 Evaluation criteria	48
5.9.3 Weight Factors	49
5.9.4 MCA results	50
5.9.5 MCA Conclusions	52
5.9.6 Final Choice	52

Chapter 5 Abstract

In this chapter the reader is presented with four original conceptual designs for storm surge barriers in sections 5.1-4. What makes them fundamentally different from existing concepts are the ways in which they can be expanded over time to deal with rising sea levels, i.e., increase of the overall structure height and width. The concepts presented in section 5.2-4 are complementary to the horizontal rolling and vertical rising type gates (Appendix F). These four concepts require a more elaborate description to better convey certain unique aspects of a design. In this chapter the concepts are designed independently from the case study area. In addition, three existing concepts are also discussed as possible protection alternatives. This chapter closes with a multiple-criteria decision analysis (MCA) in combination with technical reasoning to determine which alternative will be designed in further detail.

5.1 Conceptual Design 1: The Segment barrier

5.1.1 Introduction

The Segment barrier is an original concept for a storm surge barrier that is reconstructable and can function as a temporary or permanent barrier. The focus lies on expandability in time and a simple construction process. The barrier consists of segments which can be pieced together in horizontal and vertical direction. There is a strong focus on prefabrication for the ultimate goal of this concept is to have the entire barrier (or parts of it) be assembled and dismantled in a matter of days before the arrival of a storm surge. For example, the Segment barrier can be partly built to allow for additional navigation space, marine life crossing or tidal flow space, and be closed off in the advent of a storm surge. The concept is presented in Figures 5.1-2.

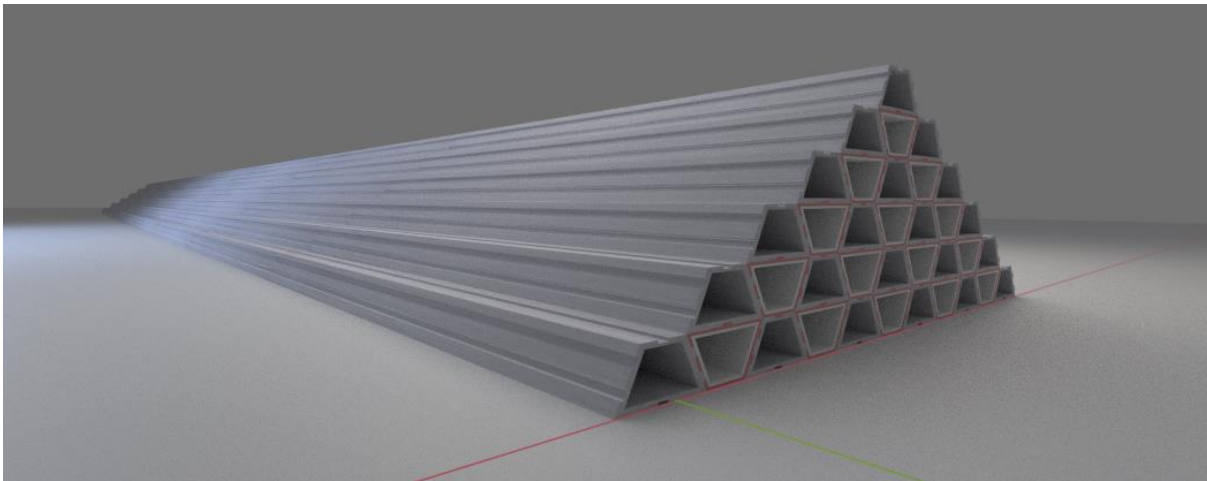


Figure 5.1 | The Segment barrier concept, cross-section.



Figure 5.2 | The Segment Barrier, side view.

A completely closed barrier is reminiscent of a classic earthen dike. This is a standard pyramid configuration in which the segments precisely align in the 'stack bond' pattern (section 6.2.6) and separates two bodies of water. In principle, this structure can have a permanent or a modular character. To what extent the barrier can already be constructed in advance of an incoming storm surge depends on the details of the design.

5.1.2 Expandability of the barrier

The main components that make up the barrier are segments which can be pieced together in both horizontal and vertical direction. The barrier can be applied in a number of ways, for example, areas only affected by sea level rise – and negligible wave loads – may desire a barrier for which the dominant input parameter is sea level rise. This would lead to the development of a segment with different characteristics, e.g., related to thickness or configuration, in contrast to a location which is dominated by periodic heavy or extreme storm surges. Naturally, this location would need a barrier configuration which can withstand the impact of frequent storm surge waves. Increasing the height of the barrier could even be a temporary solution if needed to protect against larger than expected storm surges. For example, if it is decided by the authorities that a barrier should increase in height by one segment, an entirely new row of segments could be fabricated or possibly an already existing row of segments could be temporarily dismantled and reassembled on top of the barrier. A study on the applicability of this concept in other areas is outside the scope of this thesis, however, the potential is noteworthy.

There are multiple reasons why authorities might consider changing the barrier:

- New research and insights predicting higher future water levels and more severe storms.
- The local inhabitants might view the barrier as visual pollution.
- The negative impact on the environment and ecology is greater than expected.
- The dynamics between (excess) river runoffs and tides require a different configuration, e.g., more or less flow space.

A uniform barrier is advantageous for construction workers tasked with assembling the barrier on site. Having the barrier consists of as few unique segments as possible is expected to result in a construction process that relies heavily on repetition which would make the assembling and dismantling process fast and familiar. Expansion in horizontal direction – the overall width – is also possible, which would increase the overall stability. It could also be necessary to expand the width of the structure to provide added support if the height needs to increase. Another reason for horizontal expansion could be to provide space for road and rail infrastructure.

5.1.3 Geometry

At the core of this concept lies the geometrical shape of the segments. Details on the geometry can be found in Appendix A. A number of geometrical shapes can be combined into a barrier as long as these shapes have a high degree of natural stability, meaning that on its own it the shape should have a large resistance against rotation about its axis. Circles are inadequate, squares are possible, however, the most stable natural geometry is a triangle. The geometry of choice is a trapezium. The advantages being a flat top over which segments can slide or directly stacked on top of each other. Moreover, using a triangle would require more material than a trapezium. There are a number of advantages and challenges regarding a trapezium, for example, the shape would make for a highly stable structure with a wide base and shorter top length which is advantageous, at the same time a trapezium scales unevenly, i.e., the diagonal sides thicken at a faster rate than the parallel base and top sides. A shape with unevenly thick sides has different strength properties and complicates the design even further. The mathematical derivation for this scaling problem is presented in Appendix A.

5.2 Conceptual Design 2: Rising Tower barrier

5.2.1 Introduction

The Rising Tower barrier rises from the channel floor and separates two bodies of water when fully extended. Vertical rising type structures (Appendix F) are deemed to be challenging from a maintenance perspective (USACE et al., 2019b, p. 112) since most of the structure remains submerged throughout its design life cycle. Therefore, maintenance is prioritized in this design.

5.2.2 Tower parts

Traditionally, these gates rise out of a deep gate housing which is undesired, therefore, an original rising gate design is proposed. Figure 5.3 shows a part of the barrier in open and closed position. In this example the length of one piston can be reduced by 80 percent in closed position (e.g., using a 4-stage hydraulic cylinder piston) leading to a closed barrier of almost half the height of the open barrier. Figure 5.3 includes scales for reference purpose.

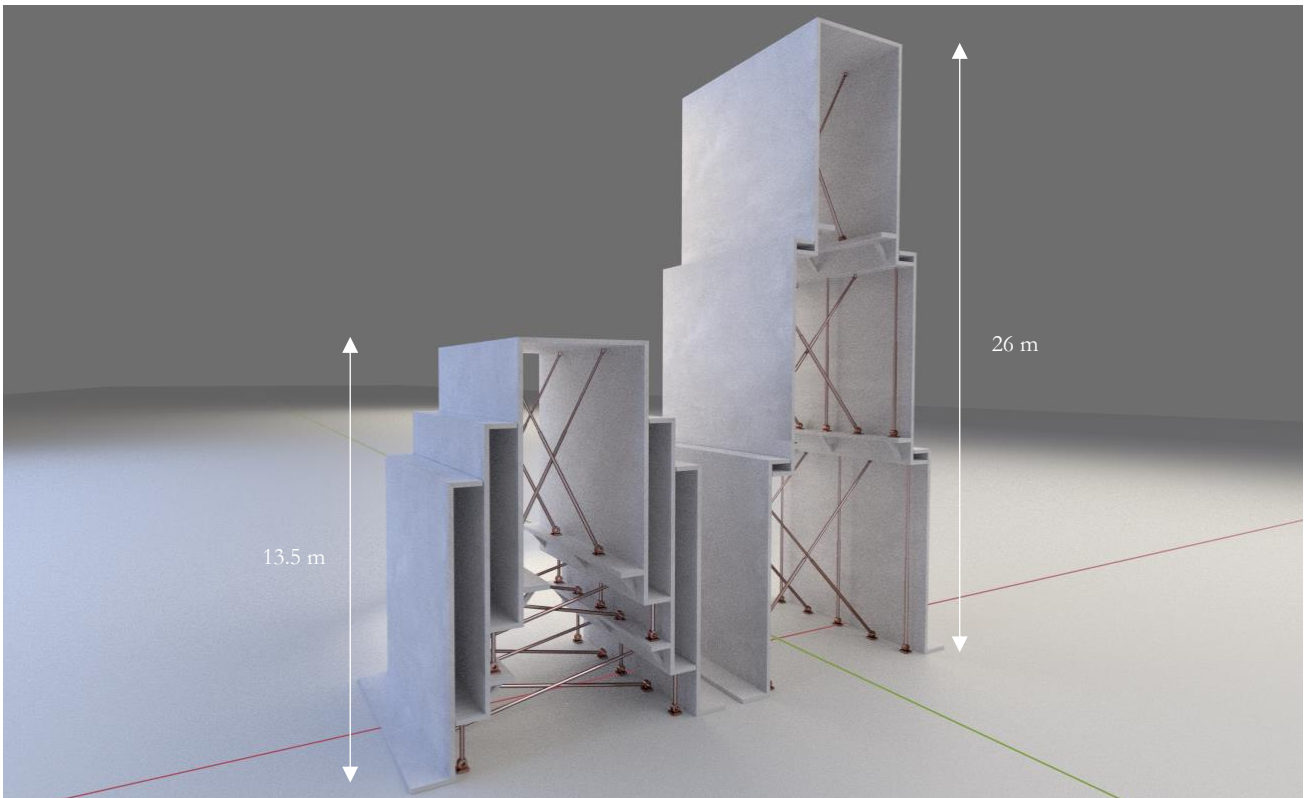


Figure 5.3 | Rising Tower barrier part in opened and closed position.

One barrier part consists of several subparts – three shown in this example – that slide along each other in vertical direction until the maximum expansion is reached. An important aspect of this design is the ability to conduct maintenance on the inside of the barrier which is spacious and contains most of the operating equipment. This means the majority of maintenance activities are carried out in a dry environment inside of the structure. Watertightness is highly prioritized and any degree of leakage will remain within tolerable levels. Hydraulic pistons are used from within the barrier for the purpose of pushing subsegments upward and providing horizontal stability. A sill provides stability for the entire gate and closes off the bottom watertight.

The examples shown in Figure 5.4 have a relatively shallow water depth, therefore a trench is dug in which the structure is housed.

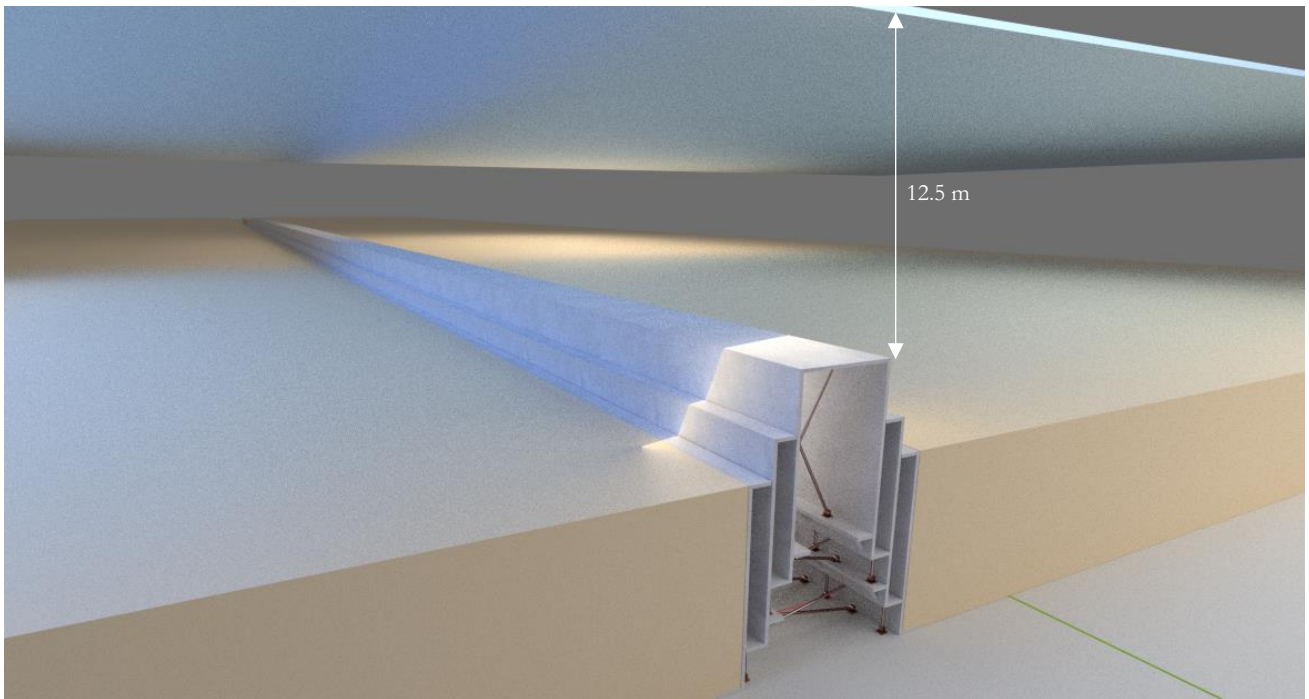


Figure 5.4 | Entranchment founded Rising Tower barrier in closed position.

In the final example presented in Figure 5.5, the structure is directly founded on the bottom of the channel and kept in place by a concrete sill which can be applied if this barrier is constructed in deeper waters and needs additional weight for stability.

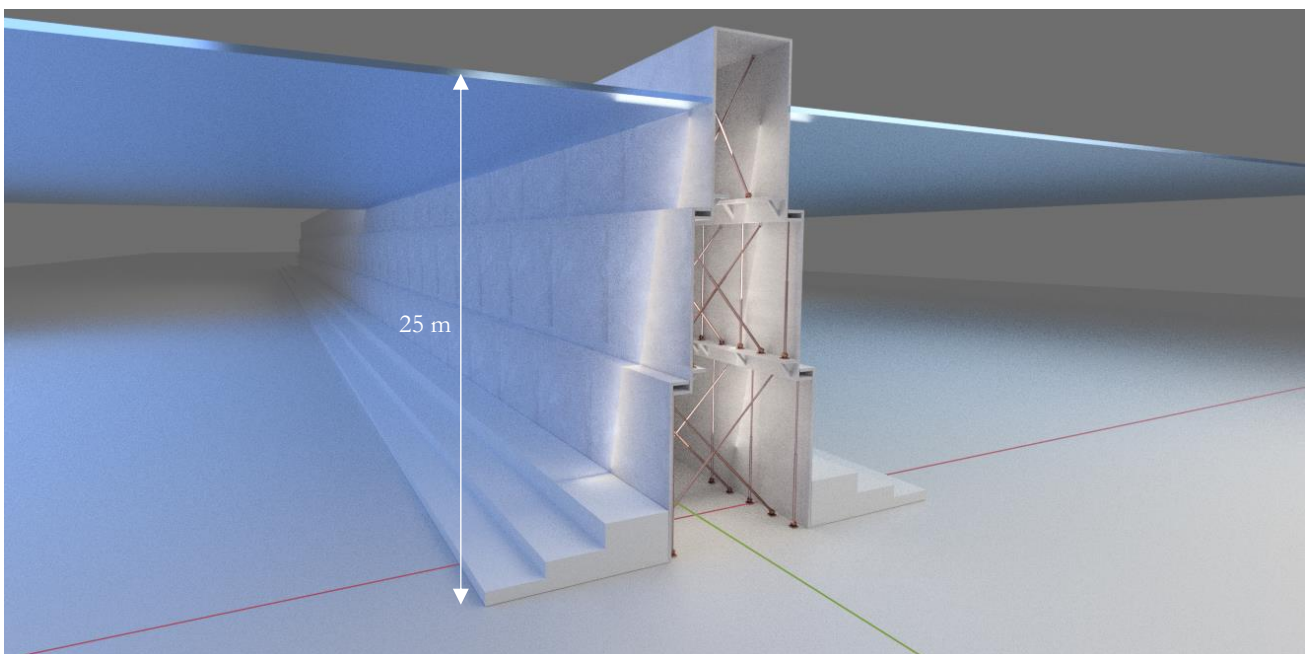


Figure 5.5 | Rising Tower barrier in deep water with a concrete sill in opened position.

5.3 Conceptual Design 3: The Rising Wall barrier

The Rising Wall barrier is a vertical rising barrier type which consist of multiple plates that slide upward along each other from a rest position at the bottom of the channel as shown in Figure 5.6 and Figure 5.7. The gates are connected to hydraulic pistons that push the plates upward and support them in horizontal direction, able to withstand tension and compression forces.

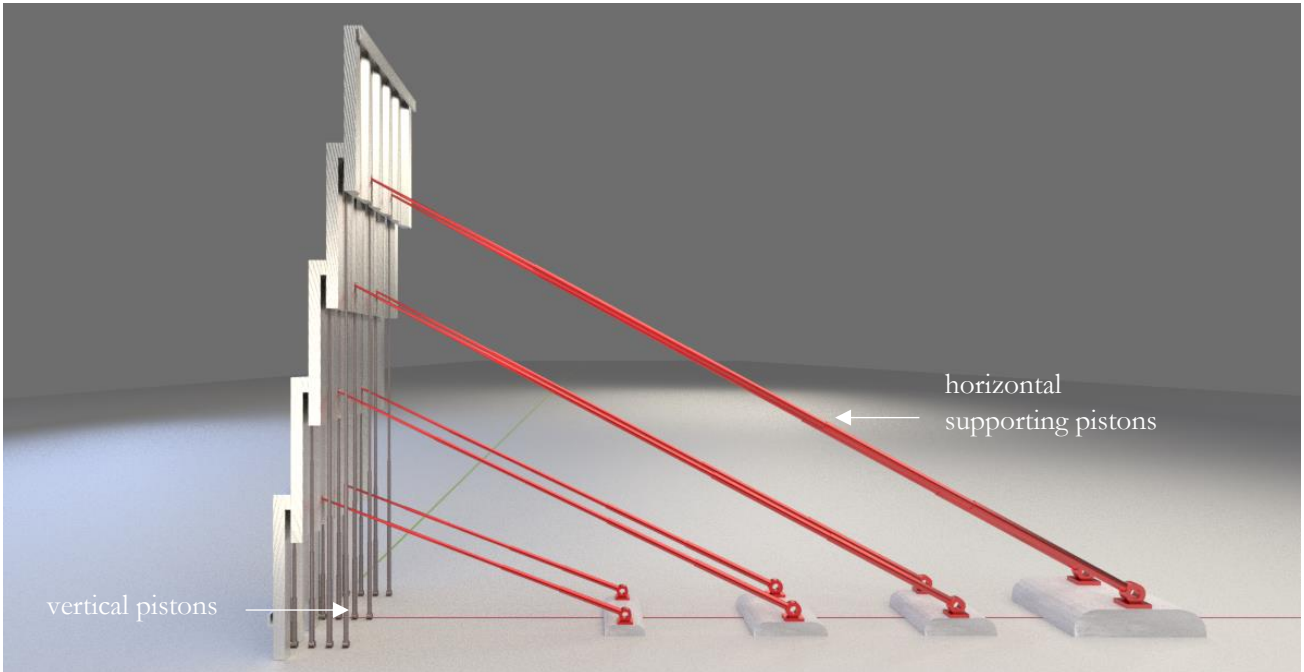


Figure 5.6 | Rising Wall barrier part in fully raised position.

A row of vertical pistons pushes a barrier plate upwards from the back. A plate is profiled so that the vertical pistons fit within that profile as shown in Figure 5.9 which is necessary to make the barrier watertight.

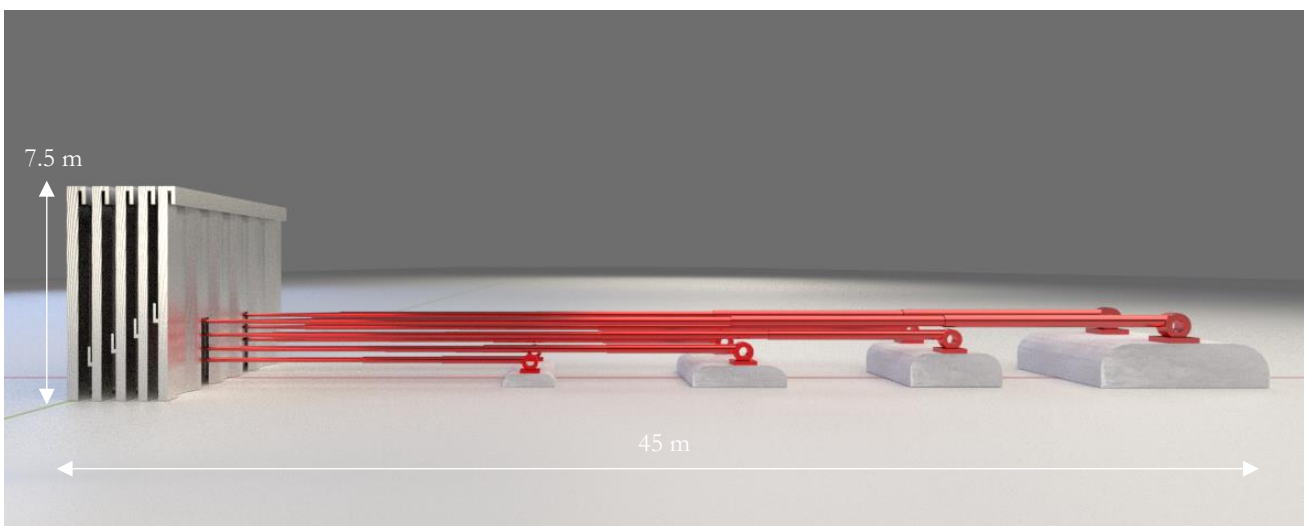


Figure 5.7 | Rising Wall barrier part in closed position.

Each gate has a number of cut-outs so that the pistons can connect to a gate. The exact number of pistons and their configurations are to be determined in a final design. Figure 5.8 shows concrete supporting blocks increasing in size as the horizontal piston length increases. When dynamically loaded the horizontal pistons are responsible for stability, transferring compression and tension forces to the concrete blocks.

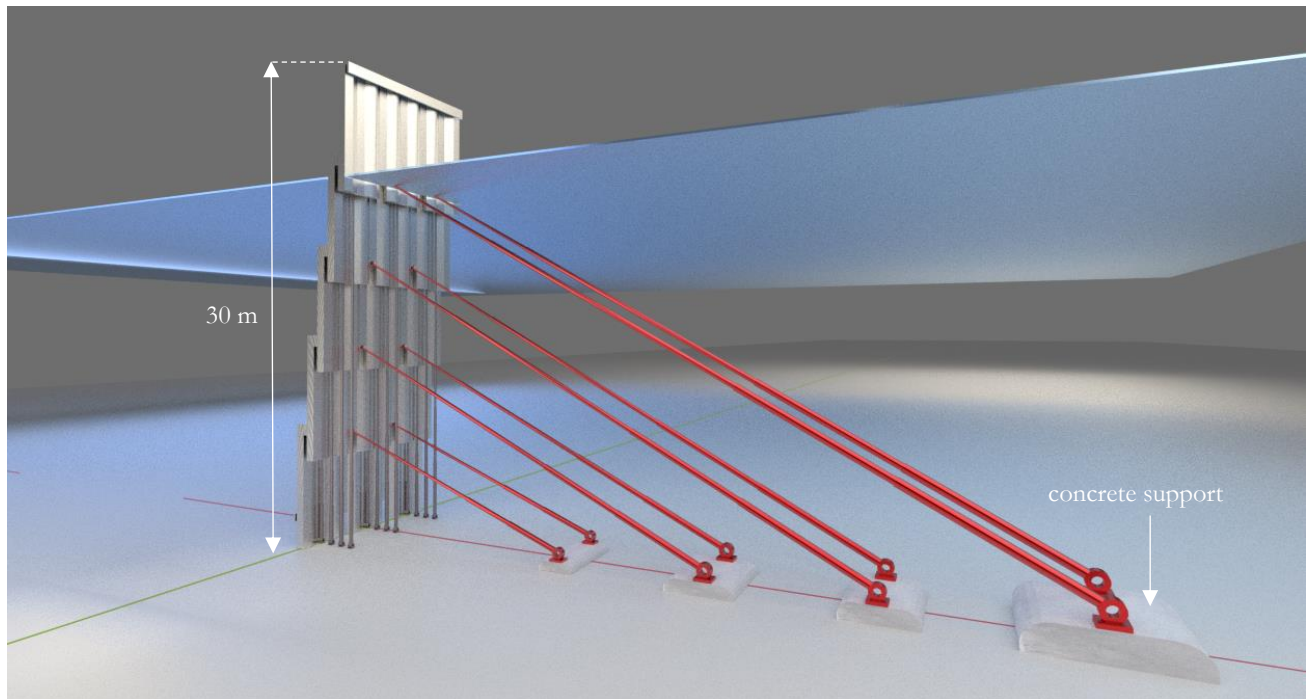


Figure 5.8 | Submerged Rising Wall barrier part.

The barrier is submerged for the majority of its life cycle; therefore, underwater maintenance is an important aspect of this alternative. Detaching the components to perform maintenance on land is possible, yet considered especially challenging. Protective measures for the horizontal supporting pistons are not shown in this phase of the design process. The horizontal pistons are especially vulnerable to collisions in raised and closed position. Vessels can damage the pistons if it is unclear where to navigate or by accidentally dropping cargo when navigation over the structure.

Figure 5.9 shows a close-up view on how these pistons connect to the gates and fit within the cut-outs. The front plate is removed to show how the grey pistons are designed to fit within the profiled shape.

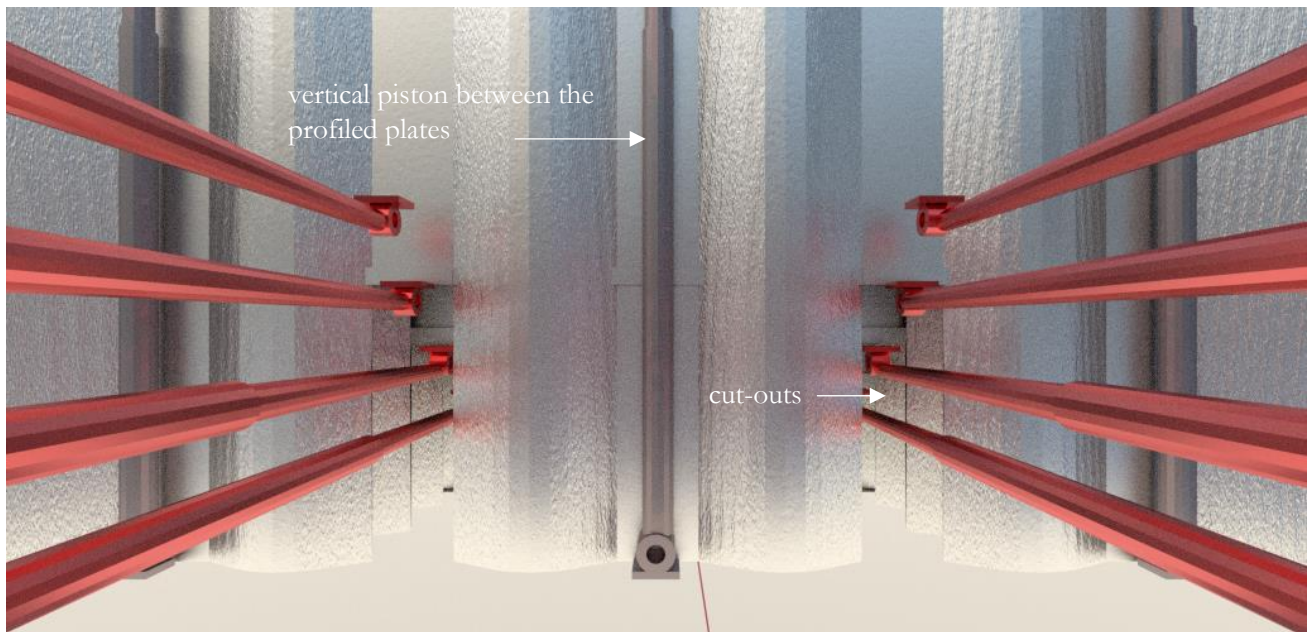


Figure 5.9 | Rising Wall barrier cut-outs with piston placements.

Finally, Figure 5.10 shows a wire frame view of Figure 5.9 and how the pistons connect behind each gate.

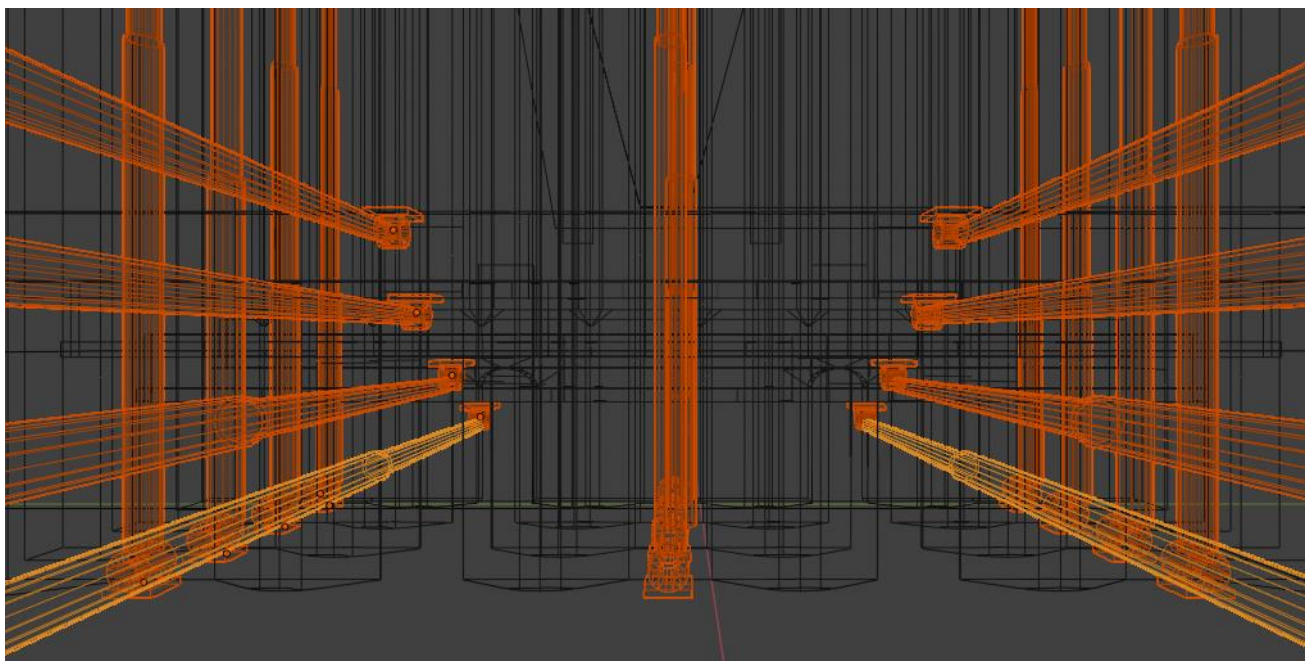


Figure 5.10 | Rising Wall barrier wire frame view.

5.4 Conceptual Design 4: The Horizontal Sliding barrier

The Horizontal Sliding barrier is a storm surge barrier type that moves horizontally from the land side dock along a bottom guiding rail. A horizontal sliding gate was deemed impractical due to the space on land required to dock the gate (USACE et al., 2019b, p. 112). An original design for a horizontal sliding gate is presented in this section to address the problem of a large docking station. Instead of one single long gate, the barrier consists of multiple shorter gates that slide along each other to close off the channel as shown in Figure 5.11 The height is included for reference purpose.

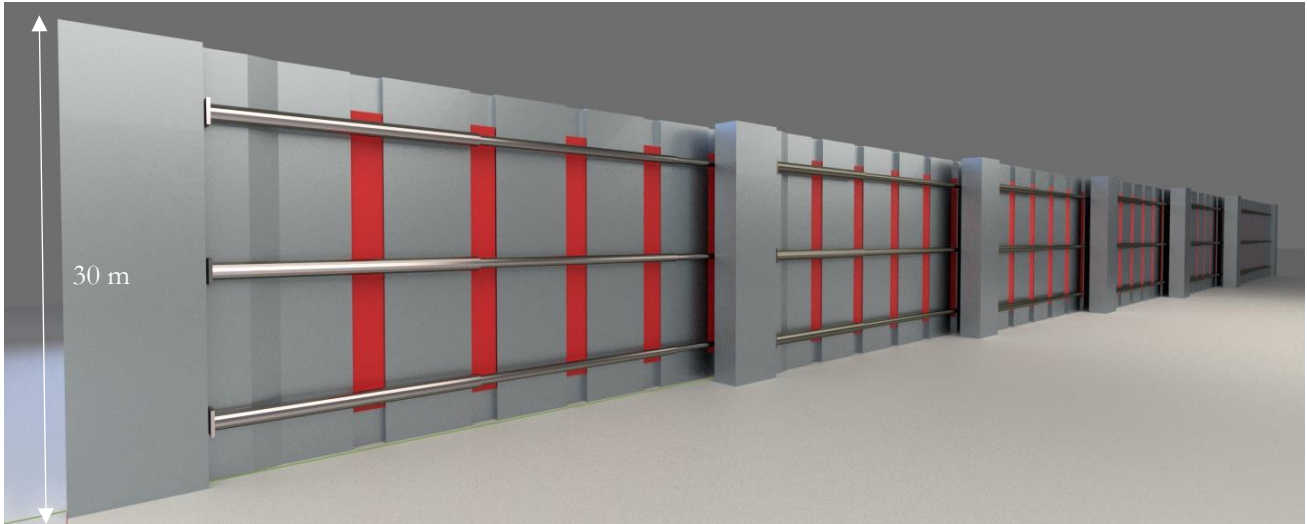


Figure 5.11 | Horizontal Sliding barrier.

Attached to each gate are movable components – red bars – that slide downwards into the foundation to provide additional support as shown in Figure 5.12.

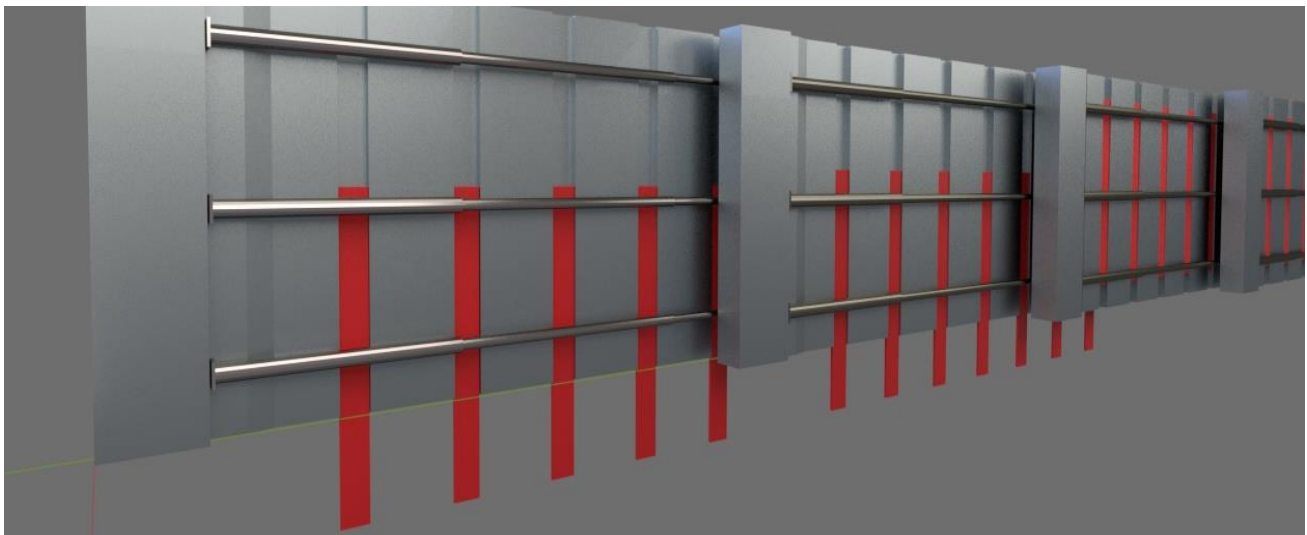


Figure 5.12 | Support bars (red) that slide in the foundation to provide extra support.

The bars will have to withstand large moments; therefore, the bars are expected to increase in thickness in a final design. The bottom foundation is specifically designed with multiple openings for each supporting bar to reside in.

Figure 5.13 shown an example of a barrier in closed position having a total length of 100 m. A conventional horizontal sliding gate would have to dock the length of a fully opened gate, approximately 400 m shown in Figure 5.14.

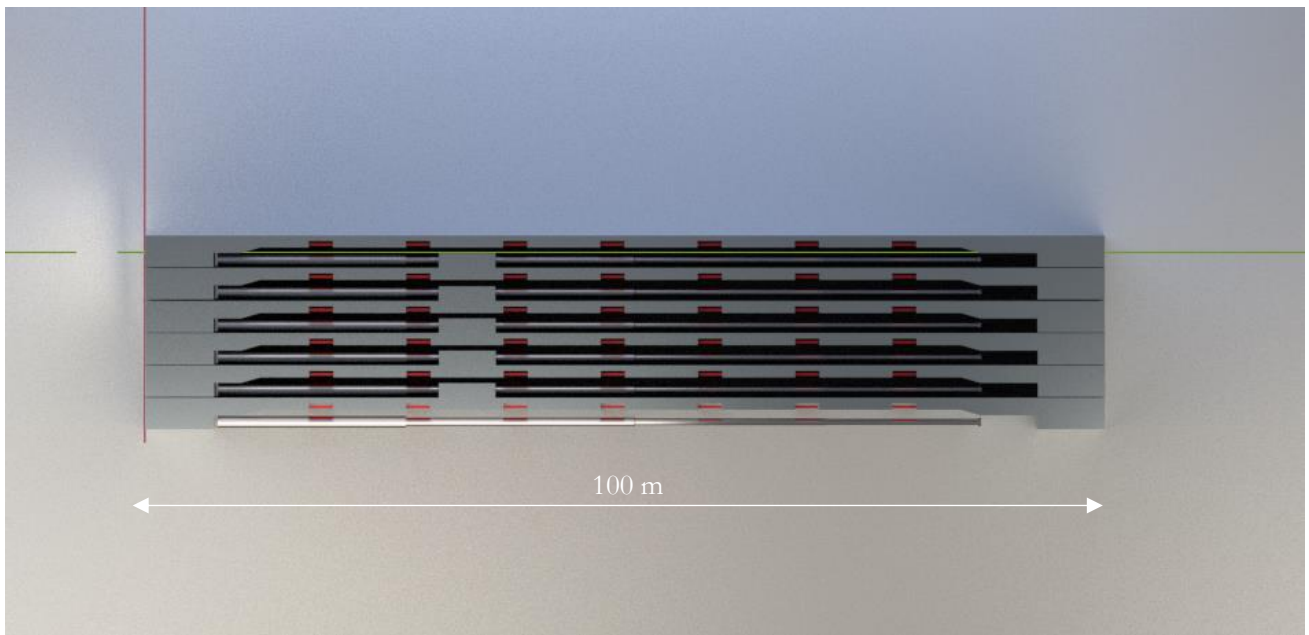


Figure 5.13 | Horizontal sliding barrier in closed position (top view).

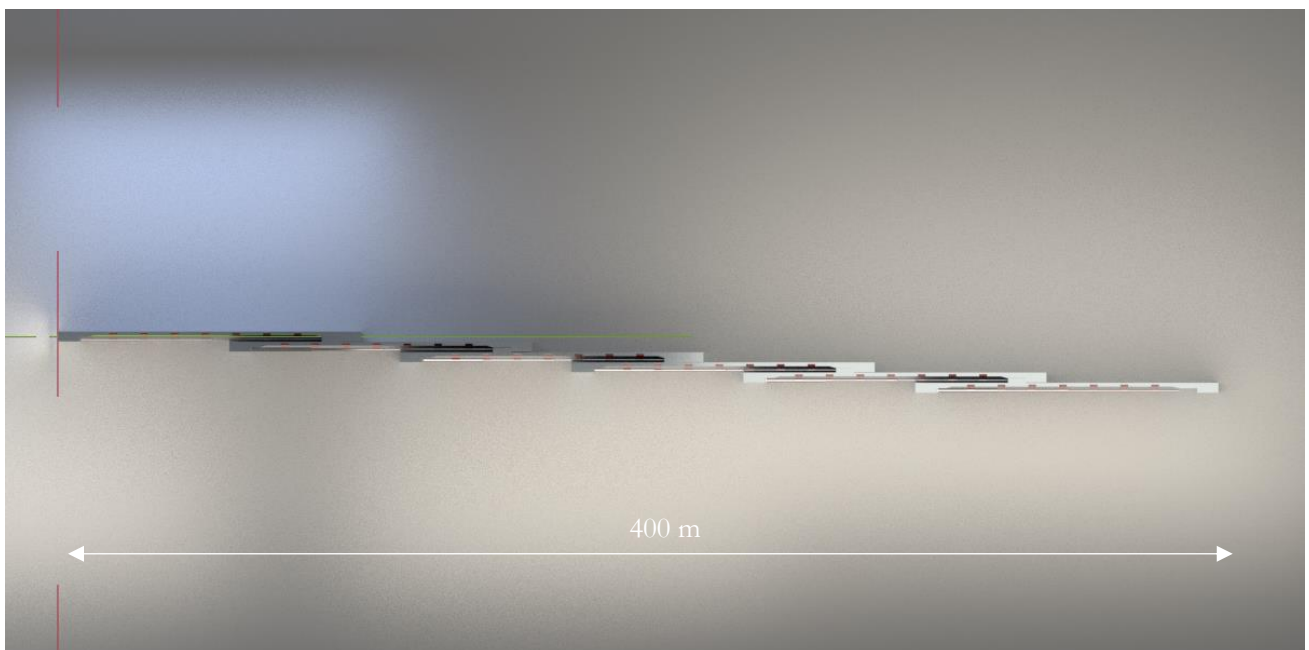


Figure 5.14 | Horizontal sliding barrier in open position (top view).

Although this is only a first conceptual design, the length reduction of the docking station can be substantial.

5.5 Conceptual Design 5: Flap gate

The flap gate is an existing design with the main components being a steel plate, hydraulic piston and rotation hinge connected to the sill. The pistons push the gate from a horizontal position upward under an angle as the gate rotates around the hinge and provide a resisting counter moment. Maintenance is challenging since most of the structure resides underwater as well as the hinges that wear off over time. The head differences that can be resisted are limited due to the large moment increase with increasing water depth which is proportional to the third power of the water depth (Bezuyen et al., p. 308). The pneumatic flap gate shown in Figure 5.15 rests in closed position with the steel gate completely filled with water. The gate rotates around a hinge due to an increasing pressure difference when water is extracted and air pumped in. The water pressure beneath the gate pushes it upwards. Pumping water in the gate causes it to move downward again (De Bakker, 2003, p. 9). Figure 5.15 summarizes the flap gate's functionality.

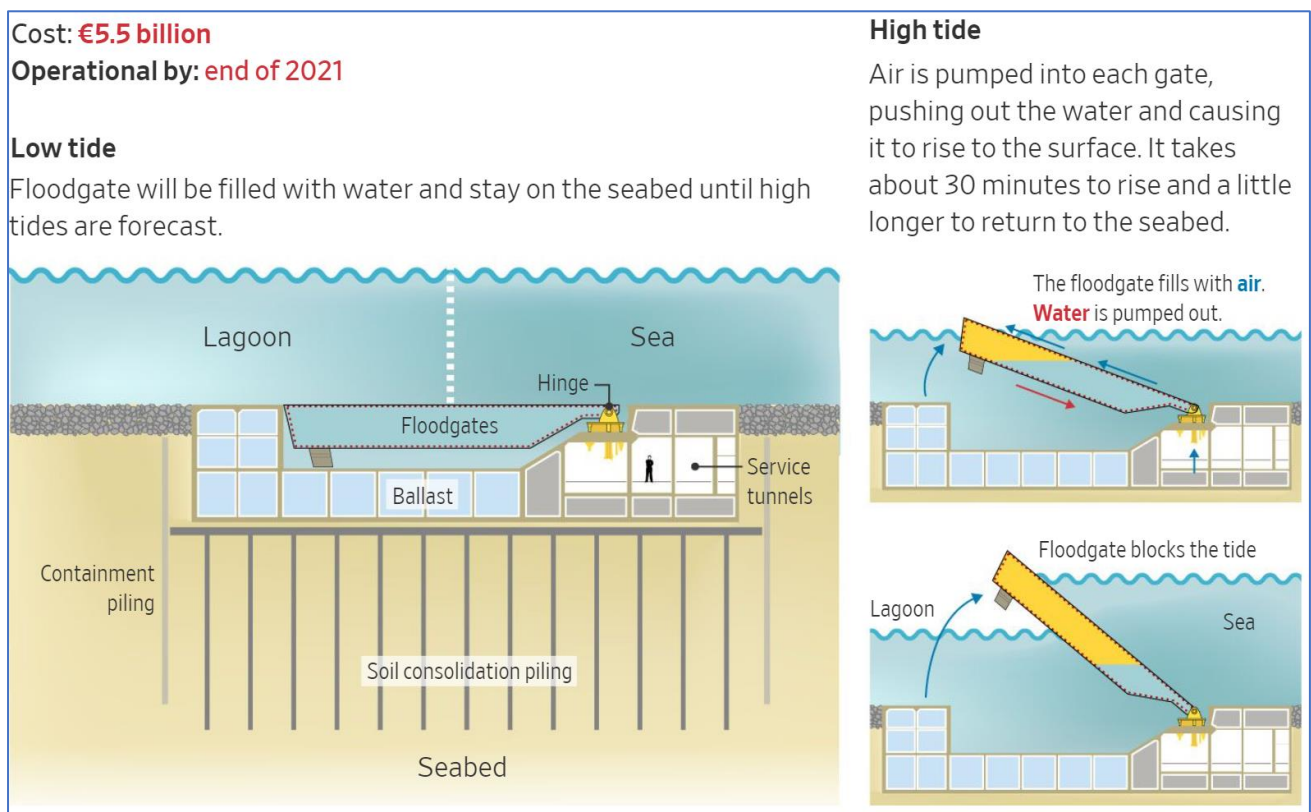


Figure 5.15 | Pneumatic flap gate, Italy (Stancati & Sylvers, 2019).

A recent example of the flap gate would be Venice's 1.6 km long Mose flood barrier project consisting of 78 flap gates and is expected to be fully operational by 2021. Each gate is 20 m wide, between 18.6 – 29.6 m in length and between 3.6 – 5 m in thickness depending on the water depth. The barriers can be fully raised in five hours. The deepest harbor mouth inlet in the lagoon is the bocca di porto di Malamocco where one part of the entire barrier project is built (Ministero delle Infrastrutture e dei Trasporti, n.d.). The main purpose of this barrier is to protect the city against high tides of up to three meters for a design period of 100 years. This concept is relatively new; therefore, lessons can be learned from the Mose flood barrier on how to improve on maintenance and the construction process if it were to be applied elsewhere. The design sea level rise scenario used for the northern Adriatic was 22 cm by 2100 which could prove to be too optimistic leaving the city unprotected after a few decades (Bastianello & Balmer, 2019).

5.6 Conceptual Design 6: Floating Sector gate

The floating sector gate consists of two gates on each land side. The steel gates are circular in shape and connect through a truss construction to a hinge from which the gates pivot along the channel. In open position the gates are floating in a dock. If the gates need to be closed, they move into position, are filled with water and sink to the bottom.

A good example of this type of barrier would be the Dutch Maeslantkering shown in Figure 5.16 located in the Nieuwe Waterweg, Zuid Holland which is part of a larger coastal protection complex designed to protect the area. Its main function is to stand in the first line of defense against ocean waves. Each gate is 200 m wide, 22 m high and 15 m thick. The gates move into position in half an hour and sink to the bottom in two hours. When inundated they reach a depth of 17 m and close of a width of 360 m. The barrier is able to withstand waves of up to 5 meters above mean water level (Rijkswaterstaat, n.d.).



Figure 5.16 | Maeslantkering, The Netherlands (Rijkswaterstaat, n.d.).

5.7 Conceptual Design 7: Lift gate

The lift gate barrier consists of multiple towers that lift the steel gates from a rest position in upward direction. The concept is similar to the USACE barrier described in section 2.4.3 with multiple auxiliary gates for tidal flows, sediment bypass and animals migrating through the barrier. There is one wider gate specifically designed for navigable passage. The Dutch Eastern Scheldt storm surge barrier shown in Figure 5.17 is an example of a lift gate type barrier applied on a large scale. The largest gate has a height of 12 m, length 42 m and weighs about 480 ton. It takes 82 minutes to close the barrier (Rijkswaterstaat, n.d.).



Figure 5.17 | Eastern Scheldt storm surge barrier, The Netherlands (Watersnoodmuseum, n.d.).

5.8 Verification of concepts

This section provides a preliminary analysis on the degree to which the concepts fulfil the functional requirements (section 3.1).

F1 – the barrier is designed with a service life of 100 years.

All concepts apply the necessary materials regarding steel structural classes and concrete thicknesses that guarantee a service life of 100 years. Whether all concepts can withstand the load increases due to severe storms over this period of time cannot be concluded at this stage.

F2 – the barrier is able to adapt to different sea level rise scenarios, including the most extreme estimation.

The segment, rising tower, horizontal sliding and vertical rising barriers are expected to be able to adapt to rising sea levels by adding segments or replacing the steel gates with larger gates. This is difficult for the flap gate as it rises from a fixed concrete casing. However, design adjustments can be made to allow the gates to be replaced with larger gates and create concrete casings that can house these larger gates. The supporting trusses and hinges of the floating sector gate require a design that allows for the addition of higher front plates when required. The same applies to the lift gate, if the design allows for the replacement of the gates with larger ones, various sea level rise scenarios can be dealt with. In general, it is expected to be possible to adjust the flap gate, lift gate and floating sector gate to deal with the long-term effects of sea-level rise, but requires a design from the ground up, therefore, it is not possible to verify this requirement without further detailed design for all concepts.

F3 – the minimum navigation width is 140 m and depth 12.2 m (Table 2.2).

The water depth and width of Long Island Sound are large enough to fulfill these requirements for all concepts.

F4 – the navigable sections of the barrier are able to close at least once per year.

Every year at least one hurricane migrates towards the eastern coast of the United States, therefore, all navigable passages for each concept are able to close at least once per year.

F5 – the navigational sections of the barrier are designed to close within one day.

Each concept's navigable spaces are expected to close within this time frame (sections 5.5-7).

5.9 Evaluation of the concepts

5.9.1 Multiple-criteria decision analysis

This section evaluates the concepts based on a multiple-criteria decision analysis (MCA) and technical reasoning. The multiple-criteria decision analysis (MCA) is a tool designed to help assess which alternative barrier is the best candidate. Historically, cost-benefit analyses have not shown to cover the full scope of relevant (side)effects of civil engineering projects. The idea is to also take into account nonmonetary comparison criteria (Beheshti, 1999, p. 194). To achieve this an evaluation matrix is used in which the vertical axis represents the criteria and horizontal axis the alternatives. It should be noted that the MCA only has a supporting role in the decision-making process and does not overrule a designer judgement.

5.9.2 Evaluation criteria

The evaluation criteria in this section are not based on structural or reliability comparisons. It is noted that thorough comparison on the structural integrity and failure probability of each alternative is essential for a complete analysis. The costs are indirectly related to most criteria, however, at this stage of the design it is not possible to obtain meaningful or reliable cost estimations. For this reason, a cost analysis is only made for the final conceptual design (section 7.3).

Criterion 1: The degree to which a barrier is adaptable

The current climate crisis is leading to an increase in global sea level rise, more severe and possibly frequent storms (section 3.2.2). As a consequence, there could be a desire to change, or modify the barrier over time to cope with changing environmental conditions. Some of the concepts are specifically designed with the ability to be modified based on changing circumstances, e.g., storm surges, sea level rise or navigation purposes. To what extent a structure can be modified relates to, for example: scalability of the structure, i.e., increase in size. Some parts of the structures are permanently fixed and cannot be changed or easily modified. Another example is the ability to change parts of the structure, e.g., install larger gates or replace damaged components.

Criterion 2: The degree to which the cross-section of channel is blocked

This criterion refers to the degree to which the barrier blocks the entire channel, thus impacting navigation for vessels and marine life. Furthermore, the presence of the barrier has an impact on local accelerations and decelerations of flows. These changes in flow patterns can lead to erosion or accretion of the bathymetry thus affecting the local water depths.

Criterion 3: The degree to which the environment is impacted

The barrier can impact the tidal flow due to a reduction in flow space. Furthermore, the funnel shape of West Sound can lead to an increase of the storm surge wave amplitude, caused by energy convergence due to width restrictions. Depending on the location, additional research will have to prove whether reflected waves pose a realistic threat to the coastlines. Another concern is upstream sewer overflow or chemical wastewater being blocked by the barriers. Fresh water should be allowed to flow in and out when necessary. Marine life which inhabits the area can experience difficulties when crossing the barrier. The negative impact on flora and fauna needs to be minimized and the applicability of compensating nature should be researched in further detail. Another important environmental impact is the way in which sediment transportation is affected. Sediment transportation is beyond the scope of this thesis for it requires extensive research and a solution in the form of a sediment bypass system. Finally, every civil engineering project generates pollution which is strongly linked to the duration of the construction project and materials being used. Measures to minimize pollution are presented in section 8.2.

Criterion 4: Integration into the environment

The visual quality of a structure is often underprioritized in civil engineering, however, the integration into the environment is very important for the end result. Although the focus is on creating alternatives that fulfill the design requirements, the importance of environmental integration is recognized in this thesis. The barriers should not only fulfill their technical and functional requirements but also inspire to a certain extent. This could boost tourism and increase recreational value for the area. A visually appealing structure could also receive more public support. Examples of environmental integrations are general color schemes, material usage and the overall geometry. The greys of concrete are often not regarded as having a positive effect on people their emotion in contrast to the greens of grass. If solutions such as these can be implemented in the final design, they will be considered.

Criterion 5: Maintenance

The amount of maintenance varies based on the complexity and scale of the barrier. If possible, limiting the number of structural components that need maintenance, e.g., connecting parts (screws, nuts and bolt) would be advantageous. The exposure to environmental conditions such as salt water, (acidic) precipitation and heat need to be taken into account. Another maintenance category is cleaning, making sure the structure as a whole maintains its visual quality which is categorized separately from technical maintenance, i.e., keeping machinery and mechanical moving parts in good condition. Another complicating factor is the barrier's overall geometry. A geometric complex structure with many edged and corners makes it harder to physically reach the entire structure.

Criterion 6: Suitability of a barrier for large distances

Some barrier types are more complicated to construct for larger channel widths, because they could become too large, complex or require many subcomponents.

5.9.3 Weight Factors

The matrix method is used to give weight to the evaluation criteria and asks which criterion is considered more important by the designer, i.e., the one on the horizontal or vertical axis. If the criterion on the vertical axis is considered more important than the horizontal axis criterion, the matrix space is given a value of '1'. If the horizontal criterion is considered more important than the vertical criterion, the shared space is marked with '0'. Horizontal summation gives the importance of the criterion. If it is unclear which criterion is prioritized, the input is '1' (Beheshti, 1999, p. 220). Table 5.1 summarizes the weight factors.

Criteria	The degree to which a barrier is adaptable	The degree to which navigation is impacted	The degree to which the environment is impacted	Integration into the environment	Maintenance	Suitability of a barrier for large distances	Total (Σ horz.)	Weight Factor
The degree to which a barrier is adaptable	1	0	0	0	0	0	2	0.13
The degree to which the cross-section of the channel is blocked.	0	1	0	0	0	0	2	0.13
The degree to which the environment is impacted	0	0	1	0	0	0	3	0.20
Integration into the environment	0	0	0	1	0	0	0	0.00
Maintenance	1	1	0	0	1	0	3	0.20
Suitability of a barrier for large distances	1	1	1	1	1	1	5	0.33

Table 5.1 | MCA weight factors.

Table 5.2 lists the importance of each criterion based on the weight factors of Table 5.1.

Priority level	Criteria	Description
1	Suitability of a barrier for large distances.	Some barrier types might not be ideal for large distances due to technical or practical reasons.
2	Maintenance.	Minimal maintenance would reduce cost and exposure to possible dangerous situation. The aim is to simplify this process and reduce the structural components that require maintenance.
	The degree to which the environment is impacted.	The environmental impact on the short- and long-term needs extensive research in order to provide a meaningful assessment. At this stage in the design, there is no way of measuring the impact.
3	The degree to which the cross-section of the channel is blocked.	Any blockage of the channel has a direct impact on navigation and economic activity. To what extent the economy is dependent on the navigational space of West Sound requires further research.
	The degree to which a barrier is adaptable.	One of the main goals is for the barrier to be able to adapt to environmental conditions, e.g., sea level rise, storm surge frequency and possibly even infrastructural demands.
4	Integration into the environment.	Although the importance of environmental integration is recognized, functionality is prioritized.

Table 5.2 | Priority list for the evaluation criteria.

5.9.4 MCA results

Table 5.3 shows the input values and results of the MCA analysis. The input values are based on a ‘5-scale’ scoring ladder in which ‘5’ is considered ideal, ‘3’ neutral and ‘0’ insufficient.

Criteria \ Concepts	Weight Factor (f)	Concept 1 Segment barrier	Concept 2 Rising Tower barrier	Concept 3 Rising Wall barrier	Concept 4 Horizontal Sliding barrier	Concept 5 Flap gate	Concept 6 Floating Sector gate	Concept 7 Lift gate
The degree to which a barrier is adaptable	0.13	5	4	0	4	0	1	0
The degree to which the cross-section of the channel is blocked.	0.13	3	4	4	3	4	3	2
The degree to which the environment is impacted	0.20	2	5	5	5	5	5	3
Integration into the environment	0.00	4	0	0	4	0	5	4
Maintenance	0.20	4	2	1	3	1	5	3
Suitability of a barrier for large distances	0.33	5	2	0	2	2	1	5
Sum (Σ)		23	17	10	21	12	20	17
MCA score (Σ x f)		3.9	3.1	1.7	3.2	2.4	2.9	3.1

Table 5.3 | MCA scores.

Motivation for criterion 1: The degree to which a barrier is adaptable

Adaptability generally refers to increasing the overall size of a structure due to an increase in storm surge severity. Adaptability is a key design objective for the Segment barrier. This is the most flexible alternative. In docked position, the Horizontal Sliding gates can be replaced or modified, e.g., higher or longer gates if required. The Rising Tower barrier, Rising Wall barrier and flap gate are permanently submerged which makes any modification of the structure more challenging. There is however still a possibility to increase the height of the rising tower gate by adding an additional tower on top of the structure. The flap gates are difficult to increase in size because the gate housing is specifically dimensioned to fit the steel gates. It is undesirable to adjust the height of a floating sector gate for this affects buoyancy and causes additional moments that have to be carried by the truss – which cannot be modified – and the hinge. The lift barrier is considered insufficiently adaptable compared to the other alternatives. The dimensions of the towers are fixed, therefore, no changes in gate width can be made. Increasing the gate height leads to extra forces and moment on the lift tower which is undesirable.

Motivation for criterion 2: The degree to which the cross-section of channel is blocked.

In open position, the Horizontal sliding barrier and floating sector gate leave a channel's cross-section completely unhindered. However, it remains to be seen how these two barriers types can be fitted over the entire span. Intermediate Islands are most likely needed. The Rising Tower barrier, Rising Wall barrier and Flap gate provide sufficient clearance depth, however, their height above the channel floor could result in undesired flow accelerations. The Segment barrier and lift gate are expected to permanently block larger portions of the channel (for large barrier lengths), thus scoring lower. Furthermore, lift gates in open position restrain the maximum vessel height which is undesirable.

Motivation for criterion 3: Impact on the environment

For this criterion the construction is not taken into account. What is mainly considered is to what degree the blockage of the channel's cross-section has an effect on the possibility of collecting wastewater, sedimentation and ability for animals to cross the barrier. The Segment barrier and lift gate permanently block a portion of the channel cross-section. The lift gate however uses auxiliary gates that is expected to let more water flow through compared to the Segment barrier, thus scores slightly higher.

Motivation for criterion 4: Integration into the environment

The Segment barrier, floating sector and lift gates are the only structures with recreational value since they are prominently visible to the public. The other alternatives are below the water surface level or in docked position, therefore (mostly) out of site.

Motivation for criterion 5: Maintenance

Maintenance is difficult for permanently submerged parts of a structure. The Rising Wall barrier consists of many submerged supporting rods spread out over a large area. The Rising Tower barrier has the majority of its operating components inside of the structure in a dry environment. The Horizontal Sliding gates can be maintained in the dry when docked, however it can be difficult to reach certain parts of the structure due to its compact design and should most likely be dismantled. The Segment barrier can be dismantled and inspected on land or on a vessel, however, this could be very time consuming. Maintenance of the floating sector gates can be done on land, thus scores highest. The steel lift gates can be maintained in raised position above the water surface level; however, the submerged concrete pillars are expected to be more challenging and requires specialized divers.

Motivation for criterion 6: Suitability for large distances

The Segment barrier and lift gates are ideal for large distances. These concepts are less dependent on the distances to the shorelines and can repeat the same construction patterns no matter how large the channel distance. The Rising Wall gate depends on many supporting rods, failure of one of these components is likely difficult to resolve. The longer the channel span, the more impractical this design becomes. The same applies for the flap gate, a longer distance requires more gates, thus increasing the possible failure rate. The Horizontal sliding barrier, Rising Tower barrier and sector gate could be used for such a large distance, but would require multiple barriers and intermediate islands to close of the channel.

5.9.5 MCA Conclusions

It should be repeated that the MCA analysis is a tool to inform the designer on the desirability of the various concepts and not a pure decision-making tool. The lift gate is one of the overall highest scoring concepts, however, the air clearance should be unrestricted for navigation purpose, making the lift gate undesirable. The fact that the Rising Wall barrier is not deemed suitable for large distances and inability to easily adapt weighs heavy on its final score. This alternative is too vulnerable because of the many mechanically driven pistons with a strong dependency on each other in order for the gates to open and close properly. Preliminary tests for the flap gate in Venice have shown the barrier to be effective at blocking flood waves, however, parts of the structure are already rusting and maintenance costs are expected to be higher than originally planned (Bastianello & Balmer, 2019). Moreover, the flap gate is considered undesirable for large distances because of the many independent gates and mechanically driven component. Both the Rising Tower and Horizontal Sliding barrier do not consist of many subcomponents compared to the flap gate or Rising Wall barrier, which makes them more desirable options. However, they cannot be standalone structures and need intermediate island to fully close off the channel.

5.9.6 Final Choice

Based on the MCA and technical judgement, the final decision is made to further advance the concept of the Segment barrier. It should be noted that other concepts could well provide solutions against flooding, however, based on technical judgement, the Segment barrier is considered to be the concept with the most potential due to its high degree of geometric flexibility, optimization and (relative) independence from mechanically driven parts.

CHAPTER 6

Barrier Configurations

Contents

CHAPTER 6 BARRIER CONFIGURATIONS	53
<u>CHAPTER 6 ABSTRACT</u>	53
6.1 INTRODUCTION	54
6.2 CONSTRUCTION PROCESS	56
6.2.1 Barrier layout	56
6.2.2 Shoreline connections	59
6.2.3 Transport of heavy equipment	60
6.2.4 Foundation	63
6.2.5 Cross-section assembling	64
6.2.6 Watertightness	65

Chapter 6 Abstract

This chapter analyses how the segments are assembled to form a barrier and how this can be applied to the locations of this case study area. Considering the highly iterative nature of the design process, the reader is presented with a number of design choices throughout this chapter that were part of the decision-making process on the final conceptual design. Section 6.1 introduces the final Segment barrier design including the barrier layout for the preferred location. Section 6.2 analysis the basic barrier layout options and how these would be implemented for other locations in Long Island Sound. Comparisons are then made between the three locations to provide an estimation on the time it takes to assemble the barrier. The remaining subsections consider multiple options for transportation, number and size of the segments, foundation, construction sequence and watertight solutions.

6.1 Introduction

The Segment barrier is a conceptual design for a storm surge barrier consisting of multiple individual prestressed concrete units that can be assembled by placing one segment on top of another in various configurations to form a complete barrier. The Segment barrier is primarily designed as a temporary structure, meaning it can be assembled before the advent of a storm surge and removed afterwards. Constructing a temporary barrier is expected to have minimal impact on the (local) ecology, flow speeds, navigation for vessels and marine life and accretion or erosion of sediment due to its temporary nature compared to a permanent barrier. However, the barrier can equally function as a permanent structure. Figure 6.1 shows a portion of the Segment barrier designed to withstand storm surges similar to those during Hurricane Sandy.

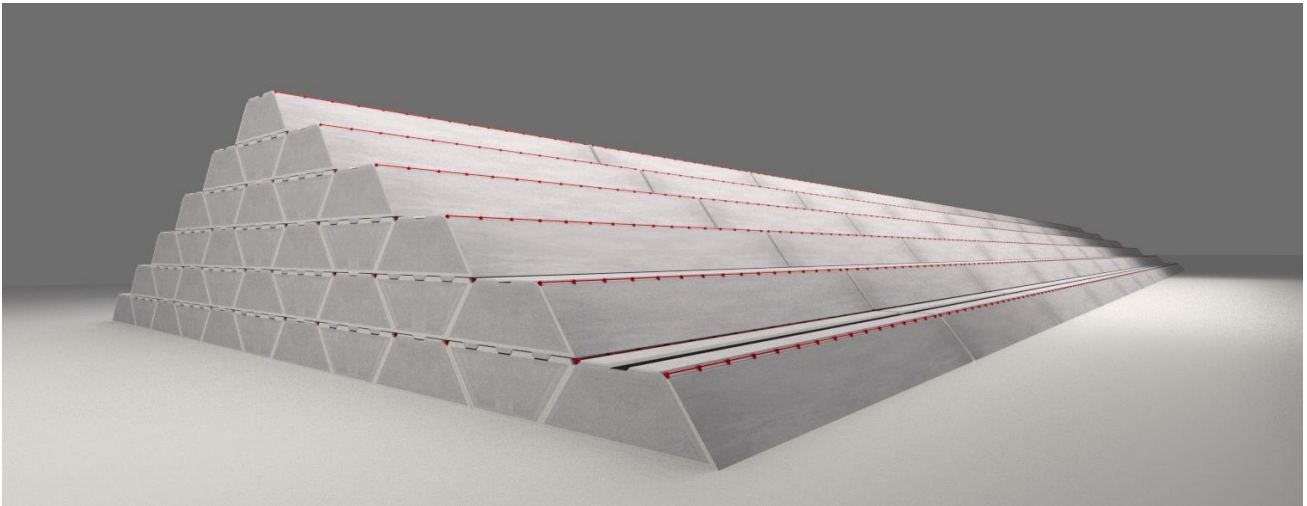


Figure 6.1 | A Segment barrier section designed to withstand forces similar to Hurricane Sandy.

These segments are designed to be used as *dam sections* or *gate sections* in. The degree to which it is feasible for the barrier to function as a temporary or permanent structure is primarily dependent on the total length and available lifting vessels that determine how long it takes to assemble the structure. Long Island Sound serves as a case study for this concept. The barrier layout for the preferred location is shown in Figure 6.2.

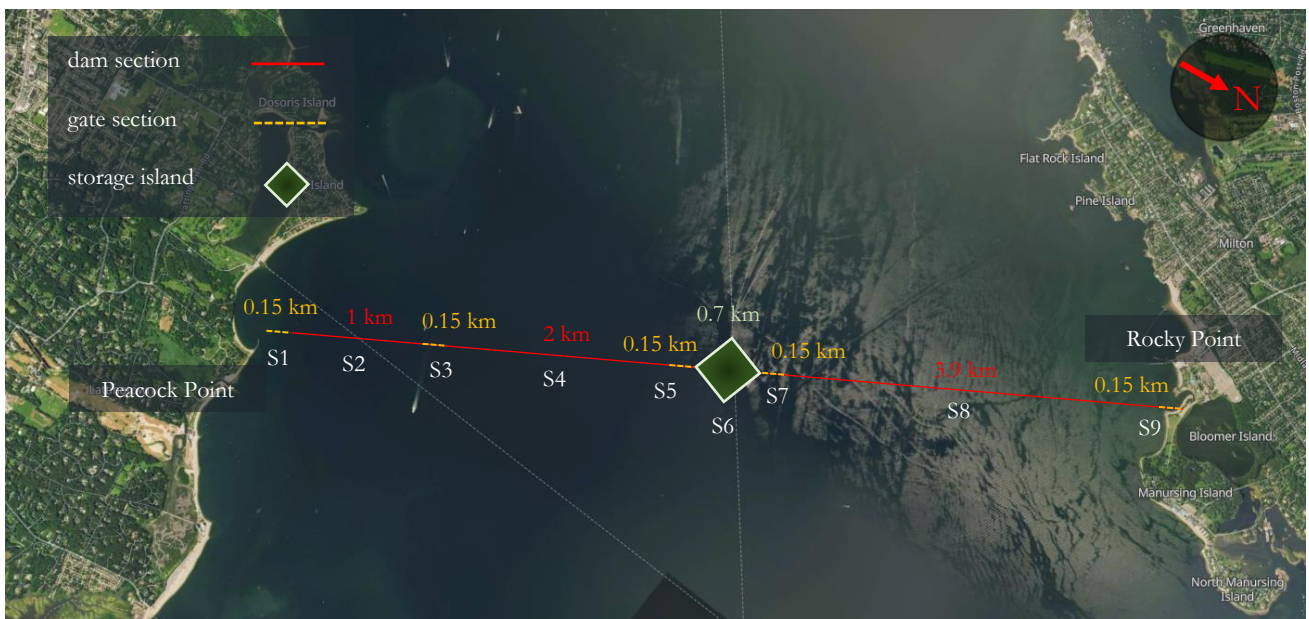


Figure 6.2 | Barrier layout between Rocky Point - Peacock Point (top view).

The total barrier length of 8.35 km is subdivided into nine sections (S1-S9). Section S2, S4, and S8 are designated as dam sections and S1, S3, S5, S7 and S9 as gate sections which allow for vessels and marine life to cross the barrier. The gate sections have a length of 150 m adhering to the minimum requirement (section 3.1). Multiple passages are incorporated into the barrier to allow for quick access to both shorelines. The total length of the five gate sections is 750 m. If it is unfeasible to close off the distance of the gate sections with segments, a different gate type gate should be considered. For example, the Horizontal sliding gate (section 5.4). For this location, it is expected to be unfeasible to reconstruct the dam sections on a yearly basis based on the large channel width. For the gate sections this will again depend on the number of available lifting vessels. The Island in the middle of the channel is designated to store segments on which maintenance can be conducted and functions as a control center. Finally, it should be noted that closing of this part of Long Island Sound had major ecological consequences, however, there is the possibility to change the dam section configuration of the barrier such that enough water and marine life can cross the barrier by removing multiple top segment layers. These layers are then reassembled before the advent of a storm surge.

6.2 Construction process

6.2.1 Barrier layout

The barrier layout in section 6.1 is based on the basic layout configuration described in this subsection. Examples are also provided on the barrier configurations for the Davenport park – Sands Point barrier and the Throgs Point – Willets Point locations. The overall layout of the entire barrier can be split into four categories: the dam section, gate section, shore connection and a segment storage space. These categories are combined to form two basic layout options schematized in Figure 6.3 and Figure 6.4 below.

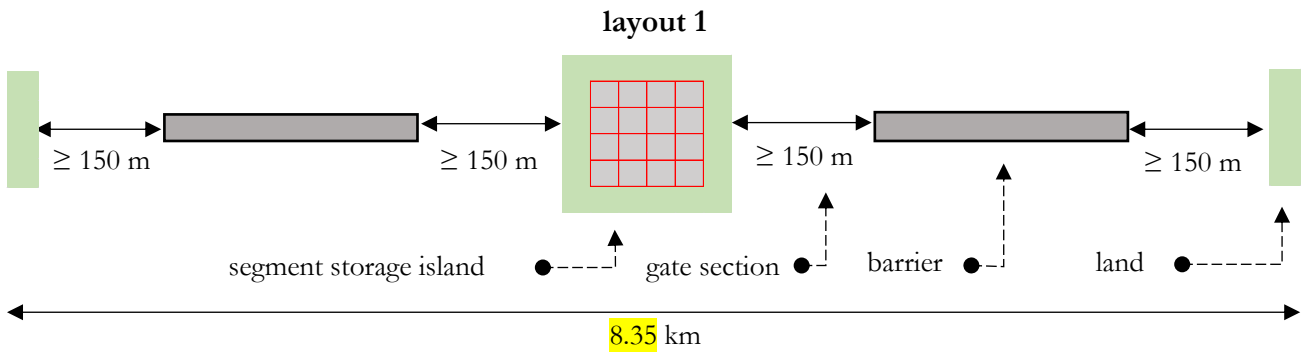


Figure 6.3 | Barrier layout 1 (top view).

Layout 1 proposes to reuse soil that has been dredged during the construction of the foundation to build an island halfway the channel that can be used to store segments needed to close off the gate sections and functions as a control center. The minimum navigation width is 150 m and present on both sides of the island which allow lifting vessels to maintain access to the stored segments. The shoreline connection remains navigable to maintain continuous access to the entire shoreline. All navigable spaces can be closed off with additional segments. If it is unfeasible to use the segments to close the gate sections, other existing barrier types (Appendix F) should be considered.

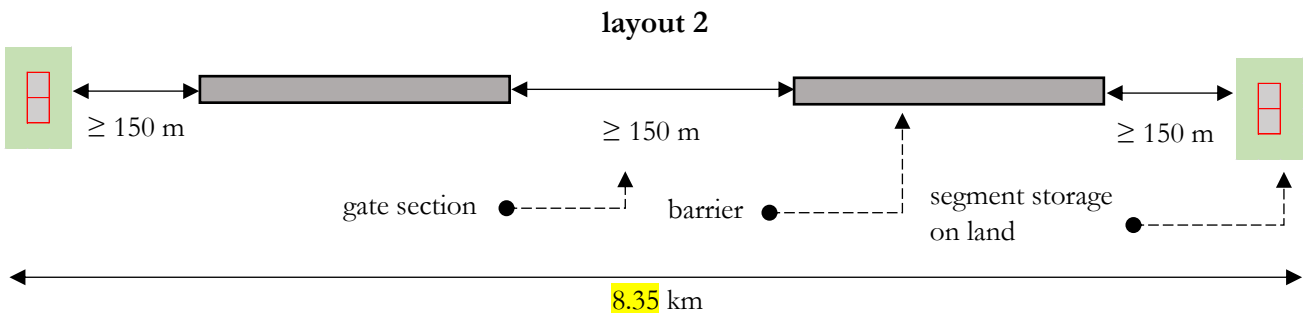


Figure 6.4 | Barrier layout 2 (top view).

Layout 2 proposes one continuous opening in the middle of the channel and two storage areas located on land. It should be noted that both layout 1 and 2 assume fully assembled dam sections, however, if additional flow space is required, the barrier can be modified by removing a number of top row segments. Further research into the environmental impact can inform the layout and determine to what extent the barrier should be constructed before the advent of a significant storm. The final barrier layout for the Rocky Point - Peacock Point location as presented in section 6.1 is based on layout 1 of Figure 6.3.

If the barrier were to be located between Davenport Park and Sands Point, layout 2 would be applied with two gate sections located along the shorelines and one in the middle of the barrier as shown in Figure 6.5.



Figure 6.5 | Barrier layout between Davenport Park – Sands Point (top view).

The final example considers Throgs Neck which is the shortest out of the three analyzed locations with three gate section and two dam sections located between Throgs Point - Willets Point as shown in Figure 6.6.



Figure 6.6 | Barrier layout between Throgs point – Willets Point.

As the length of the barrier decreases for different locations, it becomes more feasible to build the Segment barrier as a temporary structure. Table 6.1 summarizes the time it takes to build the Segment barrier for each location. It is assumed that one barrier part consisting of 36 segments, each 50 m in length can be assembled by one lifting vessel within 3 hours (section 6.2.3). The data in Table 6.1 assumes a 24/7 hour working cycle and barriers that are entirely made up of segments.

Assembling time												
location	dam section length (m)	assembling time (days)/unit vessels			gate section length (m)	assembling time (days)/unit vessels			total barrier length (m)	total assembling time (days)/unit vessels		
		1	2	3		1	2	3		1	2	3
Rocky Point - Peacock Point	6900	17.3	8.6	5.8	750	1.9	0.9	0.6	7650	19.1	9.6	6.4
Davenport park - Sands Point	4160	10.4	5.2	3.5	450	1.1	0.6	0.4	4610	11.5	5.8	3.8
Throgs Point - Willets Point	800	2.0	1.0	0.7	450	1.1	0.6	0.4	1250	3.1	1.6	1.0

Table 6.1 | Assembling time for different locations.

These values are rough estimations, but serve the purpose of showing to what extent adding more lifting vessels can reduce the assembling time. For example, from Table 6.1 it becomes clear that a Throgs Point – Willets Point barrier could be assembled in one day, making this location a more feasible option for the Segment barrier to function as a full temporary structure. The gate section alone could be closed in half a day. For the largest distance it would take at least 6 days to complete a full barrier with three vessels. Therefore, the Segment barrier might be less suitable to function as a full temporary barrier – one that has to be reassembled every year – for a channel span this large. However, it is possible to close the gate section within one day for two or more lifting vessels. This means the dam section should already be built in advance.

6.2.2 Shoreline connections

Three shoreline connections have been considered. Vessels should always be able to sail seamlessly along the shorelines. Figures 6.7-9 show the concepts. Connection 1 proposes to close the gap with additional segments. Fewer segments could be needed to close off the gape due to a shallower bathymetry.

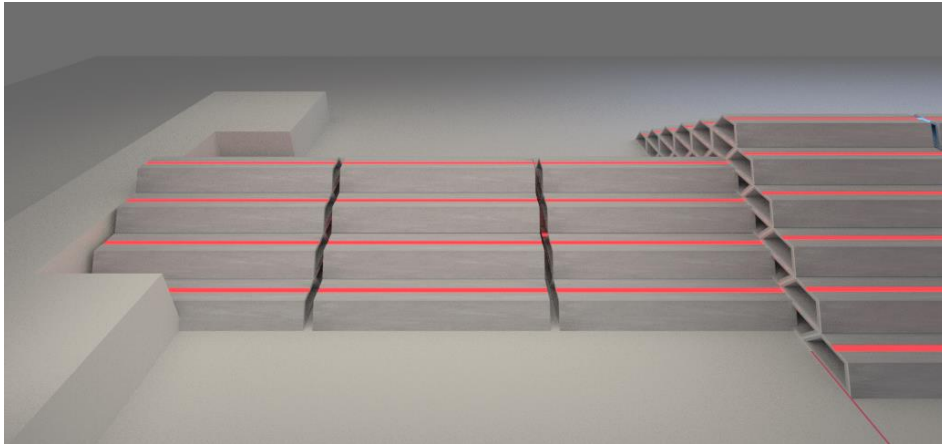


Figure 6.7 | Shoreline connection option 1.

Connection 2 uses a gate., for example, the horizontal sliding gate concept from section 5.4.

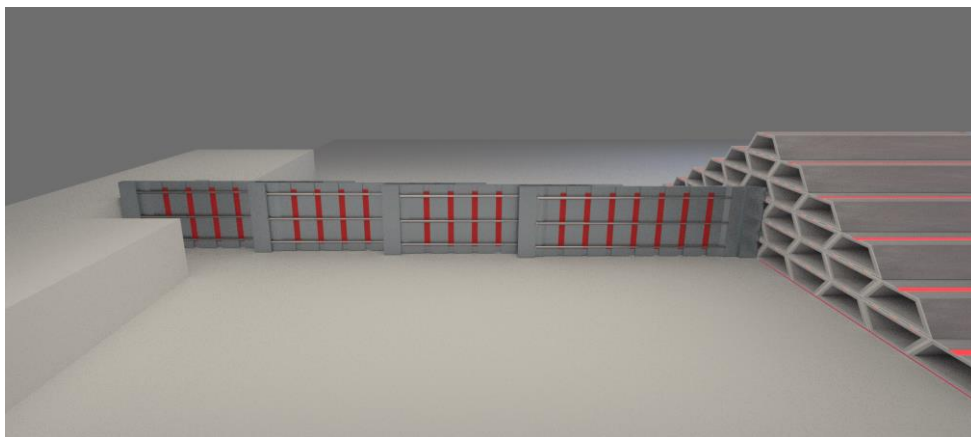


Figure 6.8 | Shoreline connection option 2.

The third option is to extend the coastline towards the barrier and create a smaller navigable opening.

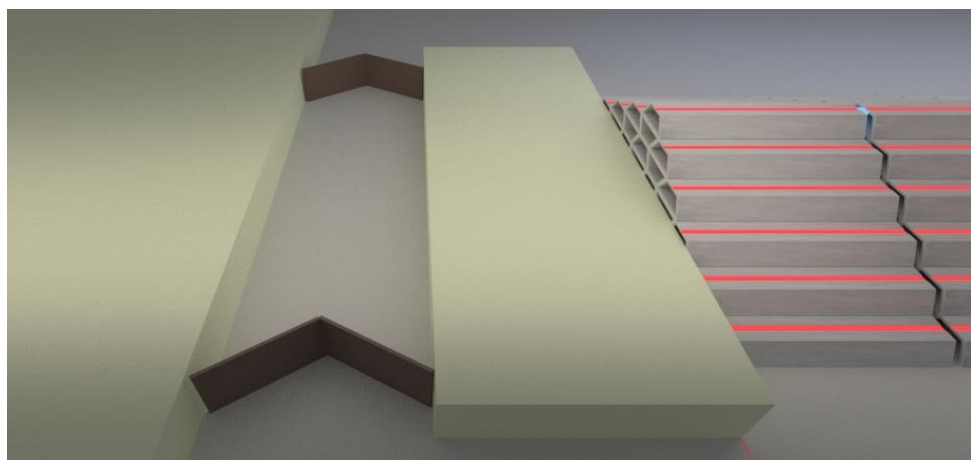


Figure 6.9 | Shoreline connection option 3.

6.2.3 Transport of heavy equipment

The first method of transportation to be considered is over land. For this example, it is assumed to be the only method to transport the barrier segments from the concrete production plant to a lifting vessel. Transporting over land limits the segment's outer dimensions to the standard maximum width of a vehicle, equal to 2.59 m, however, permits may approve of widths up to 3.66 m (State of New York Department of Transportation, p. 2). Special transport vehicles such as the Flex, Tele or ModulMAX trucks with self-steering trailers have been used for transporting long prefabricated concrete beams up to 65 m and cargo with a maximum payload of 5,000 ton (Faymonville, n.d.). Similar vehicles can be used for transporting the concrete segments. A number of long and heavy transport equipment are shown in Figure 6.10.



Figure 6.10 | Long and heavy transport equipment including a 70 m long wind turbine blade (Faymonville, n.d.).

It is preferred to have as much production activity as possible along the coast, with temporary roads from the construction facilities to the docking stations where there is ample space for vehicular transportation if needed. This way, less additional permits are expected to be required, public traffic is avoided and transport width restrictions are only limited by the carrying capacity of the vehicles.

There are three cross-sections being analyzed in this section referred to as: small, middle and large (respectively 1, 3 and 5 m in height). Each segment has a length of 50 m by design. First, the smallest size is considered of which a schematic is presented in Figure 6.11. The angle α remains 45° for every segment which is a design choice elaborated in Appendix A to ensure the strongest overall structure.

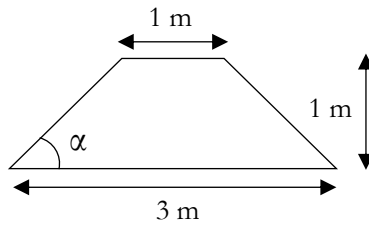


Figure 6.11 | Schematic representation of the smallest segment cross-section.

The overall height of the final structure is approximately 30 meters (determined in Appendix B3) which means the total number of segments to complete the pyramid cross-section with the smallest segments amounts to 900 units and has a base width of 119 m. Transporting segments of this size over land would be undesirable. Therefore, one option would be to build or use an existing concrete manufacturer near a channel and omit transport via public roads. A small segment weight is approximately 2,500 kN (≈ 250 ton) which means one truck – or in combination with semi-trailers – could carry the weight of 20 segments. The second option is the to use the middle size segments shown in Figure 6.12. A total of 100 segments would complete the cross-section.

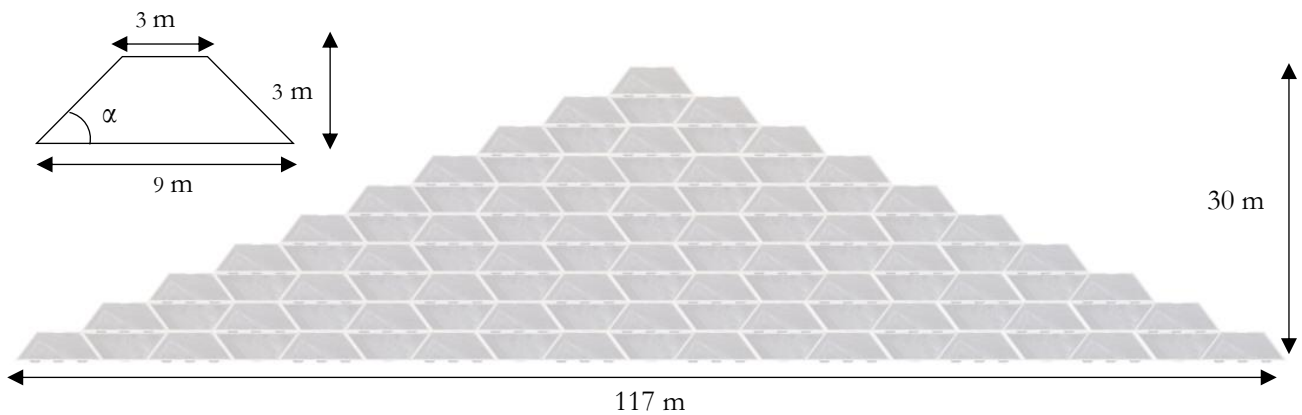


Figure 6.12 | Middle size segment of the barrier cross-section consisting of 100 segments.

The third and most economical option shown in Figure 6.13 is the large segment weighing approximately 26,100 kN ($\approx 2,620$ ton). A total of 36 segments would complete the cross-section.

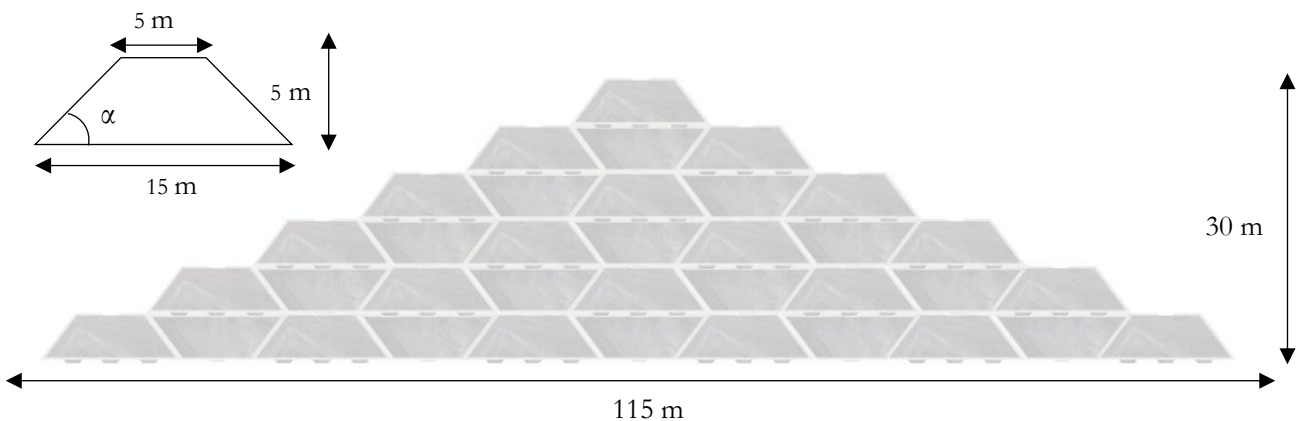


Figure 6.13 | Barrier consisting of 36 large segments.

These middle-sized segments weigh approximately 12,780 kN ($\approx 1,300$ ton) and can be easily lifted by various offshore heavy lift vessels, an example of which is shown in Figure 6.14. It should be noted that the hoisting speeds of these vessels can vary between 2-5 m/min depending on the load (Royal Boskalis Westminster N.V., n.d.). It is therefore expected to take a number of days to close off certain sections of the barrier as described in section 6.1.



Figure 6.14 | Asian Hercules II vessel with a lift capacity up to 3200 tons (Royal Boskalis Westminster N.V., n.d.).

Rather than lifting these segments on a vehicle, they can be moved from the production facility on a roller deck similar to those used at airports to the docking station and lifted onto a vessel. An example of a roller deck is shown in Figure 6.15. Section 8.2 suggest a manufacturing location where these roller decks would be applied.



Figure 6.15 | Roller deck for transporting segment (AirportTechnology, 2016).

6.2.4 Foundation

Based on the available geological data (section 3.2.8) it is assumed the barrier needs to be founded on piles over the entire length of the channel. The soil layers with sufficient bearing capacity lay beneath a layer of clayey silt material. Further research and exploratory drillings will have to result in an accurate stratigraphy. Due to the limited available data for this specific location no detailed design for the foundation is provided in this thesis, however, the desired final result for a foundation design can be explained. There are two possible ways of providing a stable and watertight foundation. Figure 6.16 shows one method which assumes piles are needed, the channel floor is dredged with the purpose to even out the channel floor first before piles are driven to the required depth. Profiled concrete floor slabs are then placed on top of the piles and the segments on top of those slabs.

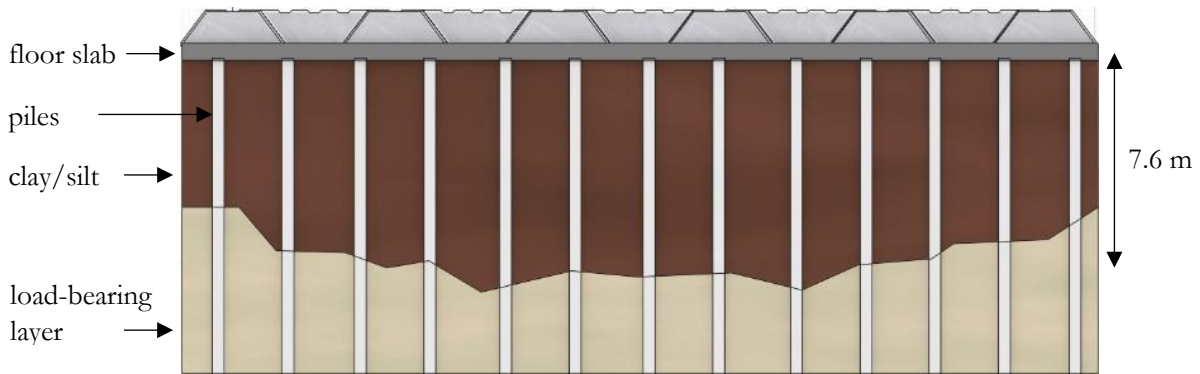


Figure 6.16 | Pile foundation (cross-sectional view).

The floor slabs have to align with sufficient accuracy when placed on top of the piles. If it is not possible to achieve this with prefabricated slabs then the concrete floor has to be cast underwater. In that case, profiled plates will be placed onto the underwater concrete before the concrete hardens out, resulting in the cross-section as shown in Figure 6.17.

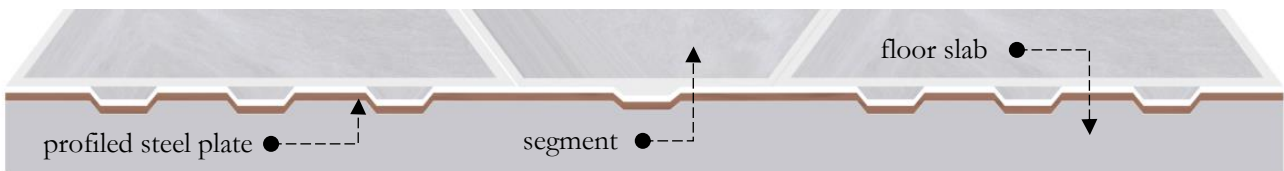


Figure 6.17 | Profiled concrete floor (cross-sectional view).

The second option shown in Figure 6.18 replaces the soft soil with a courser granular material with sufficient bearing capacity. The center row (section 6.2.6) is crucial for providing a watertight connection to prevent piping; therefore, the core layer is founded on a profiled floor slab. The concrete slab connects to a cut-off wall to prevent water from directly streaming underneath the structure.

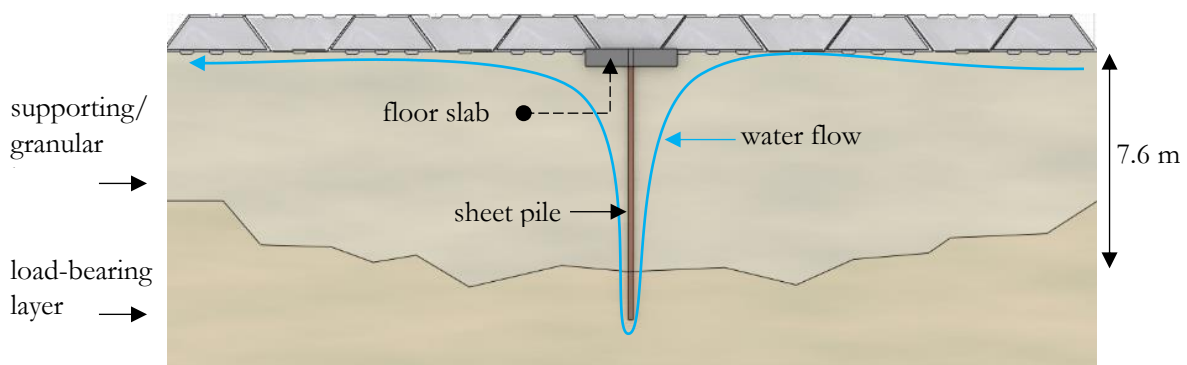


Figure 6.18 | Direct foundation on the subsoil (cross-sectional view).

6.2.5 Cross-section assembling

After the foundation has been laid, the segments are stacked in the order shown in Figure 6.19 to limit the chance of local settlements due to unevenly distributed weight.

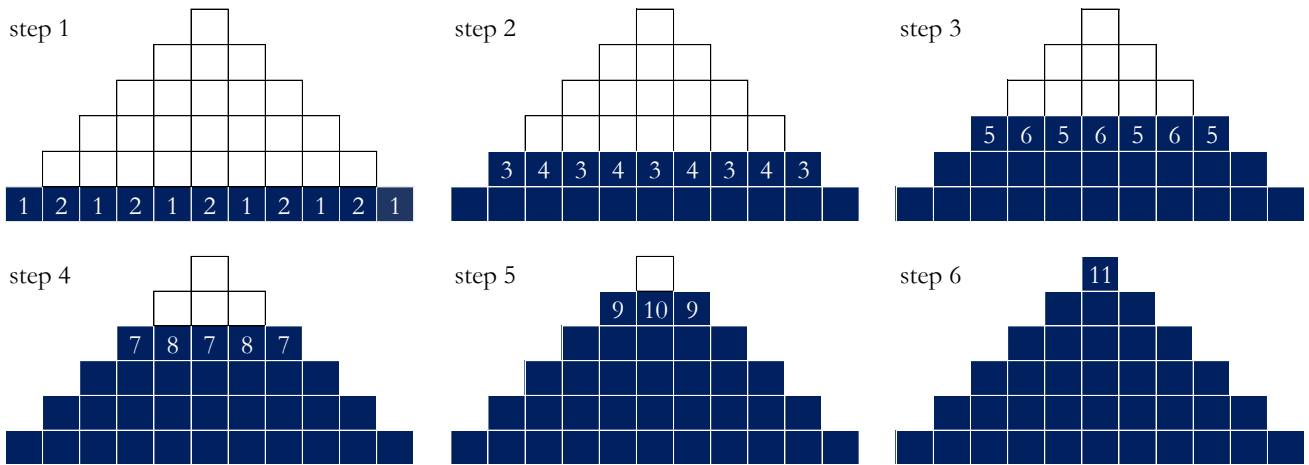


Figure 6.19 | Cross-sectional view of the stacking sequence for the large size segments.

In longitudinal direction, there are two possible ways the barrier can be assembled: the stack or brick bond pattern. First, a description is given on the stack bond pattern. The barrier is split up into parts, each part consisting of a completed pyramid shown in Figure 6.19 step 6. A guiding rail is used to help maneuver the segments into the right position according to the sequence shown in Figure 6.19. A schematic of the longitudinal view is shown in Figure 6.20.

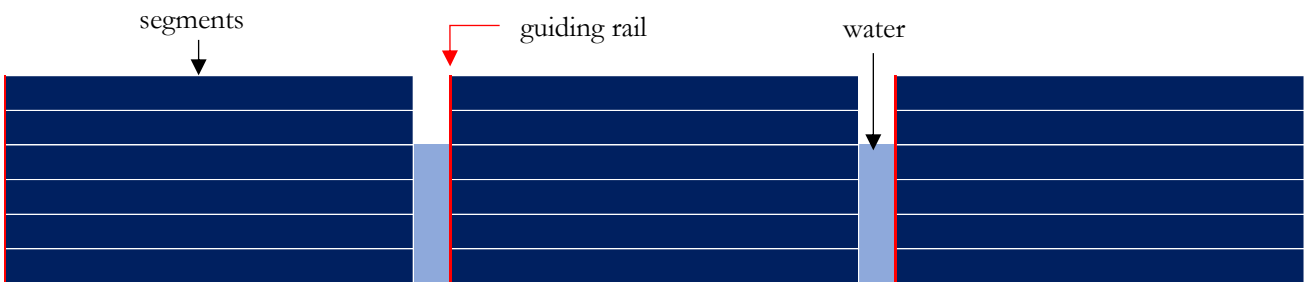


Figure 6.20 | Longitudinal view of three barrier parts (front view).

The distance between each barrier part is approximately 1 m to provide space for a watertight solution. Since every barrier section is separated by a small distance, multiple teams can work independently on the assembling process as shown in Figure 6.21. Team 1 finishes the barrier at location 1, then moves to location 4. The same applies to team 2 which moves to location 5 etc. This construction loop is repeated until the barrier is completed. Depending on the number of available lifting vessels and construction workers the entire construction process can be sped up significantly. A general estimation is made that with a hoisting speed of 5 m/min it would take approximately 3 hours to assemble one barrier part.

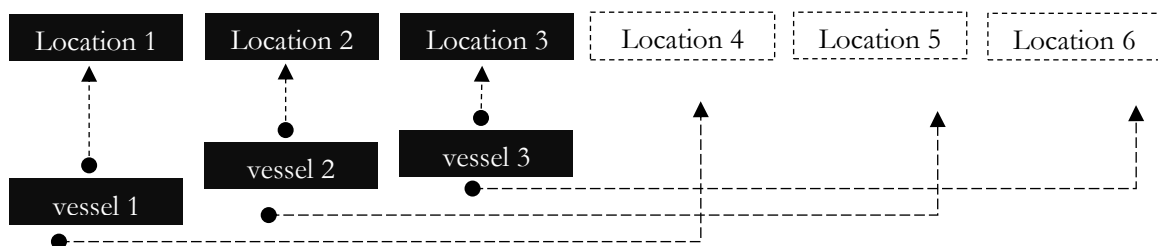


Figure 6.21 | Construction loop example for three lifting vessels.

6.2.6 Watertightness

The segments are designed with cut-outs and ridges along the top and bottom surfaces. Each segment connects by placing one on top of the other. Every cut-out has a thin layer of chloroprene rubber attached to the surface. This synthetic rubber has excellent insulation and thermal properties, corrosion resistance against salt water and can carry heavy loads (NDS Seals, n.d.). By using this material, a watertight connection can be achieved in horizontal direction. Figure 6.22 shows how the neoprene strips are connected to the concrete. For clarity reason, this material is colored red.

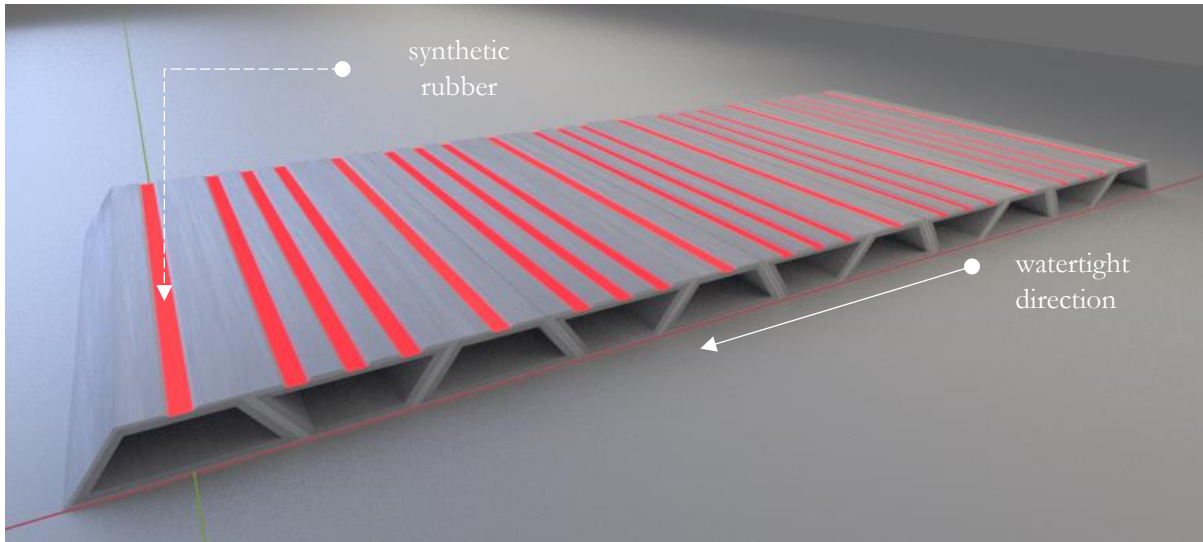


Figure 6.22 | Base layer of segments with neoprene (red) that provides watertightness in horizontal direction.

The stack and brick bond pattern are designed in such a way that both configurations can provide a vertical watertight solution. First consider the stack bond pattern. One method to achieve a watertight connection in vertical direction is to apply a 30 m long elastic synthetic bag situated in the space between barrier parts and fill it under high pressure with mortar. This method of sealing is only applied between the segments of center row; making this row the only fully watertight part of the structure. Figure 6.23 shows a top view schematic of a number of barrier parts following this pattern in which the grey segments represent the middle watertight row.

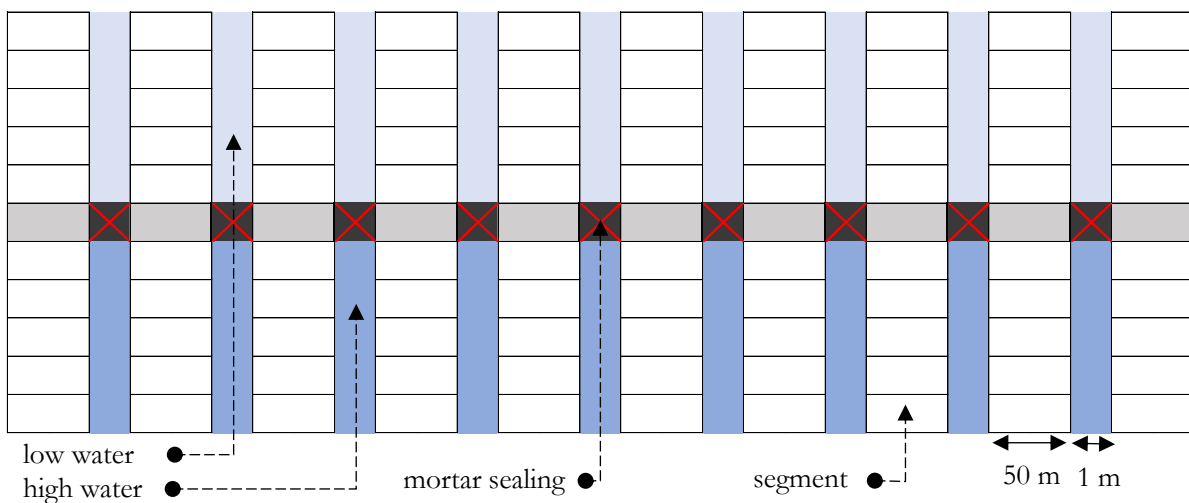


Figure 6.23 | Top view schematic of the barrier in stack bond pattern with a vertical watertight solution.

Figures 6.24-25 show realistic scale examples of the stack bond configuration. These segments are 50 m long each, corresponding to the largest segment size described in section 6.2.3. For clarity reason, the blue dots represent the locations of the mortar sealing ensuring vertical watertightness.

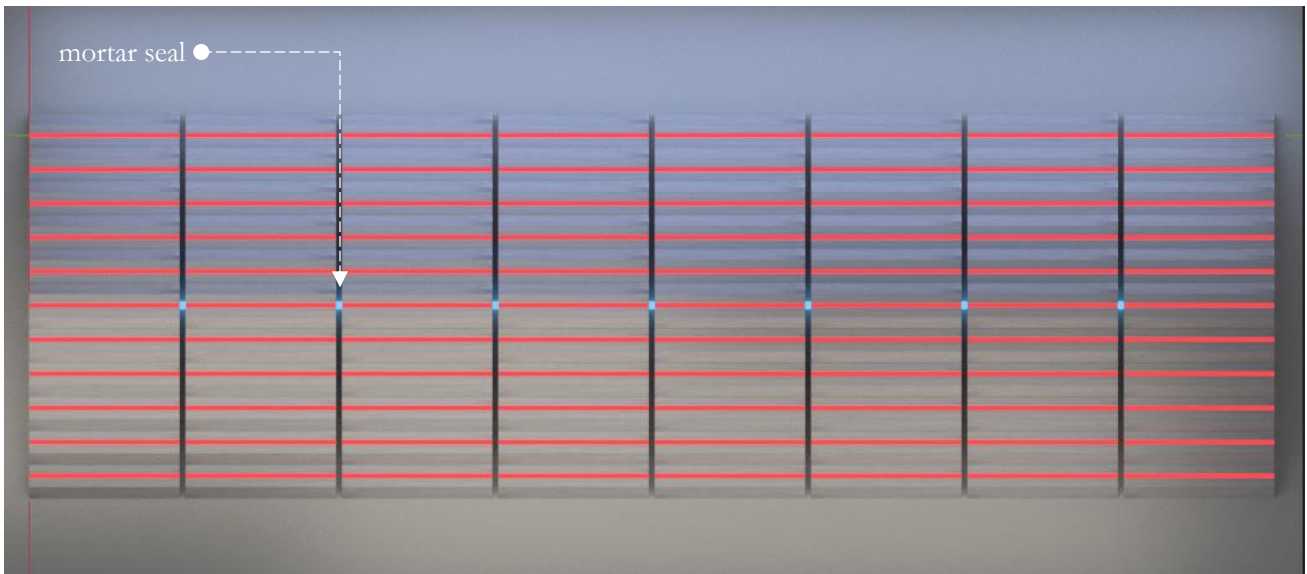


Figure 6.24 | Stack pattern scale representation (top view).

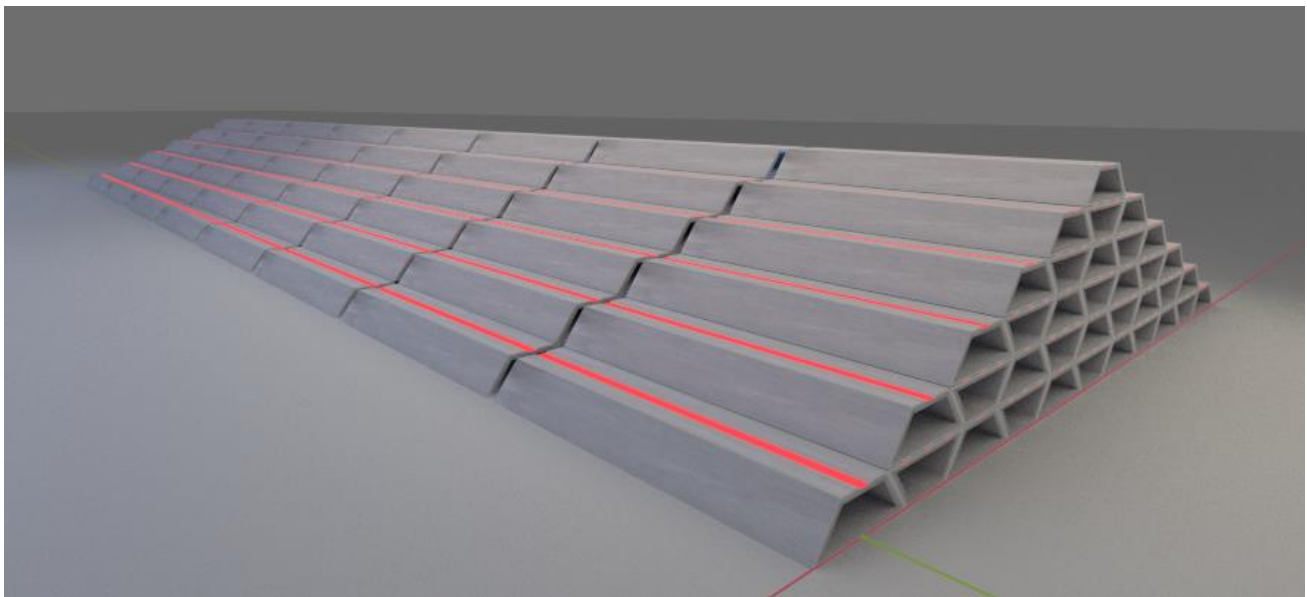


Figure 6.25 | Stack pattern on scale representation (perspective view).

The second configuration is the brick pattern which increases the overall structural strength and resistance against large horizontal pressures. There are two important steps to distinguish regarding the brick pattern: the core and the outer layers. The core, located in the middle of the barrier has the same pattern as the standard stack formation including the mortar sealing between every segment. This core row, schematized in Figure 6.26, ensures watertightness in horizontal and vertical direction. The outer layers are then positioned on both sides following the brick bond pattern configuration shown in Figure 6.27.



Figure 6.26 | Top view of the core row of the brick pattern configuration which is watertight.

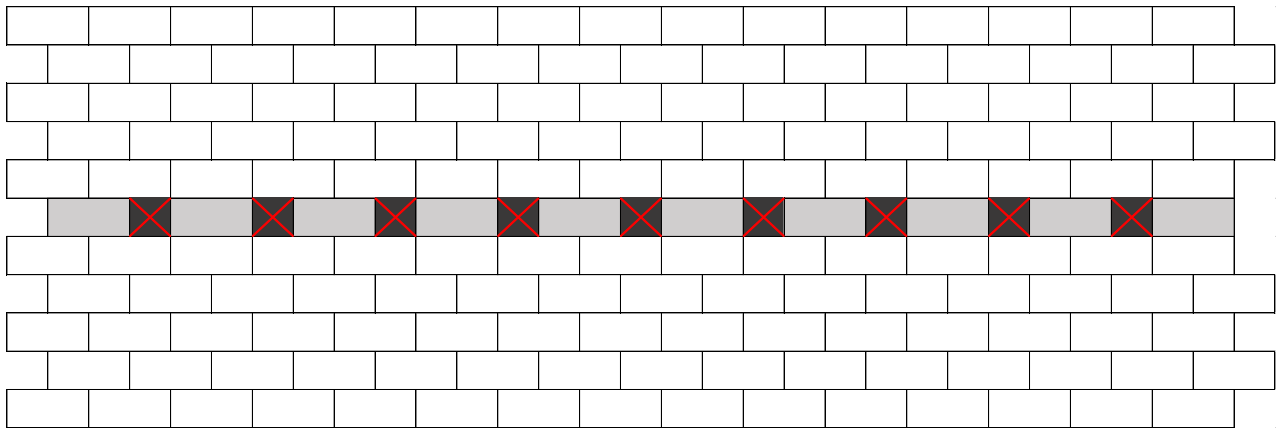


Figure 6.27 | Top view of the brick pattern configuration.

The most important advantage of this pattern is the increase in overall structural strength. The outer layers only have a structural purpose thus allowing for higher tolerable alignment deviations compared to the watertight core which should connect tightly. Aligning thousands of segments watertight would be a major challenge, therefore, the separation of the core and outer layer design provides a solution to this problem. Figures 6.28-29 show a top view of the barrier on a realistic scale. For clarity reason, the blue dots represent the location of the mortar sealing which ensure vertical watertightness. In this example each segment is 50 m long, corresponding to the largest segment size in section 6.2.3.

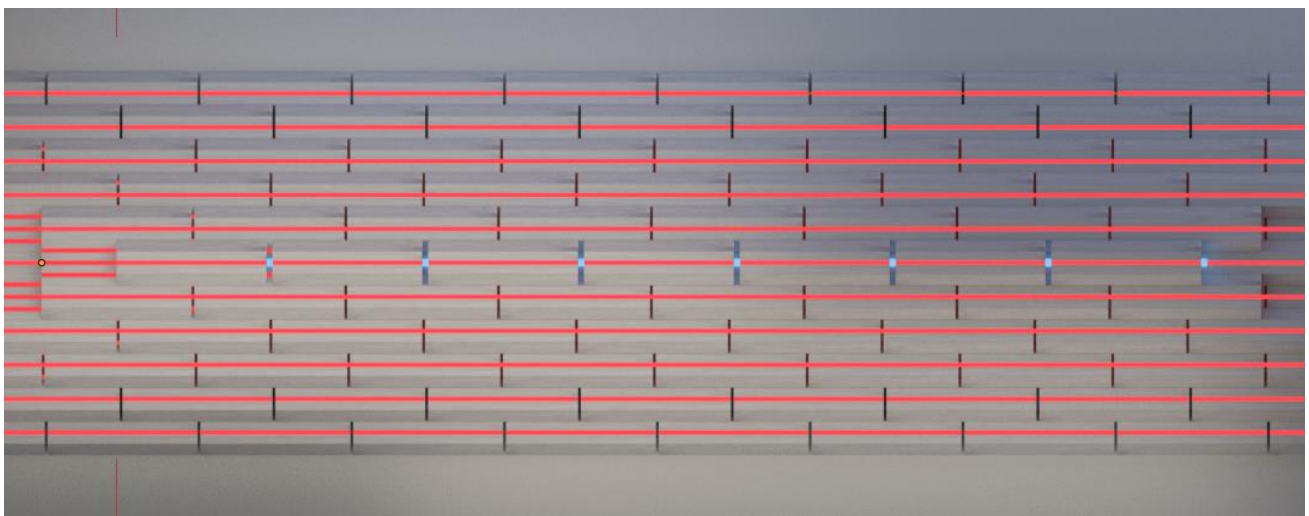


Figure 6.28 | Brick pattern top view on scale representation.

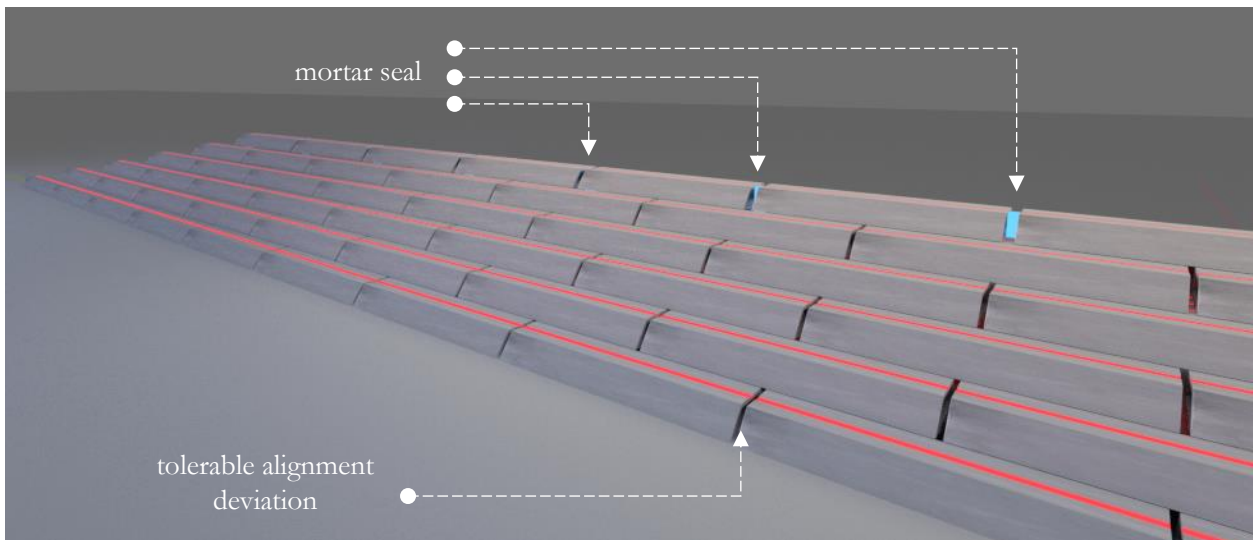


Figure 6.29 | Brick pattern perspective view on scale representation.

The final method which is discussed to ensure watertightness between the segments is by applying similar joints used for immersed tunnels (Glerum, Vrijling, & Bakker, 2018, pp. 125-129). Most suitable for these segments are the Gina gaskets. This is a continuous rubber gasket attached to the outer rim of one end of the segment during prefabrication. Figure 6.30 shows the connection components.

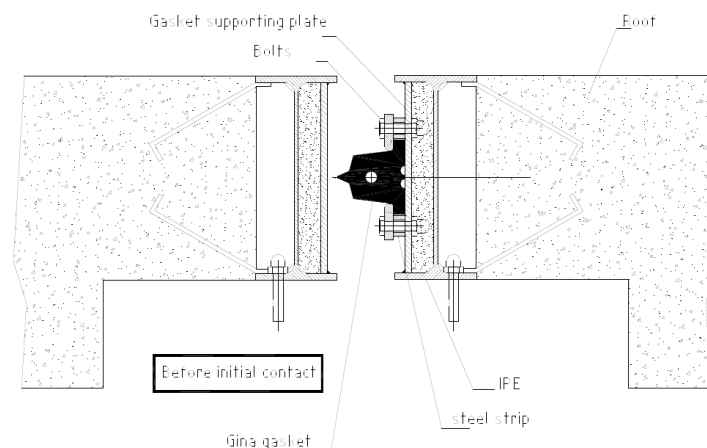


Figure 6.30 | Gina gasket before contact (Glerum, Vrijling, & Bakker, 2018, p. 126).

A steel I-plate is mounted on the concrete rims of both end of the segment. A counter-plate is then welded onto the I-section and on it the Gina gasket attached with bolted clamping stirrups. During construction, the segment is lowered and pulled towards the segment already in place. The rubber gasket is then compressed and forms a watertight seal between the segments. Now, the water between the segments is sealed off from the surrounding water. Pumping this water out creates a pressure difference between this space (low pressure) and outside water (high pressure) compressing the segments even further. One advantage of the Gina gasket is that it tolerates deviations in the vertical alignment of the segments due to for instance settlement of the subsoil. If the segment would rotate slightly, one part of the gasket would compress and the other extend due to the elasticity of the rubber.

CHAPTER 7

Structural Design

Contents

CHAPTER 7 STRUCTURAL DESIGN	69
CHAPTER 7 ABSTRACT	69
7.1 SEGMENT CROSS-SECTIONAL DESIGN	70
7.1.1 Introduction	70
7.1.2 Crest elevation of the barrier	70
7.1.3 Loads on the barrier	71
7.1.4 Concrete & steel design	72
7.2 DETAILING	75
7.2.1 Lifting connection	75
7.2.2 Chloroprene synthetic gasket	76
7.3 COST ANALYSIS	77
7.3.1 Estimations	77
7.3.2 Discussion	79
7.4 SEGMENT DETERIORATION	80
7.4.1 Causes of damage	80
7.4.2 Repairing methods	81
7.5 TECHNICAL DESIGN CHOICES	83

Chapter 7 Abstract

This chapter provides the reader with a summary of the structural design for the cross-section of the Segment barrier and a general cost estimation. The aim was to design a prestressed concrete segment which has been achieved by applying the following steps. First, the required height of the structure is determined (sections 7.1.1-7.1.2) by calculating the crest elevation based on various sea level rise scenarios. Once the height is determined, the segments can be pieced together in a pyramid configuration. From this configuration a mechanical model is made (section 7.1.3) which is used to analyze the internal forces due to the environmental loads, i.e., hydrostatic pressures, wave loads and self-weight (based on the concrete class). These loads are needed to perform strength calculation and determine the dimensions of one segment (section 7.1.4). Once the geometry is determined, it is possible to perform a stability analysis for which the reader is referred to Appendix E. Section 7.2 explains what connections are used to lift the segments and how synthetic gaskets provide a watertight connection for the final concept. In section 7.3, a basic cost estimation is provided for the barrier at the desired location between Rocky Point - Peacock Point and the shortest location between Throgs Point - Willets Point for reference purpose. Finally, section 7.4 discusses a number of technical design choices. Detailed calculations of the design can be found in Appendices A-E.

7.1 Segment cross-sectional design

7.1.1 Introduction

Section 7.1 summarizes the structural design process. Detailed calculations can be found in Appendix A-E. The barrier is designed to protect against storms with at least a 103-year return period, i.e., similar to Hurricane Sandy (significant wave height 9.9 m, wave period 13 s).

In order to achieve this the following subjects are analyzed:

- **Crest elevation of the barrier.** First, the height of the barrier will be determined. From this, the number of segments and barrier configuration can be deduced.
- **Loads.** Once the shape of the barrier is determined, a mechanical scheme is setup. The environmental loads are applied on the structure resulting in internal forces which are needed to calculate the dimensions of the segments.
- **Concrete & Steel design.** A prestressed concrete segment is designed.

The reader is referred to Appendix E, for an analysis on the stability of the structure.

7.1.2 Crest elevation of the barrier

The height of the barrier depends primarily on the wave climate. There are multiple ways of determining the wave climate, therefore, three estimations are made from which one will be governing:

- The first estimation is directly based on Hurricane Sandy's wave climate (Appendix B1). The barrier should be able to stop waves of this magnitude ($H_s = 9.9$ m and $T_s = 13$ s) in accordance with functional requirements $F3$ (section 3.1).
- The second wave climate estimation is based on the local water depth, wind conditions and fetch length (Appendix B2).
- The third wave climate estimation considers intensified conditions (Appendix B2).

The second and third estimations include global mean sea level rise predictions based on multiple different scenarios (section 3.2.2, Figure 3.2). These scenarios are combined with different steep or gentle outer slopes. A detailed analysis can be found in Appendix B. The final results are shown in Table 7.1.

Global Mean Sea Level Rise (GMSLR)		Significant Wave Height (Hs) [m]	Significant Wave Period (Ts) [m]	Crest Height (Rc) [m] slope 1 & 2 (1:1-1:2) steep	Rc + GMSLR (total height) [m]	Number of required slope segments		Crest Height (Rc) [m] slope 3 (1:3) gentle	Rc + GMSLR (total height) [m]	Number of required slope segments	Crest Height (Rc) [m] slope 4 (1:4) gentle	Rc + GMSLR (total height) [m]	Number of required slope segments
Scenario	Rise [m]					slope 1	slope 2						
contemporary	0	9.9	13	7.9	7.9	6	12	6.3	6.3	18	4.6	4.6	20
low	0.3	9.9	13	7.9	8.2	6	12	6.3	6.6	18	4.6	4.9	24
intermediate-low	0.5	9.9	13	7.9	8.4	6	12	6.3	6.8	18	4.6	5.1	24
intermediate	1	9.9	13	7.9	8.9	6	12	6.3	7.3	18	4.6	5.6	24
intermediate-high	1.5	9.9	13	7.9	9.4	6	12	6.3	7.8	18	4.6	6.1	24
high	2	9.9	13	7.9	9.9	6	12	6.3	8.3	18	4.6	6.6	24
Extreme	2.5	9.9	13	7.9	10.4	7	14	6.3	8.8	18	4.6	7.1	24

Table 7.1 | Number of required segments for various SLR scenarios and slopes.

The choice has been made to design the barrier based on the first wave climate estimation. As described in section 2.1.1, the frequency of severe storms is increasing, thus the return periods shortening. In response to this trend, the first wave climate scenario is considered the safest assumption. Finally, the GMSLR scenario 'high' (Table 7.1) in combination with a steep (1:1) outer barrier slope is chosen based on the lower number (6 instead of 7) of required segments.

7.1.3 Loads on the barrier

There are three categories of loads taken into consideration: hydrostatic pressures, wave pressure and the structure’s self-weight. In order to determine governing values for the internal forces, a mechanical scheme of the entire structure has been modeled in matrixframe (student version) as shown in Figure 7.1 which consists of so called ‘A’ (standard trapezium orientation) and ‘V’-segments (flipped orientation).

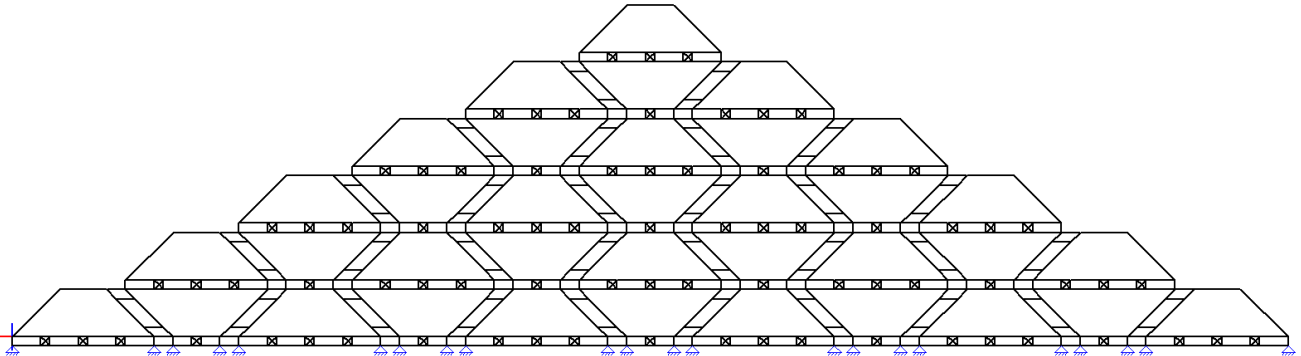


Figure 7.1 | Mechanical model of the barrier.

The connections between the bottom and top parts of each segment are modelled as uniaxial bars (crosses) as these connections cannot take up moment forces. Although the barrier height is based on the ‘high’ sea level rise scenario (Table 7.1), the loading has been analyzed for two other scenarios: the ‘contemporary’ and ‘extreme’ sea level rise cases. An example of an analysis in which all loads are combined for the contemporary scenario is shown in Figure 7.2. The seaside forces are depicted on the left which includes hydrostatic pressures (red) and wave pressure (blue). The protected side (right) is loaded by a hydrostatic pressure only (red). The difference in hydrostatic pressure is based on the maximum observed tide difference (section 3.2.1, Table 3.1). In this example, the locations of the maximum observed internal forces are encircled in Figure 7.2 as follow: maximum moment (1), shear force (2) and normal force (3).

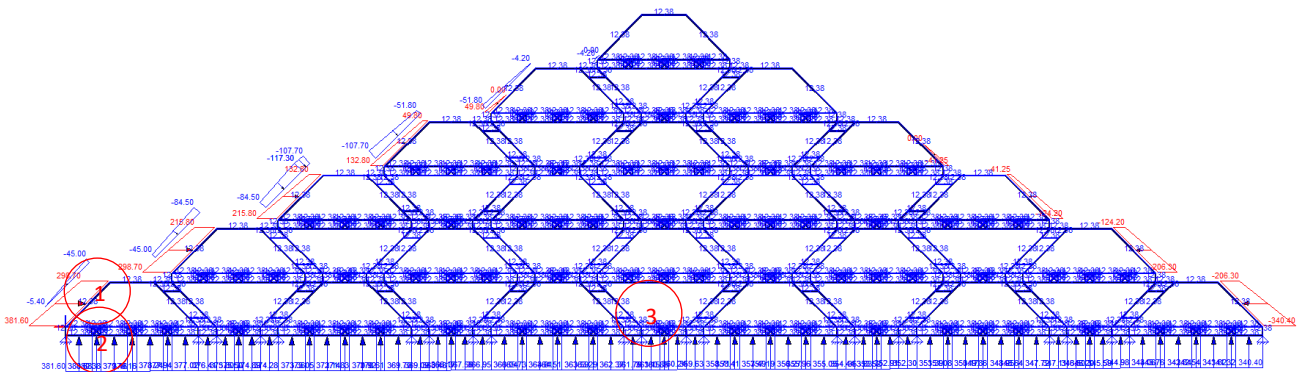


Figure 7.2 | Load combination on the structure.

Table 7.2 summarizes the internal forces for the contemporary and extreme sea level rise scenario.

Load Case	Scenario	Contemporary	Extreme	Contemporary	Extreme	Contemporary	Extreme
		Moment [kNm]		Shear Force [kN]		Normal Force [kN]	
Hydrostatic pressure		1550	1750	1780	2030	2700	3050
Wave Pressure		235	244	226	260	434	470
Self-Weight		275	275	175	175	2583	2583
Combination		2310	2800	1150	3370	4100	5400

Table 7.2 | Internal forces of the structure for contemporary and extreme GMSLR scenarios.

7.1.4 Concrete & steel design

The extreme values of Table 7.2 are governing for the calculations in this section. A prestressed segment has been designed with the intent of providing a slender cross-section, thus saving material. An overview of the material properties is presented in Table 7.3. Detailed calculations of this section can be found in Appendix D, as well as a full list of structural requirements (Appendix D2.11).

Material properties concrete	
Density	$\rho = 25 \text{ kN/m}^3$
Strength class	C50/60 ($f_{ck} = 50 \text{ N/mm}^2$)
Compressive strength design value	$f_{cd} = 50/1.5 = 33,3 \text{ N/mm}^2$
Axial tensile strength	$f_{ctm} = 4,1 \text{ N/mm}^2$
Environmental class	XS2. Corrosion induced by chlorides from sea water
Structural class	S6. Design working life of 100 years
Young's modulus of concrete (short term)	$E_{cm(0)} = 37000 \text{ N/mm}^2$
Material properties prestressing steel	
Characteristic tensile strength	$f_{pk} = 1860 \text{ N/mm}^2$
Characteristic 0,1 % proof – stress	$f_{p0.1k} = 0,9 f_{pk} = 1674 \text{ N/mm}^2$
Design value tensile strength	$f_{pd} = f_{p0.1k}/1,1 = 1522 \text{ N/mm}^2$
Initial tensile stress	$\sigma_{pm0} = 0,75 * 1860 = 1395 \text{ N/mm}^2$
Modulus of elasticity	$E_p = 195000 \text{ N/mm}^2$
Reinforcement class B500B	$f_{yd} = 435 \text{ N/mm}^2$
Material factor for prestressing steel	$E_s = 1,1$
Prestressing system	
Tendon type	19MTAI
Number of strands	19
Diameter strands	$d = 12,9 \text{ mm}$
Cross-sectional area of a strand	$A_p = 100 \text{ mm}^2$
Class A, steel name	Y1860S7
Number of wires per strand	7

Table 7.3 | Material properties of one segment.

Figure 7.3 shows the cross-section of a segment's side that is designed per 10-meter width b [m] and a variable height h [m]. The length of one segment is 50 m.

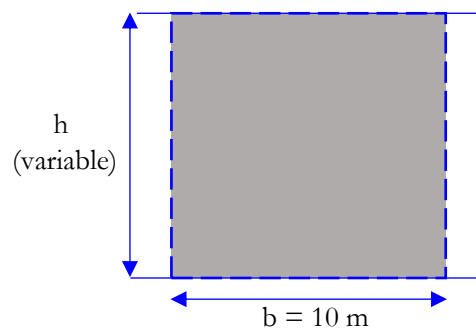


Figure 7.3 | Cross-section of a segment's top, bottom or diagonal side.

The design is based on the concept of *limited prestressing* which allows for small tensile stresses but no crack formation (Prestressed concrete, 2019, pp. 4-5). After multiple iteration, the variable height b [m] (thickness) has been reduced to 0.5 m. A segment has four sided in which the fictitious prestressed tendons are modelled as shown in Figure 7.4. In this case the weakest side of the trapezium is the base with a length of 15 m (e.g., Appendix A, Figure A.1, side A1) where the bottom fibers of the beam are loaded by outside forces.

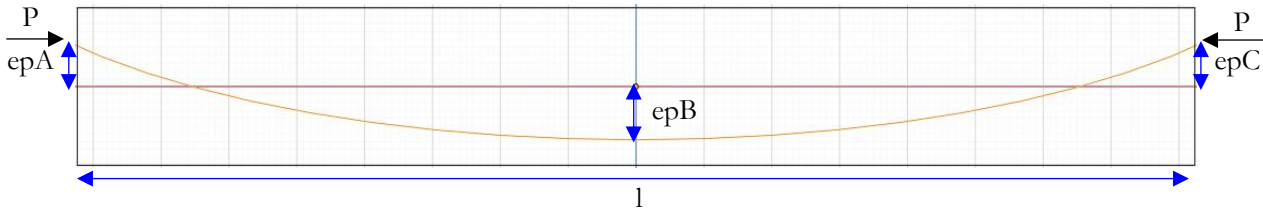


Figure 7.4 | Eccentricities of the fictitious tendon (yellow) relative to the centroidal axis (red).

The eccentricities and shape of the fictitious tendons are chosen as depicted in Figure 7.4, in which epA , epB and epC equal 140 mm. The parabola configuration of the prestressed tendon is arbitrary, other shapes and eccentricities are possible and would affect the internal moment distribution differently. In actuality the resultant of all tendons can lie within the boundaries of the *kern area* which is an area relative to the centroidal axis of the cross-section as shown in Figure 7.5. This deviation allows for proper positioning of the anchorages in practice (Prestressed concrete, 2019, p. 4-40).

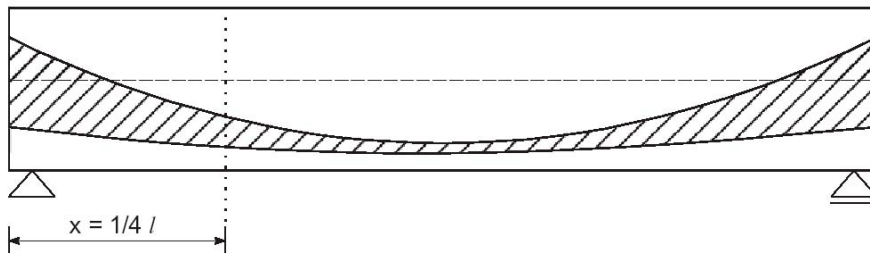


Figure 7.5 | Shaded tendon placement area (Prestressed concrete, 2019, p. 4-39).

There are three requirements with regards to prestressing:

- At $t = \infty$, it is assumed that *no* tensile forces occur at the bottom fibre of the model (Figure 7.5).
- At $t = 0$, the maximum initial prestressing cannot exceed $0.6 \cdot f_{ck}$ [30 N/mm^2].
- At $t = 0$, the prestressing load does not cause tensile stresses at the top fibre.

The result is an initial prestressing force $Pm0$ [kN] that should remain below:

$$Pm0 < 14237 \text{ kN} \tag{7.1}$$

In order to determine the amount of prestressing steel, the choice is made to apply an initial prestress force of $Pm0$ of 9500 kN. The minimum required amount of prestressing steel is 6810 mm^2 and the choice is made to use steel strands with a diameter d of 15.7 mm – area per strand A_p is 150 mm^2 – (VSL International Ltd, 2013, p. 21). The total number of strands is 46 and the choice is made to apply tendon type 19MTAI which includes 19 strands per tendon (Tensa B.V., p. 52). Therefore, three tendon(s) are applied. The prestressed tendons will experience stress losses over time which include: friction loss, elastic deformation, creep, shrinkage and relaxation losses.

The remaining prestress force after all these losses have been taken into account $P_{m\infty loss}$ is 8284 kN, which satisfies the requirement that at $t = \infty$ the prestress force should be higher than 7706 kN in order for *no* tensile stresses to occur at the bottom fiber of the model, that is:

$$P_{m\infty loss} \geq P_{m\infty} \rightarrow 8284 \text{ kN} \geq 7706 \text{ kN} \tag{7.2}$$

The concrete cover thickness is based on the environmental class *XS2* thus determined to be 60 mm. A schematic of the internal forces in the cross-section is shown in Figure 7.6, from which the bending moment capacity M_{rd} [kNm] is calculated. The choice is made to apply stirrups ($\varnothing 25$ mm) with a separation distance of 163 mm which provides sufficient shear force resistance. Additional reinforcement consisting of 36 steel bars ($\varnothing 25$ mm) spaced 275 mm is applied to achieve the overall thickness b of 0.5 m. The increase of force in the prestressing steel ΔN_p , magnitude of the concrete compressive strength N_c and reinforcement bars N_s are all depicted in Figure 7.6.

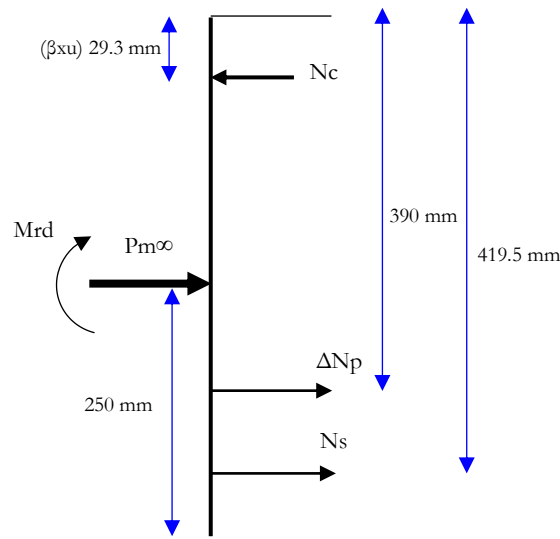


Figure 7.6 | Forces in the cross-section.

In conclusion, the final cross-section is presented in Figure 7.7 for which the bending moment capacity M_{rd} is determined to be 5700 kNm and exceeds the design bending moment M_{ed} [kNm] (Table 7.2).

$$M_{rd} > M_{ed} \rightarrow 5700 > 2800 \text{ kNm} \tag{7.3}$$

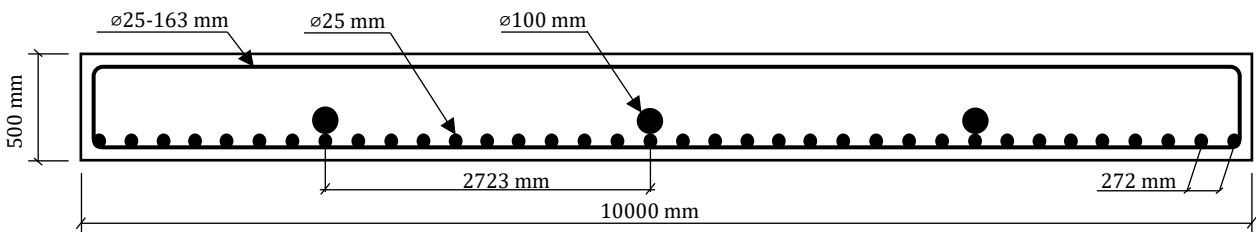


Figure 7.7 | Final result of the cross-section.

This cross-section can withstand the environmental forces for the extreme sea level rise scenario and is therefore applicable for the barrier. It should be mentioned that it is possible to only apply reinforcement steel (Appendix D2.12), however, the choice is made to apply a combination with prestressing steel which keeps the cross-section slender, thus saving material and decreasing the overall segment weight.

7.2 Detailing

7.2.1 Lifting connection

After the fabrication process is completed, the segments are lifted from the manufacturing facility onto a transporting vessel. At the construction site, the segments are lifted from the vessel and placed on the designated location. A combination of padeyes and steel rods are used to lift the segments. The padeyes are made up of a main plate, pinhole and brackets. A steel bar fits through a group of padeyes to which grab hooks can more easily attach to underwater where visibility is limited. The padeyes are connected along the edges of the concrete via anchor rods during the casting process as shown in Figure 7.8.

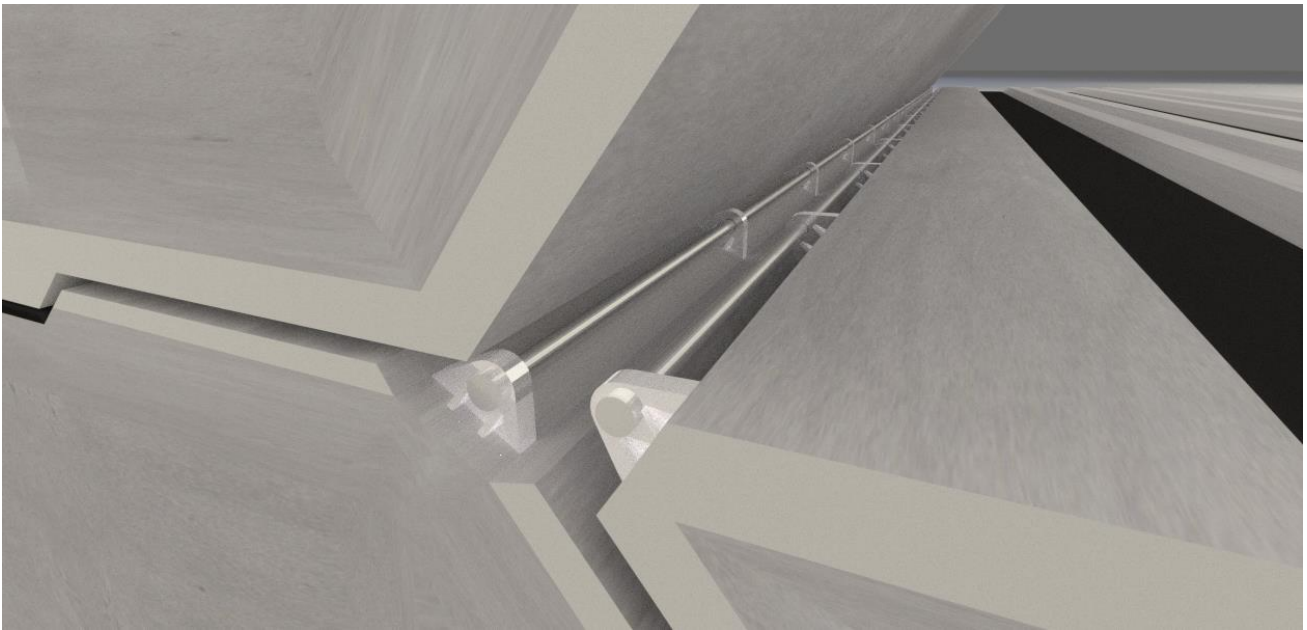


Figure 7.8 | Padeye and steel bar used for lifting of a barrier segment.

Figure 7.8 shows the exact same perspective as the image in Figure 7.9 but in wireframe view making the inside of the segment visible. The pins (highlighted yellow) align with the side of the segments.

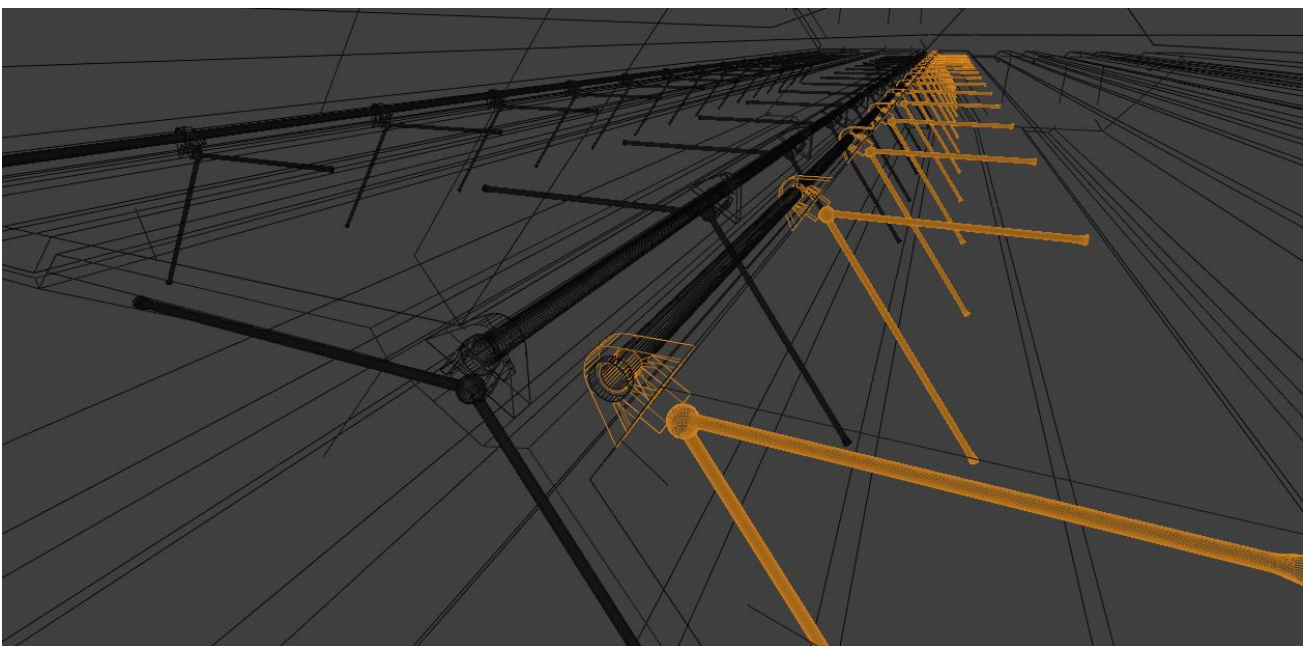


Figure 7.9 | Padeyes and steel bars used for lifting of a barrier segment (wireframe view).

A final wireframe view is presented in Figure 7.10 which shows the A- and V segment inside positioning of the lifting connections.

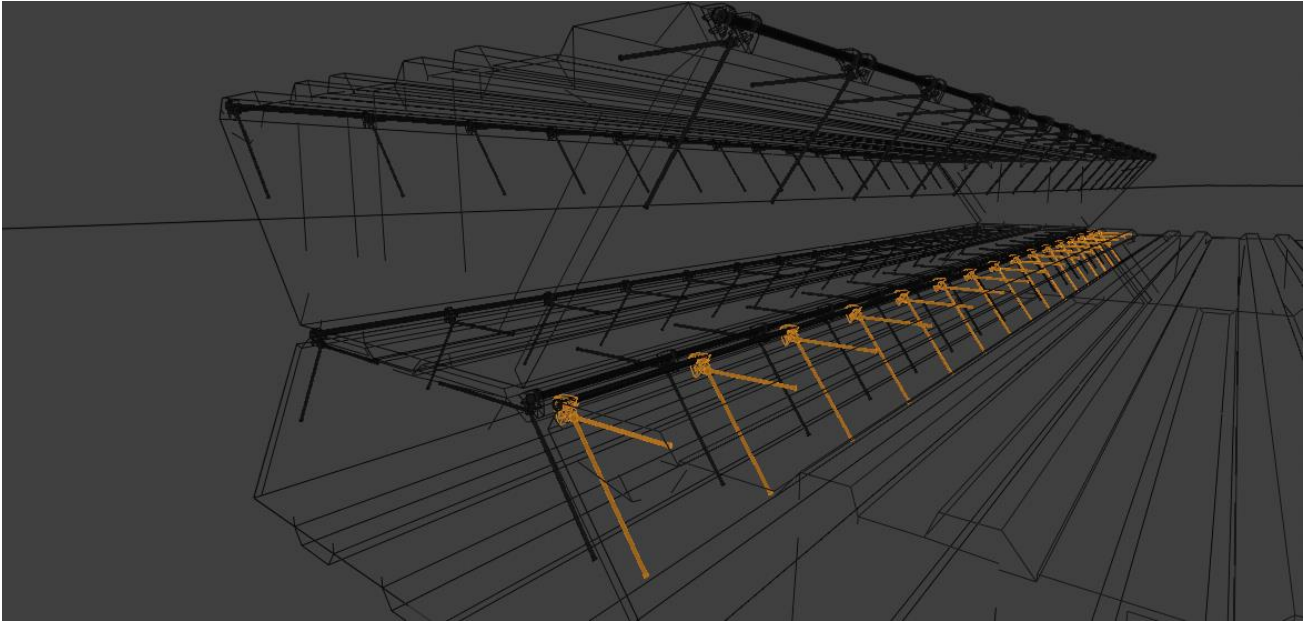


Figure 7.10 | A- and V segment inside connections (wireframe view).

7.2.2 Chloroprene synthetic gasket

Chloroprene rubber is applied as a vertical watertight seal. The seal is attached to the segment which is considered the most practical and quickest solution to achieve a watertight connection. By applying the chloroprene sealing, the number of unique segments increase. With the use of gaskets, there are four unique segments within the structure: A-and V, and two vertical sealing segments, so called ‘As’-and ‘Vs’ for the center row of the barrier. By comparison, the mortar sealing solution (section 6.2.6) uses only two unique segments: the standard A-and V segments. Figure 7.11 shows a close up of the connection where the four segments interlock. The bottom segment is removed so the gaskets can be viewed up-close.

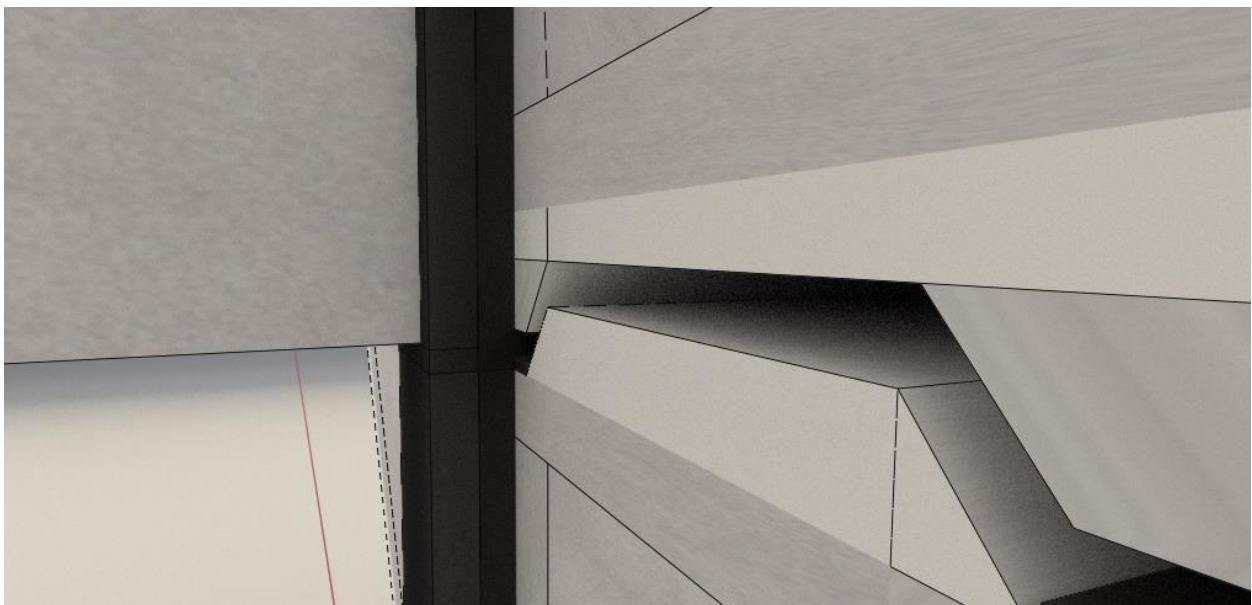


Figure 7.11 | Vertical chloroprene watertight seal for segments at the center of the barrier.

7.3 Cost analysis

7.3.1 Estimations

This section provides a basic analysis for the cost of the Segment barrier and comparison between a number of USACE concepts. It should be noted that an in-depth analysis on the barrier cost is outside the scope of this thesis. In summary, the USACE’s cost model is based on “autocorrelation tests and regression analysis” (New York-New Jersey [NYNJ] Interim Report Cost Appendix, 2019, p. 3). A detailed description of this methodology and input variables is not available, instead, the areas designated for dynamic and static barrier components (auxiliary, navigable gates and dams) are combined resulting in one single cost estimation. This resulted in an estimation of \$1 million per linear foot of dynamic length, equivalent to €2.7 million per meter (exchange rate price 2020 4th quarter [2020Q4]). It is noted that the inclusion of additional information would strengthen their cost model (NYNJ Interim Report Cost Appendix, 2019, p. 6). Table 7.4 summarized the estimated construction cost and duration for the USACE’s proposed storm surge barrier. Note the projections in Table 7.4 do not include contingencies.

Proposed Barrier	Construction Cost (No Contingency)	Duration of Construction
	[\$, 2019Q1]	[Years]
Throgs Neck	\$ 3,640,000,000	10
Sandy Hook - Breezy Point	\$ 36,455,000,000	25*
Verrazzano Narrows	\$ 8,469,000,000	18
Arthur Kill	\$ 1,671,000,000	7
Kill Van Kull	\$ 3,574,000,000	8
Jamaica Bay	\$ 2,378,000,000	9
Hackensack River	\$ 719,000,000	4
Gowanus Canal	\$ 85,000,000	2
Newtown Creek	\$ 170,000,000	3
Flushing Creek	\$ 200,000,000	3
Gerritson Creek	\$ 98,000,000	2
Sheepshead Bay	\$ 343,000,000	3
Coney Island Creek	\$ 187,000,000	3
Bronx River	\$ 150,000,000	3
Westchester Creek	\$ 170,000,000	3
Pelham Barrier	\$ 318,000,000	4

Table 7.4 | Estimated construction cost and duration for the storm surge barriers (New York-New Jersey [NYNJ] Interim Report Cost Appendix, 2019, p. 6)

The following cost model can be used to provide an estimation for the total barrier cost (M. Kluijver et al., 2019).

$$\text{Cost} = \text{€}189,000 \times \text{Navigable Area} + \text{€}111,000 \times \text{Auxiliary Area} + \text{€}20,000 \times \text{Dam Area} \quad (7.4)$$

Table 7.5 presents the results of the barrier cost estimation for the preferred barrier location in which the gate sections are assumed make use of existing gate types or segments. The Segment barrier cost estimation only uses the ‘Dam Area’ price of formula 7.4 to calculate the gate section cost.

Rocky Point - Peacock Point							
gate types	dam section length			gate section			total cost (€)
	length (m)	area (m ²)	cost (€)	length (m)	Area (m ²)	cost (€)	
existing (Appendix F)	6,900	207,000	4,140,000,000	750	22,500	4,252,500,000	8,392,500,000
segments	6,900	207,000	4,140,000,000	750	22,500	450,000,000	4,590,000,000

Table 7.5 | Rocky Point – Peacock Point barrier cost assuming the existing or segment gates.

The cost estimations in Tables 7.5 serve as a reference, however, the Segment barrier requires an additional elaborated cost model that take into account the specifics of the design. For this case study a detailed look is taken at the material costs for the segments. Table 7.6 presents an estimation of the material cost of one segment located in the core row of the barrier – which includes the gaskets – and Table 7.7 presents the cost per barrier part.

Material cost estimation per segment						
Material	price (2020Q4)	unit	quantity	unit	cost	unit
concrete grade C50/60	113.1	€/m ³	1028.33	m ³	116,304.10	€
reinforcement steel B500b (longitudinal)	389.4	€/ton	24.19	ton	9,420.79	€
reinforcement steel B500b (stirrup)	389.4	€/ton	85.83	ton	33,422.67	€
prestressing steel Y1680S7	507.6	€/ton	11.42	ton	5,798.56	€
chloroprene	238.03	€/m	235	m	55,937.05	€
carbon steel pad eyes	33	€	400		13,200.00	€
lifting anchors	0.26	€	800		208.00	€
				Total	234,300.00	€

Table 7.6 | Material cost estimation per segment.

Segment material cost estimation per barrier part (50 m, dam section)		
cost per segment with chloroprene		234,300.00 €
cost per segment without chloroprene		178,300.00 €
barrier part length	50	m
barrier part height	30	m
number of segments with chloroprene	6	
number of segments without chloroprene	30	
Total		6,756,400.00 €

Table 7.7 | Segment material cost estimation per barrier part equal to 50 m.

The total material cost for the barrier between Rocky Point – Peacock Point, including the total number of required segments, are presented in Table 7.8 It is assumed the gate sections are closed off with segments (to be situated in section S1, S3, S5, S7 and S9).

Segment material cost estimation for the full barrier					
section	section length	unit	number of segments	price (2020Q4)	unit
S1	500	m	360	64,207,481	€
S2	1000	m	720	128,414,961	€
S3	500	m	360	64,207,481	€
S4	1850	m	1332	237,567,678	€
S5	500	m	360	64,207,481	€
S6	700	m	504	89,890,473	€
S7	500	m	360	64,207,481	€
S8	2300	m	1656	295,354,410	€
S9	500	m	360	64,207,481	€
Total	8350	m	6012	1,072,264,900	€

Table 7.8 | Segment material cost estimation per section of the entire barrier.

A rough comparison is made between the dam section of the Segment barrier and an earthen sea dike. For a 20 m deep channel, the cost of the sea dike is estimated around € 150,000 m¹ (Introduction to Integral Design, 2007). For a length of 50 m (equal to a barrier part) the cost multiplies to € 7,500,000, and for an entire earthen dike barrier spanning 8.35 km the cost is roughly estimated at 1,035,000,000.

It should be noted that the traditional auxiliary gate function is provided by the Segment barrier simply by placing and removing segments at specific intervals, provided the barrier functions as a permanent structure.

The USACE’s Throgs Neck barrier with a length of 1.4 km (\$3,640,000,000 ≈ €3,090,000,000 2020Q4) is approximately six times shorter than the Segment barrier’s 8.35 km length. Table 7.9 summarizes the cost of the Segment barrier if it were constructed between Throgs Point – Willets Point (Figure 6.6) using existing gate types or segments. The water depth is estimated at 30 m.

Throgs Point - Willets Point							
gate types	dam section length			gate section			total cost (€)
	length (m)	area (m ²)	cost (€)	length (m)	Area (m ²)	cost (€)	
existing (Appendix F)	800	24,000	480,000,000	450	13,500	2,551,500,000	3,031,500,000
segments	800	24,000	480,000,000	450	13,500	270,000,000	750,000,000

Table 7.9 | Throgs Point – Willets Point barrier cost assuming the existing or segment gates.

7.3.2 Discussion

Formula 7.4 estimates €20,000 Dam Area, which means that for a barrier part (length 50 m, width 30 m) the cost would be approximately €30,000,000. Table 7.7 estimates the material cost of a barrier part to be €6,756,400, which mean the difference, €23,243,600 (77%) would make up the remaining cost, e.g., foundation, construction, manufacturing, labor, maintenance and operating costs amongst others. A significant cost reduction can be achieved if the gate sections are closed off with segments. Formula 7.4 estimates €189,000 Gate Area, making the total cost €2,551,500,000 (Table 7.9) for a 450 m gate section using traditional gate types. Applying segments instead brings the total cost at approximately €270,000,000, which is an 89% reduction in cost. It is emphasized that these comparisons ultimately require an extensive amount of research in order to provide a stronger comparing argument. Although the actual costs are expected to be higher, the differences and potential of the Segment barrier as a cheaper alternative barrier is noteworthy. Finally, it is noted that these estimations show a total cost lower than the \$19 billion in damage to New York City (section 2.1.2).

7.4 Segment deterioration

7.4.1 Causes of damage

The segments deteriorate over the life span of the structure due to the environmental conditions. A distinction is made between short- and long-term effects which is especially relevant for the Segment barrier. At its core, the Segment barrier is a temporary structure, but may need to function as a permanent one at a later stage. First consider deterioration due to long term effects caused by (ACI Committee 546, 1998, pp. 4-6):

- **Rock borers**
These are type of clam animal able to bore into porous concrete and rock, especially warmer waters with limestone aggregated concrete.
- **Acid producing bacteria**
Anaerobic and sulfur-oxidizing bacteria can produce hydrogen sulfide and turn into sulfuric acid which is a highly corrosive chemical. It attacks cement paste thus leaving the reinforcement steel exposed to corrosion.
- **Chemical attack**
Concrete is under constant external and internal chemical attack. Considering external effects, water continuously provides a fresh supply of chemicals and washes away older particles, thus exposing new surface area. Internal attack could be the result of corroded material and Alkali-silica reactions common in concrete which can be accelerated by salt water. The most common chemical attacks include: sulfate attack, magnesium ion attack and soft water.
- **Abrasion**
Small rocks, sands and debris carried by water streams which abrade the surface of concrete overtime exposing the coarser aggregates.
- **Freeze-thaw cycle**
Concrete requires adequate freeze thaw resistance to minimize deformations due to water freezing inside concrete pores, leading to internal pressure increases forcing micro cracking. Deterioration due to freeze thaw cycle is especially a concern in salt waters.

Second, consider deterioration due to short term effects which generally relates to impact loads:

- **Tensile cracking the segment stacking process**
The impact force of placing one segment on top of the other could lead to (small) cracks which increases the concrete permeability at the specific impact area allowing further chloride penetration from sea water. However, underwater corrosion is limited due to a lack of oxygen and deposit of lime from organisms and the concrete itself. The splash zone is the most critical area where corrosion can accelerate due to higher oxygen levels.
- **Heavy impact loads**
The structure can be subject to extreme loads for which it was not originally designed, e.g., seismic, extreme (periodic) wave attack, collision or explosions.

7.4.2 Repairing methods

The repairing methods vary depending on the objective. For any form of repair or maintenance, each segment can be removed from the barrier and treated on land in a dry environment compared to underwater treatment which is more difficult due to lower temperatures, currents and less light. The fact that these segments can return to a concrete facility for repair or maintenance is considered a major advantage in ensuring the highest possible quality. However, the cost of maintenance onsite versus a facility should be weighed. Consider a case in which long-term deterioration is being treated on land. Every corner can easily be reached and treated. Sprayed concrete could be applied where necessary to save on formwork costs for example.

Then there are the most complex cases in which short term impact load damages (section 7.4.1) require a solution. The barrier could be damaged to a degree where its structural integrity cannot be guaranteed and it may be necessary to redirect the loading path around the damaged area in a worst-case scenario. The Segment barrier is able to adapt to this purpose as shown in Figure 7.12.

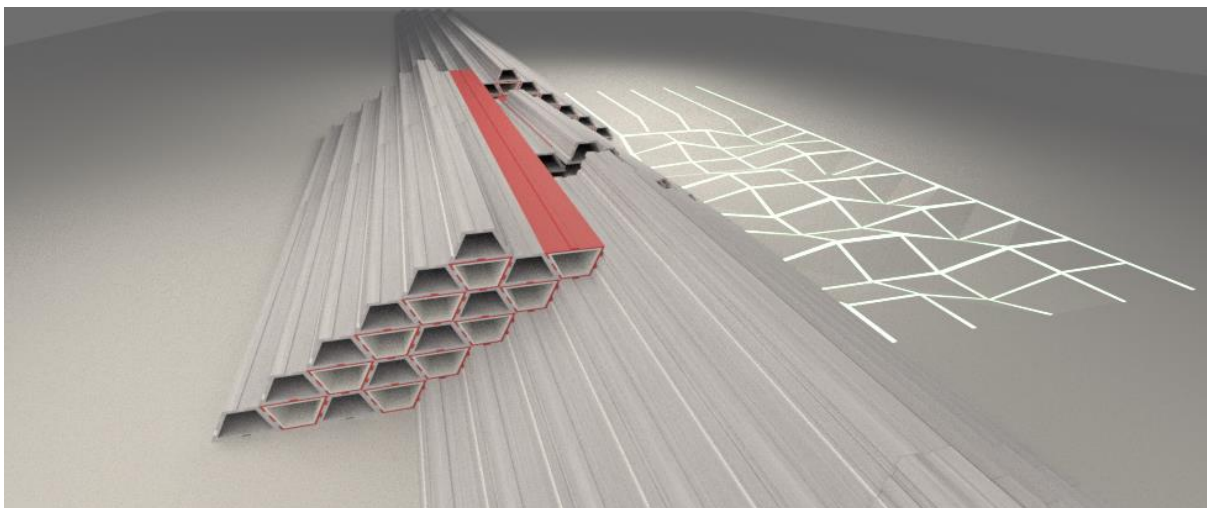


Figure 7.12 | Redirecting the load path around a major damaged area.

Figure 7.12 presents a case where damage occurred due to an explosion or earthquake where additional segments can be assembled around the damaged area. Then there is the possibility of ship collisions which is only expected to damage a handful of segments, not on the scale of what is shown in Figure 7.12. If the impact load of a ship collision breached the concrete of one segment, the empty space inside would fill up with water which poses no immediate threat to the structural stability – the additional weight of water has a positive effect on the overall stability and is not expected to cause rotational stability issues – or significant decrease in structural strength. Moreover, the only damaged segments are expected to be the ones on the outer layers of the barrier. In the long term, the accumulated salt water would corrode the segment from within, thus needs to be replaced.

If a collision leads to smaller damages such as crack formation, the concrete can be treated underwater as follow (ACI Committee 546, 1998, pp. 15-19). This analysis does not go into detail on the many concrete mixtures but only the method of treatment.

- **Using preplaced aggregate concrete**

A form with coarse aggregate is placed on the damaged area and later injected with a portland cement grout mixture. Adding fly ash or silica fume can work to reduce the grout's permeability. Typical concrete mixtures can be applied in this method.

- **Using tremie concrete**

Tremie refers to the pipe from which the concrete mixture flows downward due to gravity (not a pressurized system). This mixture has a high cementitious content which benefits compressive strength and its bond strength to the damaged area is considered excellent. However, due to the mechanics of this method it is usually not possible to create a thin overlay on the damaged area which is important if new segments would be stacked on the repaired ones at a later date. Another limitation is the requirement to have limited waterflow around the damaged location for the tremie pipe to remain steady.

- **Pumped concrete**

This is the most commonly used method for underwater concrete repairs where the concrete mixture is mixed above water and pumped through a pump line to the desired location. Due to its smaller hose, it can repair areas which are generally more difficult to reach. One of the advantages is that the repair mixture can be the same as the concrete structure. A disadvantage of this method is that pumping in surges can lead to more cement being spilled out than intended which ends up in the environment.

- **Free-fall concrete**

Perhaps the quickest solution is having a fresh concrete mixture dropped in water without any guiding pipe or pumping hose. Anti washout mixtures should be used. This method is more effective in shallow waters but may be applicable for the first row of submerged segments. Having the mixture accurately sink to the desired location in rough weather conditions might be difficult to achieve. Moreover, the segments are eventually required to have a smooth surface and must be polished during calmer weather.

Further research and experimentation into onsite repair strategies should be part of additional research.

7.5 Technical design choices

The technical design started with an analysis on different barrier sizes (section 6.2.3). Increasing the number of segments in a barrier allows it to resist higher external loads, however, at the cost of additional material and construction time. The large segment size chosen in section 6.2.3 is considered the most practical and economical and having sufficient structural strength. Scaling down could be done to apply a different barrier configuration (chapter 9) and save space. Section 6.2.5 presented two possible assembling patterns: the stack and brick bond patterns. It should be mentioned that some testing has been performed (not presented in this thesis) to determine the added advantage of the brick bond pattern over the stack bond pattern. The brick bond pattern showed overall internal forces decrease ($\approx 10-15\%$); however, the increase in structural strength does not seem worth the added complexity of the brick pattern's assembling and dismantling process. To keep it practical, the stack bond pattern is used. A construction timetable is outside the scope of this thesis; however, an estimation has been given on the time it takes to assemble one barrier part (50 m long, 36 segments) in section 6.2.3. With a hoisting speed of 5 m/min, one barrier part can be assembled in approximately 3 hours without taking into account any contingencies. If an 8.35 km barrier consisting entirely of segments (more than 6000) could be constructed in a 24/7-hour cycle without any contingencies by one lifting vessel, the assembling process could be completed within one month. This example could be more theoretical rather than practical and serves to provide a sense of scale, however, it is not unreasonable to consider the construction process to be relatively fast due to the emphasis on prefabrication and a simple execution process of this concept. The most time-consuming phases of the project are expected to be the fabrication of the segments and construction of the foundation. Instead of using the Gina gaskets (section 6.2.6), which is a proven method applied in tunnel construction, a slightly different design is applied, one with straight chloroprene gasket (Figure 7.11) on the front and back cover of the segments. Applying a Gina gasket in the exact same way used for immersed tunnels would require the water between two segments to seep into the segments when the two are pressed together. This mechanism is not part of the design, moreover this process is time consuming and complicates the process. Furthermore, the decision has been made to only apply the vertical gaskets for the center row segments which saves on material usage.

The goal was to have the segments be relatively slender while maintaining sufficient strength to resist the high periodic loading of the waves in rough environmental conditions. To achieve this, a prestressed cross-section has been designed. Prestressing steel is generally more expensive than standard reinforcement steel (Table 7.6), however, if prestressing was not applied, the concrete thickness would roughly double. Keeping the segments as identical as possible would simplify the production and assembling process. A possible drawback from this design strategy is that most of the segments in the cross-section are over dimensioned. Figure 7.2 for example shows where in the cross-section the highest loads were located, mostly along the outer segments of the structure. Due to the hexagonal shapes, the internal loads of the segments closer to the center of the barrier were generally lower, therefore, these segments could be optimized by, for example, applying less reinforcement steel or a lower concrete class.

Finally, one of the structural concerns was the presence of internal tensile forces under wave attacks. A number of tests showed that in theory, tensile forces will always be present, however, these segments are massive, and tensile forces are not expected to be an issue. What is important in making sure the segments do not uncouple, is that they do not float, which is guaranteed (Appendix E1 Buoyancy) and that water pressure gradients inside remain minimal. This can be achieved by providing enough space between the segments for water to flow out along the sides. If tensile stresses were to be a concern for any other modification to the barrier, e.g., change in size or thickness, an example for a solution is discussed in section (section 9.2).

CHAPTER 8

Evaluation

CHAPTER 8 EVALUATION 84
CHAPTER 8 ABSTRACT 84
8.1 EVALUATION MATRIX 85
8.2 ECOLOGICAL CONSTRUCTION STRATEGIES 88

Chapter 8 Abstract

This chapter provides an evaluation of the detailed Segment barrier design that was conducted in the previous chapters 6 and 7. An evaluation matrix breaks down aspects of the design into subjects which are graded based on a satisfaction level and succinctly describes how these subjects can be improved. Section 8.2 describes a number of strategies which should be implemented to reduce the ecological impact of construction activities.

8.1 Evaluation Matrix

An evaluation matrix of the Segment barrier is presented in the Table 8.1. The entire concept is broken down into subjects that were analyzed or designed in this thesis. Each subject is given a satisfaction score and description on the main reasoning and how to improve it.

EVALUATION MATRIX						
	SUBJECT	SATISFACTION			DESCRIPTION	HOW TO IMPROVE
1	barrier layout schematics (6.2.1)	2			Three main inputs inform the barrier layout: segments, gate width and storage space. More layout options are desired.	Additional input, e.g., navigation, flow and sedimentation patterns should result in new layouts.
2	barrier layout Rocky Point - Peacock Point (6.2.1)		3		unclear whether the 150 m gate openings and tidal flow through space are sufficient	additional (field) research into flow patterns and marine traffic
3	barrier layout Davenport Park – Sands Point (6.2.1)	2			Concern about the ecological impact on the nearby wildlife refuge Islands.	Research the possibility to build an earthen defense around these Islands.
4	barrier layout Throgs point – Willets Point (6.2.1)		3		Unclear whether the 150 m gate openings and tidal flow through space are sufficient.	Additional (field) research into flow patterns and marine traffic.
5	assembling time Rocky Point - Peacock Point (6.2.1)		3		The entire barrier (7.6 km) can be assembled within one week.	Deploy additional lifting vessels
6	assembling time Davenport Park – Sands Point (6.2.1)			4	The entire barrier (4.6 km) can be assembled in four days.	Deploy additional lifting vessels.
7	assembling time Throgs point – Willets Point (6.2.1)			5	The entire barrier (1.2 km) can be assembled in one day.	Deploy additional lifting vessels or increase the length of a segment.
8	Temporary character of the Rocky Point - Peacock Point barrier	2			The barrier is very long, therefore it could be unfeasible to rebuild the entire barrier on a yearly basis	Deploy additional lifting vessels or increase the length of a segment.
9	Temporary character of the Davenport Park - Sands Point barrier			4	The shorter the distance the more likely the barrier can function as a temporary structure.	Deploy additional lifting vessels or increase the length of a segment.

10	Temporary character of the Throgs point – Willets Point barrier				5	The barrier is short enough to function as a temporary barrier.	Deploy additional lifting vessels or increase the length of a segment.
11	shoreline connections (6.2.2)			3		The integration of the connections in the bathymetry is simplified.	Model the connections together with an irregular bathymetry.
12	segment size (6.2.3)				4	The largest size is the most economical and fastest to assemble.	Increase the size to the point it is no longer feasible for lifting and transportation.
13	lifting vessels (6.2.3)	1				The availability and dependency on specialized vessels is undesired	The state should own as many specialized vessels as possible to be ready for deployment on demand
14	segment transportation (6.2.3)			3		The distance of the barrier location from the production facility is large and so the distance over which pollution occurs.	Build a production facility closer to the barrier. The environmental cost of a new facility should be weighed against the already existing one.
15	foundation (6.2.4)	1				Not enough information on the stratigraphy.	Conduct exploratory drillings.
16	segment and concrete floor connection (6.2.4)				5	Using a profiled plate in combination with underwater concrete to properly align the segments solves the alignment problem.	Instead of an underwater concrete floor, a profiled prefabricated plate is preferred.
17	cross-section assembling (6.2.5)				4	The assembling sequence is currently based on one segment at a time placement.	Try assembling in bulk, for example, three segments at a time.
18	construction loop alternation for vessels (6.2.5)				5	The design allows for teams to work independently on barrier parts.	Deploy additional lifting vessels to speed up the process.
19	watertightness (6.2.6)				5	The watertight core row reduced the need for the outer layers of the barrier to be watertight and the need for sheet pile walls.	
20	mortar sealing (6.2.6)				4	Removing the hardened mortar could be challenging.	Laboratory tests are required to assess the applicability.
21	synthetic gaskets (6.2.6)				5	Fastest and most practical solution to achieve a watertight connection.	Laboratory tests are required to determine the exact thickness and shape.
22	brick bond pattern (6.2.6)			3		Estimated to moderately increases internal strength of the structure but complicates the assembling process.	
23	stack bond pattern (6.2.6)				5	fastest and simplest pattern.	

24	cross-section configuration (7.1.3)			4	The pyramid shape is very stable but requires a large number of segments.	Apply different configurations using less segments, while maintaining sufficient strength and stability.
25	mechanical model (7.1.3.)			3	The mechanical model is sufficient to continue designing the segments.	Add more components to analyze a more detailed force distribution and include a deformation or FEM analysis.
26	material properties concrete (7.1.4)			4	A high concrete class provided a slender structure.	Investigate the use of add mixtures and a lower concrete class to achieve comparable strength.
27	material properties prestressing steel (7.1.4)			4	Economic and commonly used option.	Investigate the use of additional wires, number of strands and different tensile strengths.
28	prestressing system (7.1.4)			3	The number of strands, tendons, wires are all within the boundary conditions.	Apply less material where possible while fulfilling the requirements.
29	final cross-section (7.1.4)			4	Able to achieve a relatively slender cross-section.	Apply different material classes and bar diameters to obtain a thinner cross-section.
30	lifting connections (7.2)			4	Easy to lift the segments.	Less connecting padeyes and rods to save material.
31	cost (7.3)			4	Within range of the USACE barrier costs but potential to be a cheaper solution.	In general, by optimizing the design (apply less segments, use cheaper materials) and by reducing the project timetable.

Table 8.1 | Evaluation matrix.

8.2 Ecological construction strategies

The construction process will burden and pollute the local environment. Special attention must be given to mitigating these negative effects, especially since the barrier connects to residential or recreational areas. There are three types of pollutions that deserve extra attention: noise, air and water pollution. First, consider air pollution which is primarily caused by industrial equipment and activities involving toxic chemicals (e.g., the burning of diesel engines), land removal, dredging, demolition and pile driving among others. Other noxious vapors commonly found at construction sites include oils, glues, thinners, paints, treated woods, plastics, cleaners, fumes, tar and more hazardous chemicals (Gray, 2020). Construction sites produce a lot of dust in general and the production of concrete will be a source of additional silica dust which can cause a range of respiratory problems. The segments have to be produced along a channel since transportation on land is not considered feasible. One possible location to consider is College Point Boulevard along Flushing Creek (Figure 8.1) which is an industrial area with building materials and cement production facilities.

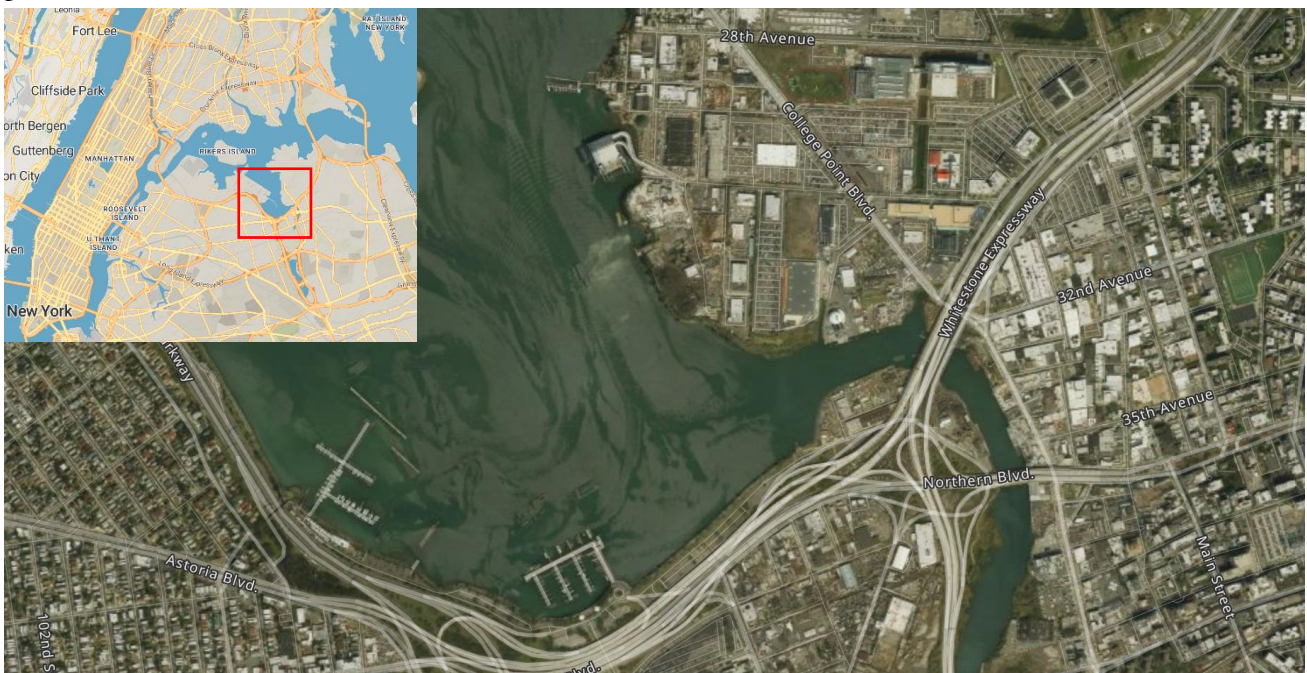


Figure 8.1 | Concrete production location (MapTiler, n.d.).

Together with local partners, a new facility and production supply chain can be realized in this area. Dust accumulates rapidly when cement, admixtures and granular materials are added together and mixed. This process has to be conducted in an enclosed space that is either moist enough or contains a sprinkler system that controls dust accumulation. To be clear, the mixing area is separated from the casting area. Since concrete is mixed in an enclosed space, workers should wear adequate protective gear that prevents too much dust from being inhaled.

Water pollution is the result of oils from machinery, solvents, paints, cleaning and other chemicals. Construction activity in combination with water (e.g., rain) makes the environment soggy or muddy which makes it easier for clean and contaminated soils to mix. The general logistics alone result in the spreading of contaminated soils in the area. The land connecting sites at Rocky Point on the northern shoreline and East beach on the southern shoreline are considered vulnerable areas. On the north side, the construction site lays in-between Rye Playland Beach and Edith G. Read natural park and Wildlife Sanctuary. Oil slick will undoubtedly develop on the surface and can be prevented from reaching the beach and the sanctuary by using oil booms which help control the spread by functioning as a floating wall. Another possible

method is the use of eco-friendly dispersants, for which the applicability should be studied first. A number of methods are in development, for example, the use of microbes in combination with nitrogen and phosphorus that degrade hydrocarbons or the use of a magnetic soap which contains iron-rich salts. Another example would be a magnetic sponge, with a magnetic nanostructure able to bind oil molecules while resisting water (Hannah, 2020). The entire theme park already has the advantage of a hard-asphalted surface which prevents contaminated water from entering the subsoil.

On the southern side, the entire area between East Beach and Peacock Point is surrounded by oil booms and this part of the beach is inaccessible to the public during the project. Any storage location of construction material will maintain sufficient distance from water sources to prevent accidental spillage along the beaches. Furthermore, waste material (e.g., plastics) always end up in the surrounding area, therefore, special attention must be given to local flow patterns that help predict where waste material will end up. Floating fences will help stop the spread of waste material.

Noise pollution experienced by residents on both coasts can be kept to a minimum by working within regular office hours. Noise pollution is expected to be less of a concern midway the channel width, however, any drilling or dredging activities could disturb local marine life. Sound measurements will have to prove at which distance from the coast construction activities can take place outside of the standard office hours as not to disturb residents. The only other option to reduce noise pollution is simply to use industrial material with the lowest decibel output, usually the most modern machinery.

It cannot be overstated how important it is to clean the construction sites regularly. A team of designated site government engineers will keep track of the amount of waste material, spillages or leakages and the areas containing high levels of contaminated soil which ultimately has to be removed and replaced especially along the beaches. The cost of polluting is often considered lower than the cost of preventing pollution, however, the damage in the long run to the environment is likely more costly than taking adequate measures to mitigate polluting construction activities. It is up to the authorities to maintain active involvement in the project ensuring contractors adhere to environmental standards and enforce them if needed.

CHAPTER 9

Conclusions and Recommendations

CHAPTER 9 CONCLUSIONS AND RECOMMENDATIONS.....	90
CHAPTER 9 ABSTRACT	90
9.1 CONCLUSIONS	91
<i>9.1.1 The Segment barrier</i>	<i>91</i>
<i>9.1.2 Applicability</i>	<i>91</i>
9.2 RECOMMENDATIONS	92

Chapter 9 Abstract

This chapter draws conclusions from the design process and provides recommendations to further develop the conceptual design.

9.1 Conclusions

9.1.1 The Segment barrier

The main objective of this thesis was to develop a conceptual design for a new type of storm surge barrier and study the applicability at Long Island Sound, USA with the purpose of protecting New York City and the coastlines of Long Island Sound within the state border from storm surges that migrate from the east side of Long Island Sound towards the city (Section 1.3). This section provides conclusions on the structure itself.

The rough wave climate conditions as a result of recurring severe storms and possible hurricanes, made Long Island Sound a favorable case study location to provide input for the design of the barrier. The end result is a new type of storm surge barrier, the Segment barrier, which is reconstructable, can function as a temporary or permanent barrier and is expandable in size to deal with multiple sea level rise scenarios.

During the design process, it became clear that the ways in which these segments and the overall concept can be optimized is considerably larger than what can be presented in this thesis. The segments have been designed with sufficient strength and stability in mind, yet, despite the their relatively slender cross-section, there are still many more optimizations that can be done regarding the overall strength, configuration and material usage. However, to do this effectively, additional constraints such as costs, timetables or fixed locations are useful.

9.1.2 Applicability

This thesis focused on whether it is possible to build a temporary reconstructable storm surge barrier. This has been achieved and the Segment barrier can be applied in all three analyzed locations to block storm surges. What cannot definitively be answered in this thesis is the barrier's feasibility as a temporary structure. This is strongly dependent on the total length, available equipment to assemble the barrier and the time interval between reconstruction periods, which is assumed to be on a yearly basis in this thesis. In general, the shorter the barrier, the more feasible it is for the structure to function as a temporary barrier. For example, a barrier at Throgs Point – Willets Point (1.25 km) is less expensive and faster to rebuild than the Rocky Point – Peacock Point (8.35 km) location. The longer the barrier gets, the more likely it is for parts of the barrier to remain permanent in position.

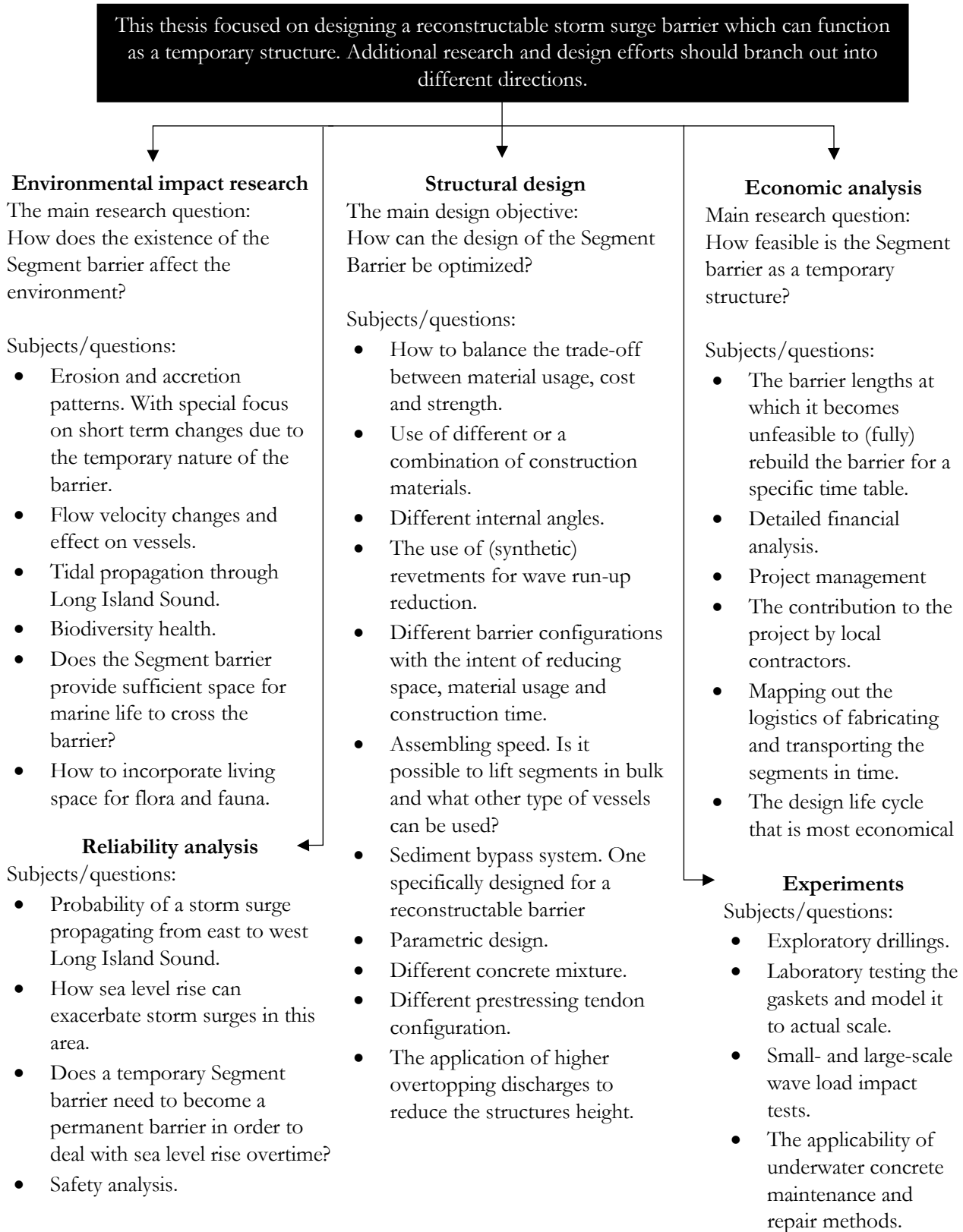
What can further be concluded is that the navigable spaces as laid out in chapter 6 can be closed within sufficient time provided there are enough vessels available. Examples have been given in section 6.2.1. The time it takes to close a navigable section decreases linearly with the number of deployed lifting vessels. The availability of lifting vessels is therefore a crucial part in determining the success of this concept.

Storm surges were the main focus in this thesis; however, the other long-term threat is sea level rise. There are four ways to deal with this: drastically reduce greenhouse gas emissions, migrate local businesses and residential areas along the shorelines land inward, embank the entire shoreline or close off Long Island Sound. It is expected that closing off Long Island Sound and controlling the waterflow through the straight is the most feasible option. The Segment barrier is then applicable as a permanent barrier.

The main objectives of this thesis have been achieved, however, with the development of a new concept, more questions arise that can be answered without in-depth research or designs. Section 9.2 provides a number of recommendations to further develop the concept.

9.2 Recommendations

This thesis laid the foundation for a fully reconstructable storm surge barrier. During the design process, there were many subjects that required in-depth research or design efforts outside the scope of this thesis. The diagram below lists possible directions which can be taken to further develop the concept and require their own dedicated research.



If there is concern regarding tensile forces that can lead to the decoupling of the segments, an adjustment to the design is made to ensure the segments stay in place and the forces are transferred to the foundation. The concept is presented in Figure 9.1 in which, for example, steel bars are fitted through the front and back cover of a segment.

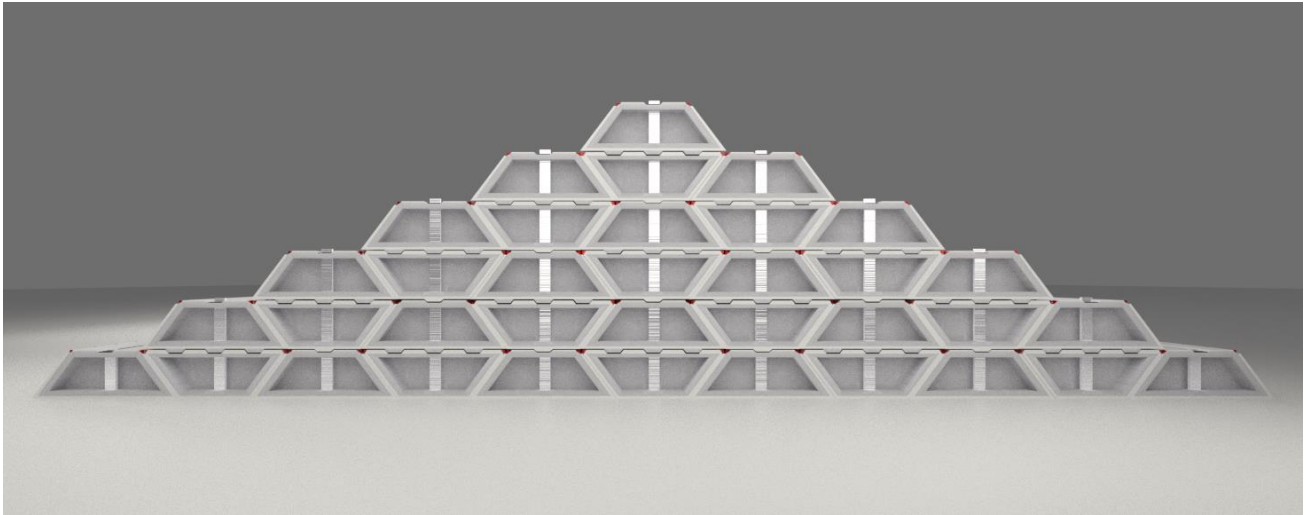


Figure 9.1 | Steel rods fitted through the front and back cover to provide additional strength and stability.

Further research and detailed designs will have to demonstrate the advantages of this configuration.

Finally, it is recommended to explore and analyze the advantages of the Segment barrier's flexibility. Due to the scope limitation of this thesis, only one barrier configuration (basic pyramid) was analyzed. A number of suggestions are presented in the Figure 9.2 below. The objective is to check whether these configurations are stable and able to withstand the environmental loads while using a lower number of segments which has the advantage of lowering cost and speeding up the construction duration.

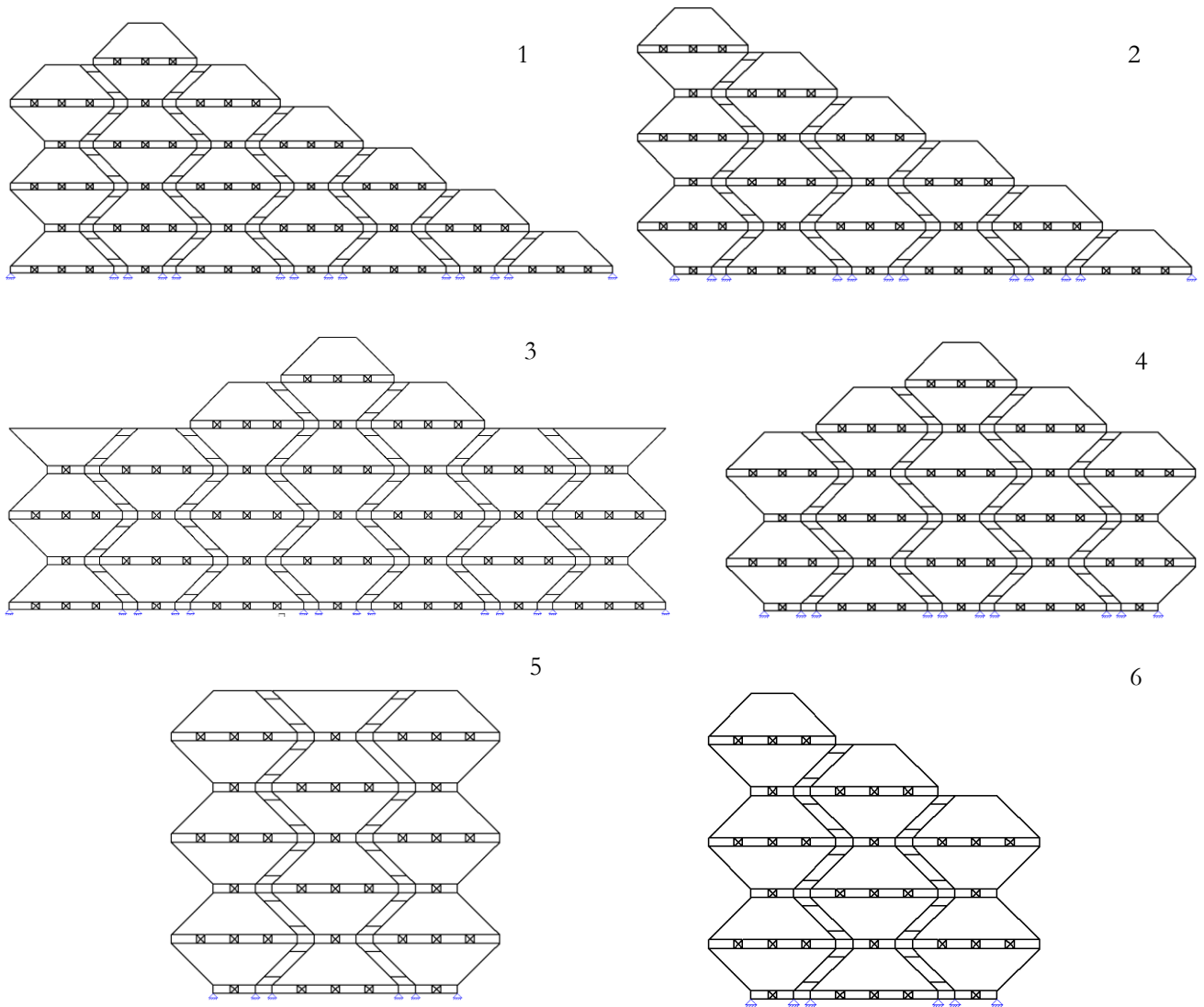


Figure 9.2| Alternate segment configurations for further research.

Finally, this concept has the potential to be applicable for multiple locations around the world, therefore, the wider applicability should be part of additional research.

References

- ACI Committee 546. (1998). *Guide to Underwater Repair of Concrete*. American Concrete Institute.
- AirportTechnology. (2016, 9 16). *DHL Builds New Brussels Hub in Belgium*. Retrieved from airport-technology: <https://www.airport-technology.com/contractors/baggage/saco/pressreleases/pressdhl-builds-new-brussels-hub-belgium/>
- Bastianello, R., & Balmer, C. (2019, November 13). *Venice still waiting for Moses to hold back the seas*. Retrieved from Reuters: <https://www.reuters.com/article/us-italy-weather-venice-mose/venice-still-waiting-for-moses-to-hold-back-the-seas-idUSKBN1XN2EQ>
- Beheshti, M. (1999). *Handboek systematisch ontwerp in de civiele techniek en bouwkunde* (3d ed.). Delft: Delft University Press.
- Bezuyen, K., Stive, M., G.J.C. V., Vrijling, J., & Zitman, T. (2012). *Inleiding Waterbouwkunde*. VSSD.
- Buccino, M., Banfi, D., Vicinanza, D., Calabrese, M., Del Giudice, G., & Carravetta, A. (2012, November 19). Non Breaking Wave Forces at the Front Face of Seawave. *Energies*, pp. 4779-4803. doi:10.3390/en5114779
- C.J.H.Aerts, J., Lin, N., Botzen, W. W., Emanuel, K., & Moel, H. d. (2013). *Low-Probability Flood Risk Modeling for New York City*. doi:10.1111/risa.12008
- Center for Operational Oceanographic Products and Services [CO-OPS]. (2018, April 9). *Datums for 8516945, Kings Point NY*. Retrieved from tidesandcurrents.noaa.gov: <https://tidesandcurrents.noaa.gov/datums.html?datum=MLLW&units=1&epoch=0&id=8516945&name=Kings+Point&state=NY>
- Center for Operational Oceanographic Products and Services. (2018, April 9). *Datums for 8516945, Kings Point NY*. Retrieved from tidesandcurrents.noaa.gov: <https://tidesandcurrents.noaa.gov/datums.html?datum=MLLW&units=1&epoch=0&id=8516945&name=Kings+Point&state=NY>
- Center for Operational Oceanographic Products and Services. (n.d.). *Water Levels - NOAA Tides & Currents*. Retrieved from tidesandcurrents.noaa.gov: <https://tidesandcurrents.noaa.gov/waterlevels.html?id=8516945&units=metric&bdate=20121029&edate=20121030&timezone=GMT&datum=MLLW&interval=6&action=>
- Center for Operational Oceanographic Products and Services. (n.d.). *Water Levels - NOAA Tides & Currents*. Retrieved from tidesandcurrents.noaa.gov: <https://tidesandcurrents.noaa.gov/waterlevels.html?id=8518750&units=metric&bdate=20121029&edate=20121030&timezone=GMT&datum=MLLW&interval=6&action=>
- De Bakker, J. (2003). *Ontwerp klepstuw*.
- DeCrow, J. (2012). *People wade and paddle down a flooded street as Hurricane Sandy approaches*. Ap Images. Retrieved from <https://apimagesblog.com/blog/2017/10/26/superstorm-sandy-fifth-anniversary>
- Dols, C. (2019). *New York-New Jersey [NYNJ] Interim Report Cost Appendix*. New York.
- Elgershuizen, J. H. (1981). Some Environmental Impacts of a Storm Surge Barrier . *Marine Pollution Bulletin*, 265-271.
- European Committee for standardization. (2004). *Eurocode 2: Design of concrete structures - Part 1-1: General rules and rules for buildings*. CEN.
- EurOtop. (2007). *Wave Overtopping of Sea Defences*.
- EurOtop. (2018). *Manual on wave overtopping of sea defences and related structures*.
- Faymonville. (n.d.). *Self-steering trailer for special & heavy-duty transport FlexMAX*. Retrieved from Faymonville: <https://www.faymonville.com/producten/naloper-dolly/flexmax/>
- Faymonville. (n.d.). *Self-steering trailer for special & heavy-duty transport FleMAX*. Retrieved from faymonville: <https://www.faymonville.com/producten/naloper-dolly/flexmax/>
- Flavelle, C. (2020, 07 14). *nytimes*. Retrieved from New Data Shows an 'Extraordinary' Rise in U.S. Coastal Flooding: <https://www.nytimes.com/2020/07/14/climate/coastal-flooding-noaa.html>
- Gates on new Panama canal - Cimolai*. (2016). Retrieved from cimolai: <https://www.cimolai.com/portfolio/gates-on-new-panama-canal/>

- Glerum, A., Vrijling, J., & Bakker, K. (2018). Lecture notes Bored and Immersed Tunnels.
- Google. (n.d.). *Middle Ground - Google Maps*. Retrieved from Google Maps:
<https://www.google.nl/maps/place/Middle+Ground/@40.7881722,-73.9250028,15z/data=!3m1!4b1!4m5!3m4!1s0x89c2f5f44f8dbcd3:0x3759cc25cc06c09e!8m2!3d40.7881568!4d-73.916248>
- Gray, J. (2020, 8 16). *Pollution From Construction*. Retrieved from sustainablebuild:
<http://www.sustainablebuild.co.uk/pollutionfromconstruction.html>
- Groll, M. (2012). *Burned-out homes in the Breezy Point section of the Queens borough*. AP Images. Retrieved from
<https://apimagesblog.com/blog/2017/10/26/superstorm-sandy-fifth-anniversary>
- Hannah, C. (2020, 10 17). *Eco-Friendly Method to Clean Oil Spills*. Retrieved from sciencetimes:
<https://www.sciencetimes.com/articles/27744/20201017/eco-friendly-methods-clean-oil-spills.htm>
- Holthuijsen. (1980). *Methoden voor golfvoorspelling*. Rijkswaterstaat. Retrieved from
<https://repository.tudelft.nl/islandora/object/uuid%3A01bec85d-4ea9-4a2a-afa1-a3c11908a217>
- Introduction to Integral Design. (2007).
- Lennihan, M. (2012). *New York Skyline*. AP Images. Retrieved from
<https://apimagesblog.com/blog/2017/10/26/superstorm-sandy-fifth-anniversary>
- Lindsey, R. (2020, August 14). *Climate Change: Global Sea Level*. Retrieved from climate.gov:
<https://www.climate.gov/news-features/understanding-climate/climate-change-global-sea-level>
- Long Island Sound Study. (n.d.). *By the numbers - Long Island Sound Study*. Retrieved from Longislandsoundstudy.net:
<https://longislandsoundstudy.net/about-the-sound/by-the-numbers/>
- Lopeman, M., Deodatis, G., & Franco, G. (2015, 4 29). Extreme storm surge hazard estimation in lower. *Natural Hazards*, pp. 355-391. doi:10.1007/s11069-015-1718-6
- M. Kluijver, C. D. (2019). Advances in the Planning and Conceptual Design of Storm Surge Barriers – Application to the New York Metropolitan Area.
- MapTiler. (n.d.). *maps preview*. Retrieved from maptiler: <https://www.maptiler.com/maps/#b992018d-d296-4562-9e33-2f86e28d0e2c/-vector/10.29/-73.8586/40.8407/-13.60/14.5>
- May, S. (2017, 8 7). *What Are Hurricanes? | NASA*. Retrieved from nasa.gov:
<https://www.nasa.gov/audience/forstudents/k-4/stories/nasa-knows/what-are-hurricanes-k4.html>
- McGeehan, P. (2019, 5 5). *6 Years After Hurricane Sandy, Here's What They Came Up With: Really Big Sandbags*. Retrieved from nytimes: <https://www.nytimes.com/2019/05/05/nyregion/hurricane-sandy-manhattan-flooding.html>
- Minchillo, J. (2012). *Sea water flooding Ground Zero construction site [Photograph]*. AP Images. Retrieved from
<https://apimagesblog.com/blog/2017/10/26/superstorm-sandy-fifth-anniversary>
- Ministero delle Infrastrutture e dei Trasporti. (n.d.). *MOSE Venezia | Bocca di Malamocco*. Retrieved from MOSE:
<https://www.mosevenezia.eu/bocca-di-malamocco-2/>
- Ministero delle Infrastrutture e dei Trasporti. (n.d.). *MOSE Venezia | Project*. Retrieved from mosevenezia:
<https://www.mosevenezia.eu/project/?lang=en>
- MOSE. (n.d.). *MOSE Venezia | Project*. Retrieved from mosevenezia:
<https://www.mosevenezia.eu/project/?lang=en>
- National Hurricane Center [NHC]. (2013). *Tropical Cyclone Report Hurricane Sandy*. Retrieved February 12, 2013, from
https://www.google.com/url?sa=t&rct=j&q=&esrc=s&source=web&cd=&ved=2ahUKEwiTkbz_jMvpAhWNzqQKHbVmDF4QFjAAegQIBhAB&url=https%3A%2F%2Fwww.nhc.noaa.gov%2Fdata%2Ftcr%2FAL182012_Sandy.pdf&usg=AOvVaw3GRzPGoGL-E7ZveYjve7RA
- NDS Seals. (n.d.). *Neopreen*. Retrieved from ndsseals: <https://www.ndsseals.com/nl/materialen/neopreen/>
- NOAA. (n.d.). *Bathymetric Data Viewer*. Retrieved from <https://maps.ngdc.noaa.gov/viewers/bathymetry/>
- NYC SIRR. (2013). *Sandy and Its Impacts*. New York.
- NYS 2100 Commission. (2013). *Recommendations to Improve the Strength and Resilience of the Empire State's Infrastructure*. Retrieved from <http://www.governor.ny.gov/assets/documents/NYS2100.pdf>.
- Oosterhoff, J. (2008). *Kracht + vorm*. Zoetermeer: Bouwen met Staal.
- Point2. (n.d.). *Real Estate | Homes for Sale & Rent by Point2*. Retrieved from point2homes.com/US:
<https://www.point2homes.com/US>

- Poppe, L., Knebel, H., Mlodzinska, Z., Hastings, M., & Seekins, B. (2000). Distribution of Surficial Sediment in Long Island Sound and Adjacent Waters: Texture and Total Organic Carbon. *Journal of Coastal Research*.
- R. M. Schwartz, C. S. (2015). The impact of Hurricane Sandy on the mental health of New York area residents. *American Journal of disaster medicine*. doi:10.5055/ajdm.2015.0216
- Rijkswaterstaat. (2013). *Maeslantkering Stormvloedkering in de Nieuwe Waterweg*. Rijkswaterstaat. Retrieved from rijkswaterstaat.
- Rijkswaterstaat. (n.d.). *Maeslantkering* | *Rijkswaterstaat*. Retrieved from Rijkswaterstaat: <https://www.rijkswaterstaat.nl/water/waterbeheer/bescherming-tegen-het-water/waterkeringen/deltawerken/maeslantkering/index.aspx>
- Rijkswaterstaat. (n.d.). *Oosterscheldekering* | *Rijkswaterstaat*. Retrieved from Rijkswaterstaat: <https://www.rijkswaterstaat.nl/water/waterbeheer/bescherming-tegen-het-water/waterkeringen/deltawerken/oosterscheldekering/index.aspx>
- Royal Boskalis Westminster N.V. (n.d.). *Heavy Lift Vessels*. Retrieved from Boskalis: <https://boskalis.com/about-us/fleet-and-equipment/offshore-vessels/heavy-lift-vessels.html>
- Stancati, M., & Sylvers, E. (2019, 11 21). *The Wall That Would Save Venice From Drowning Is Underwater*. Retrieved from wsj: <https://www.wsj.com/articles/the-wall-that-would-save-venice-from-drowning-is-underwater-11574332203>
- State of New York Department of Transportation. (n.d.). *Special Hauling Permit*. Retrieved from ny.gov: <https://www.dot.ny.gov/nypermits/special-hauling-permits>
- Tensa B.V. (n.d.). *Tensacciai Post-Tensioning System*. Breda.
- The New York Times. (2012, 10 29). *Map of Hurricane Sandy's Path*. Retrieved from nytimes.com: <http://archive.nytimes.com/www.nytimes.com/interactive/2012/10/26/us/hurricane-sandy-map.html>
- TU Delft. (2016). *General Lecture Notes Hydraulic Structures 1*. Delft.
- TU Delft. (2017). *Flood defences Lecture notes CIE5314*. Delft: TU Delft.
- TU Delft. (2018). *General Lecture Notes Hydraulic Structures 1*. Delft.
- U.S. Army Corps of Engineers [USACE], New Jersey Department of Environmental Protection [NJDEP], New York State Department of Environmental Conservation [NYSDEC], Mayor's Office of Recovery & Resilience. (2019b). *NEW YORK-NEW JERSEY JERSEY HARBOR AND TRIBUTARIES NEW YORK DISTRICT. Interim Report Engineering Analyses*. Retrieved from <https://www.nan.usace.army.mil/Portals/37/docs/civilworks/projects/ny/coast/NYNJHAT/NYNJHAT%20Interim%20Report%20Engineering%20Analyses%20Feb2019.pdf?ver=2019-02-20-121410-493>
- U.S. Army Corps of Engineers. (n.d.). *About Us*. Retrieved from USACE website: <https://www.usace.army.mil/About/>
- U.S. Army Corps of Engineers, New Jersey Department of Environmental Protection, New York State Department of Environmental Conservation, Mayor's Office of Recovery & Resilience. (2019). *NEW YORK-NEW JERSEY HARBOR AND TRIBUTARIES COASTAL STORM RISK MANAGEMENT INTERIM REPORT*. Retrieved from <https://www.nan.usace.army.mil/Portals/37/docs/civilworks/projects/ny/coast/NYNJHAT/NYNJHAT%20Interim%20Report%20-%20Main%20Report%20Feb%202019.pdf>
- U.S. Army Corps of Engineers, New Jersey Department of Environmental Protection, New York State Department of Environmental Conservation, Mayor's Office of Recovery & Resilience. (2019b). *NEW YORK-NEW JERSEY JERSEY HARBOR AND TRIBUTARIES NEW YORK DISTRICT. Interim Report Engineering Analyses*. Retrieved from <https://www.nan.usace.army.mil/Portals/37/docs/civilworks/projects/ny/coast/NYNJHAT/NYNJHAT%20Interim%20Report%20Engineering%20Analyses%20Feb2019.pdf?ver=2019-02-20-121410-493>
- U.S. Energy Information Administration. (2012, 11 9). *Electricity restored to many in the Northeast but outages persist*. Retrieved from eia.gov: <https://www.eia.gov/todayinenergy/detail.php?id=8730>
- United States Census Bureau. (n.d.). Retrieved from <https://www.census.gov/>
- United States Department of Commerce [USDC]; National Oceanic and Atmospheric Administration [NOAA]; National Ocean Service [NOS]. (2020, 1 24). *Coastal Flood Exposure Mapper*. Retrieved from [coast.noaa.gov: https://coast.noaa.gov/floodexposure/#-](https://coast.noaa.gov/floodexposure/#-)

8214793,4987057,12z/eyJiIjoizGFyayIsImgiOiJoYXphcmRDd21wb3NpdGV8MXwiLCJyIjpmYWxzZX0=

- United States Environmental Protection Agency. (n.d.). *Environmental Justice*. Retrieved from EPA: <https://www.epa.gov/environmentaljustice/factsheet-epas-office-environmental-justice>
- United States Geological Survey [USGS]. (2014). *Hurricane Sandy: Observation and Analysis of Coastal Change*. Reston. Retrieved from <https://pubs.usgs.gov/of/2014/1088/>
- United States of America Department of Commerce [USADC], USGS, United States Environmental Protection Agency [USEPA], Rutgers University. (2017). *GLOBAL AND REGIONAL SEA LEVEL RISE SCENARIOS FOR THE UNITED STATES*. Retrieved from https://tidesandcurrents.noaa.gov/publications/techrpt83_Global_and_Regional_SLR_Scenarios_for_the_US_final.pdf.
- USACE. (2019). *NY & NJ Harbor & Tributaries Focus Area Feasibility Study (HATS)*. Retrieved from New York District Website Website: <https://www.nan.usace.army.mil/Missions/Civil-Works/Projects-in-New-York/New-York-New-Jersey-Harbor-Tributaries-Focus-Area-Feasibility-Study/>
- USACE. (n.d.). *NY & NJ Harbor & Tributaries Focus Area Feasibility Study (HATS)*. Retrieved from US Army Corps of Engineers New York District Website: <https://www.nan.usace.army.mil/Missions/Civil-Works/Projects-in-New-York/New-York-New-Jersey-Harbor-Tributaries-Focus-Area-Feasibility-Study/>
- VSL International Ltd. (2013). *VSL post-tensioning solutions*.
- Walraven, J., & Braam, C. (2019). *Prestressed concrete*. Delft University of Technology.
- Watersnoodmuseum. (n.d.). *Oosterscheldekering - Watersnoodmuseum*. Retrieved from watersnoodmuseum: <https://watersnoodmuseum.nl/kennisbank/oosterscheldekering/>

Appendices

Appendix A: Mathematical derivation of the basic geometry

The basic shape of the segments which make up the barrier is the trapezium shown in Figure A.1. The decision to use trapezia is based on a higher degree of natural stability (against rotation) compared to squares and it requires less material than triangles when stacking segments. In order to maintain full control over the dimensions, the trapezium will have to scale uniformly, i.e., the thickness of each side (A1-4 in Figure A.1) will remain equal when increasing or decreasing the full geometry. This is important for determining the structural strength and the amount of required material. The mathematical derivation to achieve uniform scaling is derived in this section.

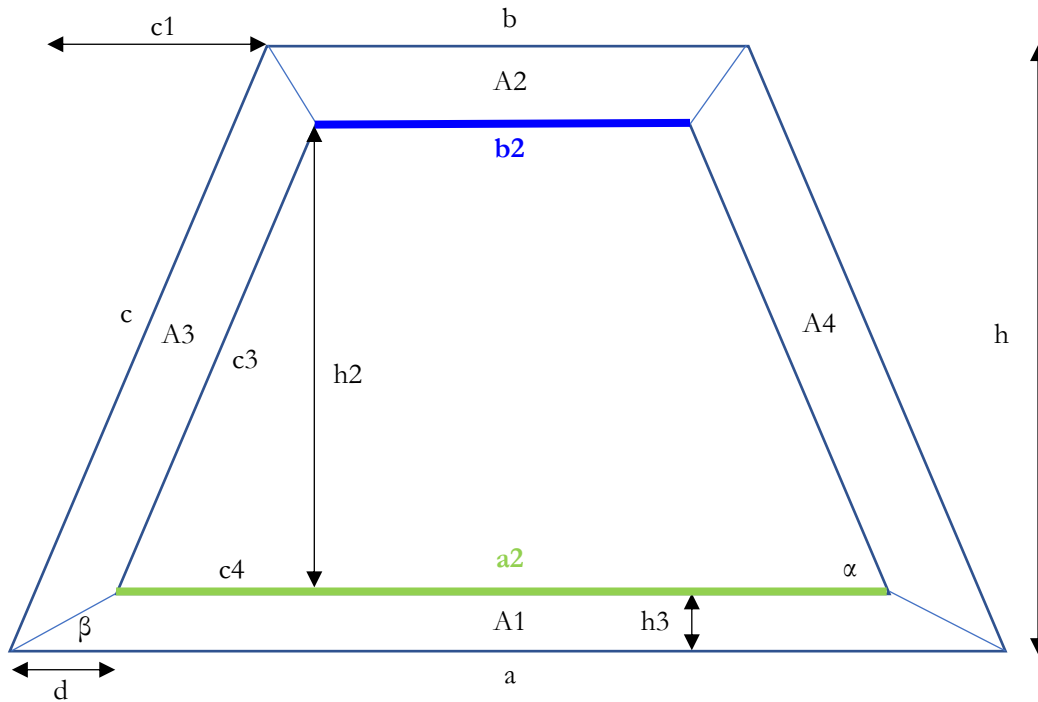


Figure A.1 | Trapezium geometry definition.

The cross-section has been subdivided into four parts with surface areas A1-4. By design, the only scalable parameters are the outer height (h), thickness (h_3), outer base length (a) and outer top length (b). The mathematical derivation to achieve uniform scaling, i.e., obtaining equally thick sides when scaling, is presented below.

For the areas A1 and A2, the thickness (h_3) must remain constant. These are determined as follow:

$$A1 = \frac{1}{2} \cdot (a_2 + a) \cdot h_3 \quad (\text{A.1})$$

$$A2 = \frac{1}{2} \cdot (b + b_2) \cdot h_3 \quad (\text{A.2})$$

The expressions for the individual sides are given by:

$$c = \sqrt{c_1^2 + h^2} \quad (\text{A.3})$$

$$c_1 = \frac{a-b}{2} \quad (\text{A.4})$$

$$c_3 = \sqrt{h_2^2 + c_4^2} \quad (\text{A.5})$$

$$c_4 = (a_2 - b_2)/2 \quad (\text{A.6})$$

The diagonal sides have the same surface areas; thus, the expression reads:

$$A3 = A4 = \frac{1}{2} \cdot (c + c_3) \cdot h \quad (\text{A.7})$$

Examining the inner trapezium, (b_2) will be expressed as a function of a_2 , h_2 and α using the trigonometric properties of a triangle:

$$b_2 = a_2 - \frac{(2 \cdot h_2)}{\tan(\alpha)} \quad (\text{A.8})$$

Finally, the left bottom corner is examined. An expression for distance a_2 and d is found as follow:

$$a_2 = a - 2 \cdot d \quad (\text{A.9})$$

$$d = \frac{h_3}{\tan(\frac{1}{2}\alpha)} \quad (\text{A.10})$$

The end result is a uniformly scalable geometry. Two arbitrary examples are shown in Figure A.2.

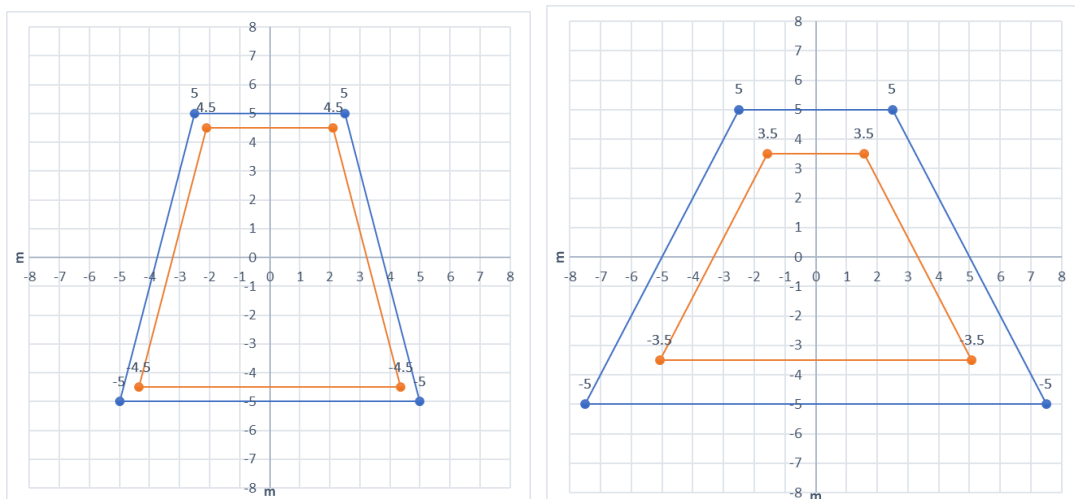


Figure A.2 | Example of uniformly scaled trapezia with evenly thick sides.

A summary of the cross-section for the final concept (section 6.1) relating to Figure A.1 is shown in Table A.1.

description	symbol	value	unit
outer base length	a	15.00	m
outer top length	b	5.00	m
outer height	h	5.00	m
thickness	h3	0.50	m
outer surface area	Aout	50.00	m ²
angle	α	45.00	degree (°)
Inner base length	a2	12.59	m
Inner top length	b2	4.59	m
Inner height	h2	4.00	m
Inner surface area	Ain	34.34	m ²
corner angle	β	22.50	degree (°)
corner length	d	1.21	m
diag. edge length	c	7.07	m
horz. edge length	c1	5.00	m
diag. edge length	c3	5.66	m
horz. edge length	c4	4.00	m
surface area 1	A1	6.90	m ²
surface area 2	A2	2.40	m ²
surface area 3	A3	3.18	m ²
surface area 4	A4	3.18	m ²
total surface area	Atot	15.66	m ²
length	l	50	m
volume	v	782.84	m ³

Table A.1 | Dimensions of the cross-section for the final concept. Input values colored red.

The resulting cross-section related to the input values of Table A.1 are shown in Figure A.3.

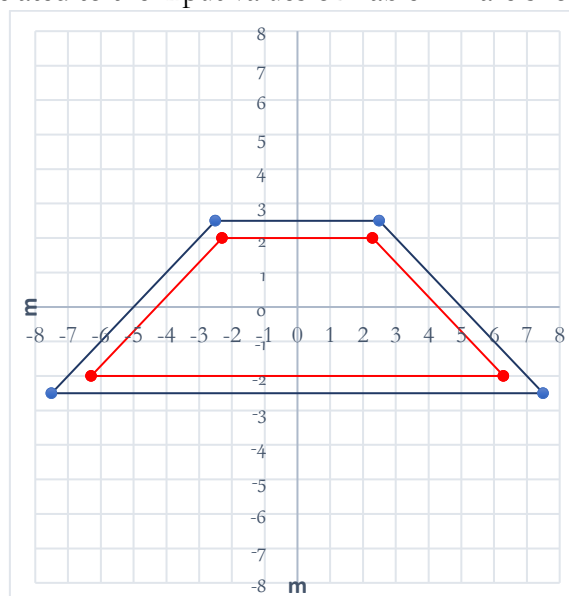


Figure A.3 | Large segment cross-section relating to Table A.1.

Appendix B: Crest elevation of the barrier

B1 Introduction

In this section the height of the barrier is calculated. In order to achieve this, an indication of the wave climate is needed which can be estimated in multiple ways, therefore, three wave climate estimations are made:

- The first estimation is directly based on Hurricane Sandy's wave climate. The barrier should be able to stop waves of this magnitude (section D2.11).
- The second wave climate estimation is based on a combination of the local water depth, wind conditions and fetch length.
- The third wave climate estimation considers intensified conditions.

One scenario will eventually be governing (section B3) and used for further analyses. It is noted that the third and second estimations take into account global mean sea level rise and different outer slope angles.

An inclined hydraulic structure experiences wave runup and possible overtopping. In order to determine the required crest elevation to achieve an acceptable overtopping discharge, it is important to understand the wave climate, i.e., the water levels and wave characteristics. Hurricane Sandy's wave climate is taken as reference for it was the most impactful storm in New York City's recorded history (NYC SIRR, 2013). Figure B.1 shows Hurricane Sandy's track and the location of three NOAA NDBC Buoy's which record wave heights and periods. Buoy 44065 is located in 50 m deep water, approximately 28 km southeast of Breezy Point (NY) which recorded a significant wave height (H_s) of 9.9 m and dominant wave period (T_s) of 13 s. These are the highest recorded values since Hurricane Irene's 2011 records (United States Geological Survey [USGS], 2014, p. 4). The Segment barrier is designed to withstand a storm surge of Hurricane Sandy's magnitude.

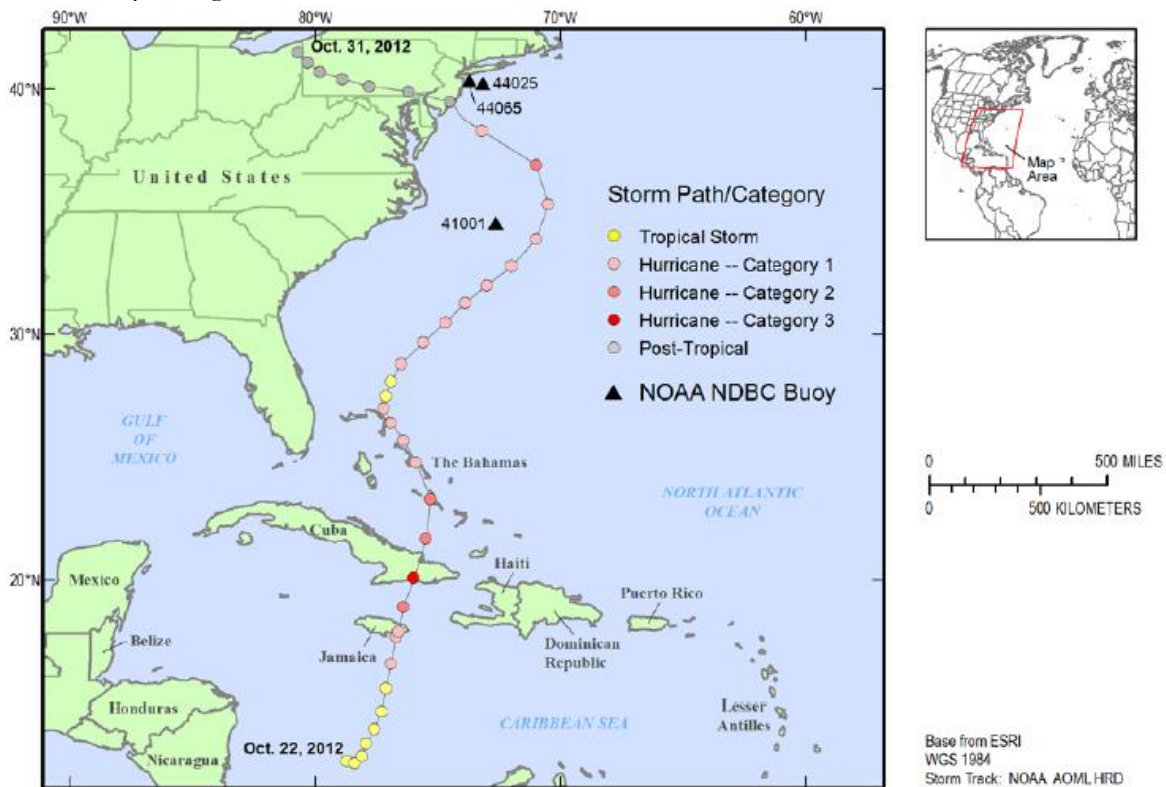


Figure B.1 | Hurricane Sandy's track, intensity and NOAA NDBC Buoy locations (United States Geological Survey [USGS], 2014, p. 3).

Figure B.2 shows how wave run-up is defined for an inclined structure with a smooth and impermeable slope. The freeboard (R_C) is calculated to determine the barrier's height.

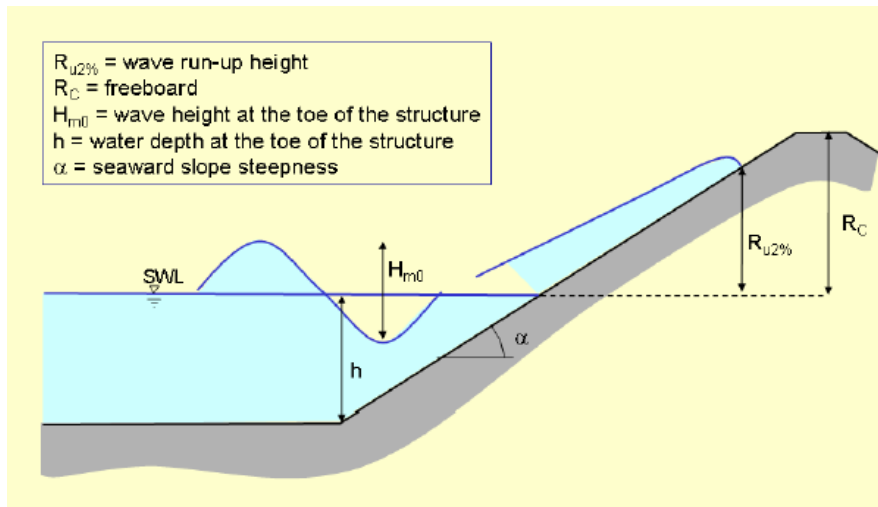


Figure B.2 | Definition of the wave run-up height $R_{u2\%}$ on a smooth impermeable slope (EurOtop, 2007, p. 69)

Table B.1 summarizes the hazard types associated with mean overtopping discharge values.

Hazard Type (ULS)	Mean Discharge q [l/s/m]	Max. Volume [l/m]
Embankment seawalls / sea dikes		
No damage if crest and rear slope are well protected	50 - 200	
No damage to crest and rear face of grass covered embankment of clay	1 - 10	
No damage to crest and rear face of embankment if not protected	0.1	
Promenade or revetment seawalls		
Damage to paved or armoured promenade behind seawall	200	
Damage to grassed or lightly protected promenade or reclamation cover	50	
Hazard type (SLS)	Mean Discharge q [l/s/m]	Max. Volume [l/m]
For pedestrians		
Trained staff, well shod and protected, expecting to get wet, overtopping flows at lower levels only, no falling jet, low danger of, fall from walkway	1 - 10	500 at low level
Aware pedestrian, clear view of the sea, not easily upset or frightened, able to tolerate getting wet, wider walkway	0.1	
For vehicles		
Driving at low speed, overtopping by pulsating flows at low flow depths, no falling jets, vehicle not immersed	10 - 50	100-1000
Driving at moderate or high speed, impulsive overtopping giving falling or high velocity jets	0.01 – 0.05	
For property behind the defence		
Significant damage or sinking of larger yachts	50	1000-10000
Sinking small boats set 5 - 10 m from wall; damage to larger yachts	10	
Building structure elements	1	
Damage to equipment set back 5 - 10 m	0,4	

Table B.1 | ULS and SLS requirements for overtopping (TU Delft, 2016, p. 104).

The overtopping discharge formula (EurOtop, 2018, p. 253) for steep slopes (1:2 to 1: (4/3)) is given by:

$$\frac{q}{\sqrt{g \cdot H_{m0}^3}} = 0.1035 \cdot \exp \left[- \left(1.35 \cdot \frac{Rc}{H_{m0} \cdot \gamma_f \cdot \gamma_\beta} \right)^{1.3} \right] \quad (\text{B.1})$$

For smooth slopes (1:2.5 to 1:4) the overtopping formula (EurOtop, 2018, p. 242) is given by:

$$\frac{q}{\sqrt{g \cdot H_{m0}^3}} = \frac{0.026}{\sqrt{\tan(\alpha)}} \cdot \gamma_b \cdot \xi_{m-1,0} \cdot \exp \left[- \left(2.5 \cdot \frac{Rc}{H_{m0} \cdot \gamma_f \cdot \gamma_\beta \cdot \gamma_b \cdot \gamma_v} \right)^{1.3} \right] \quad (\text{B.2})$$

Where:

- $a [-] = \frac{0.067}{\sqrt{\tan(\alpha)}} \cdot \gamma_b \cdot \xi_{m-1,0}$
- $b [-] = \frac{4.3}{\xi_{m-1,0} \cdot \gamma_b \cdot \gamma_f \cdot \gamma_\beta \cdot \gamma_v}$
- $\alpha [^\circ]$ = the seaward slope steepness of the structure
- $\xi_{m-1,0} [-]$ = iribarren number (breaker parameter)
- $\gamma_b [-]$ = influence factor of a berm
- $\gamma_f [-]$ = influence factor for the permeability and roughness of the slope
- $\gamma_\beta [-]$ = factor for oblique wave attack
 - $\gamma_\beta = 1 - 0.0033 |\beta|$ for $0^\circ \leq \beta \leq 80^\circ$
 - $\gamma_\beta = 0.736$ for $\beta > 80^\circ$
- $\gamma_v [-]$ = influence factor for a vertical wall on top of the crest
- $g [\text{m/s}^2]$ = gravitational acceleration
- $q [\text{m}^3/\text{s}/\text{m}]$ = overtopping discharge
- $H_{m0} [\text{m}]$ = estimate of significant wave height from spectral analysis
- $Rc [\text{m}]$ = crest height

B1.2 Steep slopes

Sections B1.2-3 analyses the first scenario for a significant wave height (H_s) of 9.9 m and dominant wave period (T_s) of 13 s. The crest height for a structure with a steep slope ($\alpha \geq 45^\circ$) is calculated as follow:

The spectral wave height H_{m0} [m] is given by:

$$H_{m0} \approx H_s \quad (\text{B.3})$$

The deep-water wave period $T_{m-1,0}$ [m] is given by:

$$T_{m-1,0} = 0.9 \cdot T_s = 11.7 \quad (\text{B.4})$$

A berm (γ_b) and vertical wall (γ_v) are not present, therefore, these values are set to '1'. The slope of the barrier is stepwise and therefore reduces the wave run-up with a roughness reduction factor ($\gamma_f = 0.3$) based on technical judgement. The influence on wave run-up reduction is assumed to be more effective than those of for example tetrapod's ($\gamma_f = 0.38$) (EurOtop, 2018, pp. 175-176). However, scale model tests are necessary to verify this.

Oblique wave attacks are assumed to be non-present, therefore $\gamma\beta = 1$. The overtopping discharge is limited to $q = 50$ l/s/m (Table B.1) based on the value for the USACE conceptual design (USACE et al., 2019b, p. 11), which still allows for vehicles to cross the barrier should this be necessary for maintenance purpose for example. No damage is expected to the structure if the crest and rear slopes are well protected.

Structures with a steep angle exceeding the lower limit (1:2) result in the same run-up. Therefore, the crest height for steep slopes (R_c) can be determined as follow:

$$\frac{q}{\sqrt{g \cdot H_{m0}^3}} = 0.1035 \cdot \exp \left[- \left(1.35 \cdot \frac{R_c}{H_{m0} \cdot \gamma_f \cdot \gamma_\beta} \right)^{1.3} \right] \rightarrow \quad (\text{B.5})$$

$$\frac{0.05}{\sqrt{9.81 \cdot 9.9^3}} = 0.1035 \cdot \exp \left[- \left(1.35 \cdot \frac{R_c}{9.9 \cdot 0.3 \cdot 1} \right)^{1.3} \right] \rightarrow R_c = 7.9 \text{ m}$$

Local ground subsidence (0.5 m) is assumed to be incorporated in the crest height (R_c) calculation.

B1.3 Gentle slopes

For gentle slopes, the seaward slope angle α is relevant for the overtopping. The value of α is based on the geometry of the overall structure when all barrier segments are stacked in a pyramid configuration. Two cases for gentle slopes (1:3 and 1:4) are considered.

The spectral wave height H_{m0} [m]:

$$H_{m0} \approx H_s \quad (\text{B.6})$$

The deep-water wave period $T_{m-1,0}$ [m] is given by:

$$T_{m-1,0} = 0.9 \cdot T_s = 11.7 \quad (\text{B.7})$$

The deep-water wave length [s] is given by:

$$L_{m,-1,0} \approx \frac{g \cdot T_{m-1,0}^2}{2 \cdot \pi} = \frac{9.81 \cdot 11.7^2}{2 \cdot \pi} = 213.7 \text{ m} \quad (\text{B.8})$$

$$\xi_{m-1,0} = \frac{\tan(\alpha)}{\sqrt{\frac{H_{m0}}{L_{m,-1,0}}}} = \frac{0.33}{\sqrt{\frac{9.9}{213.7}}} = 1.55 \quad (\text{B.9})$$

For a slope 1:3 ($\alpha = 18.4^\circ$) the crest height is determined as follow:

$$\frac{q}{\sqrt{g \cdot H_{m0}^3}} = \frac{0.026}{\sqrt{\tan(\alpha)}} \cdot \gamma_b \cdot \xi_{m-1,0} \cdot \exp \left[- \left(2.5 \cdot \frac{R_c}{H_{m0} \cdot \gamma_f \cdot \gamma_\beta \cdot \gamma_b \cdot \gamma_v} \right)^{1.3} \right] \rightarrow \quad (\text{B.10})$$

$$\frac{0.05}{\sqrt{9.81 \cdot 9.9^3}} = \frac{0.026}{\sqrt{\tan(18.4)}} \cdot 1 \cdot 1.55 \cdot \exp \left[- \left(2.5 \cdot \frac{R_c}{9.9 \cdot 0.3 \cdot 1 \cdot 1 \cdot 1} \right)^{1.3} \right] \rightarrow R_c = 6.3 \text{ m}$$

For a slope 1:4 ($\alpha = 14.0^\circ$) the crest height is determined as follow:

$$\frac{q}{\sqrt{g \cdot H_{m0}^3}} = \frac{0.026}{\sqrt{\tan(\alpha)}} \cdot \gamma_b \cdot \xi_{m-1,0} \cdot \exp \left[- \left(2.5 \cdot \frac{Rc}{H_{m0} \cdot \gamma_f \cdot \gamma_\beta \cdot \gamma_b \cdot \gamma_v} \right)^{1.3} \right] \rightarrow \quad (\text{B.11})$$

$$\frac{0.05}{\sqrt{9.81 \cdot 9.9^3}} = \frac{0.026}{\sqrt{\tan(14)}} \cdot 1 \cdot 1.16 \cdot \exp \left[- \left(2.5 \cdot \frac{Rc}{9.9 \cdot 0.3 \cdot 1 \cdot 1 \cdot 1} \right)^{1.3} \right] \rightarrow Rc = 4.6 \text{ m}$$

B1.4 Discussion

What is illustrated in sections B1.2-3 is that different sea side barrier slopes can provide the same level protection, i.e., prevent a significant wave height of 9.9 m from damaging the hinterland. However, the trade-offs should be noted when deciding which slope to apply (section B3). These relate to costs, materials, stability, segment size and construction speed. The run-up values for steep slopes above the lower limit (1:2) are the same which makes it desirable to build a 1:1 slope which save on material. This principle is schematized in Figure B.3. The trapezoidal shapes represent the large-scale segments (5 m high) on the outer slope of the barrier.

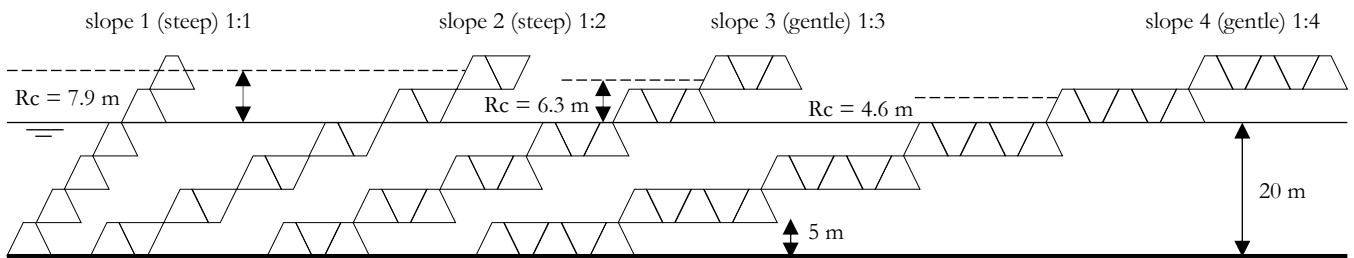


Figure B.3 | Seaside slope segments under steep and gentle angles.

For this analysis, the number of segments required to make an impermeable slope is indicative of the amount of material required for a complete barrier. Figure B.3 shows that decreasing the slope from 1:1 to 1:2 requires 6 additional segments, thus more material to achieve the same required 7.9 m crest height. Variations in gentle slopes affect the freeboard (Rc) as shown in Figure B.3. Although the crest heights are lower, the overall width of the structure increases, again increasing the amount of required material. It is noteworthy to reiterate that all segments have the exact same (optimal) geometry in order to distribute loads between segments most efficiently. Therefore, the outer slopes remain a combination of linearly (1:n) stacked identical segment. The reader is referred to (Appendix D1) for a detailed explanation on the decision-making process regarding the segment's internal angle α .

B2 Sea level rise scenarios

One of the advantages of the Segment barrier is its ability to adapt to changing environmental conditions. This section takes into account the uncertainty of sea level rise for each scenario (section 3.2.2). For the second wave climate estimation, the significant wave height (H_s) and period (T_s) are recalculated using the equations by Young and Verhagen (TU Delft, 2016, p. 89):

$$H_t = H_\infty \left\{ \tanh(0.343 \cdot d_t^{1.14}) \cdot \tanh \left(\frac{4.41 \cdot 10^{-4} \cdot F_t^{0.79}}{\tanh(0.343 \cdot d_t^{1.14})} \right) \right\}^{0.572} \quad (\text{B.12})$$

$$T_t = T_\infty \left\{ \tanh(0.10 \cdot d_t^{2.01}) \cdot \tanh \left(\frac{2.77 \cdot 10^{-7} \cdot F_t^{1.45}}{\tanh(0.10 \cdot d_t^{2.01})} \right) \right\}^{0.187} \quad (\text{B.13})$$

Where:

- $H_t [-] = \frac{g \cdot H_{m0}}{U_{10}^2}$
- $T_t [-] = \frac{g \cdot T_p}{U_{10}}$
- $F_t [-] = \frac{g \cdot F}{U_{10}^2}$
- $d_t [-] = \frac{g \cdot d}{U_{10}^2}$
- F [m] = fetch
- d [m] = water depth
- U_{10} [m/s] = wind velocity at 10 m altitude
- T_p [s] = peak wave period
- $H_\infty [-] = \text{dimensionless wave height at deep-water} = 0.24$
- $T_\infty [-] = \text{dimensionless wave period at deep-water} = 7.69$

The fetch (F) is estimated using a 30-degree angle (α) between the incoming wind direction and the nearest coast (Holthuijsen, 1980, p. 64). The Wind is assumed to travel perpendicular to the barrier as shown in Figure B.4.

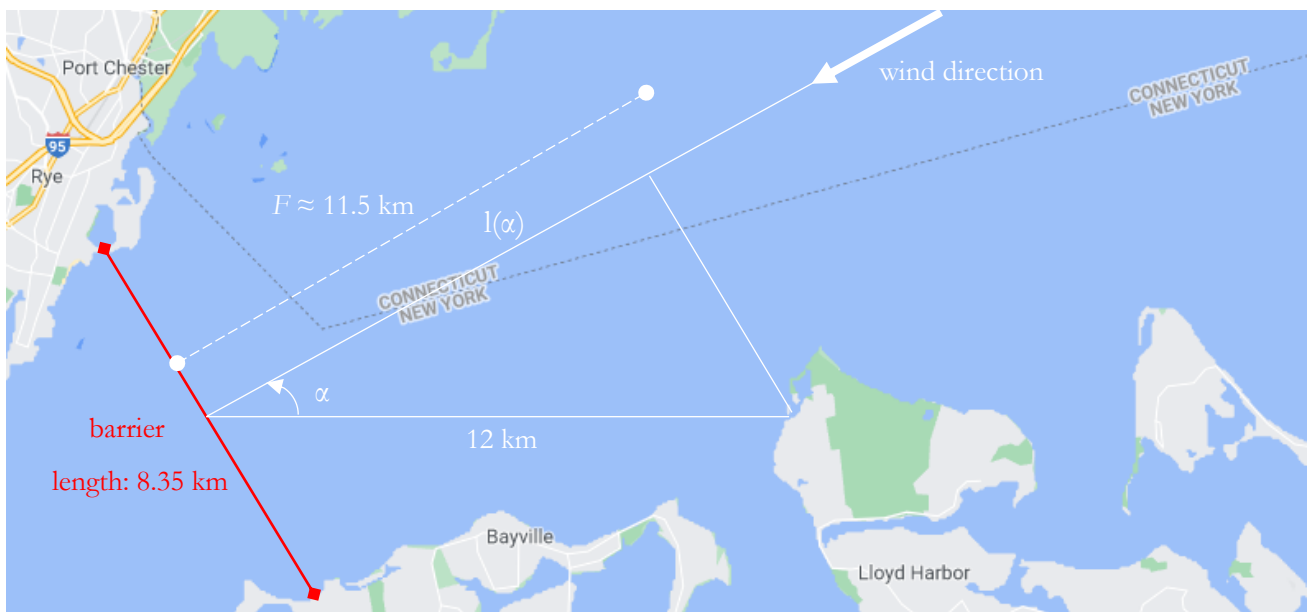


Figure B.4 | Diagram for estimating the fetch length (Google Maps).

The following relation is used to determine the fetch length (Holthuijsen, 1980, p. 64):

$$F = \frac{\int_{-\alpha_m}^{\alpha_m} (w(\alpha) \cdot l(\alpha)) \cdot d\alpha}{\int_{-\alpha_m}^{\alpha_m} w(\alpha) \cdot d\alpha} = \frac{\int_{-30}^{30} (\cos(\alpha) \cdot 12000 \cdot \cos(\alpha)) \cdot d\alpha}{\int_{-30}^{30} \cos(\alpha) \cdot d\alpha} = 11,500 \text{ m} \quad (\text{B.14})$$

For the second wave climate estimation, a maximum sustained wind velocity ($U10$) of 33.4 m/s is assumed (section 2.1.1, Figure 2.5-6) and an average water depth (d) of 20 m. The height of the barrier for steep and gentle slope configurations are calculated following the same methods as described in sections B1.2-3 while taking into account all global mean sea level rise scenarios (Figure 3.2). The results are presented in Table B.2.

Global Mean Sea Level Rise (GMSLR)		Significant Wave Height (Hs) [m]	Significant Wave Period (Ts) [m]	Crest Height (Rc) [m]	Rc + GMSLR (total height) [m]	Crest Height (Rc) [m]	Rc + GMSLR (total height) [m]	Crest Height (Rc) [m]	Rc + GMSLR (total height) [m]
Scenario	Rise [m]			slope 1 & 2 (1:1-1:2) steep		slope 3 (1:3) gentle		Slope 4 (1:4) gentle	
contemporary	0	2.58	5.44	1.44	1.44	0.8	0.8	0.6	0.6
low	0.3	2.59	5.44	1.44	1.74	0.8	1.1	0.6	0.9
intermediate-low	0.5	2.59	5.44	1.44	1.94	0.8	1.3	0.6	1.1
intermediate	1	2.59	5.44	1.44	2.44	0.8	1.8	0.6	1.6
intermediate-high	1.5	2.59	5.44	1.44	2.94	0.8	2.3	0.6	2.1
high	2	2.6	5.44	1.45	3.45	0.8	2.8	0.6	2.6
Extreme	2.5	2.6	5.44	1.45	3.95	0.8	3.3	0.6	3.1

Table B.2 | Total barrier heights accounting for different sea level rise scenarios and outer slopes.

The third wave climate estimation is based on a more severe scenario. For this analysis, the entire length of Long Island Sound contributes to fetch development. Deeper water levels are present over this distance affecting the wave development towards the barrier. Therefore, an average depth of 30 m and fetch length of 120 km are assumed and a (sustained) windspeed ($U10$) of 33.4 m/s over the entire fetch distance resulting in the following barrier heights presented in Table B.3.

Global Mean Sea Level Rise (GMSLR)		Significant Wave Height (Hs) [m]	Significant Wave Period (Ts) [m]	Crest Height (Rc) [m]	Rc + GMSLR (total height) [m]	Crest Height (Rc) [m]	Rc + GMSLR (total height) [m]	Crest Height (Rc) [m]	Rc + GMSLR (total height) [m]
Scenario	Rise [m]			slope 1 & 2 (1:1-1:2) steep		slope 3 (1:3) gentle		Slope 4 (1:4) gentle	
contemporary	0	4.71	8.82	3.15	3.15	2.39	2.39	1.74	1.74
low	0.3	4.75	8.86	3.19	3.49	2.42	2.72	1.76	2.06
intermediate-low	0.5	4.77	8.89	3.21	3.71	2.44	2.94	1.78	2.28
intermediate	1	4.84	8.96	3.27	4.27	2.49	3.49	1.81	2.81
intermediate-high	1.5	4.91	9.03	3.32	4.82	2.53	4.03	1.85	3.35
high	2	4.97	9.09	3.38	5.38	2.58	4.58	1.88	3.88
Extreme	2.5	5.03	9.15	3.43	5.93	2.6	5.1	1.9	4.4

Table B.3 | Intensified wave development for the determination of the barrier heights accounting for different sea level rise scenarios and outer slopes.

The method used for determining the fetch length in Figure B.4 is based on a closed basin (Holthuijsen, 1980, p. 64) which is not the case for Long Island Sound since both ends connects to the ocean (tidal straight). This method therefore leads to an underestimation of the significant wave height development in Table B.2 compared to Table B.3. It should be noted that the funnel shape of Long Island Sound can lead to waves converging, thus amplifying the wave height development even further in general.

B3 Discussion

Comparing the required barrier heights for all wave climate estimates (Tables B.2-3 and section B1.2), it becomes clear that the most extreme cases for the second wave climate estimation (Table B.2) with 3.95 m and the third wave climate estimation (Table B.3) with 5.93 m are well below the contemporary required 7.9 m height of the first wave climate estimation (section B1.2). A detailed study on the probability of occurrences of the different wave climates will help to inform the decision-making process, however, from a structural design perspective, the priority lies with designing a structure that can at least withstand these wave climates for they occurred in reality. Therefore, the first wave climate estimation is chosen as a reference for the design of the Segment barrier.

Global mean sea level rise is now taken into account for the first wave climate scenario. Table B.4 shows the required height of the barrier and the minimum amount of (slope) segments needed for each sea level rise scenario. Due to the height (5 m) of one segment, many sea level rise scenarios can be dealt with without adding many additional segment layers above the water level. For example, the extreme scenario requires three segment layers above the water level (15 m > 10.4 m), all other scenarios require just two segment layers (10 m > 9.9 m).

Global Mean Sea Level Rise (GMSLR)		Significant Wave Height (Hs) [m]	Significant Wave Period (Ts) [m]	Crest Height (Rc) [m] slope 1 & 2 (1:1-1:2) steep	Rc + GMSLR (total height) [m]	Number of required slope segments		Crest Height (Rc) [m] slope 3 (1:3) gentle	Rc + GMSLR (total height) [m]	Number of required slope segments	Crest Height (Rc) [m] slope 4 (1:4) gentle	Rc + GMSLR (total height) [m]	Number of required slope segments
Scenario	Rise [m]					slope 1	slope 2						
contemporary	0	9.9	13	7.9	7.9	6	12	6.3	6.3	18	4.6	4.6	20
low	0.3	9.9	13	7.9	8.2	6	12	6.3	6.6	18	4.6	4.9	24
intermediate-low	0.5	9.9	13	7.9	8.4	6	12	6.3	6.8	18	4.6	5.1	24
intermediate	1	9.9	13	7.9	8.9	6	12	6.3	7.3	18	4.6	5.6	24
intermediate-high	1.5	9.9	13	7.9	9.4	6	12	6.3	7.8	18	4.6	6.1	24
high	2	9.9	13	7.9	9.9	6	12	6.3	8.3	18	4.6	6.6	24
Extreme	2.5	9.9	13	7.9	10.4	7	14	6.3	8.8	18	4.6	7.1	24

Table B.4 | Number of required segments for different slopes.

Table B.4 further shows the trade-off between the barrier height and amount of required material. For example, the extreme sea level rise scenario can be dealt with using a 1:1 slope or 1:4 slope, however, the difference is 17 (outer slope) segments. The trade-offs between for example: material, costs and strength and the degree to which these are dependent on each other is not further analyzed and outside the scope of this thesis.

The chosen sea level rise scenario for the design of the Segment barrier is ‘high’ in Table B.4. The reason being that this scenario covers six (out of seven) different SLR scenarios without the need for more than two additional segments (above water level). Moreover, the extreme scenario is least likely to occur. In conclusion the height of the barrier is 10 m above water level, making the total height 30 m.

Appendix C: Loads on the barrier

C1 Introduction

This section analyzes the loads on the barrier. First, the basic concept of the mechanical model is explained with a simple example followed by the analysis of two scenarios: the contemporary and extreme GMSLR. For each scenario, three load cases are presented: hydrostatic loads, dynamic loads and self-weight. Finally, these load cases are combined which leads to a governing load condition from which a barrier segment can be designed.

C2 Mechanical Model

The basic mechanical scheme is modelled in matrixframe software (student version) and shown in Figure C.1. For this example, an arbitrary hydrostatic load is applied to one side and the self-weight of an arbitrary material is taken into account.

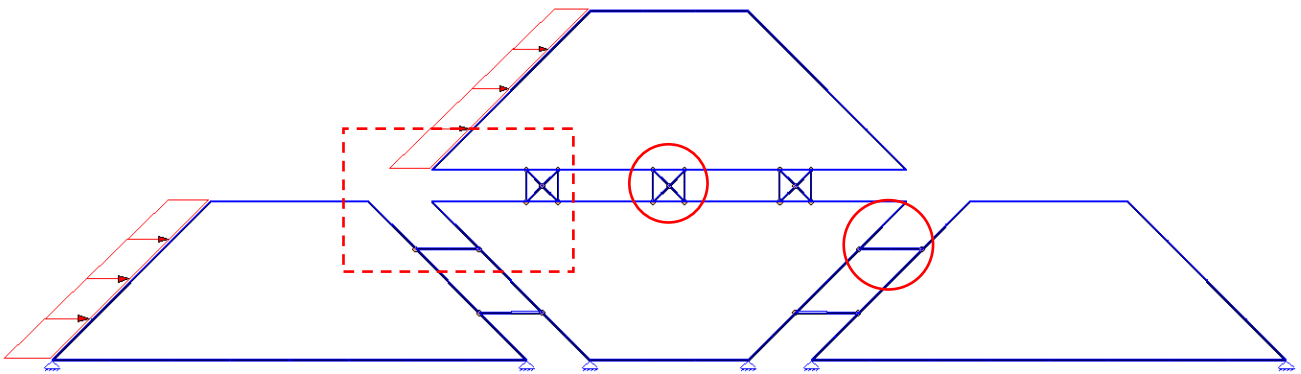


Figure C.1 | Basic mechanical model with hydrostatic loads (red) and self-weight (blue).

The encircled elements shown in Figure C.1 are uniaxial bars that can only be loaded along their axis. These bars represent the connections (ridges or cutouts) and are uniaxially loaded by design, meaning no moments are taken up by these elements. Modeling the rods in this configuration provides stability for the overall structure which is a necessity in order to perform a linear elastic calculation. Figure C.2 shows a close-up of the dotted lined area in Figure C.1 in which the axial forces within the structure are drawn.

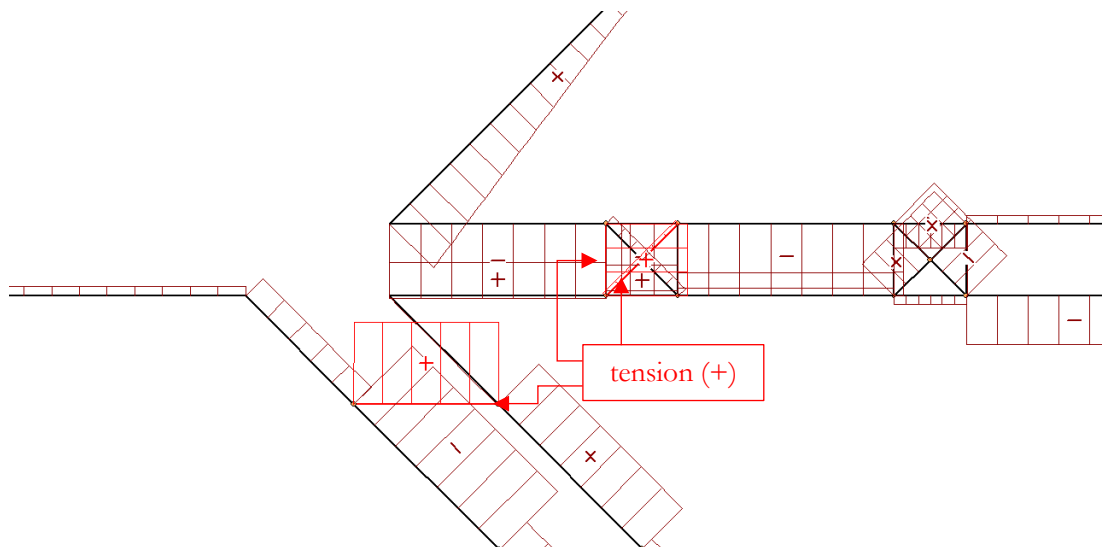


Figure C.2 | Axial forces within the structure.

Three uniaxial bars highlighted in Figure C.2 represent the connections in which axial forces are present. In reality, these connections cannot be loaded in tension, thus showing the limitations of the model. The presence of a tensile force in the model connection means the connection would release in reality. Therefore, the structure would either need to have a substantial self-weight or the tensile forces need to be taken up by a separate designed connection (section recommendation). The full mechanical model of the entire structure is presented in Figure C.3.

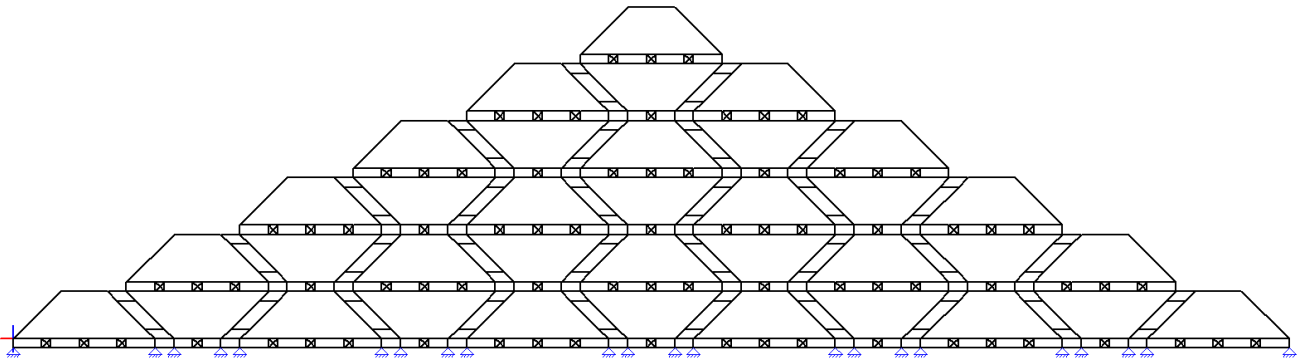


Figure C.3 | Mechanical model of the structure.

C3 Contemporary Load scenario

C3.1 Hydrostatic loads

The mechanical model including the hydrostatic loads for the contemporary scenario is presented in Figure C.4. The water depths are based on the difference between the minimum (-2.49 m) and maximum (+3.1 m) observed tides (Table 3.1).

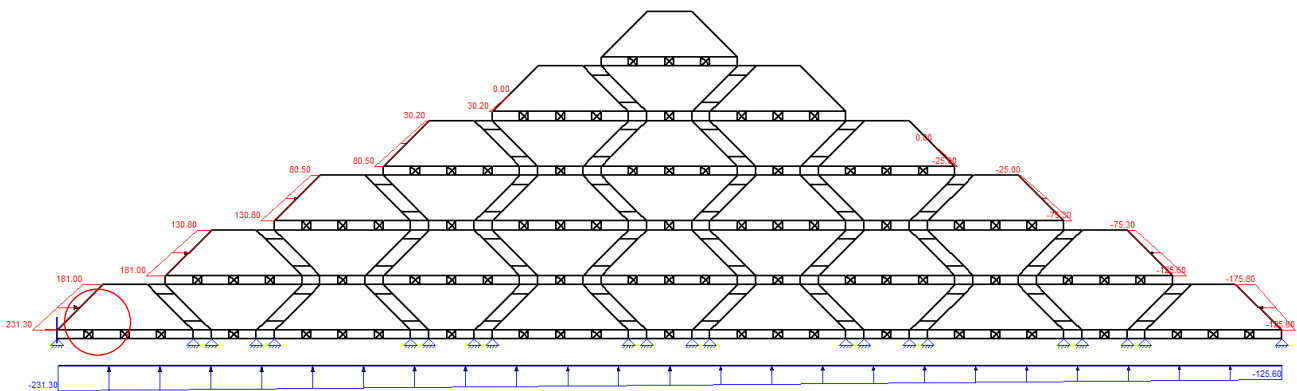


Figure C.4 | Hydrostatic loads on the structure.

The maximum internal moments and forces occur at the sea-side toe of the structure encircled red in Figure C.4. At this location, the maximum moment is 1550 kNm, shear force 1780 kN and normal force 2700 kN.

C3.2 Dynamic wave Loads

The wave pressures on a structure are estimated using Goda's empirical equations (TU Delft, 2016, p. 111). Figure C.5 shows a schematic of this principal in which the wave pressures act on a vertical structure.

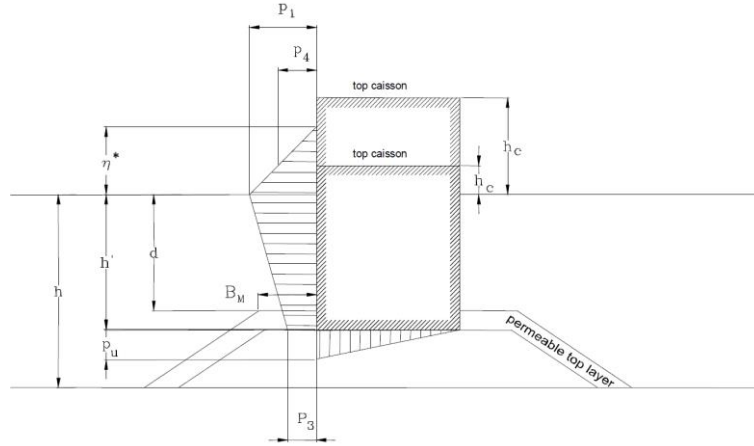


Figure C.5 | Goda's wave pressure model (TU Delft, 2016, p. 111).

The maximum wave pressures [kN/m²] on the sea side of the barrier are determined a follow:

$$P_1 = 0.5 \cdot (1 + \cos(\beta)) \cdot (\lambda_1 \alpha_1 + \lambda_2 \alpha_2 \cos(\beta)^2) \rho g H_D \quad (\text{C.1})$$

$$P_3 = \alpha_3 p_1 \quad (\text{C.2})$$

$$P_4 = \alpha_4 p_1 \quad (\text{C.3})$$

$$P_u = 0.5 \cdot (1 + \cos(\beta)) \cdot \lambda_3 \alpha_1 \alpha_3 \rho g H_D \quad (\text{C.4})$$

Where:

- β [°] = the angle of the incoming waves (assumed 0).
- η^* [m] = $0.75(1 + \cos(\beta))\lambda_1 H_D$
- $\alpha_1 = 0.6 + 0.5 \left(\frac{4\pi h/L_D}{\sinh(4\pi h/L_D)} \right)^2$
- $\alpha_2 = \min \left(\frac{\left(\left(1 - \frac{d}{h_b}\right) \cdot \left(\frac{H_D}{d}\right)^2 \right)}{3}, \frac{2d}{H_D} \right)$
- $\alpha_3 = 1 - (h'/h) \left(1 - \frac{1}{\cosh\left(\frac{2\pi h}{L_D}\right)} \right)$
- $\alpha_4 = 1 - \frac{h_c^*}{\eta^*}$
- h_c [m] = top of the structure.
- h_c^* [m] = $\min(\eta^*, h_c)$
- $\lambda_1, \lambda_2, \lambda_3$ = factors dependent on the shape of the structure and on wave conditions;
- (straight wall and non-breaking waves: $\lambda_1 = \lambda_2 = \lambda_3 = 1$)
- h_b [m] = depth at a distance $5H_D$ from the wall (assuming a constant water depth)
- H_D [m] = design wave height
- L_D [m] = design wavelength
- d [m] = water depth above the top of the sill (assuming permeable rubble layer is 1 m)
- h' [m] = water depth above the wall foundations plane
- h [m] = water depth in front of the sill

The parameters used to perform the calculations are presented below:

$h_b = 20$ m (assumed constant water depth)

$H_D = 9.9$ m (section overtopping)

$L_D = 213.7$ m (section overtopping)

$d = 18$ m (assumed foundation thickness of 1 m)

$h' = 19$ m (assumed foundation thickness of 1 m)

$h = 20$ m water depth in front of the sill.

$h_c = 10$ m

$$\eta' = 0.75(1 + \cos(\beta))\lambda_1 H_D = 0.75(1 + \cos(0))1 * 9.9 = 14.8 \text{ m} \quad (\text{C.5})$$

$$\alpha_1 = 0.6 + 0.5 \left(\frac{4\pi h/L_D}{\sinh(4\pi h/L_D)} \right)^2 = 0.6 + 0.5 \cdot \left(\frac{4\pi \cdot \frac{20}{213.7}}{\sinh\left(4\pi \cdot \frac{20}{213.7}\right)} \right)^2 = 0.9 \quad (\text{C.6})$$

$$\alpha_2 = \min \left(\frac{\left(1 - \frac{d}{h_b}\right) * \left(\frac{H_D}{d}\right)^2}{3}, \frac{2d}{H_D} \right) = \min \left(\frac{\left(1 - \frac{18}{20}\right) \cdot \left(\frac{9.9}{18}\right)^2}{3}, \frac{2 \cdot 18}{9.9} \right) = 0.01 \quad (\text{C.7})$$

$$\alpha_3 = 1 - (h'/h) \left(1 - \frac{1}{\cosh\left(\frac{2\pi h}{L_D}\right)} \right) = 1 - (13/15) \left(1 - \frac{1}{\cosh\left(\frac{2\pi * 15}{82}\right)} \right) = 0.05 \quad (\text{C.8})$$

$$h'_c = \min(\eta', h_c) = \min(14.8, 10) = 10 \text{ m} \quad (\text{C.9})$$

$$\alpha_4 = 1 - \frac{h'_c}{\eta'} = 1 - \frac{10}{14.8} = 0.33 \quad (\text{C.10})$$

The wave pressures are then determined as follow:

$$P_1 = 0.5 \cdot (1 + \cos(\beta)) \cdot (\lambda_1 \alpha_1 + \lambda_2 \alpha_2 \cos(\beta)^2) \rho g H_D \rightarrow \quad (\text{C.11})$$

$$0.5 \cdot (1 + \cos(0)) \cdot (0.9 \cdot 1 + 0.01 \cdot 1 \cos(0)^2) \cdot 1025 \cdot 9.81 \cdot 9.9 \cdot 10^{-3} = 99.5 \text{ kN/m}^2$$

$$P_3 = \alpha_3 p_1 = 0.05 \cdot 99.5 = 5 \text{ kN/m}^2 \quad (\text{C.12})$$

$$P_4 = \alpha_4 p_1 = 0.33 \cdot 99.5 = 32.5 \text{ kN/m}^2 \quad (\text{C.13})$$

$$P_u = 0.5 \cdot (1 + \cos(\beta)) \lambda_3 \alpha_1 \alpha_3 \rho g H_D \rightarrow \quad (\text{C.14})$$

$$0.5 \cdot (1 + \cos(0)) \cdot 1 \cdot 0.9 \cdot 0.05 \cdot 1025 \cdot 9.81 \cdot 9.9 \cdot 10^{-3} = 4.6 \text{ kN/m}^2$$

Goda's model is intended for vertical structures, therefore, a uniform correction factor λ_{SL} is applied to the pressures for inclined surfaces (Buccino, et al., 2012, p. 4788).

$$\lambda_{SL} = \min \left\{ \max \left\{ 1.0; -23 \cdot \frac{H}{L} \cdot \tan^2(\theta) + 0.46 \cdot \frac{1}{\tan^2(\theta)} + \frac{1}{\sin^2(\theta)} \right\}; \frac{1}{\sin^2(\theta)} \right\} \quad (C.15)$$

The uniform correction factor then becomes:

$$\lambda_{SL} = \min \left\{ \max \left\{ 1.0; -23 \cdot \frac{H}{L} \cdot \tan^2(\theta) + 0.46 \cdot \frac{1}{\tan^2(\theta)} + \frac{1}{\sin^2(\theta)} \right\}; \frac{1}{\sin^2(\theta)} \right\} \rightarrow \quad (C.16)$$

$$\min \left\{ \max \left\{ 1.0; -23 \cdot \frac{9.9}{213.7} \cdot \tan^2(45) + 0.46 \cdot \frac{1}{\tan^2(45)} + \frac{1}{\sin^2(45)} \right\}; \frac{1}{\sin^2(45)} \right\} = 1.4$$

Therefore, wave pressures on an inclined surface are corrected as follow:

$$pxf = \frac{Px}{\lambda_{SL}} \quad (C.17)$$

The entire pressure diagram in Figure C.5 can be rotated perpendicular to an inclined structure according to the method of Tanimoto and Kimura (Buccino, et al., 2012, p. 4788). The final values for the wave pressures are given by:

$$p1f = \frac{P1}{\lambda_{SL}} = \frac{99.4}{1.4} = 71.1 \text{ kN/m}^2 \quad (C.18)$$

$$p3f = \frac{P3}{\lambda_{SL}} = \frac{5}{1.4} = 3.6 \text{ kN/m}^2 \quad (C.19)$$

$$p4f = \frac{P4}{\lambda_{SL}} = \frac{32.5}{1.4} = 23.2 \text{ kN/m}^2 \quad (C.20)$$

$$puf = \frac{Pu}{\lambda_{SL}} = \frac{4.6}{1.4} = 3.3 \text{ kN/m}^2 \quad (C.21)$$

The dynamic wave forces on the structure are presented in Figure C.6. The location of the maximum moment [kNm] and shear forces [kN] are encircled (1) and maximum normal force [kN] (2).

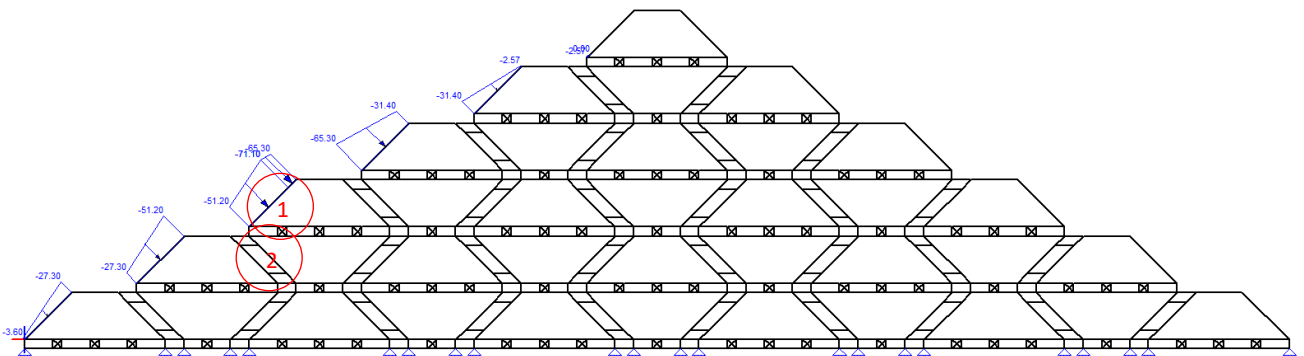


Figure C.6 | Dynamic wave loads on the structure.

The maximum internal moments and forces occur below the water surface level. At these locations, the maximum moment is 235 kNm, shear force 226 kN, normal force 434 kN.

C3.3 Self-weight

The locations of the maximum moment (1) shear forces (2) and normal force (3) are shown in Figure C.7. The maximum moment is 275 kNm, shear force 175 kN, normal force 2583 kN.

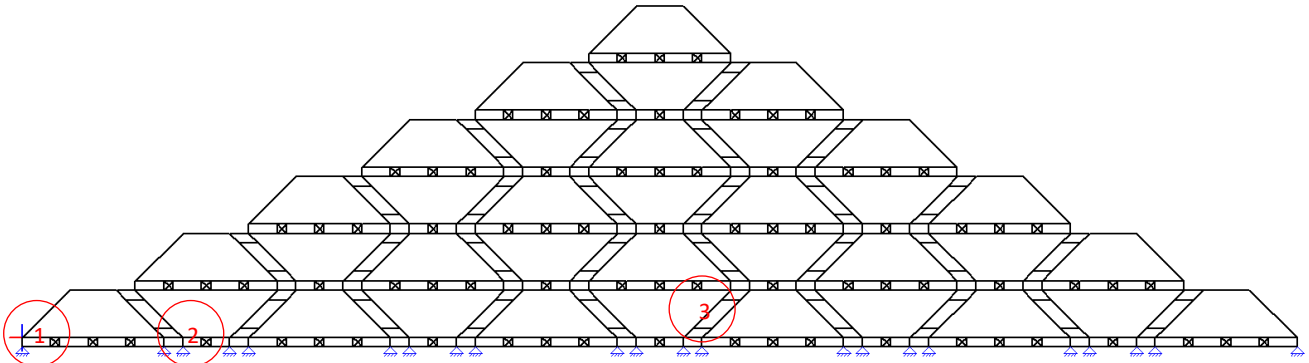


Figure C.7 | Selfweight of the structure.

C3.4 Load combinations

Permanent, variable or exceptional loads can occur separately or in combination. These load combinations are setup according to the European standards for structural design NEN-EN 1990 in which ultimate limit state (ULS) – structural stability and failure – and serviceability limit state (SLS) – deformations and vibrations – are distinguished. For ULS calculations the fundamental load combination equation is given by (Oosterhoff, 2008, pp. 10-11):

$$\sum_{j \geq k} \gamma_{G,j} G_{k,j} + \gamma_P P + \gamma_{Q,1} Q_{k,1} + \sum_{i > 1} \gamma_{Q,i} \psi_{0,1} Q_{k,i} \quad (\text{C.22})$$

Where:

G = permanent load

Q = variable load

P = prestressed load

γ_G = partial factor self-weight

γ_P = partial factor prestressed load

γ_Q = partial factor variable load

ψ = variable load factor

The concrete self-weight is favorable in this case, therefore, $\gamma_G = 0.9$. The load factors for partial factor variable load (γ_Q) is equal to 1.5 and variable load factor (ψ) equal to 1.

$$0.9 \cdot G_{k,j} + \sum_{i > 1} 1.5 \cdot Q_{k,i} \quad (\text{C.23})$$

The storm surge barrier is categorized as a CC3 (highest consequence class) due to severe economic damages and potential loss of lives; therefore, equation C.23 is multiplied by a factor K_{FL} equal to 1.1.

$$1.1 \left(0.9 \cdot G_{k,j} + \sum_{i > 1} 1.5 \cdot Q_{k,i} \right) = 0.99 \cdot G_{k,j} + \sum_{i > 1} 1.65 \cdot Q_{k,i} \quad (\text{C.24})$$

Finally, the load combination including hydrostatic, wave and self-weight pressures is presented in Figure C.8.

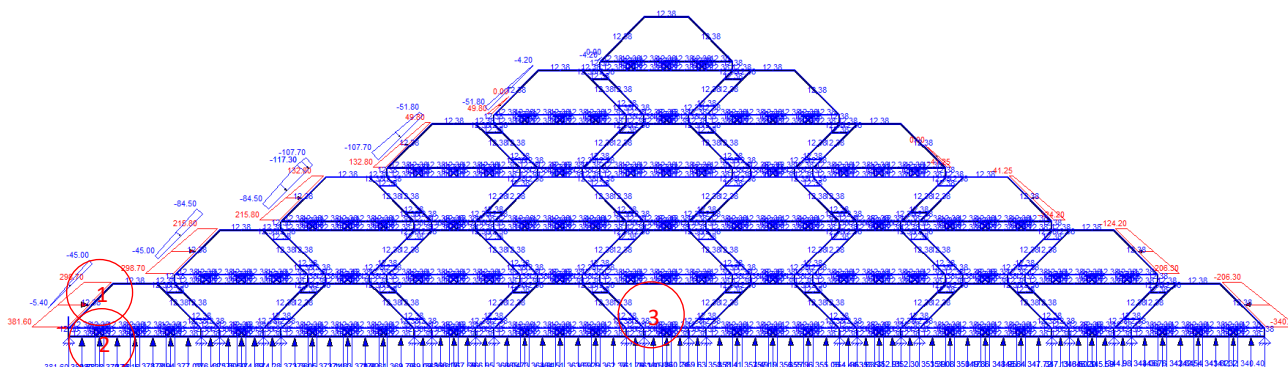


Figure C.8 | Load combination on the structure.

The maximum internal moment encircled (1) is 2310 kNm, shear force (2) 1150 kN and normal force (3) 4100 kN.

C4 Extreme load scenario

This section takes into account the extreme scenario for global mean sea level rise which delivers the maximum pressures on the structure, regardless of its probability of occurrence. An individual segment is designed to withstand these forces. For the extreme scenario, the expected surface water level elevation increase is 2.5 m; therefore, the hydrostatic water levels are increase by this amount while assuming the tidal range remains unchanged. The wave pressure is calculated according to the same method applied in section C3.2 with a water depth of 22.5 m. This leads to a reduction factor for wave pressure λSL of 1.28. The wave height and length are assumed to increase by 10%. The results of the internal forces in the structure for the contemporary (section C3) and extreme load scenarios are summarized in Table C.1.

Load Case \ Scenario	Contemporary	Extreme	Contemporary	Extreme	Contemporary	Extreme
	Moment [kNm]		Shear Force [kN]		Normal Force [kN]	
Hydrostatic pressure	1550	1750	1780	2030	2700	3050
Wave Pressure	235	244	226	260	434	470
Self-Weight	275	275	175	175	2583	2583
Combination	2310	2800	1150	3370	4100	5400

Table C.1 | Internal forces on the structure for contemporary and extreme GMSLR scenarios.

Appendix D: Concrete & steel design

D1 Internal angle

The cross-section of a segment is dimensioned with the purpose of minimizing the internal forces which simultaneously optimizes the transfer of forces between segments. Therefore, the outer slope of the trapezium should be inclined by 45-degrees (angle α denoted in Appendix A, Figure A.1). This can be illustrated by determining the moment distribution within the cross-section. The mechanical model of a trapezium and load configuration are shown in Figure D.1. The loads are assumed to be uniform.

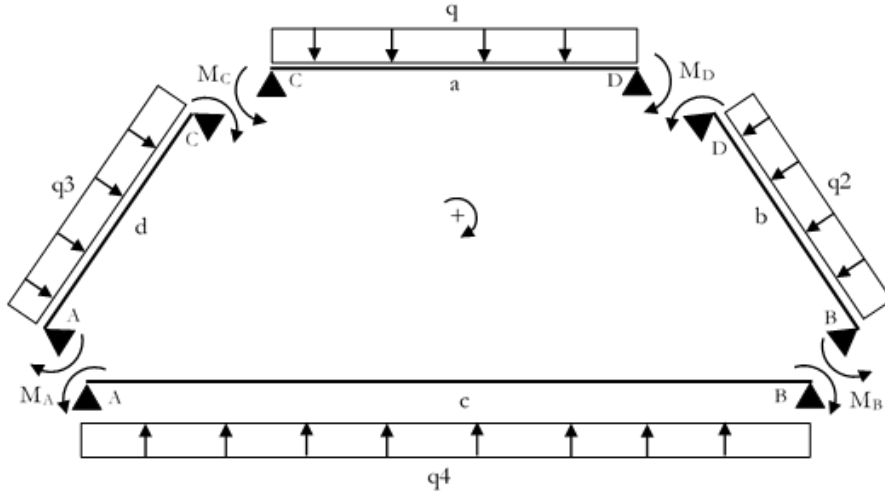


Figure D.1 | Mechanical scheme for the base segment geometry.

The moment distribution is calculated by placing arbitrary loads ($q - q4$) on every side of the structure for which the transitional moment distribution equations are written as follow:

$$\varphi A_{AB} = \frac{-M_A \cdot c}{3EI} - \frac{M_A \cdot c}{6EI} - \frac{q_4 \cdot c^3}{24EI} \quad (D.1)$$

$$\varphi A_{AC} = \frac{M_A \cdot d}{3EI} - \frac{M_C \cdot d}{6EI} + \frac{q_3 \cdot d^3}{24EI} \quad (D.2)$$

$$\varphi C_{AC} = \frac{-M_A \cdot d}{6EI} + \frac{M_C \cdot d}{3EI} - \frac{q_3 \cdot a^3}{24EI} \quad (D.3)$$

$$\varphi C_{CD} = \frac{-M_C \cdot a}{6EI} - \frac{M_C \cdot a}{6EI} + \frac{q \cdot a^3}{24EI} \quad (D.4)$$

$$\varphi B_{AB} = \frac{M_B \cdot c}{3EI} + \frac{M_A \cdot c}{6EI} + \frac{q_4 \cdot b^3}{24EI} \quad (D.5)$$

$$\varphi B_{BD} = \frac{-M_B \cdot b}{3EI} + \frac{M_D \cdot b}{6EI} - \frac{q_2 \cdot b^3}{24EI} \quad (D.6)$$

$$\varphi D_{BD} = \frac{-M_B \cdot b}{3EI} + \frac{M_B \cdot b}{6EI} + \frac{q_2 \cdot b^3}{24EI} \quad (D.7)$$

$$\varphi D_{CD} = \frac{M_D \cdot a}{3EI} + \frac{M_C \cdot a}{6EI} - \frac{q \cdot a^3}{24EI} \quad (D.8)$$

The transitional moments can be determined by solving the following set of equations:

$$\varphi A_{AB} = \varphi A_{AC} \quad (D.9)$$

$$\varphi C_{AC} = \varphi C_{CD} \quad (D.10)$$

$$\varphi B_{AB} = \varphi B_{BD} \quad (D.11)$$

$$\varphi D_{BD} = \varphi D_{CD} \quad (D.12)$$

In order for the outside slopes to have a 45-degree angle, the top length is one-third the base length. If the lengths of b and d (Figure D.1) – which are equal – are shorter or longer than the length under an angle α of 45-degree, there will always be an internal moment that is larger than the moment under a 45-degree angle. To illustrate this, an arbitrary loads $q \cdot q4 = 10 \text{ kN/m}$, base length $c = 10 \text{ m}$ and top length $a = 5 \text{ m}$ are chosen. The angle is modified and the internal moments are presented in Figure D.2.

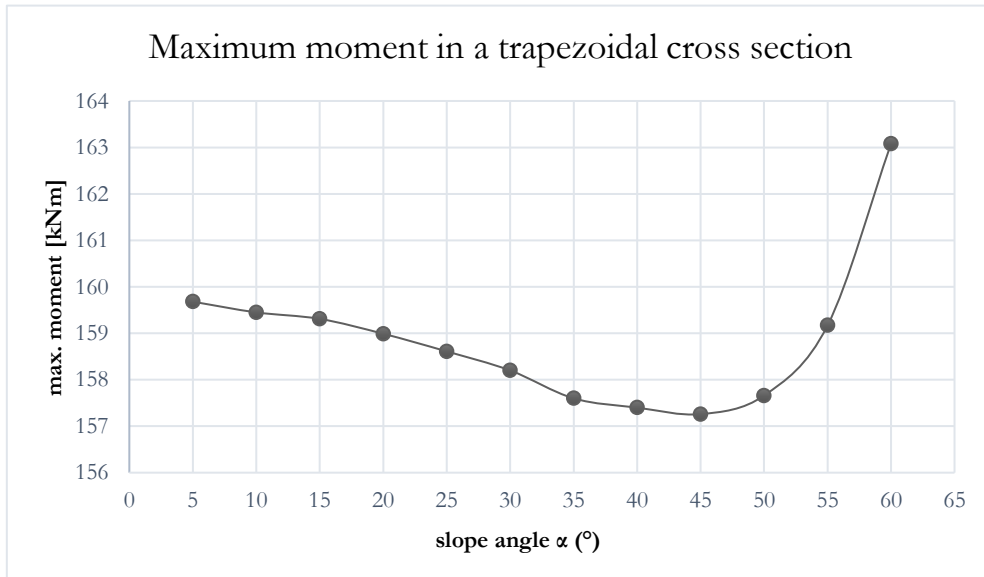


Figure D.2 | Internal moment of one segment under various angles.

Figure D.2 shows how the maximum internal moment in the cross-section decreases to a minimum until an angle of 45-degrees is reached. The angle is changed by increasing/decreasing the height of the structure. Considering this information, the choice is made to design the segments under an internal 45-degree angle.

D2 Concrete & Steel design

D2.1 Material properties

In this section a prestressed segment is designed for the large size segment (section 6.2.1) based on the loading conditions presented in section C4 Table C.1. The reader is referred to section D2.11 for a comprehensive list of all the structural requirements. Table D.1 provides an overview of the concrete and steel material properties used for this design.

Material properties concrete	
Density	$\rho = 25 \text{ kN/m}^3$
Strength class	C50/60 ($f_{ck} = 50 \text{ N/mm}^2$)
Compressive strength design value	$f_{cd} = 50/1.5 = 33,3 \text{ N/mm}^2$
Axial tensile strength	$f_{ctm} = 4,1 \text{ N/mm}^2$
Environmental class	XS2. Corrosion induced by chlorides from sea water
Structural class	S6. Design working life of 100 years
Young's modulus of concrete (short term)	$E_{cm}(0) = 37000 \text{ N/mm}^2$
Material properties prestressing steel	
Characteristic tensile strength	$f_{pk} = 1860 \text{ N/mm}^2$
Characteristic 0,1 % proof – stress	$f_{p0.1k} = 0,9 f_{pk} = 1674 \text{ N/mm}^2$
Design value tensile strength	$f_{pd} = f_{p0.1k}/1,1 = 1522 \text{ N/mm}^2$
Initial tensile stress	$\sigma_{pm0} = 0,75 * 1860 = 1395 \text{ N/mm}^2$
Modulus of elasticity	$E_p = 195000 \text{ N/mm}^2$
Reinforcement class B500B	$f_{yd} = 435 \text{ N/mm}^2$
Material factor for prestressing steel	$E_s = 1,1$
Prestressing system	
Tendon type	19MTAI
Number of strands	19
Diameter strands	$d = 12,9 \text{ mm}$
Cross-sectional area of a strand	$A_p = 100 \text{ mm}^2$
Class A, steel name	Y1860S7
Number of wires per strand	7

Table D.1 | Material properties.

Figure D.3 shows the cross-section of a segment's side which is designed per 10-meter width b [m] and a variable height h [m].

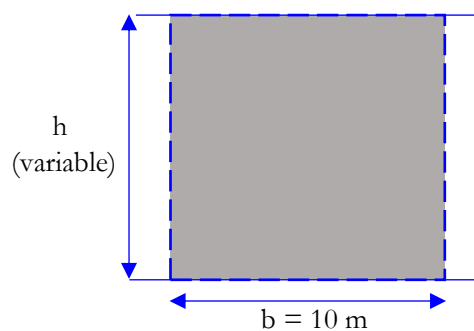


Figure D.3 | Cross-section of a segment's side (top, bottom or diagonal).

The design is based on the concept of *limited prestressing* which allows for small tensile stresses but no crack formation (Prestressed concrete, 2019, pp. 4-5).

Cross-sectional characteristics of concrete

For the initial design, the width $b = 10$ m and height $h = 0.5$ m. The moment of inertia I_c [m⁴] is given by:

$$I_c = \frac{1}{12} \cdot b \cdot h^3 = 0.1042 \text{ m}^4 \tag{D.13}$$

The resisting moments for the top W_{ct} and bottom W_{cb} [m³] are given by:

$$W_{ct} = W_{cb} = \frac{I_c}{\frac{h}{2}} = 0.4166 \text{ m}^3 \tag{D.14}$$

In this case, $h/2$ refers to the distance from the centroidal axis to the bottom and top fibre of the cross-section. The surface area A_c [m²] is given by:

$$A_c = b \cdot h = 5 \text{ m}^2 \tag{D.15}$$

Tendon characteristics

The eccentricities and shape of the *fictitious* tendon are chosen as depicted in Figure D.4, in which ep_A , ep_B and ep_C are 0.14 m.

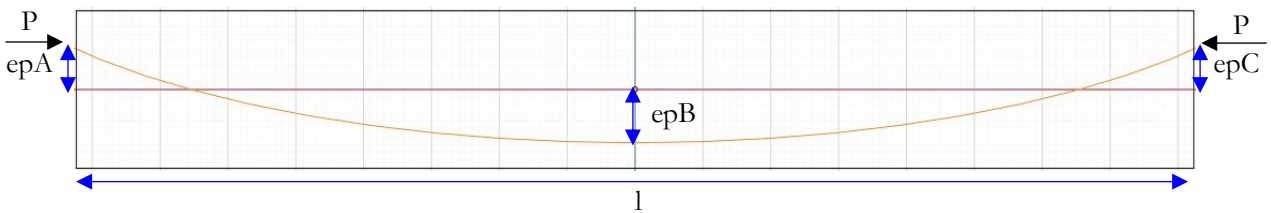


Figure D.4 | Eccentricities of the fictitious tendon (yellow) relative to the centroidal axis (red).

In actuality, the resultant of all tendons final position can lie within the boundaries of the *kern area* which is an area relative to the centroidal axis of the cross-section as shown in Figure D.5. It is noted that the kern area at the ends of the beam will be thicker by design. This is to ensure a more gradual transition between the sides instead of a sharp corner.

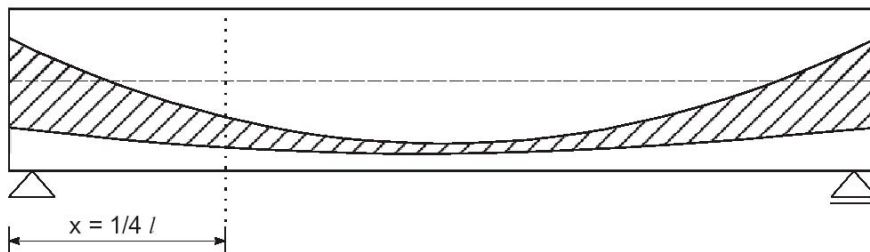


Figure D.5 | Shaded area in which the tendons can be placed in actuality (Prestressed concrete, 2019, pp. 4-39).

The radius R [m] of the fictitious tendon (yellow line Figure D.4) is determined as follow:

$$y = epA + epB \quad (\text{D.16})$$

$$x = \frac{l}{2} \quad (\text{D.17})$$

$$R = \frac{x^2}{2 \cdot y} \quad (\text{D.18})$$

The governing side in the trapezium cross-section is the bottom side considering it has the longest of all sides and experiences the largest loads. The radius of the fictitious tendon for this side is 100.4 m.

The bending moment diagram for the fictitious tendon is shown in Figure D.6.

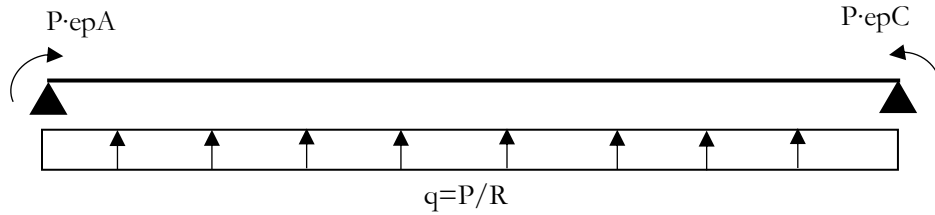


Figure D.6 | Mechanical scheme of the bending moment contribution by the prestressed tendon.

Prestressing force requirements

The time related scenarios that need to be analyzed are $t = 0$ and $t = \infty$. At $t = \infty$, no tensile stresses are allowed in the concrete fibres. The working prestressing force $P_{m\infty}$ which is needed to fulfil this requirement is determined by using the internal moments calculated in section C4 for the extreme sea level rise scenario (Table C.1) which is considered governing for the entire segment.

Consider $t = \infty$.

The bending moment M^∞ [kNm] is determined in section C4 Table C.1. The expressions for the q-load qp^∞ [kN/m] and related bending moment Mp^∞ [kNm] of the fictitious tendon are given by:

$$qp^\infty = \frac{P_{m\infty}}{R} \quad (\text{D.19})$$

$$Mp^\infty = \frac{1}{8} \cdot qp^\infty \cdot l^2 \quad (\text{D.20})$$

At $t = \infty$, the prestressing force is determined as follow. It is assumed that *no* tensile stresses occur at a governing fibre, which in this case assumed to be at the bottom of the cross-section.

$$qp^\infty = 0.00995 \cdot P_{m\infty} \quad (\text{D.21})$$

$$Mp^\infty = 0.279 \cdot P_{m\infty} \quad (\text{D.22})$$

$$-\frac{P_{m\infty}}{Ac} - \frac{Mp^\infty}{W_{cb}} + \frac{M^\infty}{W_{cb}} \leq 0 \rightarrow P_{m\infty} \geq 7706 \text{ kN} \quad (\text{D.23})$$

Consider $t = 0$.

The initial prestressing force $Pm0$ [kN] is limited by the maximum allowed compressive concrete stress (European Committee for standardization, 2004, p. 77). During stressing, the maximum allowed prestressing stress σ_c [N/mm²] is limited by:

$$\sigma_c = f_{ck} \cdot 0.6 = 30 \text{ N/mm}^2 \quad (\text{D.24})$$

At $t = 0$, the maximum initial prestressing force $Pm0$ [kN] is given by:

$$qp0 = \frac{Pm0}{R} \quad (\text{D.25})$$

$$Mp0 = \frac{1}{8} \cdot qp0 \cdot l^2 \quad (\text{D.26})$$

$$-\frac{Pm0}{Ac} - \frac{Mp0}{Wcb} + \frac{M_\infty}{Wcb} \geq -\sigma_c \cdot 10^3 \rightarrow Pm0 \leq 42110 \text{ kN} \quad (\text{D.27})$$

Additionally, it is required that the prestressing is not loaded to such extremes causing tensile stresses at the top fibre. The initial prestressing is therefore limited by:

$$-\frac{Pm0}{Ac} + \frac{\frac{1}{8} \cdot \frac{Pm0}{R} \cdot l^2}{Wct} - \frac{M_\infty}{Wct} \leq 0 \rightarrow Pm0 \leq 14237 \text{ kN} \quad (\text{D.28})$$

Therefore, the governing initial prestressing force $Pm0$ [kN] at $t = 0$ should remain below 14237 kN.

The choice is made to apply an initial prestressing force:

$$Pm0 = 9500 \text{ kN} \quad (\text{D.29})$$

Number of strands per tendon

The choice is made to base the number of strands and tendons on a $Pm0$ of 9633 kN. The minimum required amount of prestressing steel is then determined as follow:

$$A_{ptot} \geq \frac{Pm0 \cdot 10^3}{\sigma_{pm0}} = \frac{9500 \cdot 10^3}{1395} = 6810 \text{ mm}^2 \quad (\text{D.30})$$

The choice is made to apply steel strands with a diameter d of 15.7 mm and area per strand A_p is 150 mm² (VSL International Ltd, 2013, p. 21). The total number of strands become:

$$\#strands = \frac{A_{ptot}}{A_p} = 45.4 \rightarrow 46 \quad (\text{D.31})$$

The choice is made to apply tendon type 19MTAI which includes 19 strands per tendon (Tensa B.V., p. 52). The number of tendons is then given by:

$$\#tendons = \frac{\#strands}{19} = 2.4 \rightarrow 3 \text{ tendons} \quad (\text{D.32})$$

D2.2 Prestress losses

Prestressing steel with steel grade Y1860 can be stressed up to a maximum σ_{pmax} of 1488 N/mm², equivalent to a maximum force:

$$\sigma_{pmax} \cdot (\#strands \cdot A_p) \cdot 10^{-3} = 10267 \text{ kN} \quad (\text{D.33})$$

This stress level is required not to be exceeded. Furthermore, directly after anchoring the stress must remain below the initial tensile stress σ_{pm0} of 1395 N/mm², equivalent to

$$\sigma_{pm0} \cdot (\#strands \cdot A_p) \cdot 10^{-3} = 9625 \text{ kN} \quad (\text{D.34})$$

The choice is made to stress the tendons from one end up to $dPm0 = 9500$ kN, which is within the upper limit. It is verified whether after anchoring the initial stress remains below σ_{pm0} 1395 N/mm² due to friction loss ΔP_μ in section D2.3.

D2.3 Friction loss

The expression for friction loss is given by:

$$\Delta P_\mu(x) = P_{max} \cdot (1 - e^{-\mu(\theta+k \cdot x)}) \quad (\text{D.35})$$

Where:

θ [rad] = rotation of the prestressing tendon (angle in rad.)

k [rad/m] = 0.01. wobble-effect

ΔP_μ [kN] = loss due to friction

μ [-] = 0.19. friction coefficient

P_{max} [kN] = design prestressing force

The prestressing loss due to friction is determined as follow:

$$\theta = \frac{l}{R} = 0.149 \quad (\text{D.36})$$

$$\Delta P_\mu = dPm0 \cdot (1 - e^{-\mu(\theta+k \cdot x)}) = 9500 \cdot (1 - e^{-0.19(0.149+0.01 \cdot 15)}) = 525.2 \text{ kN} \quad (\text{D.37})$$

The force and stress per tendon after friction loss is calculated as follow:

$$F_{tendon} = \frac{dPm0 - \Delta P_\mu}{\#tendons} = 2991 \text{ kN} \quad (\text{D.38})$$

$$\sigma = \frac{F_{tendon} \cdot 10^3}{\frac{A_{ptot}}{A_p}} = 1300.7 \text{ N/mm}^2 \quad (\text{D.39})$$

This stress is below the required 1395 N/mm². It now has to be verified whether the design value $dPm0$ is sufficient. It is requirement that after taking into account additional time dependent losses (creep, shrinkage and relaxation), the prestress force remains higher than the minimum required prestress force at $t = \infty$, i.e.:

$$Pm_{loss}^\infty \geq Pm^\infty (7706 \text{ kN}) \quad (\text{D.40})$$

D2.4 Creep

Creep is a time dependent deformation. The concrete stress at the level of the prestressing steel at the midspan of Figure D.4 is given by:

$$\sigma_{cc} = -\frac{dPm0 \cdot 10^3}{Ac \cdot 10^6} - \frac{(dPm0 \cdot epB) \cdot 10^3}{Ic \cdot 10^{12}} + \frac{M_{\infty} \cdot epB \cdot 10^3}{Ic \cdot 10^{12}} = 1.85 \text{ N/mm}^2 \quad (\text{D.41})$$

The creep coefficient is $\varphi = 1.7$ (European Committee for standardization, 2004, p. 31) and concrete strain is determined as follow:

$$\varepsilon_{cc} = \frac{\varphi \cdot \sigma_{cc}}{E_{cm}} = 8.5 \cdot 10^{-5} \quad (\text{D.42})$$

The creep loss is given by:

$$\Delta\sigma_{creep} = \varepsilon_{cc} \cdot E_p \quad (\text{D.43})$$

$$\Delta P_{creep} = \Delta\sigma_{creep} \cdot A_{ptot} \cdot 10^{-3} = 114.4 \text{ kN} \quad (\text{D.44})$$

D2.5 Shrinkage

The shrinkage strain is assumed (European Committee for standardization, 2004, p. 33):

$$\varepsilon_{cs} = 0.15 \cdot 10^{-3} \quad (\text{D.45})$$

The stress loss due to shrinkage is given by:

$$\Delta\sigma_{shrinkage} \cdot E_p = 29.2 \text{ N/mm}^2 \quad (\text{D.46})$$

$$\Delta P_{shrinkage} \cdot \Delta\sigma_{shrinkage} \cdot A_{ptot} \cdot 10^{-3} = 201.8 \text{ kN} \quad (\text{D.47})$$

D2.6 Relaxation

The stress loss caused by relaxation is determined as follow:

$$\Delta\sigma_{pr} = \sigma_{pi} 0.66 \cdot \rho_{1000} \cdot e^{9.1 \cdot \mu} \cdot \left(\frac{t}{1000}\right)^{0.75 \cdot (1-\mu)} \cdot 10^{-5} \quad (\text{D.48})$$

Where:

$\Delta\sigma_{pr}$ [N/mm²] = the absolute value of the relaxation losses of the prestressing steel.

σ_{pi} [N/mm²] = σ_{pm0} the initial stress in the prestressing steel (after anchoring).

t [hrs] = 500000. time after tensioning.

$\mu = \sigma_{pi}/f_{pk}$, where f_{pk} is the characteristic value of the tensile strength of the prestressing steel.

$\rho_{1000} = 2.5\%$ is the value of relaxation loss (%), at 1000 hours after tensioning and at a mean temperature of 20 °C.

When combined with creep and shrinkage, a reduction factor of 0.8 can be applied to the relaxation loss (European Committee for standardization, 2004, p. 80).

$$\rho_{1000} = 2.5 \quad (\text{D.49})$$

$$\mu = \frac{\sigma_{pm0}}{f_{pk}} = \frac{1395}{1860} = 0.75 \quad (\text{D.50})$$

$$\Delta\sigma_{pr} = \sigma_{pi} \cdot 0.66 \cdot \rho_{1000} \cdot e^{9.1 \cdot \mu} \cdot \left(\frac{t}{1000}\right)^{0.75 \cdot (1-\mu)} \cdot 10^{-5} = 67.9 \text{ N/mm}^2 \quad (\text{D.51})$$

Taking shrinkage and creep into account, the relaxation loss ΔP_{rlx} [kN] is determined as follow:

$$\Delta P_{rlx} = 0.8 \cdot \Delta\sigma_{pr} \cdot A_{ptot} \cdot 10^{-3} = 375 \text{ kN} \quad (\text{D.52})$$

D2.7 Elastic deformation

Elastic deformation of the concrete is calculated as follow. The variation of stress at the center of gravity of all tendons is given by:

$$\Delta\sigma_{cp} = -\frac{dPm0}{Ac \cdot 10^6} \cdot \left(1 + \frac{epB^2 \cdot Ac}{Ic}\right) \quad (\text{D.53})$$

$$j = \left(\frac{n-1}{2 \cdot n}\right) \quad (\text{D.54})$$

Where:

n = the number of tendons

The mean loss of all tendons is calculated as follow:

$$\Delta P_{el} = \left(\frac{A_{ptot}}{\#tendons}\right) \cdot Ep \cdot \left(j \cdot \frac{\Delta\sigma_{cp}}{Ecm}\right) = 14.9 \text{ kN} \quad (\text{D.55})$$

D2.8 Summary of all losses

The working prestressing force after taking into account all losses is given by:

$$Pm^{\infty}_{loss} = dPm0 - \Delta P_{\mu} - \Delta P_{creep} - \Delta P_{shrinkage} - \Delta P_{rlx} - \Delta P_{el} = 8269 \text{ kN} \quad (\text{D.56})$$

The stress per tendon is then given by:

$$\sigma_{pm^{\infty}_{loss}} = \frac{Pm^{\infty}_{loss}}{\left(\frac{A_{ptot}}{\#tendons}\right)} = 1198 \text{ N/mm}^2 \quad (\text{D.57})$$

The equivalent force per tendon is 2756 kN.

D2.9 Bending moment capacity

In this section the bending moment resistance M_{rd} [kNm] is calculated. For a serviceability limit state calculation (SLS) the concrete is linear-elastic in compression and assumed to have no strength when loaded in tension. First, the thickness of the concrete cover is calculated.

The nominal concrete cover is defined as a minimum cover plus allowed deviation (European Committee for standardization, 2004, pp. 48-52):

$$c_{nom} = c_{min} + \Delta C_{dev} \quad (D.58)$$

The minimum cover c_{min} is defined as:

$$c_{min} = \max \{c_{min,b}; c_{min,dur} + \Delta c_{dur,\gamma} - \Delta c_{dur,st} - \Delta c_{dur,add}; 10 \text{ mm}\} \quad (D.59)$$

Where:

$c_{min,b}$ [mm] = 19.35. minimum cover due to bond requirement

$c_{min,dur}$ [mm] = 60. minimum cover due to environmental conditions

$\Delta c_{dur,\gamma}$ = 0. additive safety element

$\Delta c_{dur,st}$ = 0. reduction of minimum cover for use of stainless steel

$\Delta c_{dur,add}$ = 0. reduction of minimum cover for use of additional protection

It is assumed a barrier segments can be produced with a high degree of accuracy, allowing for ΔC_{dev} to be 0 mm, thus the nominal cover c_{nom} is:

$$c_{nom} = \max\{19.35; 60; 10 \text{ mm}\} = 60 \text{ mm} \quad (D.60)$$

The height of the concrete compression zone is determined as follow. A minimum longitudinal reinforcement A_{smin} [mm²] of 0.0013·b·d. is required (European Committee for standardization, 2004, p. 152) which is equals:

$$A_{smin} = 0.0013 \cdot b \cdot d = 6500 \text{ mm}^2 \quad (D.61)$$

The choice is made to apply 36 longitudinal reinforcement bars with a diameter of 25 mm².

$$A_s = \frac{\pi}{4} d^2 \cdot 36 = 17674 \text{ mm}^2 \quad (D.62)$$

The height of the compression zone x_u [mm] for rectangular cross-sections is given by:

$$x_u = \frac{(A_s \cdot f_{yd} + A_{ptot} \cdot \sigma_{pu})}{\alpha \cdot b \cdot 1000 \cdot f_{cd}} = \frac{(17673 \cdot 435 + 6750 \cdot 1606)}{0.75 \cdot 1 \cdot 1000 \cdot 33.3} = 75.0 \text{ mm} \quad (D.63)$$

The concrete should 'warn' when failing and prevent brittle failure to occur. This is verified as follow:

$$\frac{x_u}{d_{eff}} \leq 1 - \frac{f}{500 + f} \rightarrow 0.2 \leq 0.5 \quad (D.64)$$

Where:

$$f = \frac{\left(\frac{f_{pk}}{y_s} - \sigma_{pm\infty}\right) \cdot A_{ptot} + f_{yd} \cdot A_s}{A_p + A_s} = 451 \quad (D.65)$$

Thus, this condition is satisfied.

The strain development is assumed to be linear over the height of the cross-section. Figure D.7 shows the strain distributions for the prestressing tendon (located along the black line) and reinforcement steel (located along the red line).

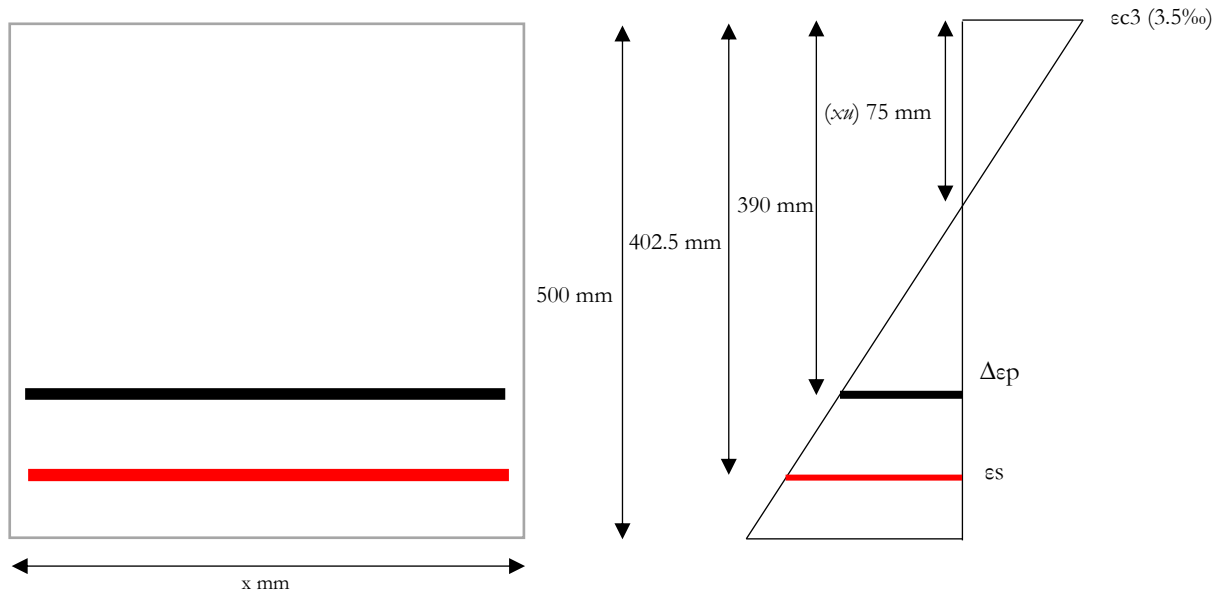


Figure D.7 | Concrete cross-section and strain distribution diagram.

The effective height $deff$ [mm] is chosen to be 402.5 mm (including $\text{Ø}25$ mm stirrups). The strain values are:

$$\varepsilon_s = \frac{(deff - xu)}{xu} (h - xu - 80.5) = 15.3 \cdot 10^{-3} \quad (\text{D.66})$$

$$\Delta\varepsilon_p = \frac{(dp - xu)}{xu} \cdot (390 - xu) = 14.7 \cdot 10^{-3} \quad (\text{D.67})$$

It is assuming the prestressed steel reaches a tensile stress σ_{pu} [N/mm^2] given by:

$$\sigma_{pu} = \frac{0.95 \cdot fpk}{y_s} = 1606 \text{ N/mm}^2 \quad (\text{D.68})$$

It is then verified whether the stress in the prestress steel reached the assumed tensile stress σ_{pu} [N/mm^2]. This is determined as follow:

$$\varepsilon_p = \frac{\sigma_{pm\infty loss}}{E_p} + \Delta\varepsilon_p = 2.08 \cdot 10^{-2} \quad (\text{D.69})$$

$$\sigma_p = 1522 + \frac{(1691 - 1522) \cdot (\varepsilon_p \cdot 10^3 - 7.81)}{(35 - 7.81)} = 1603 \text{ N/mm}^2 \quad (\text{D.70})$$

The value of the stress in the prestressing steel σ_p is below the assumed σ_{pu} $1606 \text{ N}/\text{mm}^2$.

The bending moment capacity M_{rd} [kNm] for the cross-section can be calculated as follow. Figure D.8 summarizes the forces in the cross-section.

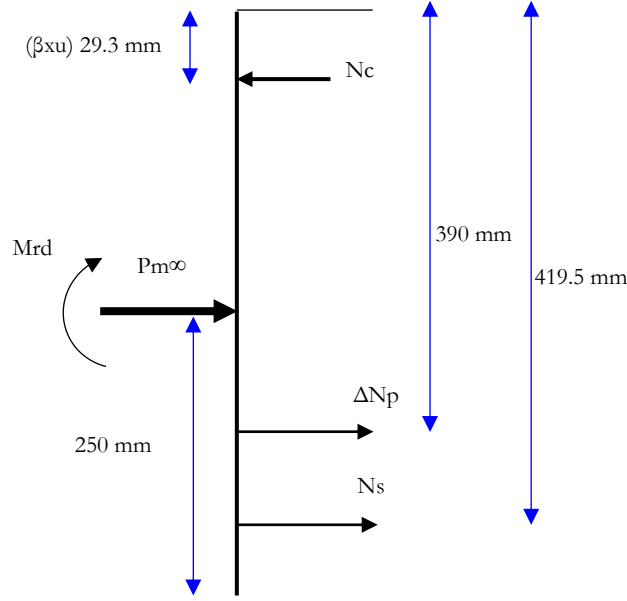


Figure D.8 | Forces in the cross-section.

$$N_s = A_s \cdot f_{yd} \cdot 10^{-3} = 7684 \text{ kN} \quad (\text{D.71})$$

$$\Delta N_p = A p_{tot} (\sigma_p - \sigma_{pm\infty}) \cdot 10^{-3} = 2791 \text{ kN} \quad (\text{D.72})$$

From the horizontal force equilibrium, the magnitude of the concrete compressive force N_c [kN] follows:

$$N_c - P m_{\infty loss} - N_s - \Delta N_p + N_{s2} = 0 \rightarrow N_c = 18744 \text{ kN} \quad (\text{D.73})$$

Finally, the bending moment capacity is given by:

$$(N_c \cdot \beta \cdot x_u \cdot 10^{-3}) - M_{rd} - P m_{\infty loss} \cdot 0.5 \cdot h - \Delta N_p \cdot \left(\frac{h}{2} + e p B\right) \cdot 10^{-3} - N_s \cdot d_{eff} \cdot 10^{-3} = 0 \rightarrow$$

$$M_{Rd} = 5700 \text{ kNm} \quad (\text{D.74})$$

The maximum bending moment capacity for this cross-sectional design is sufficient to resist the loads for the extreme sea level rise scenario (2800 kNm, Table C.1), i.e.:

$$M_{Rd} > M_{Ed} \rightarrow 5700 > 2800 \text{ kNm} \quad (\text{D.75})$$

A verification on the cracking moment is conducted to ensure the cross-section cannot fail without warning.

$$M_{crack} = \left(\frac{P m_{\infty loss}}{A_c} + f_{ctm}\right) \cdot W_{cb} = \left(\frac{8284}{5 \cdot 1000} + 4.1 \cdot 1000\right) \cdot W_{cb} = 2397 \text{ kN} \quad (\text{D.76})$$

$$M_{crack} < M_{Rd} \quad (\text{D.77})$$

The cross-section satisfies the cracking requirement.

D2.10 Shear reinforcement

A verification on the shear capacity is conducted in which the shear capacity $V_{rd,c}$ [kN] should exceed the governing shear force for the extreme sea level rise scenario (Table C.1) V_{ed} is 3370 kN, that is:

$$V_{rd,c} > V_{Ed} \quad (\text{D.78})$$

The shear capacity is determined as follow (European Committee for standardization, 2004, pp. 85-86):

$$V_{rd,c} = \left[C_{Rd,c} \cdot k \cdot (100 \cdot \rho_l \cdot f_{ck})^{\frac{1}{3}} + k_1 \cdot \sigma_{cp} \right] b \cdot d \quad (\text{D.79})$$

Where:

$$k = 1 + \sqrt{\frac{200}{d}} \leq 2.0 \text{ with } d \text{ in mm}$$

$$k_1 = 0.15$$

$$C_{rd,c} = 0.12$$

$$\sigma_{cp} = \frac{N_{ED}}{A_c} < 0.2 \cdot f_{cd} \text{ [MPa]}$$

$$\rho_l = \frac{A_{sl}}{b \cdot d} \leq 0.02$$

A_{sl} [mm²] = the area of tensile reinforcement

b [mm] = the smallest width of the cross-section in the tensile area

f_{ck} [N/mm²] = concrete strength class

A_c [mm] = area of the concrete cross-section

The shear capacity is determined as follow:

$$k = 1 + \sqrt{\frac{200}{914.5}} \leq 2.0 \rightarrow 1.7 \leq 2.0 \quad (\text{D.80})$$

$$\rho_l = \frac{A_{sl}}{b \cdot d} \rightarrow \frac{\left(\frac{18656}{2}\right)}{10000 \cdot 402.5} = 0.00220 \leq 0.02 \quad (\text{D.81})$$

$$\sigma_{cp} = \frac{N_{ED}}{A_c} \rightarrow \frac{5400 \cdot 10^3}{5 \cdot 10^6} = 1.1 \text{ [MPa]} < 6.6 \text{ [MPa]} \quad (\text{D.82})$$

$$V_{rd,c} = \left[C_{Rd,c} \cdot k \cdot (100 \cdot \rho_l \cdot f_{ck})^{\frac{1}{3}} + k_1 \cdot \sigma_{cp} \right] b \cdot d \rightarrow \quad (\text{D.83})$$

$$\left(\left[0.12 \cdot 1.7 \cdot (100 \cdot 0.00220 \cdot 50)^{\frac{1}{3}} + 0.15 \cdot 1.1 \right] \cdot (10000 \cdot 10^3) \cdot 402.5 \right) \cdot 10^{-3} = 2265 \text{ kN}$$

The shear capacity is insufficient. Therefore, shear reinforcement is required.

D2.11 Final Results

As described in the previous sections (D2.1-10), the design has to fulfil a number of structural requirements. A brief summary of these requirements is provided below which are all satisfied:

- The barrier is designed to protect against storms with a 103-year return period, i.e., similar to Hurricane Sandy (significant wave height 9.9 m, wave period 13 s).
- At $t = \infty$, it is assumed *no* tensile forces occur at the bottom fibre of the model (Figure 6-33), i.e.:

$$Pm_{\infty} \geq 7706 \text{ kN} \quad (\text{D.86})$$
- At $t = 0$, the maximum initial prestressing cannot exceed $0.6 \cdot f_{ck}$ (30 N/mm^2), i.e.:

$$Pm_0 \leq 42110 \text{ kN} \quad (\text{D.87})$$
- At $t = 0$, the prestressing load does not cause tensile stresses at the top fibre, i.e.:

$$Pm_0 \leq 14237 \text{ kN} \quad (\text{D.88})$$
- The minimum required amount of prestressing steel is 6810 mm^2 . Applied: 6900 mm^2 .
- Prestressing steel with steel grade Y1860 can be stressed up to a maximum σ_{pmax} of 1488 N/mm^2 , i.e., 10267 kN .
- Directly after anchoring the stress must remain below the initial tensile stress σ_{pm0} of 1395 N/mm^2 , i.e., 9625 kN .
- The initial prestressing force should be larger than the prestress force at $t = \infty$ after taking into account all losses., i.e.:

$$Pm_{\infty loss} > Pm_{\infty} \quad (\text{D.89})$$
- The concrete cover thickness should be based on the environmental class.
- The concrete should warn against brittle failure.
- The assumed tensile stress in the prestressed steel $\sigma_{pu} = 1606 \text{ [N/mm}^2]$ should not be exceeded.
- The design value Med [kNm] must remain below the bending moment capacity Mrd [kNm] i.e.:

$$Med < Mrd \quad (\text{D.90})$$
- The cracking moment M_{crack} [kNm] must remain below the bending moment capacity Mrd [kNm] i.e.:

$$M_{crack} < Mrd \quad (\text{D.91})$$
- The internal shear reinforcement distance s [mm] should lie between 150-374 mm.

The final design of the cross-section is presented in Figure D.10.

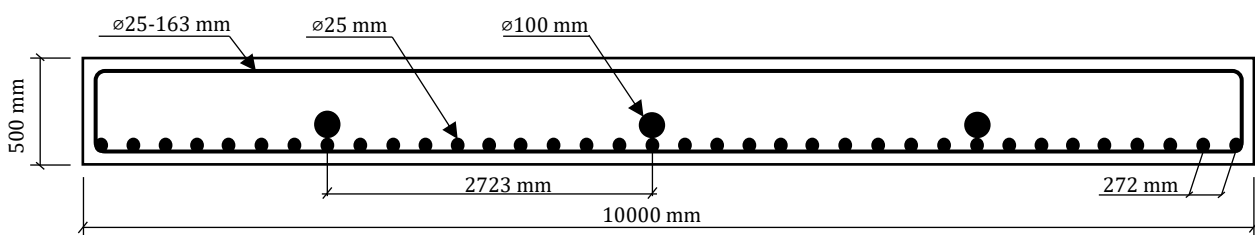


Figure D.10 | Final result of the concrete and steel prestressed design.

D2.12 Reinforcement only

Another possibility would be to only apply reinforcement steel. In order to make a comparison to the prestress design, all material properties in Table D.1 remain the same. A verification of the bending moment capacity will illustrate the difference. It is chosen to apply the same stirrups ($\text{Ø}25$ mm), reinforcement bar diameters ($\text{Ø}25$ mm) and 60 mm concrete cover. A concrete cross-section with a width of $b = 1$ m is analyzed. The cross-section should be able to withstand the maximum bending moment M_{ed} 2800 kNm (Table C.1). This can be achieved with the following input. By applying a thickness of 1 m the minimum longitudinal reinforcement A_{smin} [mm^2] and effective height d_{eff} [mm] become:

$$A_{smin} = 0.0013 \cdot b \cdot d = 1300 \text{ mm}^2 \quad (\text{D.92})$$

$$d_{eff} = 1000 - 25 - 25 - 60 = 902.5 \text{ mm} \quad (\text{D.93})$$

The choice is made to apply 16 longitudinal reinforcement bars with a diameter of 25 mm.

$$A_s = \frac{\pi}{4} d^2 \cdot 16 = 7855 \text{ mm}^2 \quad (\text{D.94})$$

The height of the compression zone x_u [mm] for rectangular cross-sections is then given by:

$$x_u = \frac{(A_s \cdot f_{yd})}{\alpha \cdot b \cdot 1000 \cdot f_{cd}} = \frac{(7855 \cdot 435)}{0.75 \cdot 1 \cdot 1000 \cdot 33.3} = 136.6 \text{ mm} \quad (\text{D.95})$$

The maximum compression zone is limited to:

$$x_{max} = 0.488 \cdot d_{eff} = 404 \text{ mm} \quad (\text{D.96})$$

The forces in the cross-section and reinforcement steel N_s [kN] are shown in Figure D.11.

$$N_s = A_s \cdot f_{yd} \cdot 10^{-3} = 3415 \text{ kN} \quad (\text{D.97})$$

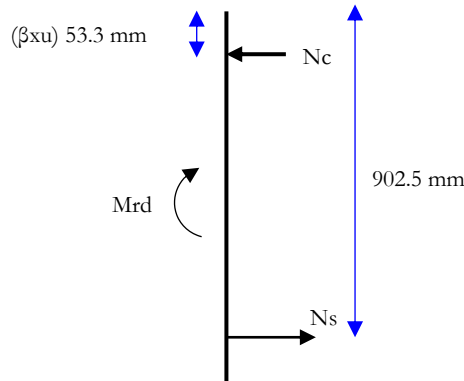


Figure D.11 | Forces in the cross-section.

$$Mrd - N_s \cdot d_{eff} \cdot 10^{-3} + N_c \cdot (\beta \cdot x_u) \cdot 10^{-3} = 0 \rightarrow Mrd = 2900 \text{ kNm} \quad (\text{D.98})$$

In this example, 16 reinforcement steel bars and a concrete thickness of 1 m are needed to fulfil the bending moment requirement. There are trade-offs between the reinforcement steel A_s , [mm^2], compression zone x_u [mm] and concrete thickness b [m] which introduces limitations. For example, a 0.5 m thick cross-section would require too much steel, thus exceeding the compression limit. The only remaining option is to increase the concrete thickness, in this case to 1 m. It could be possible to achieve a thinner thickness by adjusting the concrete mixture (e.g., higher concrete classes), however this optimization is outside the scope of this thesis. Suffice to say that without prestressing the cross-section would thicken. The choice is made to apply prestressing steel to keep the cross-section slender, thus saving material and decreasing the overall segment weight.

Appendix E: Stability

E1 Buoyancy

In this section, the buoyancy for an individual segment is analyzed. In order for a segment to float, the draught must not exceed the object's height. A segment might be of such considerable size that the only method of transportation is to towing it from the manufacturing location to the construction site. This can be achieved by using floating support structures or a specifically designed geometry which is able to float. According to Archimedes principal, the upward directed buoyant force $F_{buoyancy}$ must be equal to the downward directed weight of the object F_w , that is:

$$F_w = F_{buoyancy} \quad (\text{E.1})$$

The buoyancy force is equal to the product of the volumetric weight of water and volume of the displaced water given by:

$$F_{buoyancy} = V_{water} \cdot \gamma_{water} \quad (\text{E.2})$$

$$V_{water} = \frac{1}{2} \cdot (a + b_{sub}) \cdot d \cdot l \quad (\text{E.3})$$

In equation E.3, b_{sub} is the top width of the submerged volume shown in Figure E.1. The orientation of Figure E.1 is similar to that of a so called A-segment.

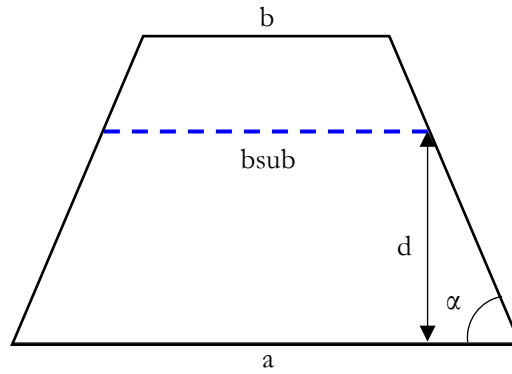


Figure E.1 | Defenition of the submerged distance.

$$b_{sub} = a - 2 \cdot \frac{d}{\tan(\alpha)} \quad (\text{E.4})$$

The draught d [m] would then follow from the following relation:

$$F_w = \frac{1}{2} \cdot \left(a + \left(a - 2 \cdot \frac{d}{\tan(\alpha)} \right) \right) \cdot d \cdot l \cdot \gamma_{water} \quad (\text{E.5})$$

However, this equation has no meaningful solution for the draught, i.e., complex numbers are the resulting outcomes. Only if the segment consisted of a material with a lower volumetric weight than water ($\leq 10 \text{ kN/m}^3$) e.g., polymers, the segment could float in this orientation. Thus, for concrete ($\approx 25 \text{ kN/m}^3$) the trapezium is unable to float.

The geometry has the potential to float when orientated similar to a V-segment as shown in Figure E.2. For the segments on the inside of the barrier, this orientation is the most critical as these tend to float more easily due to uplifting pressures along the diagonal sides. The draught d can be determined as follow:

$$F_w = \frac{1}{2} \cdot \left(b + \left(b + 2 \cdot \frac{d}{\tan(\alpha)} \right) \right) \cdot d \cdot l \cdot \gamma_{\text{water}} \quad (\text{E.6})$$

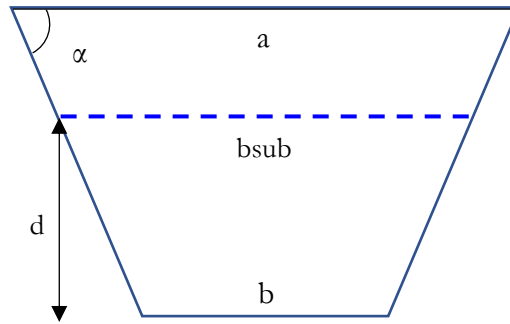


Figure E.2 | Possible floating orientation of a trapezium.

The expression for the draught d is then given by the following relation.

$$d = \frac{-b \cdot l \cdot \gamma_{\text{water}} + \sqrt{(b \cdot l \cdot \gamma_{\text{water}})^2 - 4 \cdot \frac{l \cdot y}{\tan(\alpha)}}}{2 \cdot \frac{l \cdot y}{\tan(\alpha)}} \quad (\text{E.7})$$

In this thesis, both A-and V-segments should *not* float. The segments are lifted on a vessel and transported to the construction site. When the segments are placed into position, the A-segments sink naturally due to their orientation. The V-segments can float or sink depending on the thickness of the cross-section, which in this case is relatively slender (0.5 m) compared to the overall dimensions. In order for the V-segments to sink, a front and back cover are incorporated into the design as shown in Figure E.3. The V-segment will sink for a front and back cover thickness equal to at least 3.8 m. The A-segments have the same cover thickness as the sides (0.5 m).

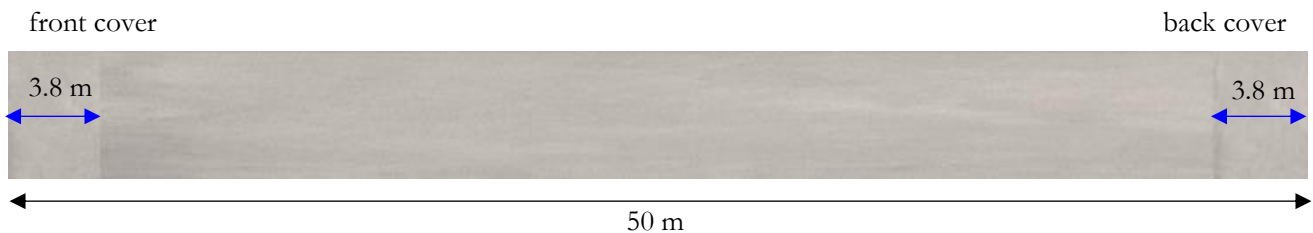


Figure E.3 | Segment with front and back cover width for a V-segment (side view).

E2 Rotational stability

In order to determine the overall stability of the structure, the combinations of horizontal and vertical forces are schematized in Figure E.4 and the resulting moments presented in Table E.1.

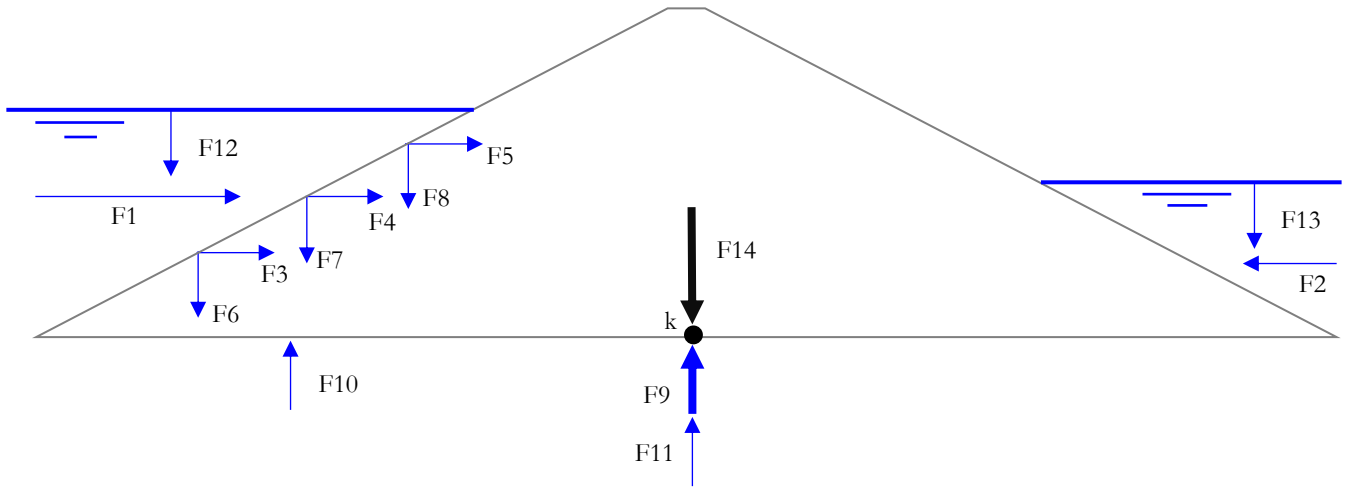


Figure E.4 | Schematic representation of the forces on the structure.

The moments are calculated around the bottom center of the structure (point k).

Horizontal forces	force [kN]	arm [m]	moment [kNm]
F1: hydrostatic load sea side	2683	7.7	20657
F2: hydrostatic load back side	-1540	5.8	-8982
F3: wave load component	54	7.5	405
F4: wave load component	506	10.0	5060
F5: wave load component	377	18.5	6975
sum horizontal forces (ΣH)	2080		
Vertical forces			
F6: wave load component	54	50	-2700
F7: wave load component	506	47.5	-24035
F8: wave load component	377	39	-14703
F9: hydrostatic component	-14444	0	0
F10: hydrostatic component	-6078	19.2	116693
F11: buoyancy force	-1450	0	0
F12: water load sea side	5131	43	-220632
F13: water load back side	2947	46.3	136467
F14: self-weight	14094	0	0
sum vertical forces (ΣV)	1138		
sum moments (ΣM)			15205

Table E.1 | Forces on the structure.

The stability calculations are conducted as follow (TU Delft, 2016, pp. 258-259). The vertical acting forces are: F9, F10 and F11 and the forces responsible for the acting moments are: F1, F3, F4, F5, F10 and F13. Rotational stability is given by:

$$e_r = \frac{\sum M}{\sum V} < \frac{1}{6}b \rightarrow \frac{286257}{21972} < \frac{1}{6} \cdot 115 \rightarrow 13 < 19.2 \quad (\text{E.8})$$

Where:

- e_r [m] = distance from the middle of the structure (point k) to the intersection point of the resulting force and the bottom line of the structure.
- $\sum V$ [kN] = total acting vertical forces.
- $\sum M$ [kN] = total acting moments.
- b [m] = width of the structure.

Therefore, rotational stability is guaranteed.

E3 Vertical stability

The barrier induces an acting load $\sigma_{k,max}$ on the subsoil which should remain below the maximum bearing capacity of the subsoil p'_{max} :

$$\sigma_{k,max} < p'_{max} \quad (\text{E.9})$$

If this is not achieved, the structure needs to be supported with piles. The acting load is calculated as follow:

$$\sigma_{k,max} = \frac{\sum V}{b \cdot l} + \frac{\sum M}{\left(\frac{1}{6}\right)b^2 \cdot l} = \frac{21972}{115 \cdot 1} + \frac{286257}{\left(\frac{1}{6}\right) \cdot 115^2 \cdot 1} = 321 \text{ kN/m}^2 \quad (\text{E.10})$$

This resulting maximum effective soil stress should not exceed the vertical bearing capacity of the soil which can be calculated using the theory of Prandtl & Brinch Hansen (TU Delft, 2016, pp. 182-186).

$$p'_{max} = c'N_c s_c i_c + N_q s_q i_q + 0.5y'BN_y s_y i_y \quad (\text{E.11})$$

Where:

y' = relative specific weight $y' = y_s - y_w = 15 - 10 = 5 \text{ kN/m}^2$ (y is clay, slightly sandy, weak)

φ' =angle of internal friction = 22.5°

N_q [-] = factor for surcharge $N_q = \frac{1+\sin(\varphi')}{1-\sin(\varphi')} \cdot e^{\pi \tan \varphi'} = \frac{1+\sin(22.5)}{1-\sin(22.5)} \cdot e^{\pi \tan(22.5)} = 8.23$

N_y [-] = factor for subsoil $N_y = (N_q - 1) \cdot \cot(\varphi') = 17.7$

N_c [-] = bearing factor $N_c = (N_q - 1) \cdot \cot \varphi' = (8.23 - 1) \cdot \cot(22.5) = 17.45$

S_y [-] = shape factor for the foundation $s_y = 1 - 0.3 \cdot \frac{b}{l} = 1 - 0.3 \cdot \left(\frac{1}{115}\right) = 0.997$

i_y [-] = factor for horizontal load $i_y = \left(1 - \frac{\sum H}{\sum V + A \cdot c' \cdot \cot(\varphi')}\right)^3 = \left(1 - \frac{2080}{21972 + 115 \cdot 1 \cdot 5 \cdot \cot(22.5)}\right)^3 = 0.76$

s_q [-] = shape factor $s_q = 1 + \frac{B}{L} \cdot \sin(\varphi') = 1 + \frac{1}{115} \cdot \sin(22.5) = 0.39$

s_c [-] = shape factor $s_c = \frac{s_q N_q - 1}{N_q - 1} = \frac{0.39 \cdot 8.23 - 1}{8.23 - 1} = 0.305$

i_q [-] = Inclination factor $i_q = \left(1 - \frac{0.7 \sum H}{\sum V + A \cdot c' \cdot \cot(\varphi')}\right)^3 = \left(1 - \frac{0.7 \cdot 2080}{21972 + 115 \cdot 1 \cdot 0 \cdot \cot(22.5)}\right)^3 = 0.82$

i_c [-] = Inclination factor $i_c = \frac{i_q N_q - 1}{N_q - 1} = \frac{0.814 \cdot 17.7 - 1}{17.7 - 1} = 0.80$

Due to the limited geological data, it is assumed a weak clayey silt bathymetry spans the entire channel section near the state border (Figure 3.3). The effective soil stress next to the foundation is assumed negligible, its effect would be too favorable, moreover, the soil is relatively weak. The bearing capacity is therefore:

$$p'_{max} = c' N_c s_c i_c + 0.5 y' B N_y s_y i_y \rightarrow$$

$$5 \cdot 17.45 \cdot 0.305 \cdot 0.8 + 0.5 \cdot 15 \cdot 1 \cdot 17.7 \cdot 0.997 \cdot 0.76 = 122 \text{ kN/m}^2 \quad (\text{E.12})$$

The bearing capacity of the subsoil is insufficient to carry the weight of the barrier:

$$\sigma_{k,max} > p'_{max} \rightarrow 321 > 122 \quad (\text{E.13})$$

A pile foundation is necessary which is elaborated in section 6.2.4.

E4 Horizontal stability

The resulting horizontal forces acting on the barrier need to be resisted by the friction force of the subsoil (TU Delft, 2018, pp. 257-258):

$$\sum H < f \cdot \sum V \quad (\text{E.14})$$

Where:

f [-] = friction coefficient.

$$f = \tan\left(\frac{2}{3} \cdot \varphi\right) = 0.267 \quad (\text{E.15})$$

The horizontal stability is determined as:

$$\sum H < f \cdot \sum V \rightarrow 2080 \text{ kN} < 0.267 \cdot 21972 = 5867 \text{ kN} \quad (\text{E.16})$$

Thus, horizontal stability is guaranteed.

E5 Piping Resistance

Piping resistance is verified according to the methods of Bligh and Lane (TU Delft, 2018, pp. 259-260).

Piping method Bligh:

$$L \geq \gamma \cdot C_B \cdot \Delta H \rightarrow 115 \geq 1.5 \cdot 18 \cdot 5.6 (= 151) \quad (\text{E.17})$$

Piping method Lane:

$$\frac{L}{3} \geq \gamma \cdot C_B \cdot \Delta H \rightarrow 115 \geq 1.5 \cdot 8.5 \cdot 5.6 \rightarrow 38.3 \geq 71.4 \quad (\text{E.18})$$

In which:

L [m] = 115. is the total seepage distance

C_B [-] is Bligh's constant, depends on soil type. For silt: 18.

C_L [-] is Lane's constant, depends on soil type. For silt 8.5 (-)

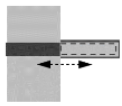
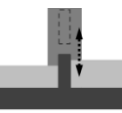
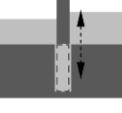
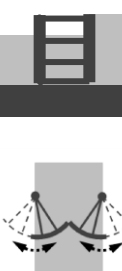
ΔH [m] = 5.6 m. is the head difference across the structure (max tide – min tide)

γ [-] = safety factor (1.5)

This shows that the current situation will lead to piping below the construction. Section 6.2.4 presents a solution against piping.

Appendix F: Gate Types

Table F.1 shows a complete overview of the gate types that were considered in the NYNJHAT study (USACE et al., 2019, p. 142).

Gate Type	section	Cursory Review Throgs Neck	Description	Example Location
Horizontal rolling gate		Impractical due to area needed to dock the gate		
Vertical Lift Gate		Not suitable since unrestricted air clearance is required	Vertical lift gates are moved vertically towards the sill. A tower supports the gate during its operation. Overhead cables, sheaves and bull wheels or hydraulic cylinders lift the gate	Seabrook (USA), IHNC (USA), Eastern Scheldt (NL), Hollandse IJssel (NL), Ems (GER)
Vertical Rising Gate		Deemed too challenging from a maintenance perspective and no proven concept for such a large gate span	Vertical rising gates rest beneath the sill in open position. The gates are lifted vertically to close the barrier. Both in open and in closed position the gates are for the most part submerged. In most applications, gates can be lifted above water to allow for maintenance.	St. Petersburg Barrier (RU)
Tainter Gate		Not suitable since unrestricted air clearance is required	The tainter gate rotates around a horizontal axis, which passes through the bearing center. In closed position, the tainter gate rests on the sill and in open position it is lifted and locked. It is also referred to as a radial or segment gate	St. Petersburg Barrier, Eider (GER), Thames (UK), Ems (GER), Fox Point Barrier (MA, USA)
Rotating Segment Gate		Not suitable for such a large span (no proven constructed concept)	Similar to a tainter gate the rotary segment gate has a horizontal axis. However, in recessed positions, it rests in a concrete sill housing at or near the river bed. Thus, it is possible for maritime traffic to pass over the gate in opened position. Operation of the gate is achieved by approximately 90-degree rotation to raise the gate to the flood protection position. An additional 90 degree of rotation places the gate in the raised position and completely out of the water to facilitate inspection or maintenance.	Thames (UK), Ems (GER)
Sector Gate (Vertical Axis)		Not suitable for such a large span (no proven constructed concept)	A sector gate consists of a double gate complex. Each gate has a circular shape, transferring forces through a steel frame to the hinges at each side of the opening. It operates by rotating around two vertical axes. During operation the gates will rest on the sill of the structure. In non-operational condition, each gate is stored in a gate housing or recess besides the waterway.	Seabrook (USA), New Bedford (USA), IHNC (USA), Harvey Canal (USA), West Closure (USA)

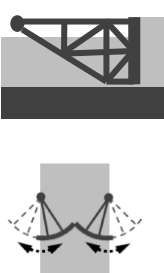
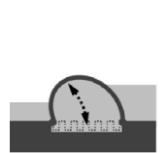
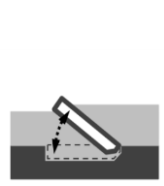
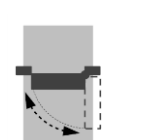
<p>Floating Sector Gate</p>		<p>Suitable, proven concept for large navigable opening.</p>	<p>A floating sector gate consists of a double gate complex. Each gate has a circular shape, rotates around a spherical hinge at each side of the opening transferring forces through a steel frame to the hinges and to the foundation. The gate leaves are buoyant and float into place. During operation the gates will rest on the river bed. In non-operational condition, the doors are stored in a gate housing (dry dock) besides the waterway in the river banks</p>	<p>Maeslant Barrier (NL), St. Petersburg Barrier (RU)</p>
<p>Inflatable Gate or Dam</p>		<p>Not suitable for such a large deep span (no proven constructed concept)</p>	<p>An inflatable gate is essentially a sealed tubular structure made of a flexible material, such as synthetic fiber, rubber, or composite plastics. It is anchored to the sill and walls by means of anchor bolts and an air- and watertight clamping system. The gate is inflated with air, water, or a combination of both.</p>	<p>Ramspol Barrier (NL)</p>
<p>Flap Gate</p>		<p>Possible, as a series of flap gates, but not suitable for reverse head conditions and deemed too challenging from a maintenance perspective</p>	<p>Flap gates consist of a straight or curved gate leaf surface, pivoted on a fixed horizontal axis. The axes can be submerged (Venice, Stamford) or above water (Billwerder Bucht). The gates are operated by filling or emptying them with air, water or a combination of both or actuated with a hoisting mechanism.</p>	<p>MOSE Venice (IT), Stamford (USA)</p>
<p>Barge Gate</p>		<p>Not suitable for such a large span (no proven constructed concept)</p>	<p>A barge gate is a floating caisson stored on one side of a waterway, pivoting around a vertical axis to close. A barge gate may be buoyant or equipped with gated openings to reduce hinge and operating forces. This type of gate is also referred to as a swing gate or caisson gate.</p>	<p>IHNC Barrier (USA)</p>
<p>Miter Gate</p>		<p>Not suitable for such a large span or reverse head conditions</p>		

Table F.1 | Gate types considered in the NYNJHAT report (USACE et al., 2019, p. 142).

Appendix G: Earthen embankment and concrete segment comparisons

The new barrier has a number of advantages over a regular earthen dyke worth considering. Figure G.1 shows the most common failure mechanism for an earthen dike.

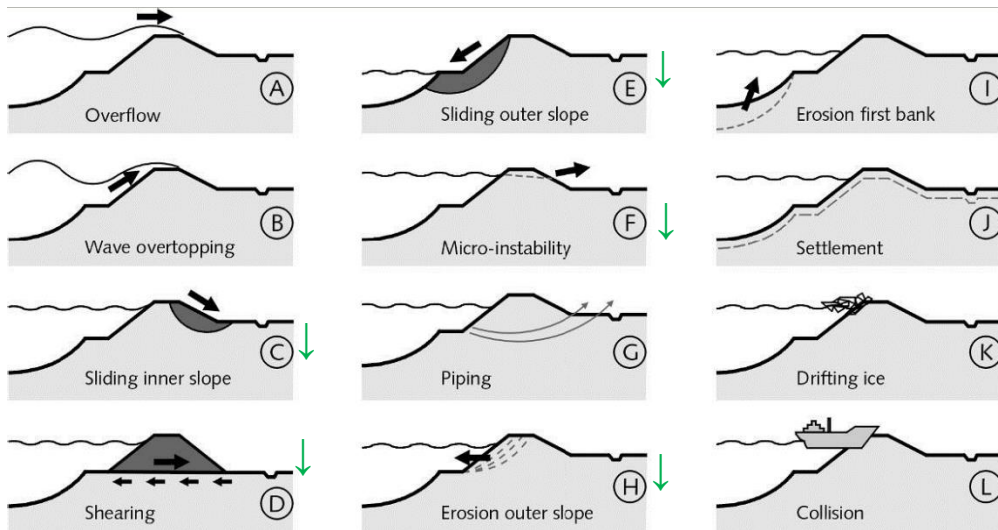


Figure G.1 | Earthen dyke failure mechanisms (TU Delft, Flood defences Lecture notes CIE5314, 2017, p. 20).

There are a number failure mechanisms having less of an impact on the Segment barrier indicated with a downward arrow (↓) in Figure G.1. For example, overflow (A) occurs when the still water levels exceed the crest level. What is then especially damaging is waterflow along the inner slope which can erode and ultimately breach the dyke (TU Delft, Flood defences Lecture notes CIE5314, 2017, p. 19). Erosion of the slopes is not relevant for the Segment barrier. In fact, the Segment barrier is less sensitive to most failure mechanisms relating to erosion in general due to its concrete design. Sliding of the inner slope (C) is the most common stability problem (for river dykes) due to increasing pore pressures from rising water levels, reducing the effective stress and shear strength which can lead to sliding planes in the dyke (TU Delft, Flood defences Lecture notes CIE5314, 2017, p. 21). A somewhat similar failure mechanism is sliding of the outer slope (E). An example would be a high flood wave which can cause a sudden drop in water level in front of the dyke. The pressure difference that develops can lead to sliding. Not only is the Segment barrier fundamentally different due to its concrete design, but the space between segments (Figure 6.23) is expected to allow for a faster flow through of water resulting in a lower pressure gradient. Micro-instability (F) is of no concern and the structure is not expected to be significantly less impacted compared to a dyke by piping (G) or settlements (J) as these failure mechanisms mostly depends on the makeup of the subsoil. However, settlements due to a drop in water level have no effect on the barrier.

Appendix H: Tidal Ranges

Table H.1 shows the tidal elevation data for Kings Point, NY (Center for Operational Oceanographic Products and Services, 2018) which is used as a reference for the entire West Sound area.

NOTICE: All data values are relative to the NAVD88.		
Elevations on NAVD88		
Station: 8516945, Kings Point, NY		
Status: Accepted (Apr 9 2018)		
Units: Meters		
Control Station: 8467150 Bridgeport, CT		
T.M.: 0		
Epoch: 1983-2001		
Datum: NAVD88		
Datum	Value	Description
MHHW	1.109	Mean Higher-High Water
MHW	0.999	Mean High Water
MTL	-0.092	Mean Tide Level
MSL	-0.082	Mean Sea Level
DTL	-0.08	Mean Diurnal Tide Level
MLW	-1.183	Mean Low Water
MLLW	-1.268	Mean Lower-Low Water
NAVD88	0	North American Vertical Datum of 1988
CRD OFFSET		Columbia River Datum Offset
STND	-5.195	Station Datum
GT	2.376	Great Diurnal Range
MN	2.182	Mean Range of Tide
DHQ	0.109	Mean Diurnal High-Water Inequality
DLQ	0.085	Mean Diurnal Low Water Inequality
HWI	4.03	Greenwich High Water Interval (in hours)
LWI	10.73	Greenwich Low Water Interval (in hours)
Max Tide	3.073	Highest Observed Tide
Max Tide Date & Time	10/30/2012 02:00	Highest Observed Tide Date & Time
Min Tide	-2.491	Lowest Observed Tide
Min Tide Date & Time	01-06-18 2:30	Lowest Observed Tide Date & Time
HAT	1.674	Highest Astronomical Tide
HAT Date & Time	10/16/1993 16:12	HAT Date and Time
LAT	-1.761	Lowest Astronomical Tide
LAT Date & Time	01/21/1996 23:30	LAT Date and Time
Tidal Datum Analysis Periods		
09/01/1999 – 08/31/2011		
02/01/2012 – 01/31/2015		
09/01/2016 – 08/31/2017		

Table H.1 | Tidal Ranges (CO-OPS, 2018).